Report No. FAA-RD-76-206

EXPERIMENTAL RELATIONSHIPS BETWEEN MODULI FOR SOIL LAYERS BENEATH CONCRETE PAVEMENTS

J.B. Forrest P.S. Springston
M.G. Katona J. Rollins

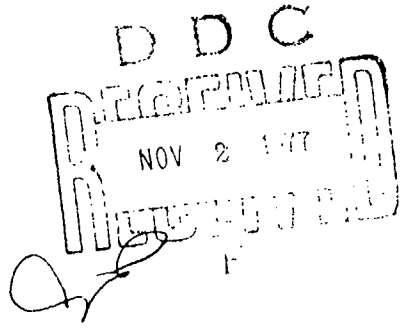

JUNE 1977

FINAL REPORT

Prepared for

U.S. DEPARTMENT OF TRANSPORTATION
FEDERAL AVIATION ADMINISTRATION
Systems Research & Development Service
Washington, D.C. 20590

NOTICE

This document is disseminated under the sponsorship of the Department of Transportation in the interest of information exchange. The United States Government assumes no liability for its contents or use thereof.

Technical Report Documentation Page

1. Report No.	2. Government Accession No.	3. Recipient's Catalog No.
FAA-RD-76-206		

4. Title and Subtitle
Experimental Relationships between Moduli For Soil Layers Beneath Concrete Pavements

5. Report Date
June 1977

6. Performing Organization Code

8. Performing Organization Report No.

7. Author(s)
J. B. Forrest, P. S. Springston, M. G. Katona J. Rollins

9. Performing Organization Name and Address
Civil Engineering Laboratory
Naval Construction Battalion Center
Port Hueneme, California 93043

10. Work Unit No. (TRAIS)

11. Contract or Grant No.
DOT-FA74WAI-487

13. Type of Report and Period Covered
Final Report.
June 1975 - January 1976

12. Sponsoring Agency Name and Address
U.S. Department of Transportation
Federal Aviation Administration
Washington, D.C.
(243 p.)

14. Sponsoring Agency Code
ARD-430

15. Supplementary Notes

16. Abstract

Two subgrades and four rigid pavement test sections were constructed and instrumented to recover experimental information of soil/rigid pavement behavior beneath static loadings. Pavement deflections and pavement/soil strain data were recorded for incremental static loads applied to a 30 inch diameter steel plate. Tests were conducted for comparison of experimentally collected data with Westergaard and elastic layer analyses of the test sections to investigate whether a consistent mathematical relationship exists between the two methods of analysis. To this end material characterizations were carried out for the component materials in the 4 different pavement sections and analytically predicted and experimentally obtained response data were compared.

17. Key Words	18. Distribution Statement
Airport pavements Pavement response Pavement Testing Rigid Pavements	Document is available to the public through the National Technical Information Service, Springfield, Virginia 22151.

19. Security Classif. (of this report)	20. Security Classif. (of this page)	21. No. of Pages	22. Price
UNCLASSIFIED	UNCLASSIFIED	236	

Form DOT F 1700.7 (8-72) Reproduction of completed page authorized

391 111

PREFACE

The study described in this report was sponsored by the Federal Aviation Administration under Inter-Agency Agreement No. DOD-FA/74WA1-487, "Theoretical Relationship Between Moduli for Soil Layers Beneath Concrete Pavements." This report is the second of two reports to be completed under this agreement and covers the work accomplished between June 1975 and January 1976.

The assistance of U. S. Naval Mobile Construction Battalions Four and Ten in providing the equipment and labor for construction of the subgrades and pavement sections is appreciated. Also the dedication and excellent assistance of Mr. Leonard Woloszynski in supervising the construction and testing activities is greatfully acknowledged.

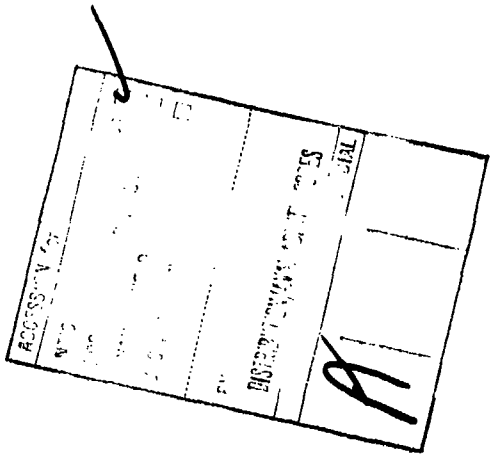

CONTENTS

LIST OF ILLUSTRATIONS

LIST OF ILLUSTRATIONS (Continued)

LIST OF ILLUSTRATIONS (Continued)

LIST OF ILLUSTRATIONS (Continued)

LIST OF ILLUSTRATIONS (Continued)

LIST OF ILLUSTRATIONS (Continued)

LIST OF TABLES

LIST OF TABLES (Continued)

NOTATIONS

a	soil parameter
$[C]$	constitutive matrix
C_{ij}	components of the constitutive matrix
e	void ratio
E	Young's modulus
E_n	Young's modulus for the nth pavement layer
G	shear modulus
G_{max}	maximum value of shear modulus for a particular soil
G_s	secant shear modulus
k	Westergaard, subgrade stiffness parameter
K	coefficient of lateral earth pressure or bulk modulus
K_w^1	Westergaard displacement functional
p	pressure
PI	plasticity index
q	dimensionless parameter used in expression to calculate ν_s
S	percent saturation
S_1, C_1	soil parameters
δ	peak deflection
γ	accumulated maximum shear stress
γ_h	hyperbolic shear strain
γ_r	reference shear strain
γ_{rz}	engineering shear strain
$\{\epsilon\}$	strain tensor

ε_{kk}	sum of normal strains (approximately equal to volumetric strain)
$\{\sigma\}$	stress tensor
σ_{11}, σ_{22}, σ_{33}	principal stresses
σ_{kk}	sum of normal stresses (i.e., = $\sigma_{11} + \sigma_{22} + \sigma_{33}$)
σ_{rr}, ε_{rr}	normal stress/strain in R - coordinate direction
σ_{rz}, ε_{rz}	tensor shear stress/strain in R, Z plane
$\sigma_{\theta\theta}$, $\varepsilon_{\theta\theta}$	normal stress/strain in θ - coordinate direction
σ_{zz}, σ_{zz}	normal stress/strain in Z - coordinate direction
ν	Poisson's ratio
ν_n	Poisson's ratio for the nth pavement layer
ν_{min} and ν_{max}	Poisson's ratio at zero shear strain and at large shear strain
ν_s	secant Poisson's ratio
τ	accumulated maximum shear stress

INTRODUCTION

BACKGROUND

This report is the second phase of a study initiated to provide valid, mathematically consistant relationships between the Westergaard method of analysis and the elastic layer method of analysis for rigid (portland cement concrete) airfield pavements. The study was required in order to explain the different results which sometimes occurred from application of the two different design methods to the same field situation.

The first phase of this study (Reference 1) developed mathematical expressions relating the subgrade modulus used in Westergaard design to the parametric values defining the various layers in elastic layered systems. Several mathematical relationships were presented which related the Westergaard analysis for rigid pavements to the elastic layered method used for both rigid and flexible pavement design. Twenty three actual pavement sections representing a wide variation of rigid pavement types were selected to illustrate the use of the developed relationships. Within the context of linear analysis it was demonstrated that designs based upon peak pavement stress were compatible by either analysis. However, peak displacements by the two different methods of analysis were found to differ by a rather consistant 70 percent. For the range of loadings and types of pavement sections considered, the Westergaard analysis consistantly underpredicts the peak deformation calculated by elastic layered analysis.

The relationships demonstrated that the problem of correlating the two methods can usually be related primarily to inconsistancies in material input, in one or both of the two methods, and to a considerably lesser extent to the disparities in the mathematical idealizations.

This phase of the study reported herein was designed to both validate, under controlled conditions, with well defined pavement test sections, the conclusions reached theoretically in the first phase, and to establish regions of validity.

PROGRAM ELEMENTS

A test facility was constructed at the Civil Engineering Laboratory (CEL), for the purpose of providing data. This data also provides a measure against which the appropriateness of various pavement analysis procedures can be assessed.

The CEL Pavement Test Facility consists of two sites, A and B, containing a sand subgrade and a compacted clay subgrade, respectively. Various pavement sections were constructed over these subgrades allowing an economical construction of test sections while concurrently providing instrumented subgrades whose properties were well defined.

The four test sections, were as follows:

Test	Site	Pavement Section Placed on Subgrade
A1	A	9 inches of portland cement concrete (PCC)
A2	A	6 inches of concrete over 6 inches of asphalt base
B1	B	9 inches of concrete (PCC)
B2	B	6 inches of concrete over 8 inches of lime stabilized clay

These sections were constructed and loaded in a manner to minimize boundary effects and to simulate as nearly as possible the idealizations associated with the various analysis procedures. The loads were applied using a 30 inch plate, with a maximum level of 90 kips. This load limitation was of major consideration in establishing the pavement thickness. A description of the field tests is presented in Chapter 3, and Appendices A and B.

One very important aspect of this study was characterization of the pavement material responses for input into the analytic treatments. A comprehensive set of experimental data was available on a uniform sand which was modelled in the sand subgrade. The fat highly plastic cohesive clay used for the compacted clay subgrade had not been subjected to extensive previous testing, therefore it was necessary to carry out a comprehensive laboratory study to define its response characteristics. Material characterizations for both of these materials are developed in Chapter IV. (Summaries of the actual laboratory test data are included in Appendix C).

In addition to the imported subgrade materials it was necessary to evaluate the response parameters of the other materials incorporated in the pavement test sections, namely the portland cement concrete, the asphaltic base course material and the lime stabilized clay. The scope of the project prohibited as extensive a testing program for these latter more conventional pavement materials, as was conducted for the untreated subgrades. Material characterizations for these latter materials are also developed in Chapter IV.

Chapter V provides discussion of the validity of the theoretically derived conclusions presented in Reference 1. This chapter also discusses limits of applicability of the relationships, and any shortcomings or limitations in the current study. The complexity of parameter interactions are also discussed together with the validity of various parameter evaluation techniques.

Conclusions based upon the overall study are presented in Chapter VI together with recommendations regarding steps to be taken to both optimize and advance the accomplishments of this study.

THEORETICAL RELATIONSHIPS

The original Westergaard idealization of a pavement considers a plate of infinite extent supported by a fluid with a modulus of subgrade reaction, or resistance to deflection denoted by k, in units of force per unit area (length ^{2}) per unit deflection (length). Obviously it would be impossible to relate the response of such a system to an elastic layered system at least on a one-to-one basis unless certain restrictions are defined, such as size of the loaded area, strain or deformation levels, material parameters etc. For this reason a completely general treatment is rigorously impossible. The loaded area throughout this study is assumed to be that of a 30 inch diameter plate (the size specified in Westergaard design). The load ranges and materials are limited to those that would be encountered in Federal Aviation Administration approved airfield pavement practice.

The responses used for controlling design by the Westergaard approach are the maximum tensile stress in the plate (the concrete pavement) and the maximum deflection under the center of applied load. The elastic layer method of analysis is based upon the theory of elasticity, and considers a series of N layers of infinite horizontal extent. The top N-1 layers are of finite thickness while the bottom layer is considered a semi-infinite half-space. Expressions for calculating the appropriate stresses and deflections for both of these two idealizations have been presented in Reference 1. A computer code ELAST, for calculating these quantities and also the values of the derived functionals relating them, has been presented in Reference 1.

Three different definitions for calculating an equivalent subgrade modulus, k, for elastic layered systems were utilized:

1. Computation of subgrade moduli, k_w^1, based upon simulation of a plate bearing test on a layered elastic system.

2. Computation of subgrade moduli, k_w^2, for an elastic layered system such that it would give the same pavement deflection as that predicted by a Westergaard analysis.

3. Computation of subgrade moduli, k_s^1, for an elastic layered system such that it would give the same maximum tensile pavement stress as that predicted by a Westergaard analysis.

Thus for any elastic system a k value could be calculated which would be compatible with either a measured k value or either of the two prescribed pavement response criteria. Unfortunately these various k values were not equal due to the basically different natures of the two theoretical idealizations, and are a function of both the system material parameters and the applied loading. Reference 1 discusses the implications of the differences between the various k values.

Except for the k value calculated prior to placement of a specific pavement, all the relationships (for any particular test section) between Westergaard and Elastic layered analysis are load related. Thus it would be informative to note how these relationships are affected by different ranges of applied loading during the field tests.

The k value calculated for the pavement subgrade system prior to application of the surfacing should first be compared with measured values, to evaluate the validity of the material characterizations. By making comparisions between the "ideal" granular subgrade section and the compacted fat clay sections, some indication as to the validity of the relationships with different types of material can be achieved.

Such comparisons can also be made with regard to the relationships for the surfaced pavement sections, for different load levels. Also the contributions of the different pavement component materials used in the test sections should be evaluated individually and compared to estimates of their behavior based upon theoretical considerations. This includes comparison between measured deflections and tensile stresses and theoretical values predicted by the two analytical approaches.

Considerable further analytic detail concerning shear strain distributions, stress levels in various component layers etc., could be carried out, which would be very pertinent to advancing pavement design technology. In addition, such stresses could be supported by the extensive experimental data presented in this report. Unfortunately such complex considerations are outside the scope of the present objectives.

FIELD TESTS

CONSTRUCTION OF PAVEMENT TEST FACILITY

The subgrades and pavement sections were constructed and tested at a site located within the Construction Battalion Center, Port Hueneme. A 300-foot section of existing embankment was selected as a site for the two subgrades (Figure 1). Placement of the 8 to 9 foot deep subgrades within the embankment insured that the subgrades would be above the natural water table.

The fifteen-foot high embankment consisted of a well graded fill sand (SW, E-1)[a] constructed over in-situ clayey sand (SC, E-6). Debris was removed from the north side of the embankment and the embankment was excavated for placement of the clay subgrade. The clay subgrade was constructed concurrently with widening of the embankment with SC fill material (Figure 2a). After completion of the clay subgrade, the embankment was cut for construction of the sand subgrade which proceeded in the same manner (Figure 2b). Construction specifications for earthwork are presented in Appendix A.

Clay Subgrade Construction

After excavation into the embankment, the bottom of the cut was compacted with a self-propelled vibratory roller with a smooth drum, and a plate test was conducted on the fill sand of the embankment (elev + 12.23) (see Appendix B). Polyethylene was then spread over the bottom of the cut and the first clay lift was placed and compacted. Temporary forms were used to control clay placement and polyethylene was placed along the sides of the clay lifts to retard moisture migration into the clay subgrade after construction. Sand, previously excavated from the embankment, was backfilled between the forms and the sides of the excavation and compacted with an electrical tamper (Figure 3).

Clay was pulverized and mixed with water by a rototiller at an offsite location and transported to the subgrade for spreading and compaction. The clay was compacted in lifts with a self-propelled vibratory roller with a sheepsfoot drum. Five moisture/density tests of the compacted clay were accomplished with a nuclear meter (ASTM D2922, Reference 4) for each lift and readings were averaged to determine the representative lift density and moisture content. Fifteen moisture/density tests were conducted using a sand cone apparatus (ASTM D1556, Reference 5) to calibrate the nuclear meter with the clay soil. Moisture/density tests

---

[a] Throughout this report, the first soil classification designation in parentheses indicates the classification according to the Unified Soil Classification System (Reference 2). The second designation indicates the Federal Aviation Administration (FAA) soil classification (Reference 3).

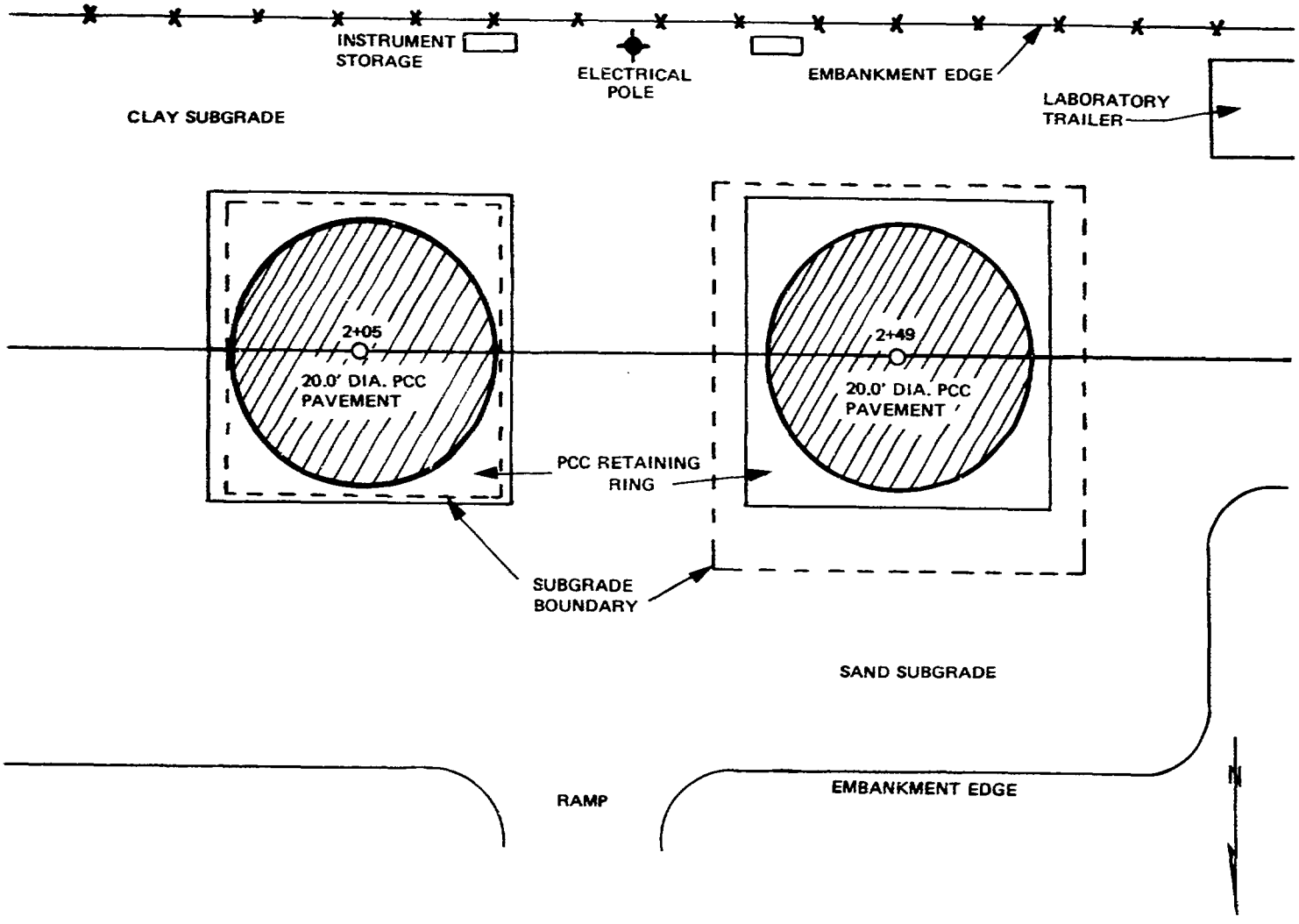

Figure 1. Pavement Test Facility Plan View

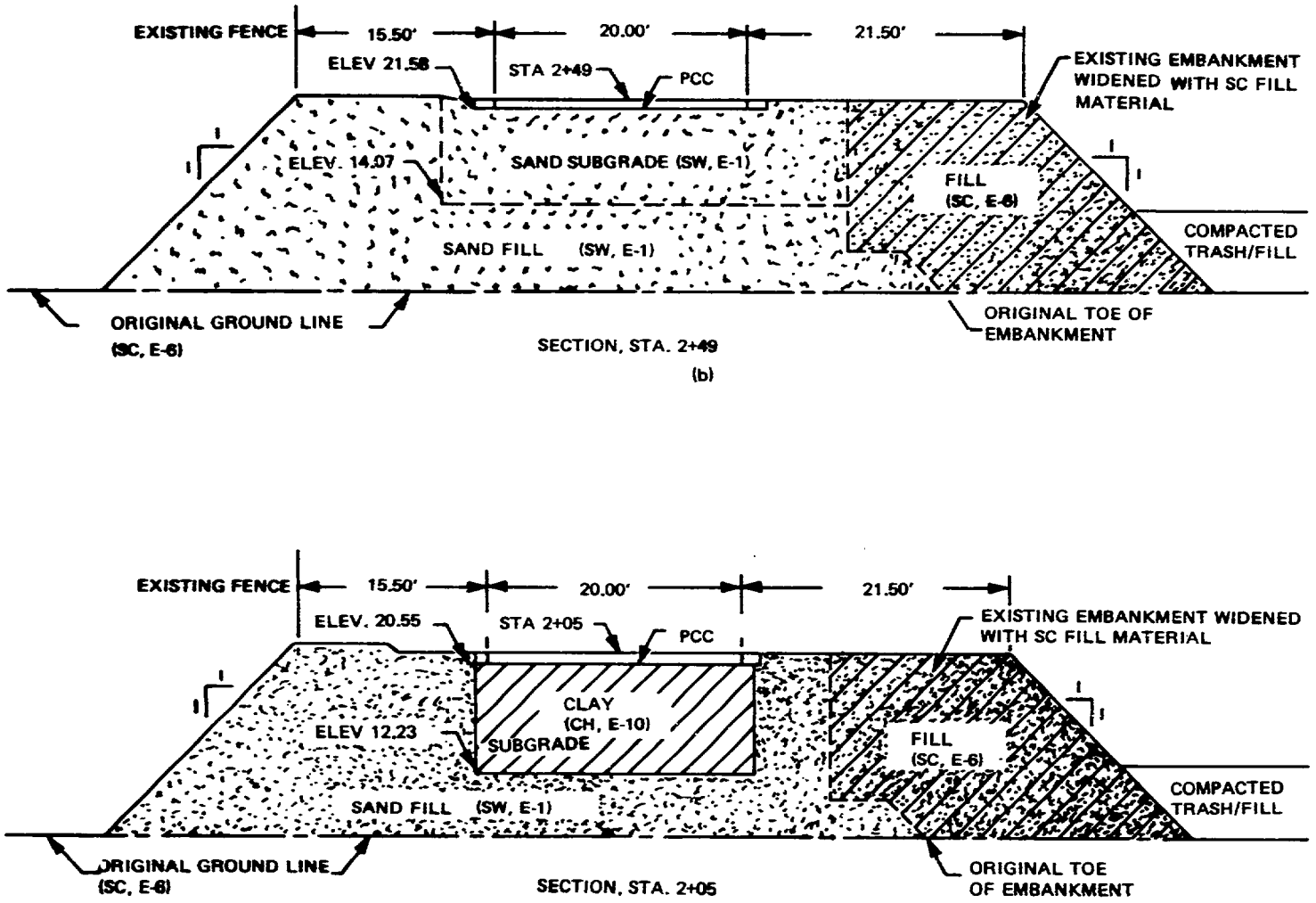

Figure 2. Subgrade Cross Sections

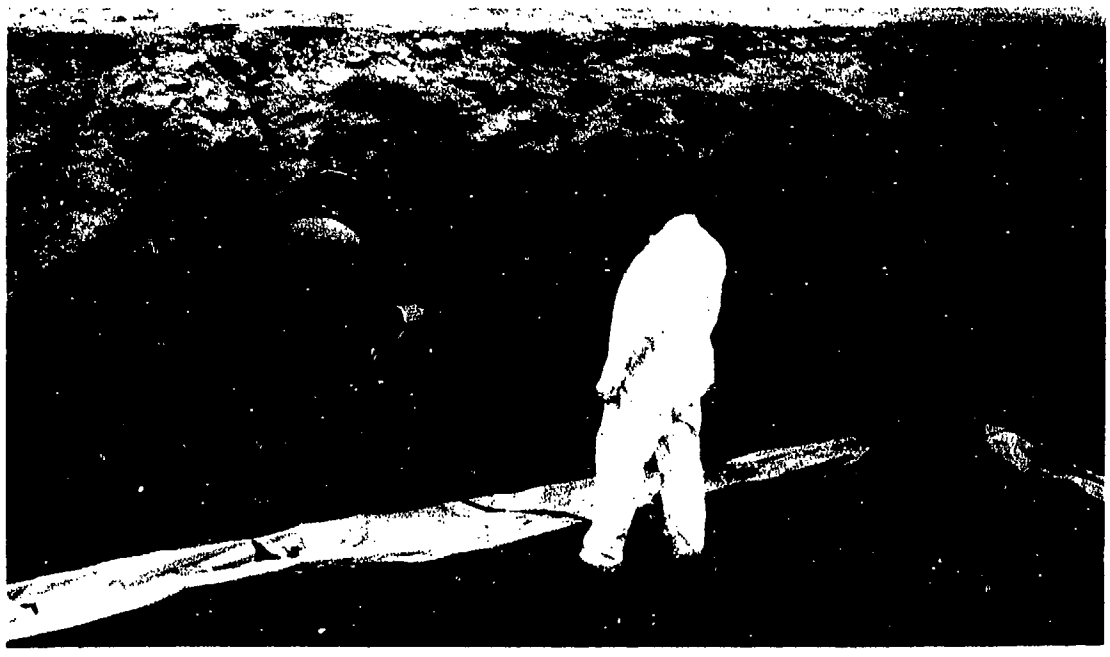

Figure 3. Compaction of Clay Subgrade Boundaries
(NOTE: Polyethylene moisture barrier)

were also performed at various elevations along the clay subgrade boundaries in the compacted fill sand. Moisture/density data are summarized in Appendix B.

Bison soil strain gages were placed within the clay subgrade at spacings of approximately 8 inches during subgrade construction. The 4-inch diameter Bison gages were stacked from bottom to top at 8-inch nominal spacings along the vertical centerline of the subgrade, and one pair of gages was placed on the subgrade surface 15 inches radially from the subgrade center (Figure 4). Soil strain gage installation is discussed in detail below.

After subgrade instrumentation was completed, forms were set and the PCC pavement was placed for Test Section B1.

Sand Subgrade Construction

The embankment was excavated from the north for placement of unwashed fill sand (SW, E-1) for the sand subgrade. After excavation to the desired elevation, the bottom of the cut was compacted with a self-propelled vibratory roller with a smooth drum and moisture/density tests were performed. A plate test using a 30-inch diameter plate was conducted (Appendix B), and the first lift of sand was spread and compacted. Water was added to the fill sand during placement and the sand was compacted in lifts. An electrical tamper was used for compaction adjacent to the sides of the excavation.

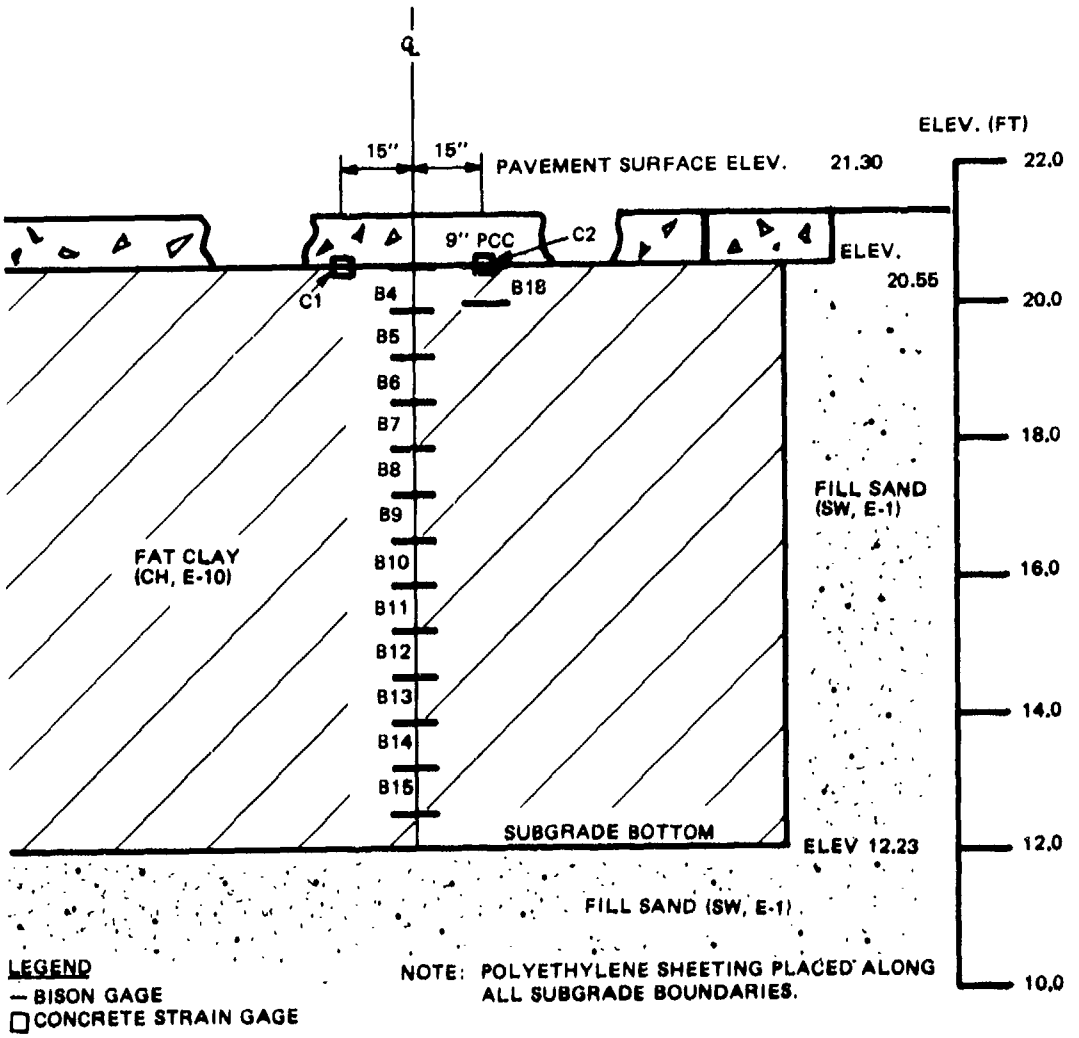

Figure 4. Clay Subgrade Profile, Test Section B1

Five moisture/density tests with a nuclear meter (ASTM D2922, Reference 4) were recorded for each lift. Ten moisture/density tests were conducted with a sand cone apparatus (ASTM D1556, Reference 5) for calibration of the nuclear meter. Moisture/density data are summarized in Appendix B.

Soil strain gages were placed within the sand subgrade during construction. Gage locations are illustrated in Figure 5. After the subgrade reached the specified elevation, instrumentation was installed, forms were set, and the PCC pavement was placed for Test A1.

INSTRUMENTATION

Instrumentation was included in each subgrade and the various test sections to record quasi-static loading response data. Vertical soil strain, horizontal concrete strain, and pavement surface deflection were measured. Locations of instrumentation have been shown for each pavement section test, Figures 4 and 5. The following paragraphs present a brief description of the various types of instrumentation.

Soil Strain Sensors

The soil strain sensors were manufactured by Bison Instruments, Inc., Minneapolis, Minn. The sensors are individual disk-shaped coils which operate through electromagnetic mutual inductance coupling of any two sensors (Reference 6). The 4-inch diameter sensors were placed in near parallel and coaxial alignment, and were separated with a nominal gage length of 8 inches over which the soil strain was averaged. The sensors were not connected and were "free floating" in the soil; thus, they contributed minimal interference with soil movement. The sensors were connected by coaxial cable to a switch box and a Bison Instruments Model 4101A Soil Strain Instrument which contained the driving, amplification, balancing, calibration and recording controls, and a self-contained power supply.

Movement of one sensor with respect to an adjacent sensor was detected by the change in electromagnetic coupling between them. The electromagnetic coupling between sensors is generally a nonlinear function of spacing change; however, for the small strains measured, a linear function was assumed. The sensors were accurately calibrated and changes in sensor spacing were determined by reference to voltage output displayed on a digital voltmeter.

One sensor pair was used as a calibration reference for each subgrade. These two sensors were securely fastened at either end of a block of wood and buried within the subgrade (Figure 6a). The spacing between sensors of the calibration pair was constant and, for a given amplitude, output voltage after nulling was constant. A calibration amplitude was chosen and, prior to reading data from other sensors, the sensitivity (gain) of the Soil Strain Instrument was adjusted to the selected setting by referencing the output voltage of the calibration sensor pair.

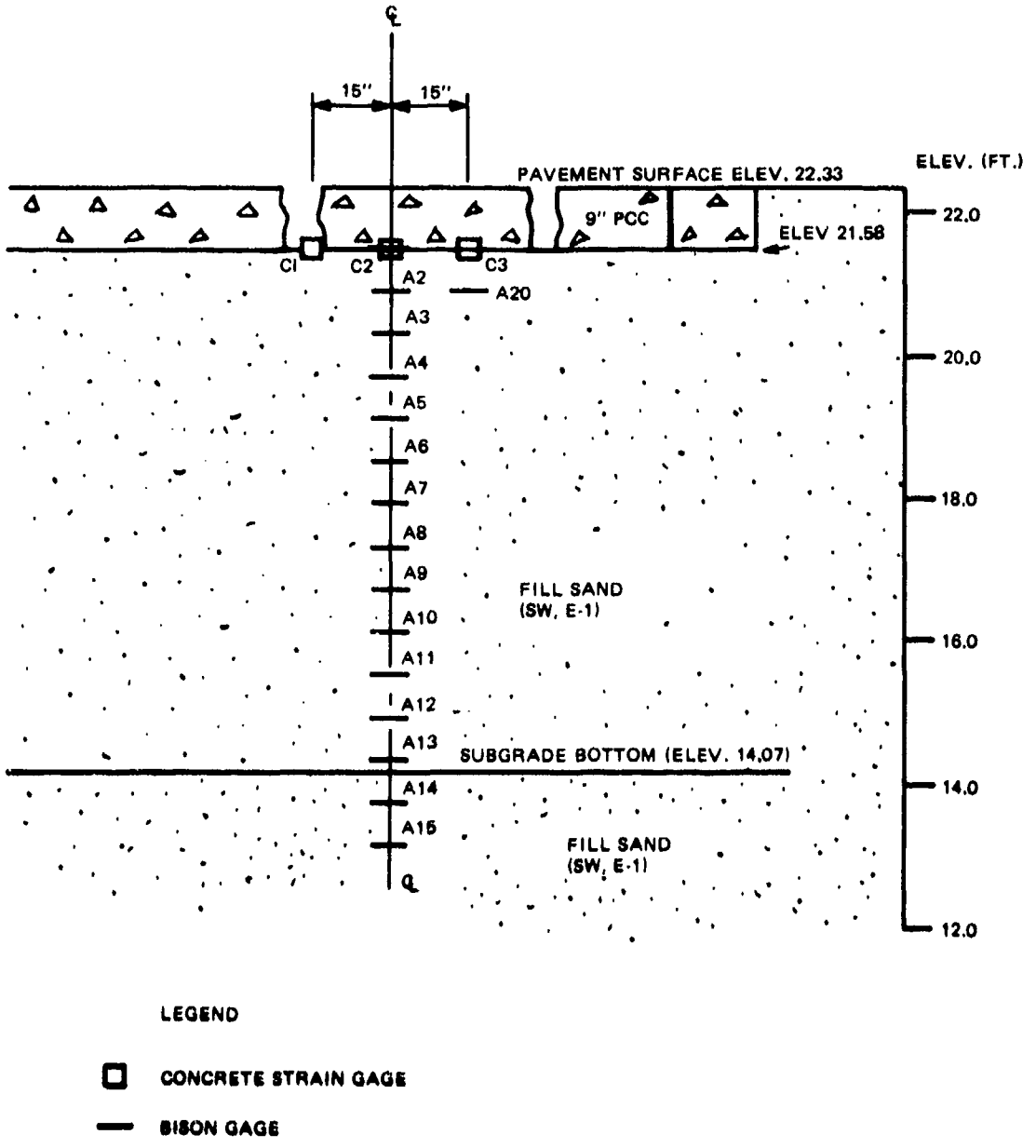

Figure 5. Sand Subgrade Profile, Test Section A1

The soil strain sensors were calibrated on a calibration fixture with a micrometer, see Figure 6b. Although spacing resolution was .0001 inch, field tests indicated a spacing measurement repeatability of .0013 $\pm$.0009 inch. The sensors that were to be in close proximity to the loading plate were calibrated at their respective distances from the plate to correct for influence of the steel plate on the sensor inductance (Figure 6b).

Sensors were installed as the subgrades were constructed in such a manner that the uppermost sensor was from 9 to 12 inches below the subgrade surface to minimize its movement by compaction equipment. They were implanted by augering a hole to the desired depth, leveling and tamping the bottom surface of the hole, and placing the sensor. Initial sensor elevation (spacing) was determined electrically by the readout from the 4101A Instrument and a small spirit level was used to insure the sensors were horizontal (Figure 7). Sensor alignment was accomplished electrically and, through optical surveying. After the sensor was positioned, the hole was backfilled in stages and hand tamped to the approximate density of the surrounding soil.

Concrete Strain Gages

Embedment strain gages (Figure 8) manufactured by AILTECH (formerly MICRODOT Instrumentation Division) were placed near the bottom surface of the test section concrete slabs. Gage placement depths and orientation for the various tests are given in Appendix B. Each gage consisted of a self temperature-compensated nickel chrome strain sensing filament encased within a twisted stainless steel tube. The embedment gages had a 6.00 $\pm$.03 inch gage length and a rated strain level of $\pm$20,000 microinches per inch with an apparent strain with temperature of $\pm$50 microinches per inch (Reference 7).

Perforated metal discs at the ends of the strain tube provided a means of securing the gages during concrete placement. Gages were secured by driving nails into the subgrade and fastening the discs to the nails with string. The gages were initially within a wood form which allowed hand placement of concrete around the gages. When concrete screeding advanced to the form, the form was removed and the concrete surface was screeded. Workers were not permitted to step within the area of the gages during concrete placement.

Deflection Gages

Pavement surface deflection was measured by mechanical dial gages capable of measuring deflection with a resolution of .0001 inch. The dial gages were supported by a 3.5 inch diameter steel pipe which spanned 24 feet clearing the circular test pavement and the encompassing concrete retaining ring (Figure 9a). The pipe was supported on a steel cradle founded in concrete, and was clamped at one support. Dial gages were positioned on the loading plate and, radially from the plate to the pavement edge. Except as noted, the dials and support beam were covered with

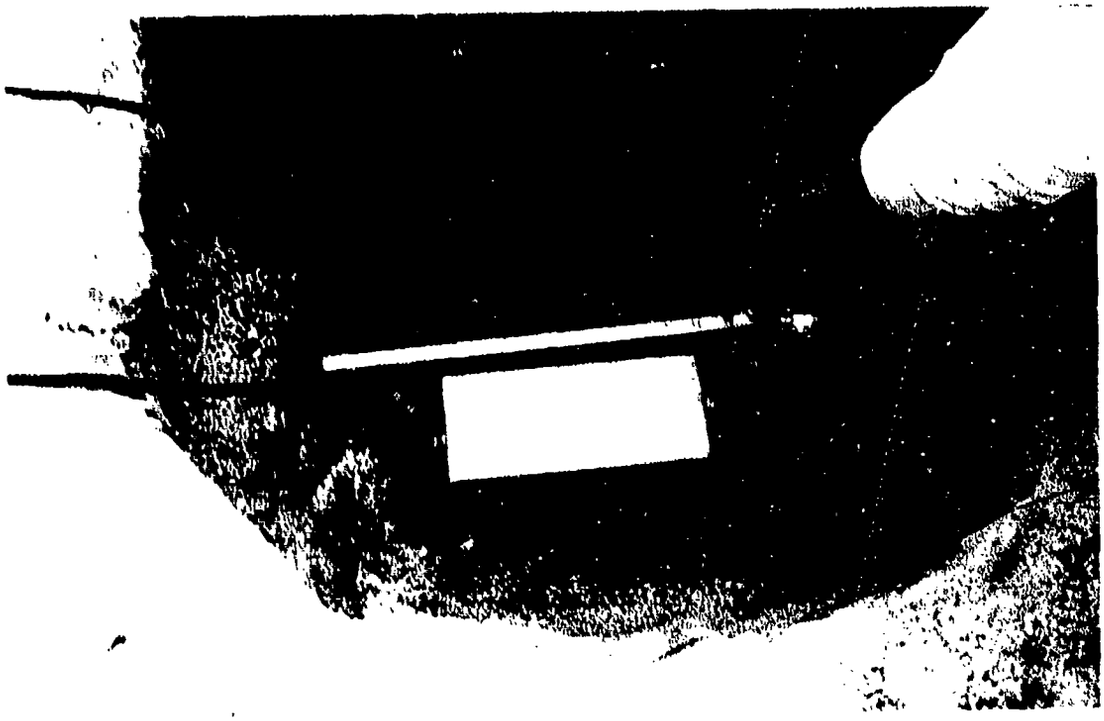

(a) Calibration Block

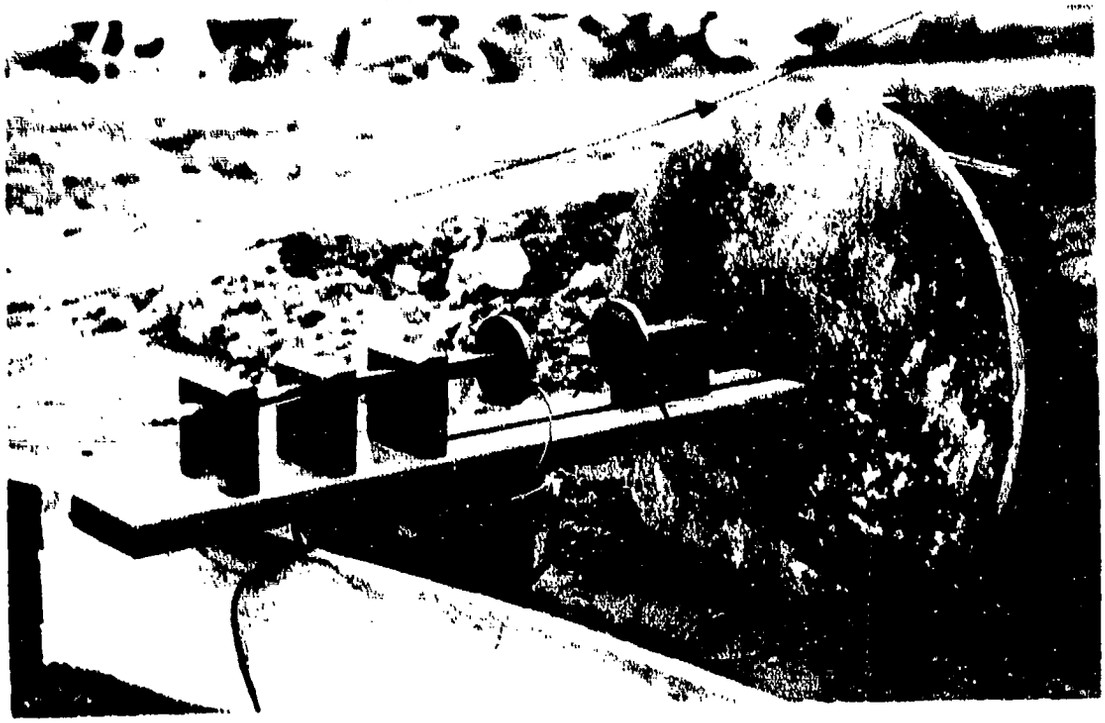

(b) Calibration Device

Figure 6. Soil Strain Gage Calibration

Figure 7. Levelling Strain Gage Coil

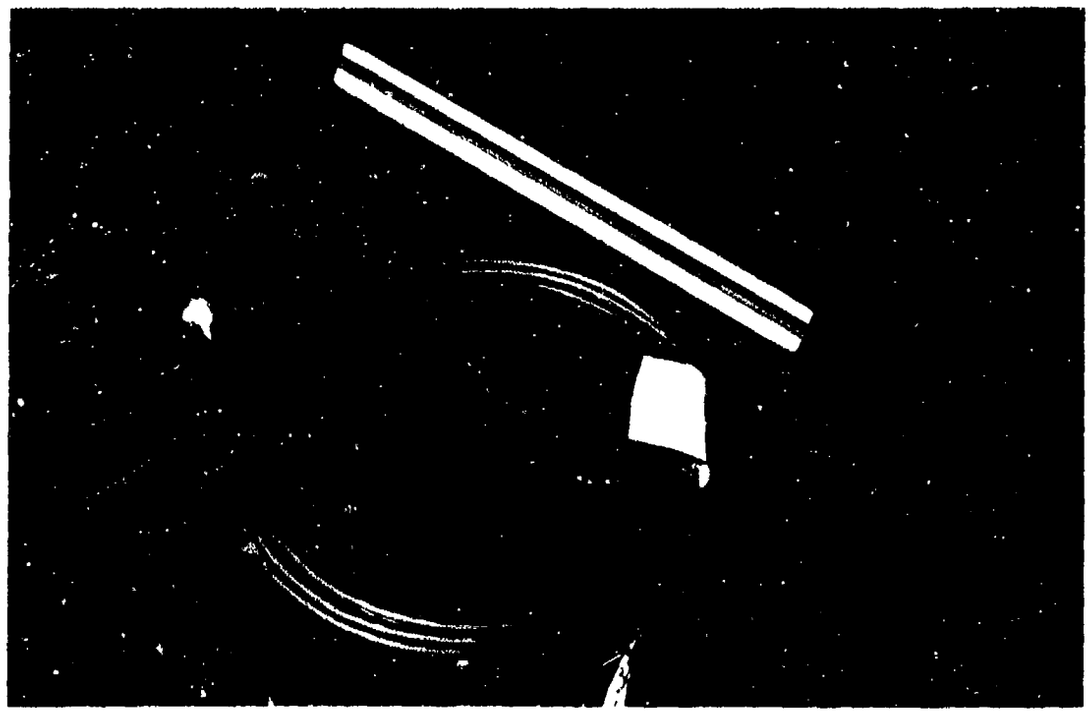

Figure 8. Embedment Strain Gage

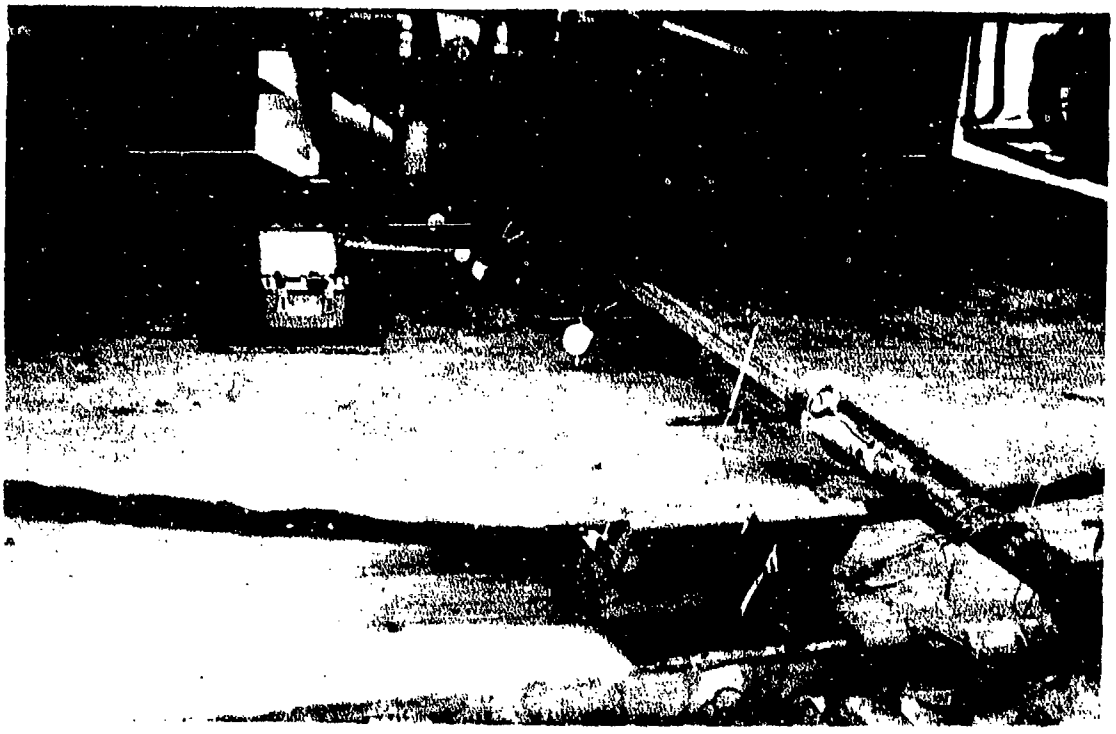

(a)

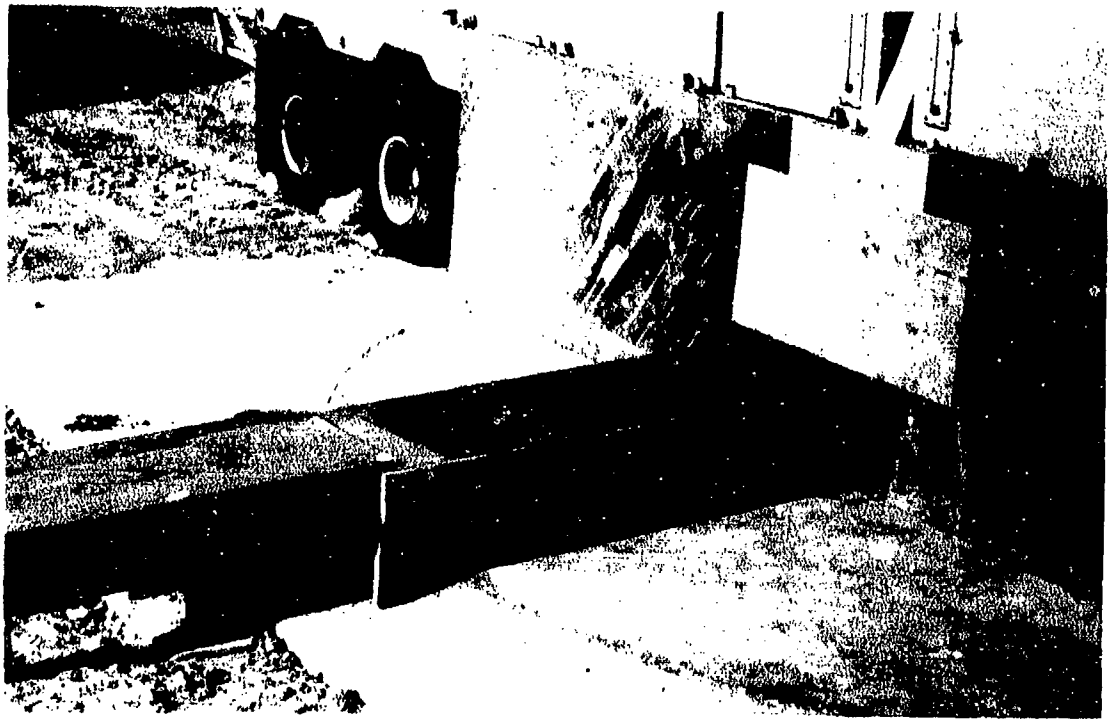

(b)

Figure 9. Typical Surface Deflection Gage Setup

shades to minimize temperature errors (Figure 9b). Field measurements indicated temperature induced error to be on the order of .0037 $\pm$.0025 inch.

TEST PROCEDURES AND DATA RECORDED

Static plate load tests of the pavement sections were conducted using a trailer designed by CEL. Water tanks mounted on the trailer provided a maximum plate load of 90 kips. The trailer, supported by sixteen wheels with a clearance between inside wheels of 22 feet was positioned so that no wheels were in contact with the circular test pavement.

Load was applied to a 30-inch diameter steel plate in increments and data from all instrumentation (soil strain gages, deflection gages and concrete strain gages) were recorded when surface deflections (from gages located on the loading plate) fell to less than .0001 inch movement in one minute. Generally, several load cycles were completed in one day of testing. Load test descriptions and dates are listed in Table 1.

Section A1

Test section A1 consisted of a 9-inch thick concrete pavement placed on the sand subgrade, see Figure 5. Three concrete strain gages were located approximately 0.5 inch from the bottom of the slab and were diametrically oriented with two gages positioned at 15 inches from the load center and one gage at the load center (Figure 10).

As shown in Table 1, load testing was accomplished in two days with load cycles 1 and 2 completed on the first day and cycles 3 and 4, on the second. Load was applied in 30 kip increments to a maximum of 90 kips for the first cycle; thereafter, the full 90 kip load was applied and released. No data were recorded for load cycle 2 since the load trailer became unbalanced necessitating quick load release without recording of data. All instrumentation data were recorded at the beginning of load cycle 3. Ultimate concrete compressive strength for the PCC slab during load testing was determined from site-cured test cylinders and is presented in Appendix B.

Following completion of testing of section A1, an opening was cut in the pavement, and a plate test was conducted on the subgrade surface (Figure 11). Five load cycles were completed to determine the subgrade load/strain response characteristics. The modulus of subgrade reaction (corrected plate for bending and seating) was found to be 606 psi per inch. Data from load testing are presented in Appendix B.

Section A2

Test section A2 consisted of a 6-inch concrete pavement over a 6-inch bituminous concrete base course on the sand subgrade (Figure 12). The bituminous base course was constructed (Figure 13) to the specifications of Appendix A and then load tested. For load testing of the base course,

Table 1. Plate Load Test Description and Sequence

Load Test Description/Location	Load Cycle	Date	Figures Containing Results
Bottom of Clay Subgrade at Elevation 12.23 (Δ)[a]	1	6/26/75	B-3
Surface of Clay Subgrade at Elevation 20.55 (Δ)	1-4	8/7/75	B-4
Bottom of Sand Subgrade at Elevation 13.94 (Δ)	1-5	8/13/75	B-1
Section B1 (ε_c,[b] ε_s,[a] Δ)	1	8/20/75	Appendix B Part B-4
	2 and 3	8/22/75	
	4 and 5	9/15/75	
	6 and 7	9/16/75	
Section A1 (ε_c, ε_s, Δ)	1 and 2	9/25/75	Appendix B Part B-2
	3 and 4	9/26/75	
Surface of Sand Subgrade at Elevation 21.58 (Δ)	1-5	11/3/75	B-2
Bituminous Concrete, Base Course of Section A2 (ε_s, Δ)	1 and 2	11/18/75	Appendix B Part B-3
	3	11/20/75	
Section B2 (ε_c, ε_s, Δ)	1	12/4/75	Appendix B Part B-5
	2 and 3	12/8/75	
	4 and 5	12/8/75	
	6 and 7	12/11/75	
Section A2 (ε_c, ε_s, Δ)	1	12/16/75	Appendix B Part B-3
	2 and 3	12/17/75	
	4 and 5	1/6/76	
Lime Stabilized Clay, Subbase of Section B2 (Δ)	1-4	1/8/76	Appendix B Part B-5

[a] Δ denotes plate deflection and pavement deflection (when applicable) measurements.

[b] ε_c denotes concrete strain measurement.

[c] ε_s denotes soil strain measurement.

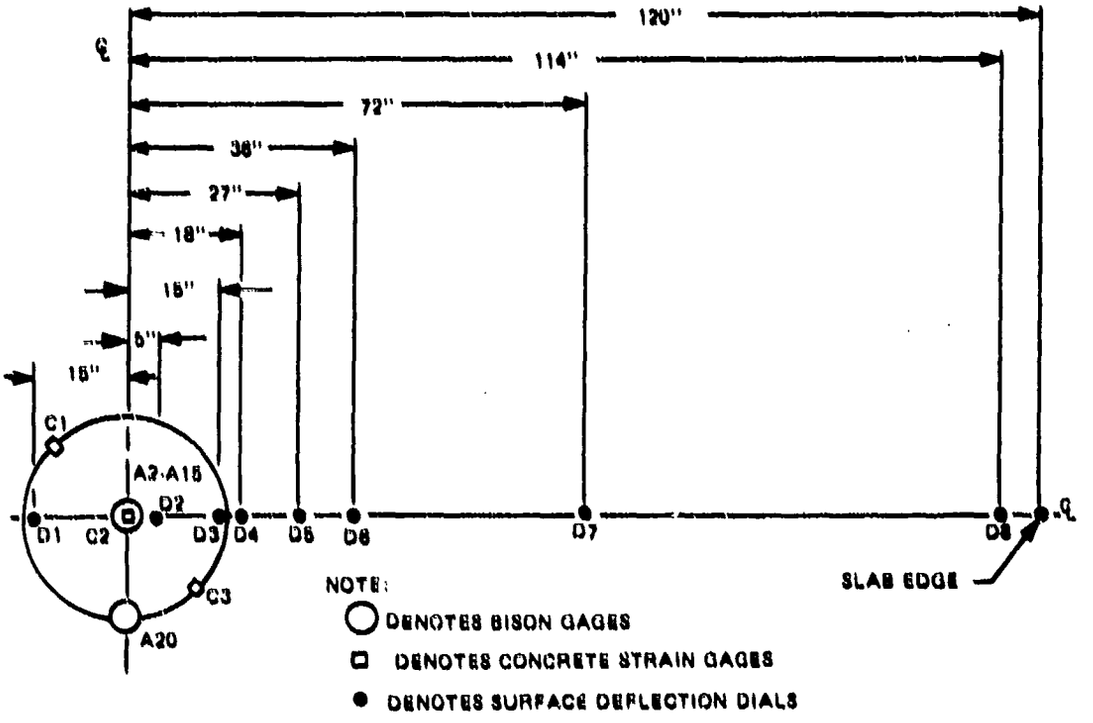

Figure 10. Instrumentation Layout for Test A1

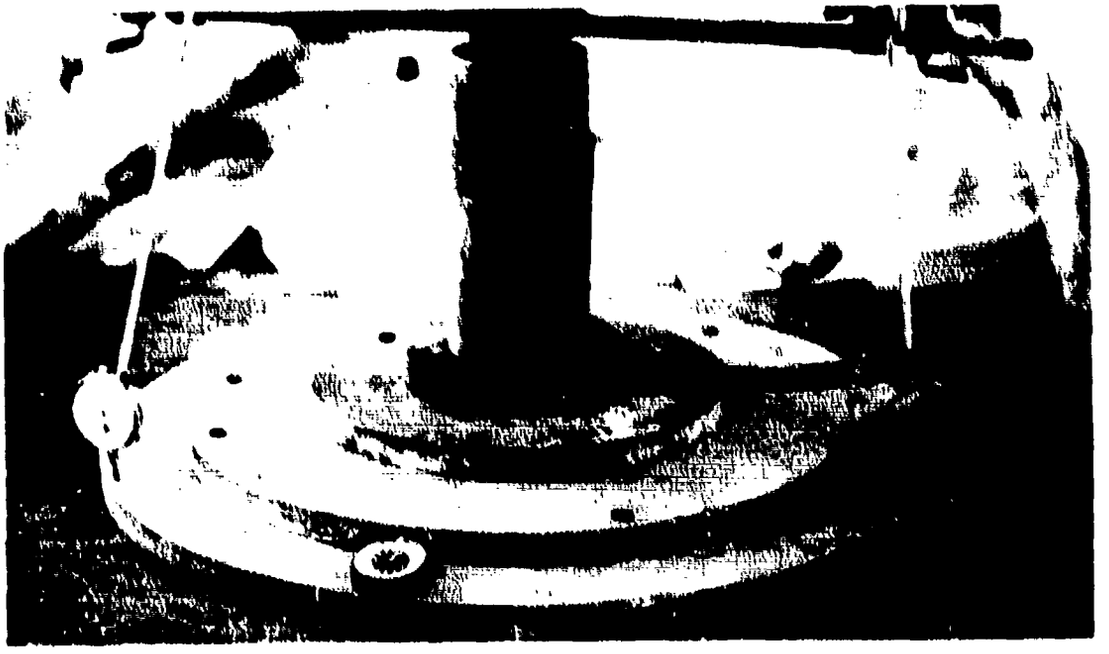

Figure 11. Plate Test on Sand Subgrade

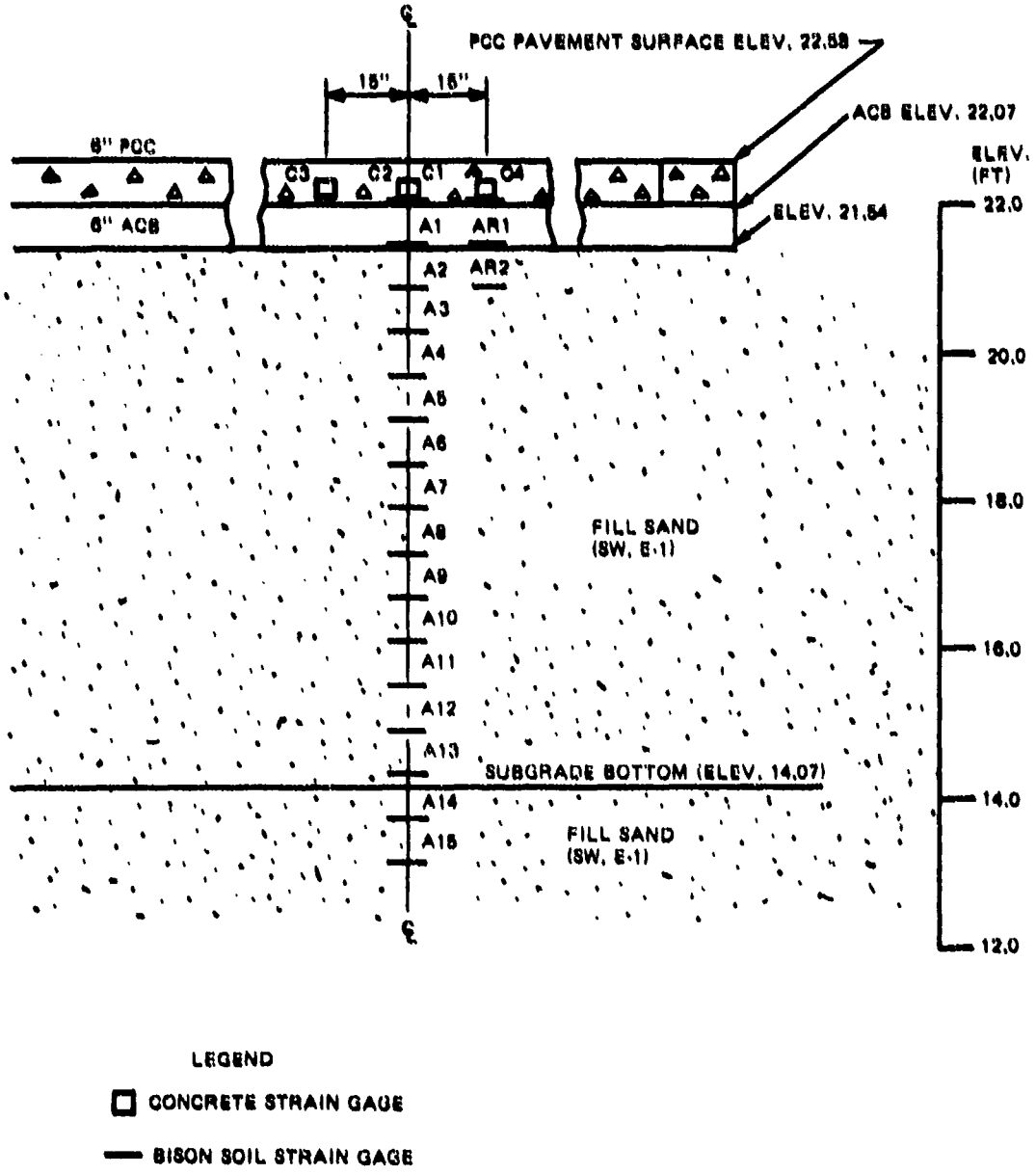

LEGEND

CONCRETE STRAIN GAGE

BISON SOIL STRAIN GAGE

Figure 12. Sand Subgrade Profile, Test Section A2

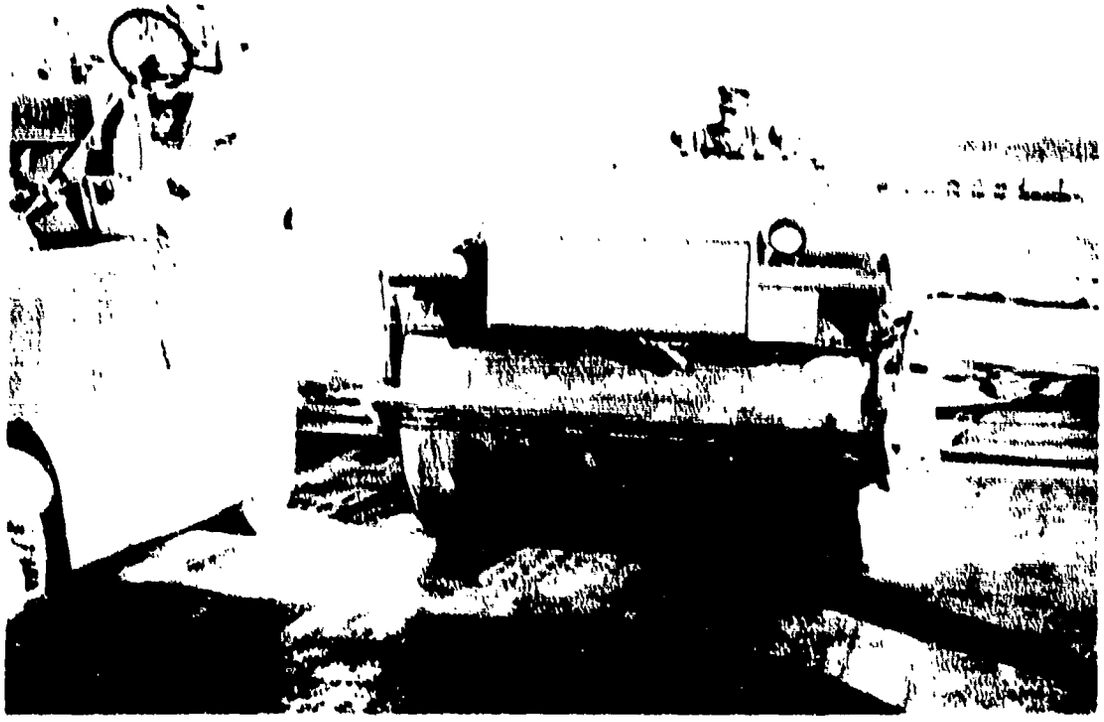

(a)

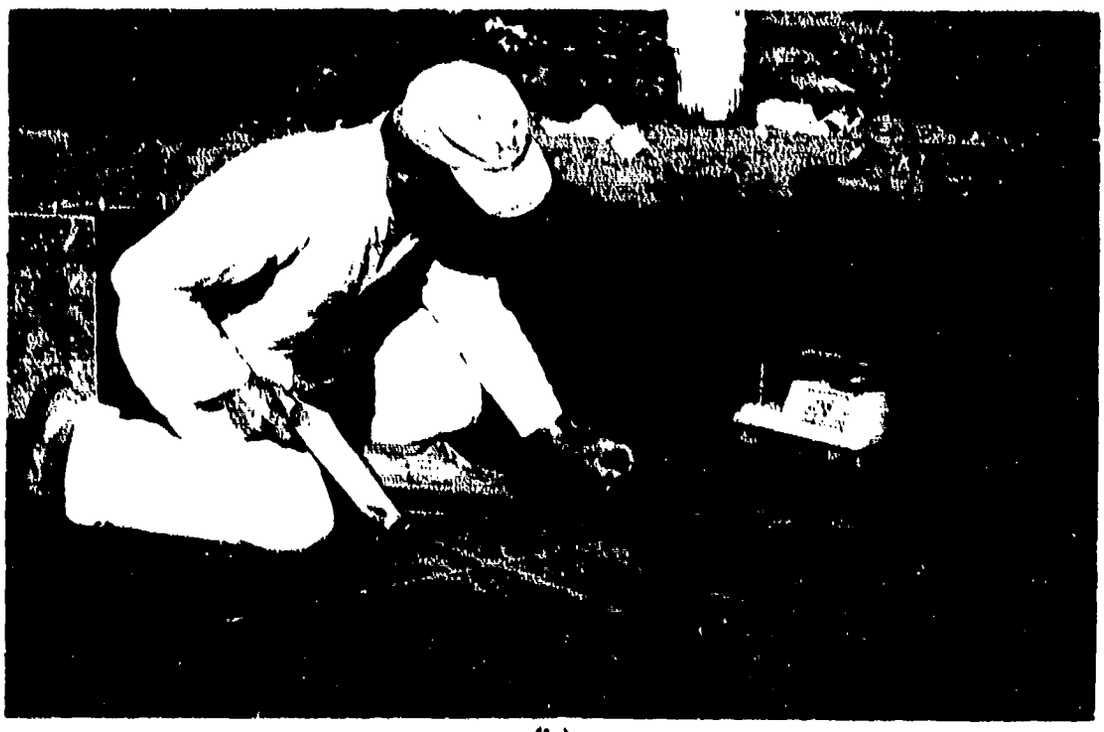

(b)

Figure 13. Compaction and Testing Bituminous Base Course of Test Section A2

three deflection gages were situated on the edge of the loading plate and three others, diametrically at spacings of 21, 27, and 45 inches from the plate center. The test was conducted over the soil strain sensors within the subgrade. The base course strain and deflection data are presented in Appendix B.

Two load cycles, to a maximum load of 39 kips, were completed on the initial day of base course testing. A one kip preload was used as a zero load and load was applied and released in two increments for load cycle 1 and one increment for load cycle 2. At the start of testing the weather was overcast and shades were not placed over the deflection gage support beam. The weather cleared during load cycle 2, affecting the surface deflection gage readings and possibly influencing the soil strain readings for that cycle. A second day of testing was considered necessary and one additional load cycle was completed. Load was applied, without preload, in 15 kip increments to a maximum load of 45 kips. Data from cycle 3 correlated with that from cycle 1 and base course testing was terminated.

After base course load testing, forms were set and a 6-inch PCC pavement was placed to the specifications of Appendix A. During concrete placement, four concrete strain gages were positioned within 0.5 inch of the bottom surface of the concrete slab with two gages at the intended load center and two at 15 inches from the center.

Five load cycles to a maximum plate load of 70 kips were applied over three days of testing of the completed pavement section A2. Results are shown in Appendix B. A 10 kip preload served as zero load for each cycle. The first day, cycle 1 was completed in two loading and unloading increments. For cycles 2 and 3, on the second day, load was applied in a single 70 kip increment. On the final day of testing, load was applied and released in two increments for cycle 4 and one increment for cycle 5. The ultimate compressive strength and unit weight of the PCC slab, during load testing, was determined from field cured cylinders and is presented in Appendix B.

Section B1

After construction of the clay subgrade, a plate test was conducted to determine the subgrade load response. Four load cycles to 21.2 kips were completed; the data are shown in Appendix B. The modulus of subgrade reaction (corrected for plate bending and seating) was found to be 278 psi per inch.

Subgrade load testing was followed by placement of a 9 inch thick PCC slab on the subgrade as test section B1 using the specifications of Appendix A. A 6 mil polyethylene moisture barrier at the subgrade/slab interface prevented the clay from absorbing moisture from the fresh concrete. Two embedment concrete strain gages were located diametrically opposite each other at a distance of 15 inches from the pavement center and within 0.5 inch of the slab bottom surface, see Figure 14.

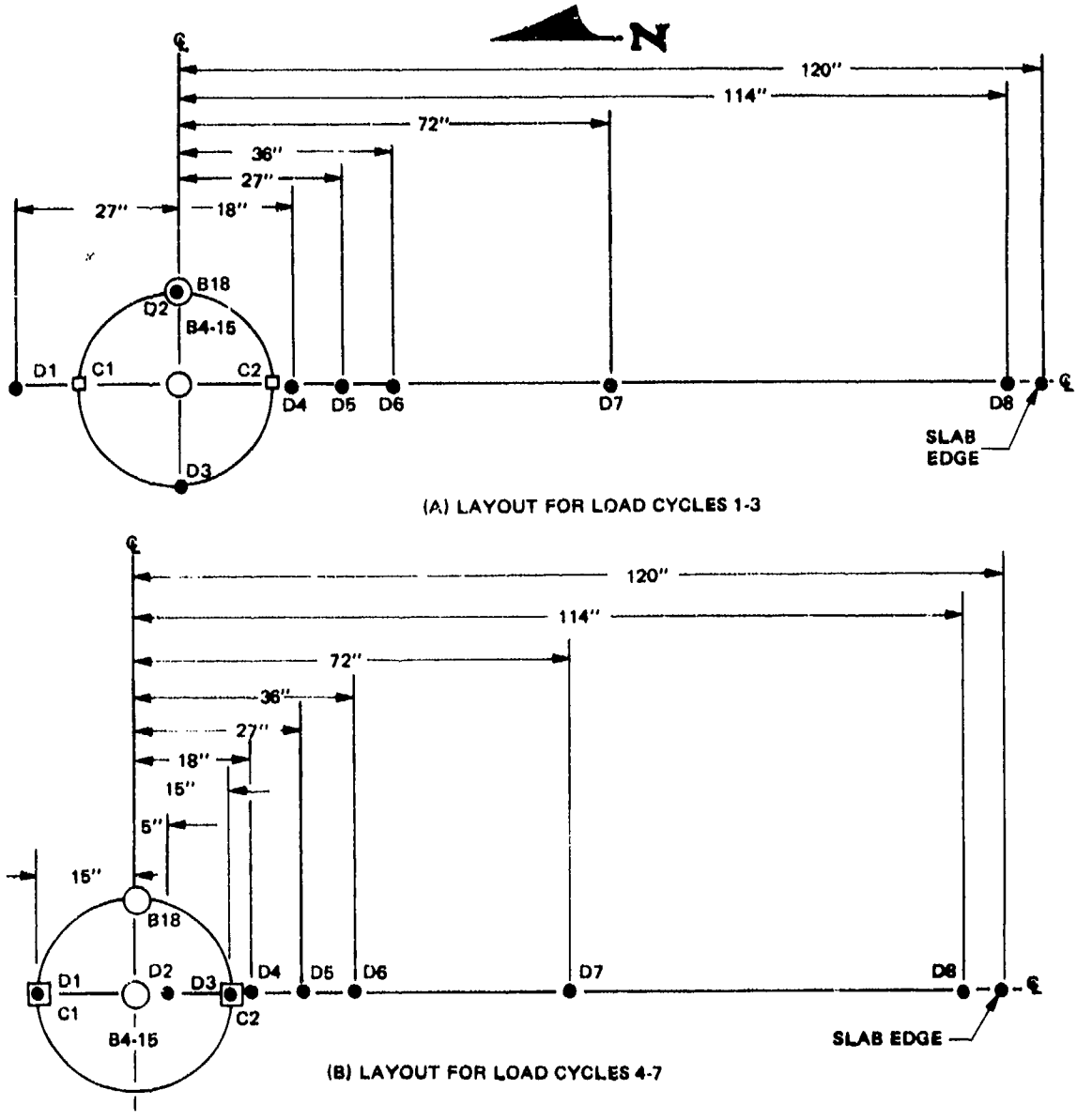

NOTES: 1. ☐ DENOTES CONCRETE STRAIN GAGES. BOTH GAGES PLACED 1/4" TO 1/2" FROM BOTTOM OF SLAB. MIDPOINT OF 6" GAGE LENGTH WAS POSITIONED BENEATH PLATE EDGE. GAGES WERE RADIALLY ORIENTED.
2. ● DENOTES SURFACE DEFLECTION DIALS.
3. ◯ DENOTES BISON GAGES.

Figure 14. Instrumentation Layout for Pavement Section B1

As shown in Table 1, seven load cycles were applied to Section B1 in 4 days of testing over a period of 28 days. Results are given in Appendix B. A detailed description of the loading procedures is presented as follows:

Test day 1. Load was added in 10 kip increments to a maximum plate load of 90 kips and released in two increments. Distortion of soil strain data was noted, and after completion of the load cycle, a calibration sensor pair was installed in the subgrade for fine adjustment of amplifier sensitivity (gain).

Test day 2. Load was applied in four increments to 90 kips and released in two increments to complete load cycle 2; then the full 90 kip load was applied and released in one increment for load cycle 3. The calibration sensor pair improved the quality of the soil strain data. Soil and concrete strain calculations were referenced to the zero load data for cycle 2.

Note: During cycles 1, 2, and 3, the loading plate was seated in a thin bed of sand. The sand proved to be too compressible and the test setup was modified for cycles 4 through 7 by seating the plate in Hydrostone compound. The locations of the dial gages were also changed as shown in Figure 14b. These additional cycles were performed for data comparison with the previous cycles and to gain further information concerning the cyclic load response of the test section.

Test day 3. Loading was accomplished in four increments to 90 kips and load was released in three increments to conclude load cycle 4. Load was applied to 90 kips and released for cycle 5. Soil and concrete strain calculations were referenced to the zero load data for cycle 4.

Test day 4. Load was applied to 90 kips and released to complete load cycles 6 and 7. Soil and concrete strain calculations were referenced to the zero load data for cycle 4.

Note: Soil strain data from cycles 4 through 7 generally correlated with that from cycles 2 and 3. Plate deflection data from cycles 4 through 7 for the upper range of plate loads indicated approximately 0.02 inch less deflection than was evidenced in cycles 2 and 3 which was attributed to the firmer plate seating and an increase in concrete flexural strength. All pavement section tests subsequent to section test B1 were conducted with the loading plate seated in Hydrostone.

Ultimate compressive strength for the PCC slab during the different cycles of testing was determined from site-cured concrete cylinders and is presented in Appendix B.

Section B2

A 6-inch PCC slab overlying 8 inches of lime stabilized clay on the clay subgrade constituted pavement test section B2 (Figure 15). The 6 percent by weight lime stabilized clay mixture was prepared to the specifications of Appendix A. Clay was initially pulverized by a rototiller;

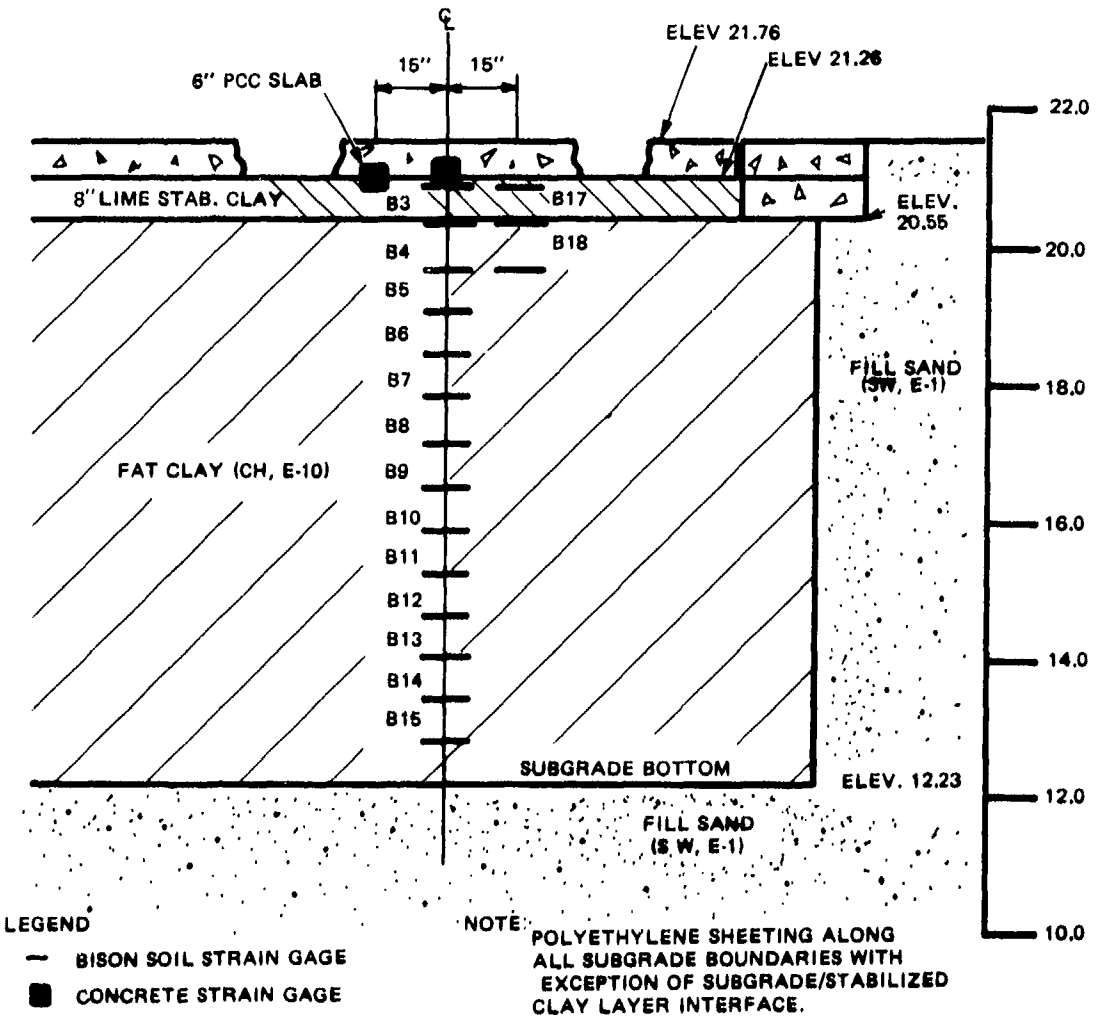

Figure 15. Clay Subgrade Profile for Test Section B2

and the lime, water, and clay were batched in a mixer. The freshly mixed material was deposited on the clay subgrade, cured for 48 hours, and remixed with the rototiller to the extent that 64 percent, by weight, of the clods passed a No. 4 sieve, see Figure 16. Tests of the stabilized clay after final compaction and trimming indicated an average soil dry density of 94.5 pcf (95 percent of maximum as per AASHO Test T180, Reference 8) with a moisture content of 21.9 percent. Following construction of the stabilized layer, the 6-inch PCC slab was formed and placed to the specifications of Appendix A. The compacted lime mixture was cured for 54 days before load testing.

Section B2 was load tested over a period of 8 days. Results are shown in Appendix B.

Test day 1. Load was applied and released in three increments to complete load cycle 1. A 10 kip preload was utilized as a zero load and a maximum plate load of 80 kips was obtained. Data from the soil strain sensors were found to be erroneous and were disregarded.

Test day 2. Load was applied to a maximum plate load of 70 kips and released to complete cycles 2 and 3. Soil strain data for cycle 3 were distorted and were discounted; whereas, soil strain and surface deflection data for cycle 2 appeared valid and were recorded.

Test day 3. The switch box for the soil strain channels was insulated to minimize temperature and humidity influences which were estimated to have caused the poor soil strain data cycles 1 and 3. Load cycle 4 was completed in three loading and unloading increments with a maximum plate load of 70 kips and load cycle 5 was completed by applying and releasing the maximum plate load of 70 kips. All data appeared valid and correlated with that obtained from load cycle 2.

Test day 4. Load was applied and released in three increments for load cycle 6 and one increment for load cycle 7 with a maximum plate load of 70 kips. Data correlated with that from cycles 2, 4, and 5. Ultimate concrete compressive strength and the unit weight for the PCC slab during testing was determined and is presented in Appendix B. A 10 kip preload was used as the zero load for all load cycles applied to test Section B2.

After completion of load testing for Section B2, an opening was cut in the PCC pavement to allow plate testing of the lime stabilized clay layer (Figure 17) which was tested in 4 load cycles. Load cycle 1 was accomplished by loading in four increments to a maximum load of 40 kips and unloading in two increments. Three additional cycles of alternately loading to 40 kips and unloading were completed. A 5 kip preload was used as zero load for each cycle. The modulus of subgrade reaction (corrected for plate bending and seating) was found to be 467 psi per inch. See Appendix B.

Figure 16. Cured and Pulverized Lime/Clay Mixture

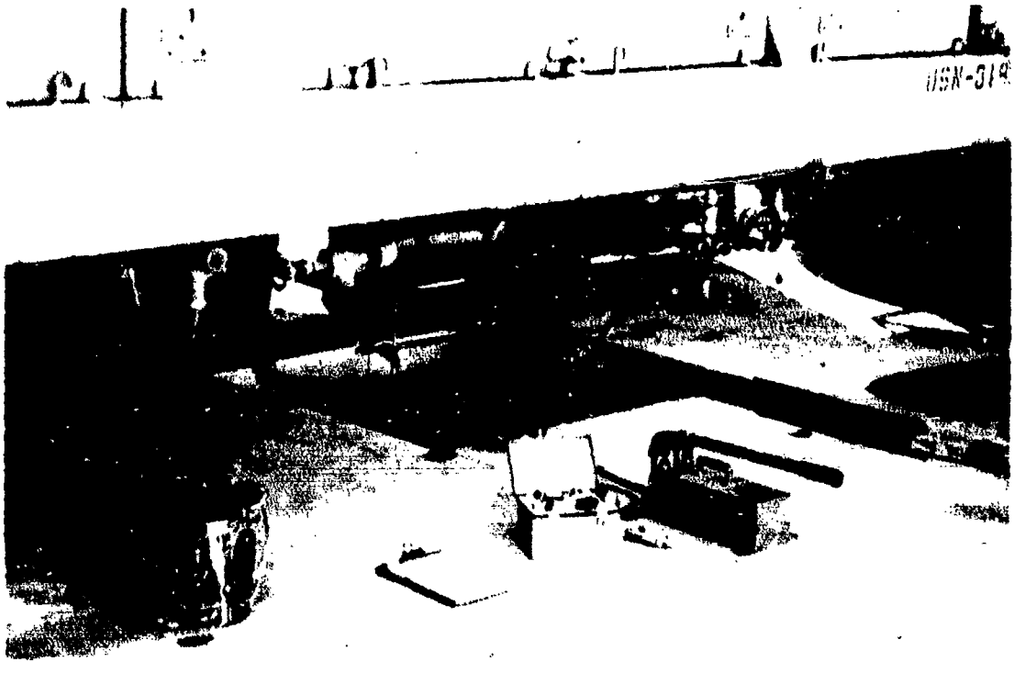

Figure 17. Plate Test on Lime Stabilized Clay Layer

MATERIAL RESPONSE PARAMETERS

MATERIALS TESTING

The primary purpose of this report is to use refined experimental data to validate the results of theoretical developments. For this reason it was required that extensive efforts be made to define the mechanical properties of the CEL test sections. That is, it was necessary to establish values or functions of such parameters as "equivalent" Young's modulus, shear modulus, and Poisson's ratio for the pavement constituents with special attention paid to the unique materials, i.e., the clay and sand subgrades.

Thus the first step in characterizing the materials making up the pavement sections was to acquire sufficient experimental test data to permit defining the various material responses, at least within certain ranges. Obviously, since airfield pavements are subjected primarily to dynamic loadings, then dynamic soil tests would appear most applicable. However this direction was not pursued for the following reasons:

1. The available field loading capability was limited to quasi-static operations, at least within the ranges of loading required for the proposed prototype pavement sections;

2. It is well known that long term static loading presents a more critical situation for airfields than short term dynamic loadings;

3. Dynamic testing presents a whole new order of complexity in material response evaluations by the introduction of time effects.

Thus quasi-static material response relationships were pursued here. These response relationships were restricted to very limited ranges of density and moisture content, and, for the clay subgrade, degree of saturation. Even with these limitations, attempting to correlate the broad spectrum of theoretical analyses; highly refined large scale field tests; and material parameter definitions within the scope of a project of this size is an extremely ambitious endeavor. The material for the sand subgrade was selected to model a uniform sand upon which a comprehensive set of experimental data (Reference 9) was available for the purposes of the soil study. This material, known as Cook's bayou sand, was in a dense dry condition. The characteristics of this material have been reported in the literature (Reference 10). That data pertaining to the final conclusions are included in this section; more complete data is reported in Appendix C. The available test data consisted of nine tests conducted using conventional triaxial apparatus. All test specimens were 2.8 inches in diameter by 6 inches high (7.1 cm x 16.8 cm) and were initially compacted to 112 $\pm$0.5 lb per cubic foot (1814 $\pm$ 8 kg/m^3) dry density, resulting in void ratios of 0.51 $\pm$ 0.01. A summary of the data for all 9 tests is shown in Tables 2, 3 and 4. All calculations concerning specimen response assume a homogeneous state of stress and strain throughout the specimens. Although this is not precisely true, it is considered sufficiently accurate for prediction purposes. All correlations are based upon the levels of strain occurring during the first load cycle.

Table 2. Summary of Hydrostatic Compression Tests on Sand

TEST NO. 1		TEST NO. 2	
Confining Pressure (psi)	Volumetric Strain ($X10^{-3}$)	Confining Pressure (psi)	Volumetric Strain ($X10^{-3}$)
5.00	0.00	5.00	0.00
10.00	0.41	25.00	1.62
20.00	1.06	50.00	2.73
40.00	2.19	75.00	3.53
50.00	2.72	100.00	4.49
5.00	0.53	125.00	5.12
50.00	2.92	150.00	5.67
75.00	3.78	175.00	6.23
100.00	4.53	200.00	6.66
5.00	.94	225.00	7.12
100.00	4.77	250.00	7.53
125.00	5.44		
150.00	6.00		
5.00	1.26		
150.00	6.24		
175.00	6.72		
250.00	7.23		
5.00	1.80		
200.00	7.70		
225.00	8.23		
250.00	8.52		

Table 3. Summary of Uniaxial Strain Test on Sand

TEST NO. 3			TEST NO. 4		
Axial Stress (psi)	Radial Stress (psi)	Axial Strain ($X10^{-3}$)	Axial Stress (psi)	Radial Stress (psi)	Axial Strain ($X10^{-3}$)
2.17	2.00	0.00	2.02	2.00	0.00
27.37	10.00	1.36	33.25	10.00	1.06
52.88	20.00	2.25	66.25	20.00	2.00
80.76	30.00	3.15	97.49	30.00	2.91
131.95	50.00	4.31	128.04	40.00	3.70
207.07	75.00	5.72	156.70	50.00	4.46
275.41	150.00	6.80	20.37	20.00	2.18
347.65	125.00	7.89	191.20	60.00	5.20
415.83	150.00	8.79	245.43	80.00	6.25
483.67	175.00	9.65	295.18	100.00	7.25
552.69	200.00	10.44	41.43	40.00	3.92
619.68	225.00	11.14	313.40	100.00	7.45
683.62	250.00	11.79	385.31	125.00	8.34
			460.13	150.00	9.19
			51.49	52.00	4.10
			461.16	150.00	9.58
			533.24	175.00	10.41
			597.24	200.00	11.10
			83.12	84.00	6.10
			603.60	200.00	11.40
			664.85	225.00	12.08
			734.87	250.00	12.72

Table 4. Summary of Triaxial Shear Tests on Sand

Test No. 5 (σ_3 = 25 psi)			Test No. 6 (σ_3 = 50 psi)			Test No. 7 (σ_3 = 100 psi)		
Deviator Stress (psi)	Axial Strain ($X10^{-3}$)	Radial Strain ($X10^{-3}$)	Deviator Stress (psi)	Axial Strain ($X10^{-3}$)	Radial Strain ($X10^{-3}$)	Deviator Stress (psi)	Axial Strain ($X10^{-3}$)	Radial Strain ($X10^{-3}$)
0.33	0.00	0.00	.16	0.00	- 0.00	0.99	0.00	- 0.00
15.13	0.41	- .04	13.27	.33	- .04	26.48	0.63	- .04
32.13	.94	- .18	30.30	.65	- .11	77.44	1.91	- .22
49.11	1.57	- .40	64.33	1.74	- .37	128.31	3.33	- .58
66.05	2.48	- .80	98.26	3.23	- .91	179.01	5.04	- 1.34
82.91	3.92	-1.54	132.01	5.61	- 1.87	229.30	7.31	- 2.48
99.51	7.40	-3.33	164.98	10.30	- 4.83	278.72	10.75	- 4.86
111.17	13.01	-6.40	196.14	20.58	-11.45	326.16	17.08	- 9.57
						359.72	26.21	-16.81

Test No. 8 (σ_3 = 150 psi)			Test No. 9 (σ_3 = 250 psi)		
Deviator Stress (psi)	Axial Strain ($X10^{-3}$)	Radial Strain ($X10^{-3}$)	Deviator Stress (psi)	Axial Strain ($X10^{-3}$)	Radial Strain ($X10^{-3}$)
2.71	0.00	- 0.00	8.58	0.00	- 0.00
19.76	1.83	- .04	33.00	.25	- .07
70.88	2.49	- .15	118.38	1.08	- .18
138.96	3.98	- .44	220.73	2.24	- .44
206.88	5.80	- .95	322.86	3.91	- .88
291.22	8.62	- 2.20	424.56	5.90	- 1.61
357.59	12.27	- 4.32	541.90	9.39	- 3.33
421.84	18.07	- 8.31	639.89	14.71	- 6.34
467.79	24.70	-13.03	732.76	24.02	-12.09
496.53	31.00	-17.64	802.56	38.64	-20.74
			822.29	76.37	-39.34

For tests cycled at various increments of loading, the strains considered are those experienced by the soil the first time the load reached that level. Complete stress path and response history were recorded electronically for each test, and the experimental results were reasonably consistent between similar types of tests.

The clay subgrade test sections were meant to represent pavements placed upon the poorest possible foundation materials. Initially it was planned to select a subbase material for which extensive test information was available. However it became evident that the quantities of material required made shipment of such a material from a source outside the local area financially prohibitive. It was necessary to use a local highly plastic clay upon which negligible experimental response information existed. This necessitated generation of extensive experimental data which was carried out by means of an interagency agreement between the Civil Engineering Laboratory and the U.S. Army Corps of Engineers Waterways Experiment Station, at Vicksburg, Mississippi.

Triaxial test results on three series of compacted clay specimens at three different nominal moisture contents are shown in Figure 18, 19, and 20. This data, taken from Reference 11 (which is reproduced in part in Appendix C) provides triaxial data pertaining to the clay subgrade at Site B of the CEL Pavement Test Facility. This material is a highly plastic clay, designated a CH under the Uniform Classification System, with a liquid limit (LL) and a plasticity Index (PI) of 69 and 38 respectively. The specific index property values for the various test specimens are presented in Table 5 (reprint of Table 3.2 of Reference 11).

For the more conventional pavement component materials, which were the portland cement concrete, the bituminous base course material, and the lime stabilized clay base, laboratory testing programs of the scope of those used for the sand and clay subgrades were not possible. In these cases only a nominal amount of laboratory testing could be carried out, primarily to identify the basic material properties. For the complex response relationships required in some of the analyses it was necessary to rely heavily on published response data from the literature. Basic material properties for the portland cement concrete, the bituminous base and the lime stabilized clay are reported in Appendix C.

RESPONSE MODELS

Since it is not possible to measure the response of any material under all possible test situations, it is generally attempted to hypothesize some form of response relationship or constitutive relation that will be valid over at least a prescribed range of conditions. With soils the difficulties are even more pronounced than with most materials in that every soil represents a different material and this material may undergo changes in its basic properties during testing. The stress-strain response for soils is not only dependent upon stress and strain states but also upon such parameters as void ratio, or density and degree of saturation.

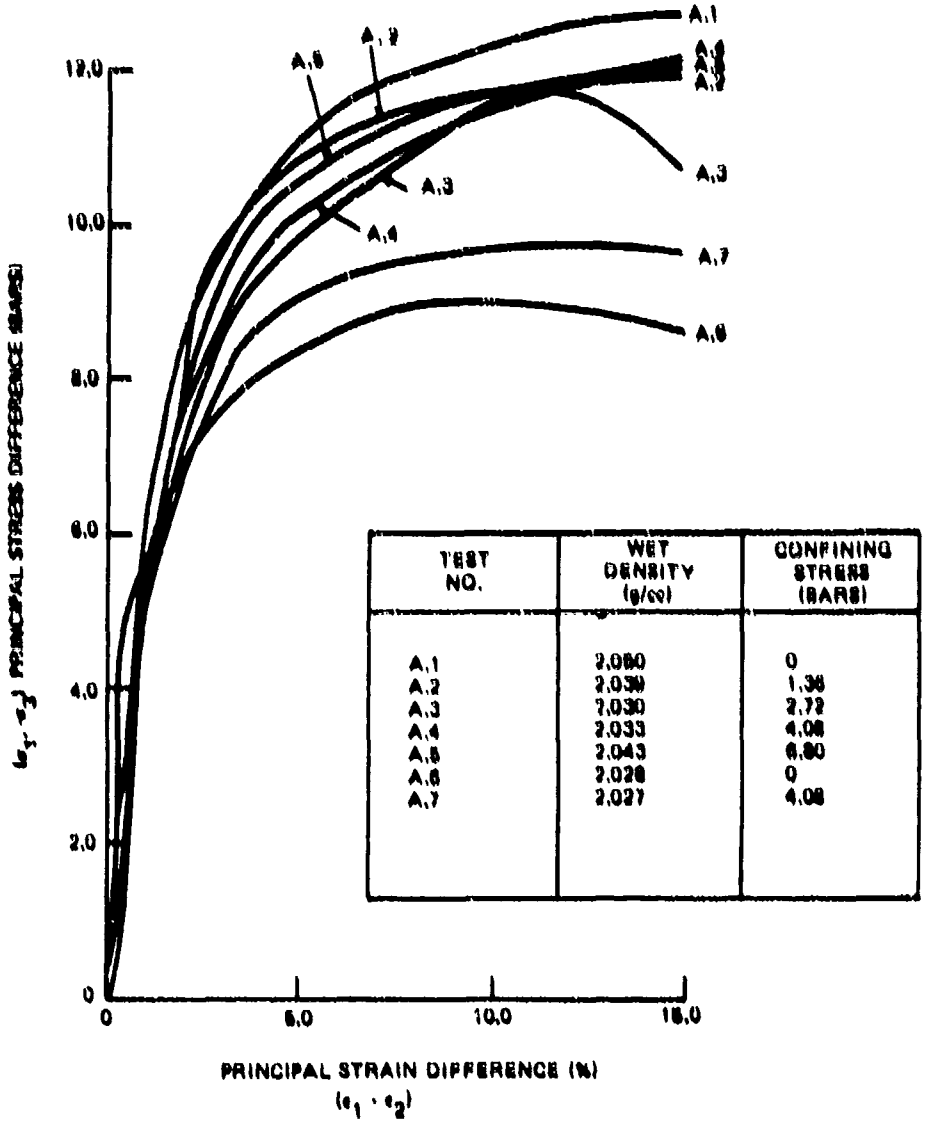

Figure 18. Triaxial Shear Test Data for Series A Tests

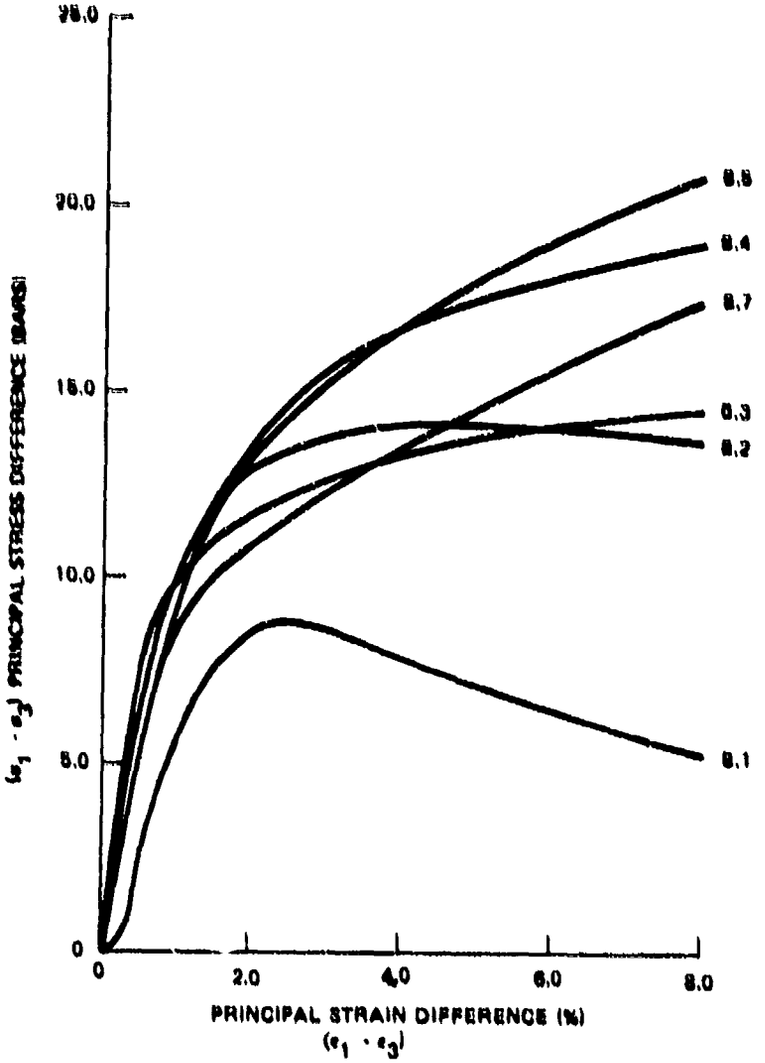

Figure 19. Triaxial Shear Test Data for Series B Tests

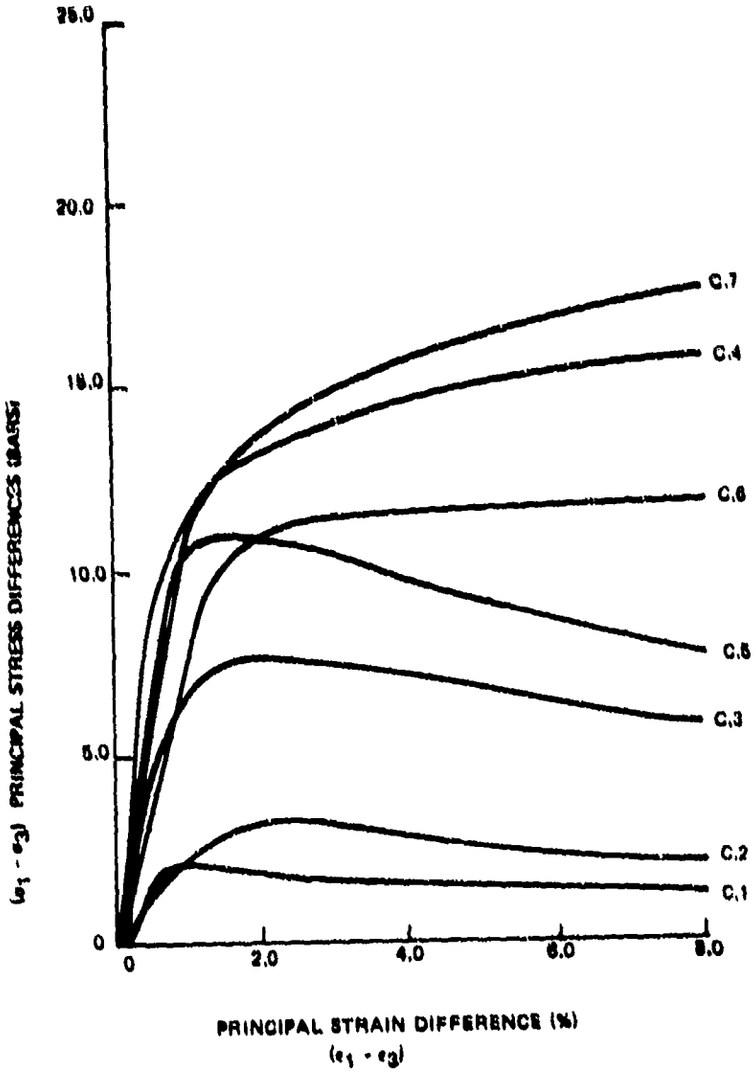

Figure 20. Triaxial Shear Test Data for Series C Tests

Table 5. Composition Properties for Triaxial Tests on Clay

Test No.	Wet Density γ (g/cc)	Water Content w (percent)	Dry Density γ_d (g/cc)	Degree of Saturation S (percent)	Void Ratio e	Air Voids V_a (percent)
A.1	2.050	19.67	1.713	90.4	0.5939	3.57
A.2	2.039	20.47	1.692	91.2	0.6130	3.36
A.3	2.030	20.26	1.689	89.7	0.6164	3.92
A.4	2.033	20.11	1.693	89.6	0.6127	3.95
A.5	2.043	20.53	1.695	91.8	0.6107	3.12
A.6	2.028	21.38	1.671	92.1	0.6339	3.07
A.7	2.027	21.50	1.668	92.2	0.6366	3.03
A.8	2.025	20.40	1.682	89.4	0.6227	4.05
A.9	2.031	20.65	1.684	90.7	0.6215	3.56
A.10	Sample Lost Before Testing					
A.11	2.045	Sample Leaked				
A.12	2.065	20.74	1.710	94.9	0.5965	1.90
B.1	1.832	15.15	1.591	57.8	0.7157	17.61
B.2	1.846	15.19	1.603	59.0	0.7032	16.94
B.3	1.838	15.27	1.595	58.5	0.7121	17.24
B.4	1.839	15.20	1.596	58.4	0.7104	17.27
B.5	1.842	15.25	1.598	58.8	0.7080	17.08
B.6	1.833	15.25	1.590	58.1	0.7169	17.51
B.7	1.848	15.03	1.606	58.7	0.6994	17.01
B.8	1.852	15.03	1.610	59.0	0.6956	16.82
B.9	1.810	15.04	1.574	55.9	0.7349	18.69
B.10	1.900	14.99	1.653	62.8	0.6518	14.69
B.11	1.836	Sample Leaked				
B.12	1.871	15.40	1.621	61.5	0.6841	15.66
C.1	1.630	10.21	1.479	32.9	0.8462	30.74
C.2	1.682	10.12	1.528	35.1	0.7870	28.58
C.3	1.708	10.22	1.550	36.6	0.7613	27.38
C.4	1.684	10.11	1.530	35.2	0.7845	28.50
C.5	1.669	9.99	1.518	34.1	0.7987	29.24
C.6	1.641	10.22	1.489	33.5	0.8335	30.24
C.7	1.674	10.19	1.519	35.2	0.7912	28.88
C.8	1.668	10.02	1.516	34.2	0.8004	29.26
C.9	1.693	9.86	1.541	34.9	0.7717	28.37
C.10	1.656	Sample Leaked				
C.11	1.660	Sample Leaked				
C.12	1.639	10.92	1.478	35.2	0.8471	29.72

This section presents a general discussion of material models which is followed by an introduction to the employment of a relatively simple nonlinear model that can be used in conjunction with linear analysis. This simple model is used to define the mechanical properties of the subgrade based on the extensive laboratory tests made on the clay and sand. While these models are usually associated with nonlinear analyses, they may be used for linear analyses also. As mentioned in Reference 1, material characterization plays an important role in limiting the disparities between the Westergaard and elastic layer idealizations.

As part of this research effort a literature survey was conducted in an attempt to select an appropriate constitutive model(s), i.e., a stress-strain law representative of pavement soils and applicable to pavement type loadings. From this study, it was evident that opinions differ markedly on soil modeling, not only in the pavement community, but in the general field of soil-structure interaction. Proposed soil models range from simple elastic relations (Hook's law) to highly complicated plasticity models requiring the determination of many "material" parameters. For a given soil there is a multitude of state variables that influence the stress-strain relationship, such as, the stress/strain history, which includes previous stress/strain magnitudes; stress reversals, no. of stress cycles, load rate, and particular loading path. In addition, the effects of void ratio, percent saturation, temperature, and other basic soil properties all interact with each other and the stress/strain history to further complicate the stress-strain relationship.

In view of the above, it is not likely there is one "universal" soil model that is applicable to all ranges of the state variables. Rather, the job of the researcher is to choose a constitutive model that works reasonably well for a small domain of the state variables that are anticipated for a particular boundary value problem.

In Appendix D a particular soil model is developed based on the work of Hardin (References 12, 13). The Hardin model is representative of a group, variable modulus models, utilizing a hyperbolic form originally proposed by Kondner (References 14, 15).

For the remainder of this section, the general character of constitutive models is discussed from the viewpoint of form and solution methodology.

A soil model is a mathematical relationship which is used to relate a stress state to a strain state at a point within a soil mass. In matrix form this relationship is denoted as:

$$\{\sigma\} = [C]\ \{\varepsilon\}$$

where $\{\sigma\}$ is the stress state at a point

$[C]$ is the constitutive matrix or operator whose components may be stress/strain dependent

$\{\varepsilon\}$ is the strain state at a point

One of the simplest forms of this expression is that used in linear, isotropic elastic layer analysis. In particular, assuming axisymmetric geometry, the relationship is:

$$\begin{Bmatrix} \sigma_{rr} \\ \sigma_{zz} \\ \sigma_{\theta\theta} \\ \sigma_{rz} \end{Bmatrix} = \begin{bmatrix} C_{11} & C_{12} & C_{13} & 0 \\ C_{21} & C_{22} & C_{23} & 0 \\ C_{31} & C_{32} & C_{33} & 0 \\ 0 & 0 & 0 & C_{44} \end{bmatrix} \begin{Bmatrix} \varepsilon_{rr} \\ \varepsilon_{zz} \\ \varepsilon_{\theta\theta} \\ \gamma_{rz} \end{Bmatrix}$$

where $C_{11} = C_{22} = C_{33} = \dfrac{E(1-\nu)}{(1+\nu)(1-2\nu)}$

$$C_{12} = C_{13} = C_{21} = C_{23} = C_{31} = C_{32} = \frac{\nu E}{(1+\nu)(1-2\nu)}$$

$$C_{44} = \frac{E}{2(1+\nu)}$$

In this case the C_{ij} are based on the two elasticity constants, E and ν, which are assumed to remain constant regardless of the magnitudes of stress or strain. In the more general case the C_{ij} are functions of stress, strain and time. Mathematical relationships for these cases are usually described as nonlinear soil models. A brief overview of time-independent nonlinear soil models follows. A more thorough development can be obtained elsewhere (see Reference 16).

Nonlinear Soil Models. For purposes of this discussion only two types of nonlinear soil models are considered: plasticity models and variable modulus models. The former group is based on the theory of plasticity which in general requires a yield criterion, a hardening rule, and a flow rule. A yield criterion defines the onset of plastic yielding and is usually assumed to be a function of the stress invariants. The hardening rule redefines the yield criterion after plastic deformation has occurred and is usually assumed to be a function of plastic work and stress level. Lastly, the flow rule relates increments of plastic strain to increments of stress after the yield criterion is satisfied. Examples of plastic models applied to soils are the Drucker-Prager, Mohr-Coulomb, and capped models (Reference 17).

From an academic viewpoint, the plasticity models are more rigorous than the variable modulus models (discussed next) because they generally satisfy theoretical requirements and are inherently capable of treating unloading. On the negative side, plasticity models are generally

difficult to correlate with actual soil test data, making it relatively difficult to determine the model's parameters.

Variable modulus models are based on the hypothesis that stress increments can be related to strain increments by an "elastic" constitutive matrix wherein the components of the constitutive matrix are dependent on the level of stress and strain, i.e., $\{\Delta\sigma\} = [C]\{\Delta\varepsilon\}$, where $\{\Delta\sigma\}$ and $\{\Delta\varepsilon\}$ are increments of stress and strain and [C] is the "elastic" constitutive matrix whose components C_{ij} are dependent on the current total level of stress and strain. The variable modulus models represent materials of the so-called "hypoelastic" classification, that is, the constitutive components are dependent upon initial conditions and the stress path. Consequently, the term "nonlinear elastic" is not appropriate for variable modulus models since "nonlinear elastic" implies path independence.

Variable modulus models differ among themselves in two important ways. First is the particular material law or relationship used to determine the constitutive matrix. Second is the associated methodology for updating the constitutive matrix. Four methods are most commonly employed: secant, tangent, modified tangent, and chord methods. These methods are illustrated in Figure 21. The secant method implies that the total load is applied in one step and the solution is iterated to find the secant constitutive components satisfying both equilibrium and the associated material law. For the tangent method the load is applied in a series of steps. At the end of each step the tangent of the material law is evaluated at the accumulated stress/strain level to provide the constitutive components for the next load step. Note the stress and strain responses calculated by the method increasingly diverge from the material law under monotonic loading. The modified tangent method avoids this divergence by iterating within the load step to determine constitutive components that are based on weighted averages of the material law tangents evaluated at both the beginning and the end of the load step. The chord method is the secant method applied in a step-by-step fashion. Thus, the chord method satisfies equilibrium and the material law at every load step and is generally the most accurate method.

The significant advantage of the variable modulus models is their freedom to closely approximate experimental data and the relative ease of determining the parameters of the model. For these reasons and their computational simplicity, variable modulus models are commonly employed in soil problems. For the present, the variable modulus technique appears useful for pavement analysis. A particularly useful variable modulus model (Hardin) is presented in Appendix D. A computer program (XHARDN) implementing this model for use with linear analysis techniques is described in Appendix E.

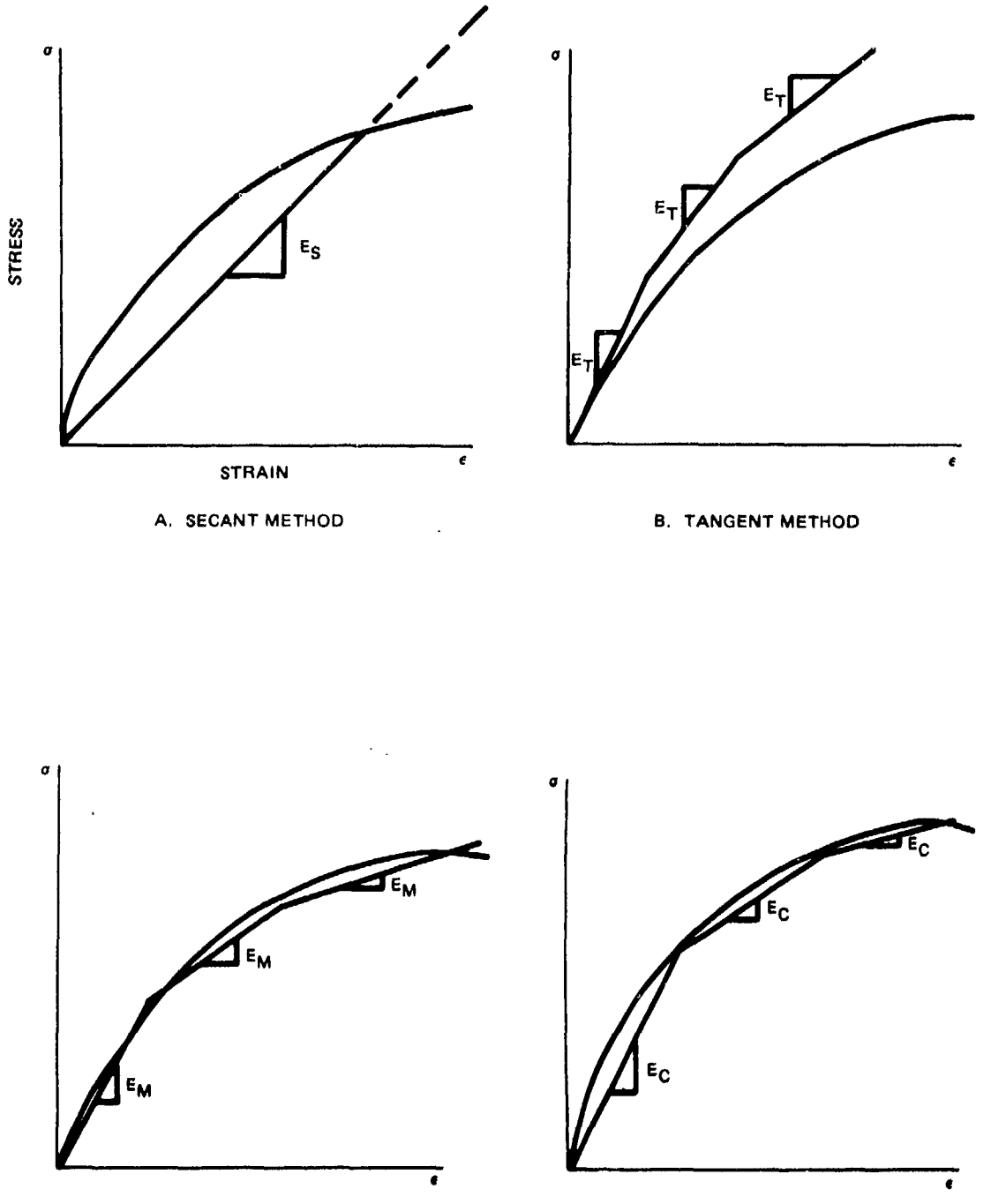

Figure 21. Solution Strategies for Nonlinear Materials

In fairness, it must be pointed out that current research on capped plasticity models shows a great deal of promise with regard to characterizing the dilation and load cycling phenomena of soils. If plasticity model parameters can be standardized or predicted in a fashion similar to the Hardin development (Appendix E), this could provide a major step toward a better soil model.

MODELING THE PAVEMENT COMPONENT MATERIALS

Based upon the experimental data in the Appendices, and upon the references cited, constitutive models for characterizing the various pavement section materials are developed below:

Sand and Clay Subgrades. For the sand and clay subgrades, their shear moduli and Poisson ratios are described with nonlinear relationships by the extended Hardin soil model presented in Appendix D. Basically, the Hardin model defines the secant shear modulus for a specific soil having specific index properties as a function of maximum shear strain and spherical pressure, such that increasing shear strain decreases the shear modulus, whereas increasing spherical pressure increases the shear modulus. The shear modulus function is characterized by three input parameters; S_1, C_1, and a, that are dependent on the soil material and character.

In a similar manner, the extended Hardin Poisson ratio relationship is also defined in terms of a function of maximum shear strain and spherical pressure, such that increasing shear strain increases Poisson's ratio and increasing spherical pressure decreases Poisson's ratio. The Poisson ratio function is characterized by three input parameters; ν_{min}, ν_{max}, and q dependent on the soil character.

The extended Hardin soil parameters used to characterize the sand and clay subgrades of this study were determined (see Appendix D) from material data presented in Appendix C and are summarized in Table 6.

Table 6. Extended Hardin Soil Parameters for the Subgrade Materials

Hardin Parameter	Sand Subgrade	Clay Subgrade
S_1	5993	2000
C_1	9.8×10^6	3.0×10^6
a	3.2	0.5
ν_{min}	0.1	0.1
ν_{max}	0.49	0.49
q	0.258	1.0

*Shear parameters are applicable to in-lb system of units.

Bituminous Base Course. Based upon available test data (See References 18, 19 and 20) and Appendices A and C the relationship depicted in Figure 22 has been selected to represent the stiffness. A Poisson ratio value of 0.4 is considered appropriate.

Lime Stabilized Base. The lime stabilized clay layer consisted of 6 percent type S hydrated lime, mixed with the clay at the proper moisture content (see Appendices A and C) by means of batch plant. This material was then permitted to cure for 48 hours in place then remixed in place with a rototiller and recompacted. This material was selected to meet FAA specifications as outlined in Reference 21.

Values of resilient modulus for the lime stabilized clay base were measured using the test method outlined in Reference 22. Based upon the results of several tests, together with data from Reference 23, the following parameters are selected to model the lime stabilized clay:

Resilient Modulus (Modulus of Elasticity) = 25,000 psi

Poisson's Ratio = 0.25

COMPUTER MODEL

To facilitate usage of the extended Hardin model, a computer program, XHARDN, was written (See Appendix E for further details). This program is designed to be run in two modes: (1) either using input from triaxial tests directly or (2) using the other procedure described in Appendix D (i.e., using e, PI, S and G_{max} etc., to computer G_s and selection of a default value of ν_s. The first mode is preferred, but for many soil types, expediency will permit utilization of the second mode. It should be noted here that the second mode is not considered suitable for compacted plastic clays. For these "problem" materials only mode (1) is considered adequate.

To illustrate the program's capability a parameter study was conducted for the granular material reported in Appendix C. Young's modulus was computed for various heights of overburden and void ratios, using G_s and the parameters of Appendix D to determine ν_s (where $E = 2G(1+\nu)$). To make this study, it is necessary to assume that Poisson's ratio is unaffected by void ratio (i.e., the data of Appendix C that was used in the computation of q, ν_{min}, and ν_{max} is derived for only one void ratio, e = .51). It is regrettable that this compromise must be made

here; however, it is circumstances such as this that provide motivation for establishing a much needed testing program for ν_s similar to Hardin's work for G_s.*

Figure 23 shows the effects that the amount of overburden (which controls the value of σ_m) has on Young's modulus (E_s **) at a particular point in the soil mass for various void ratios. For most rigid pavements, only a few "psi" of live load ever reach the soil, and within a few feet from the bottom of the concrete the live load stress is completely overshadowed by the deadload stress. Thus, at least for most of the soil layers it is necessary to include the gravity effects (i.e., overburden) in any soil characterization.

The most important parameter for Hardin's model is G_{max}. For the granular material shown in Figure 23, G_{max} is computed from σ_m by equation (D-3). Where σ_m is the average of the principal stresses in the soil mass. However, equation (D-3) is intended only as an approximate procedure***, and for soils whose behavior is markedly affected by their degree of saturation, this computation is inaccurate. For these cases G_{max} must be measured experimentally either using triaxial specimens, hollow core cylinders as Hardin did, or vibratory techniques similar to those discussed in References 24 and 25.

---

*ν is a much neglected parameter because the parameters G or E have what appears to be a much more profound effect on response. This notion is presumably derived from 1-dimensional test associated with the definition of E where ν plays a negligible role. However, for 2 or 3-dimensional structures like pavements, ν can be as important as any of the other parameters. This can be demonstrated by using some of the basic relationships among the various elasticity material parameters (G,ν,K). For example, $K = 2G(1+\nu)/3(1-\nu)$ implies that for acceptable values of ν (0 to .5) K ranges from 2/3G to G/0+. ν plays a predominant role in the spreading out of the load and in the distribution of dilational versus deviatoric response.

**The secant modulus (E_s) is used interchangeably with E for linear elastic analysis although E_s is a more accurate terminology. A similar situation occurs for ν_s and ν, and G_s and G.

***Another approximate procedure which might also be used involves usage for CBR values, where $G_{max} = CBR/(1+\nu)$. This is derived from the relationship for sonic E, i.e., E = 1,500 CBR, [27].

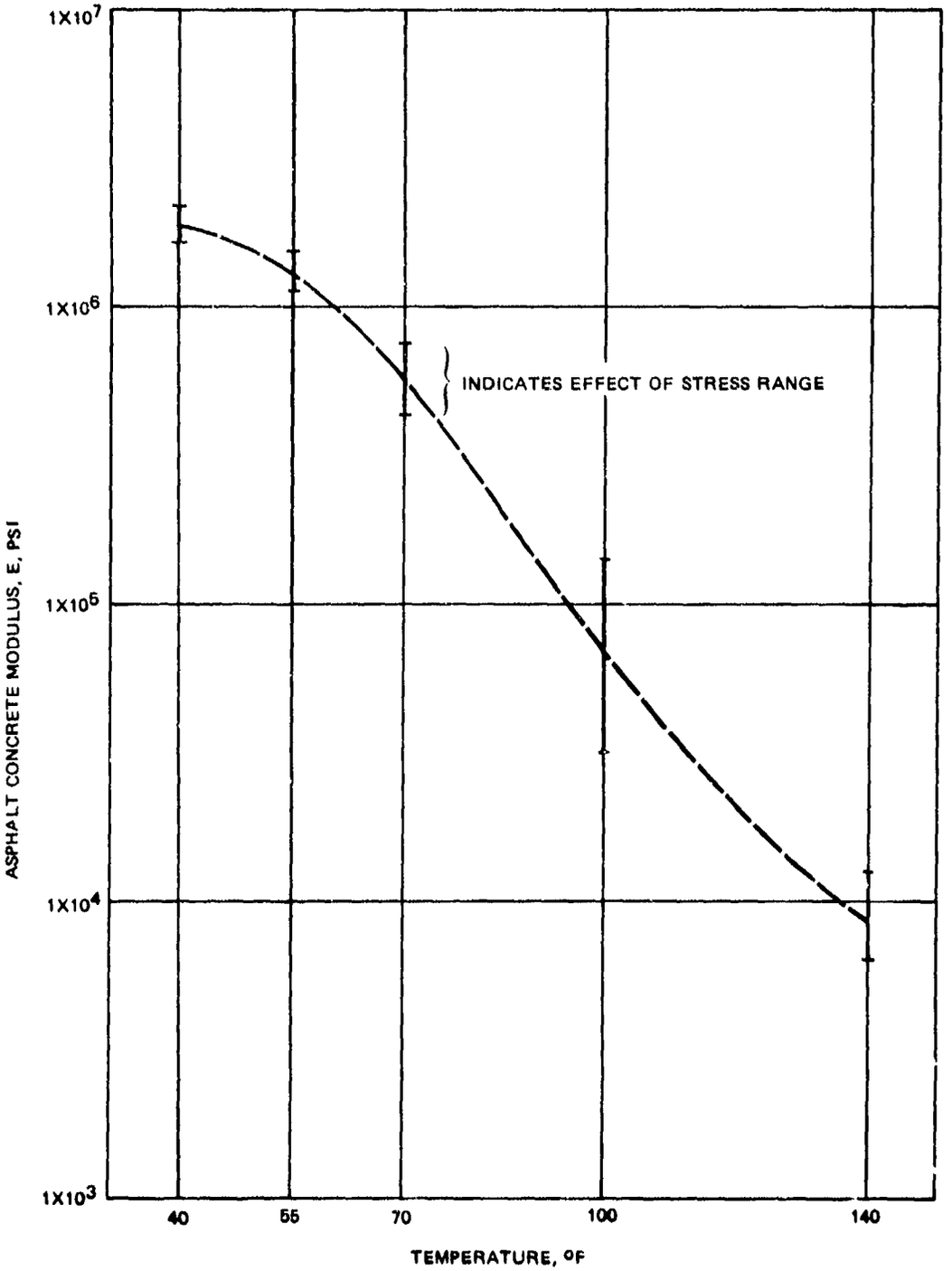

Figure 22. Temperature Dependence of Asphalt Concrete Modulus

Based upon work by Hardin, (12, 13) it is obvious that curves similar to Figure 23 could be developed for many normally consolidated clays, silts, and sands. With an appropriate selection of values of ν, then with respect to linear elastic analysis* a good estimate of material parameters could be obtained for most practical situtations, even without resorting to testing. This is extremely valuable because often in an airfield analysis, the engineer does not possess knowledge of the soil material's actual constitutive properties.

---

*For nonlinear analysis it is necessary to incorporate curves like Figure 23 into a computer program which is especially geared for this form of analysis.

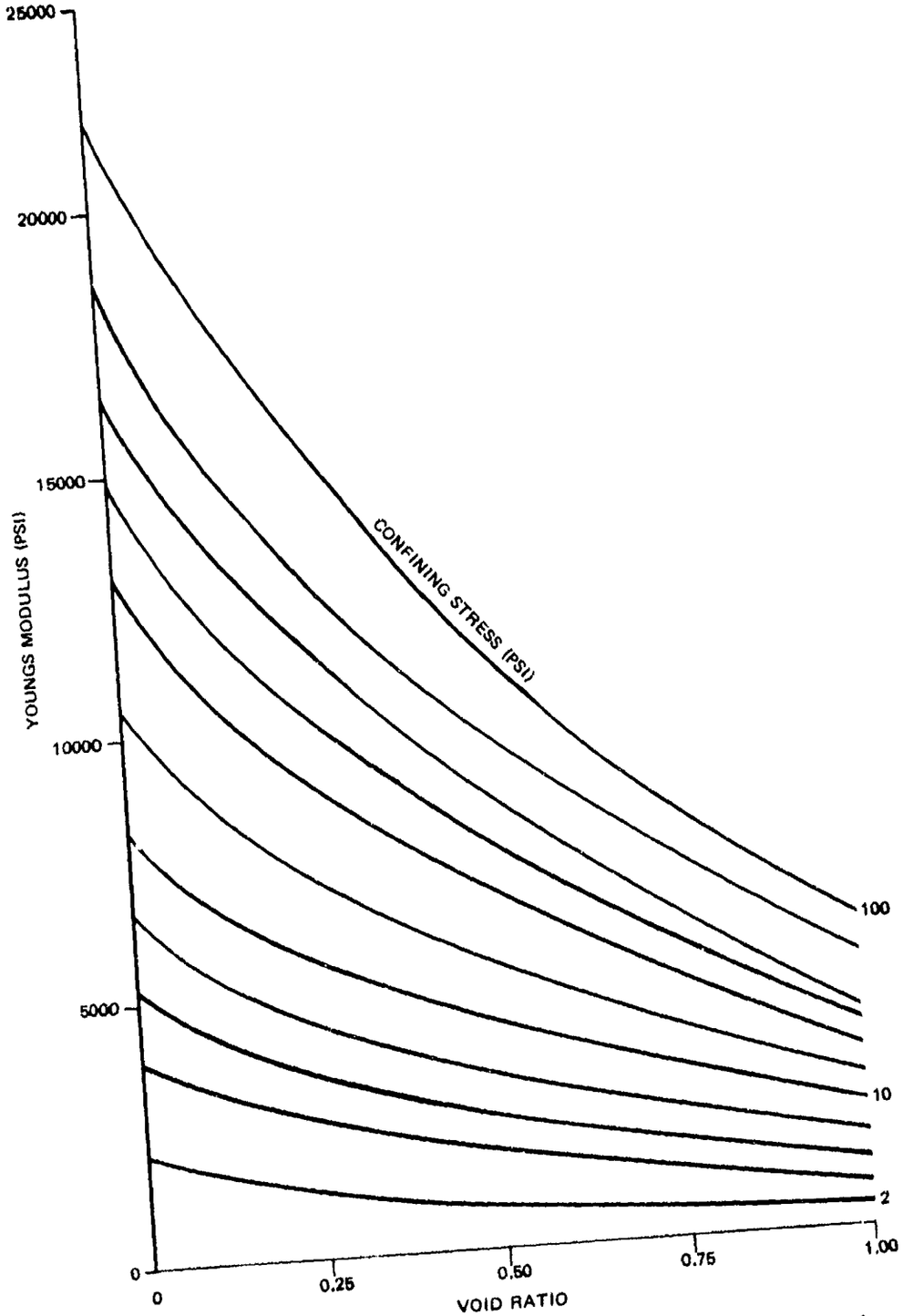

Figure 23. Variation of Young's Modulus with Overburden and Void Ratio for a Granular Soil

DISCUSSION OF RESULTS

In using elastic layer idealizations of pavement systems, the first major difficulty to be encountered is how to account for the changes that take place in material properties under applied load. The influence of static confining stress can be accounted for in some measure by dividing the pavement section into numerous layers+, (up to a limit, depending upon the degree of complexity that can be tolerated). However, the applied pavement loading both increases the level of confining stress and increases the level of shear strain. Since both confining stress and shear strain level exert a major influence on the stiffness of most soils (as may be noted by reference to the previous chapter) this influence of material nonlinearity is difficult to ignore. This problem is particularly apparent for interpreting plate load tests conducted directly upon the soil subgrade. In this case major volumetric and shear stresses are transmitted directly into the nonlinear subgrade material. Theoretically the analysis of this situation must first estimate the increases in shear strain and confining stress to be transmitted to the soil and continue to modify the solution iteratively. Thus soil stiffness parameters must be selected based upon an estimated stress regime and the final solution checked against the initial assumptions. Should there be disagreement between the calculated stress and strain states and those initially assumed, a new assumption of stress state must be made, material parameters revised and the calculation repeated, etc.

This is not by any means the major difficulty to be encountered here. A homogeneous subgrade under a plate load experiences a broad variation of stress states, and hence simultaneously encompasses a broad range of material parameter response values. However only one set of elastic response "constants" can be selected for elastic analysis. The question becomes: what single stress state is representative of the average for calculating the response of the plate-subgrade system?

With finished pavement systems the foregoing problem is not so prominent in that response properties of the surface layers, particularly the portland cement concrete are not so sensitive to the stress state. The more nonlinear materials such as the subgrade, are at greater depth and are not subjected to a broad range of stress variations.

Thus for layered pavement systems it might be acceptable to select constant values of material response parameters based upon the initial or static stress levels.

+One must still estimate the coefficient of lateral earth pressure in order to accurately evaluate the true volumetric or confining stress.

For the situation where plate loads are placed directly upon the more nonlinear pavement component materials such as the subgrade or granular base it will generally be unacceptable to ignore the effects of applied load on the material stiffnesses. In the cases where live load must be considered in this context, it is important to realise that the material properties will be totally different under different levels of applied load. This will be illustrated in the following:

Figures 24 and 25 show measured and calculated load-deflection plots for the surfaces of the sand and clay subgrades respectively, and the "corrected" subgrade moduli, as discussed in Field Tests. In order to compare this measure modulus with those calculated by elastic layer analysis, basic assumptions must be made regarding the representative stress state. Two different assumptions were investigated herein.

First, the influence of the plate load was ignored and only the static load stresses were considered, with regard to selecting material parameter values. In order to account for the variation in static strength with depth, the homogeneous subgrades were divided up into 6 layers having 6", 6", 6", 12", 30" and infinite thicknesses, respectively. The soil stiffness parameters for the various layers were modelled using the soil constants given in Table 6. The calculated load deflection plots in Figures 24 and 25, which consider only the influence of static load on the soil response parameters, indicate softer materials than are shown by the measured curves. Whereas the measured load deflection curves indicate a stiffening of the subgrade with increased load, the analytical curves, using constant elastic parameters, give no recognition to increased confinement, and are unable to predict this increased stiffness.

In order to incorporate the effects of increased confinement and increased shear strain levels on the subgrade material, an analysis was carried out which considered the plate loading only, and neglected the effects of static load. Because the subgrade stresses induced by the plate load are concentrated primarily within a region directly below the plate, the representative stress state for confinement level for the subgrade was taken as that at a depth of one radius below the center of the plate. The representative state for the shear strain was considered that which occurs below the edge of the plate, also at a depth of one plate radius. Using the stress and strain levels at these points, and connecting these values iteratively, the calculated load deflection curves which consider live load influence on the material properties were calculated and shown in Figures 24 and 25. It is noted that for low load levels, the level of confinement is such that the calculated load-deflection response is softer than that measured. With increased load, beneficial effects of increase in confinement outweigh the weakening influence of increase in shear strain, and the subgrade resistance to settlement improves.

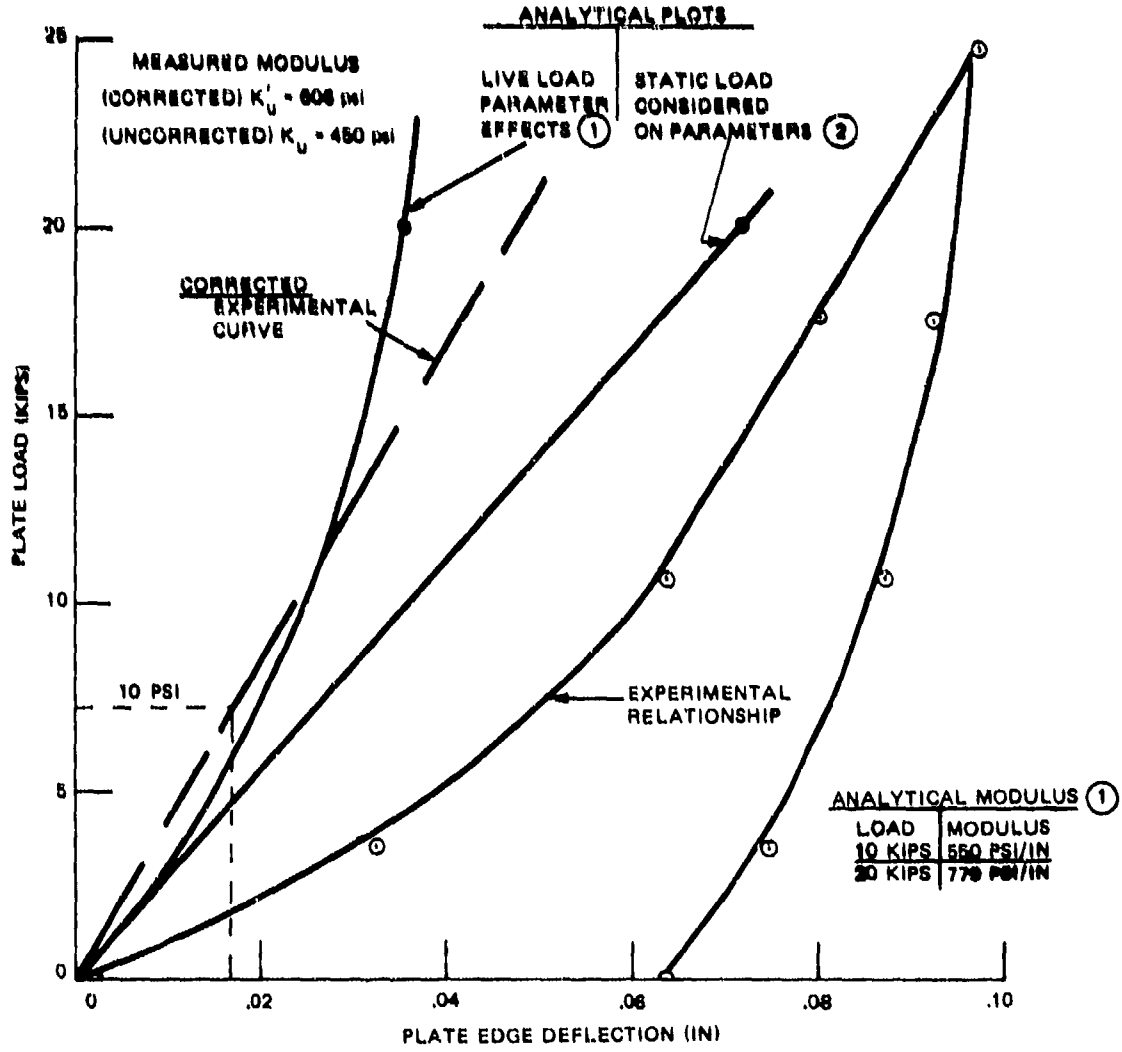

Figure 24. Measured Versus Calculated Deflections for Sand Subgrade

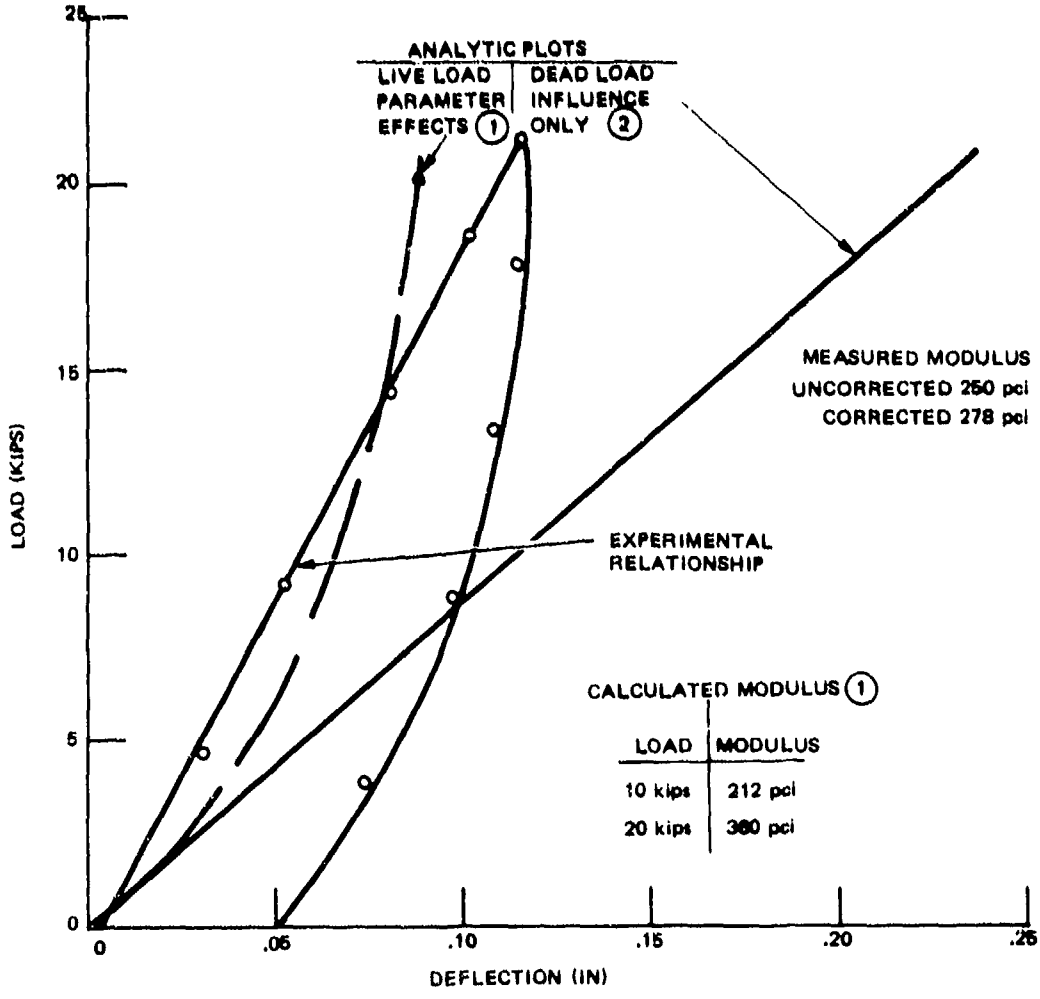

Figure 25. Measured Versus Calculated Deflections for Compacted Clay Subgrade

Thus the material parameters selected to monitor the subgrade response bracket the actual measured subgrade modulus. This emphasizes the fact that any calculated subgrade modulus, based upon realistic soil models is load sensitive. It is interesting to note here that the analytically derived stiffness, based upon the stress and strain states at a depth of one plate radius, and located below the center and edge of the plate, respectively, bracket the corrected subgrade modulus measured for this load range. If static confinement in addition to the confinement due to the plate had been considered the calculated moduli would be slightly higher. On the other hand if stress and strain states, at locations within the subgrade that were different from those selected are used as the representative states, either stiffer or weaker analytical response would be determined. Nevertheless for the two materials tested herein, the use of the recommended soil model and selection of the representative stress and strain states used herein provides analytical values of subgrade modulus that bracket the (corrected) measured values. The foregoing, however, clearly illustrate the limitations of elastic theory in characterizing subgrade response. Although the reference stress states were selected empirically, it is apparent that they are reasonably representive.

Thus it appears that the average stress conditions for volumetric and shear response beneath a loaded plate may be taken as the stresses existing at a depth of one plate radius, beneath the center and edge of the plate, respectively. By using the stress states at these locations as representative states, using a realistic soil model, as outlined in the previous Chapter, and staying within applicable load ranges, elastic theory is shown to be able to predict subgrade stiffness to plate loading. The foregoing applies to situations wherein the nonlinear relationship between applied load level, and material response stiffness cannot be ignored. Where the applied loading is transmitted through less nonlinear materials, such as portland cement concrete, the effects of loading on the material response parameters will be considerably less. Whether or not the effects of live load on material response can be ignored in these latter cases is investigated below.

When a plate load is applied to a pavement section such as A-1 (Figure 5) or B-1 (Figure 4), which permits considerable load distribution by the stiff surface layer, it may not be necessary to consider the changes in material response parameters under applied loading.

To investigate this situation, elastic layered solutions for plate loads applied to the concrete surfaces of Sections A-1 and B-1 are presented in Figures 26 and 27, which also show measured plate load-deflection response for one load cycle. It may be noted on the figures that the elastic layered solutions give deflection response that is relatively consistent with the measured values.

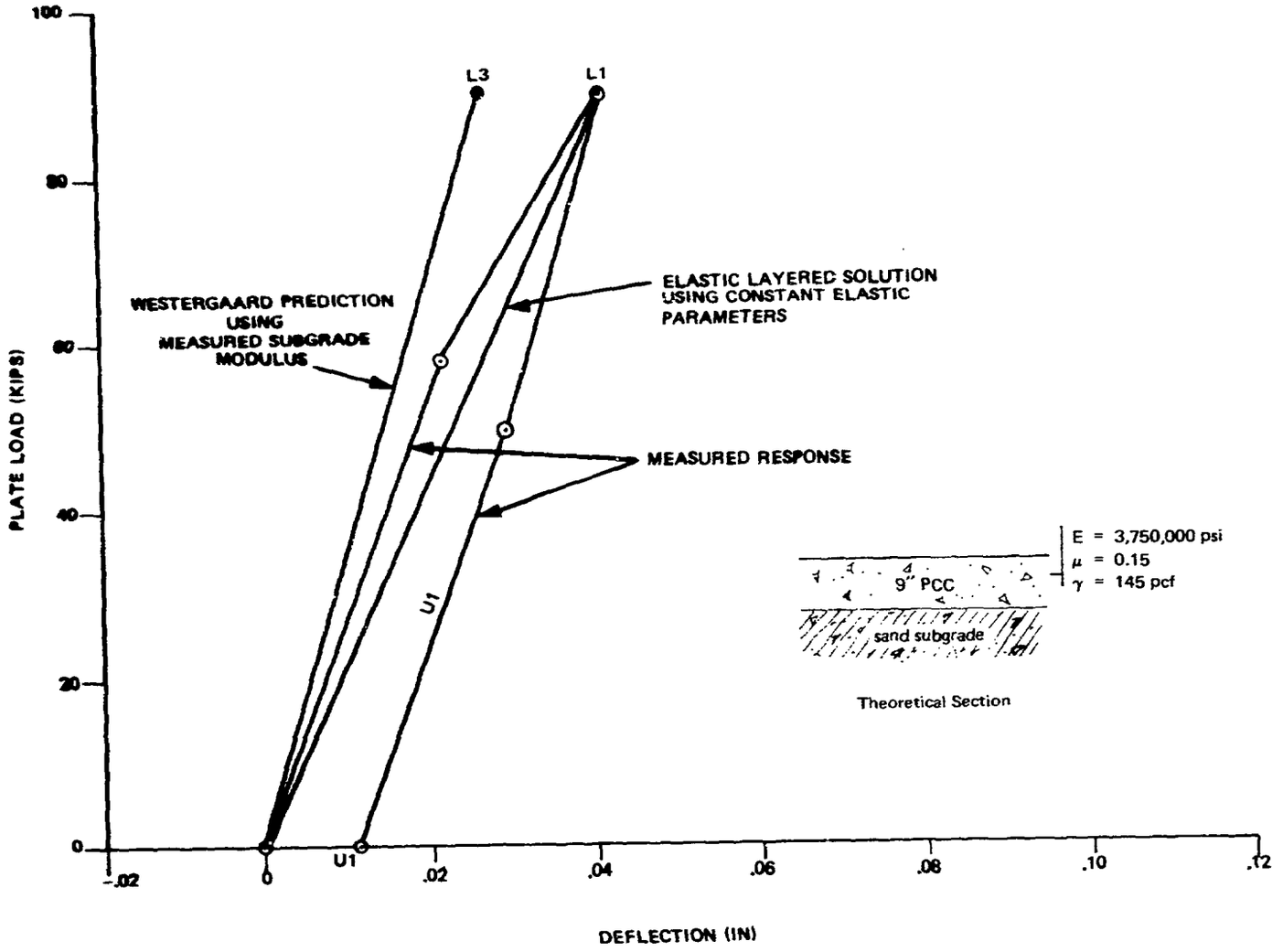

Figure 26. Measured Versus Calculated Deflections for Section A-1

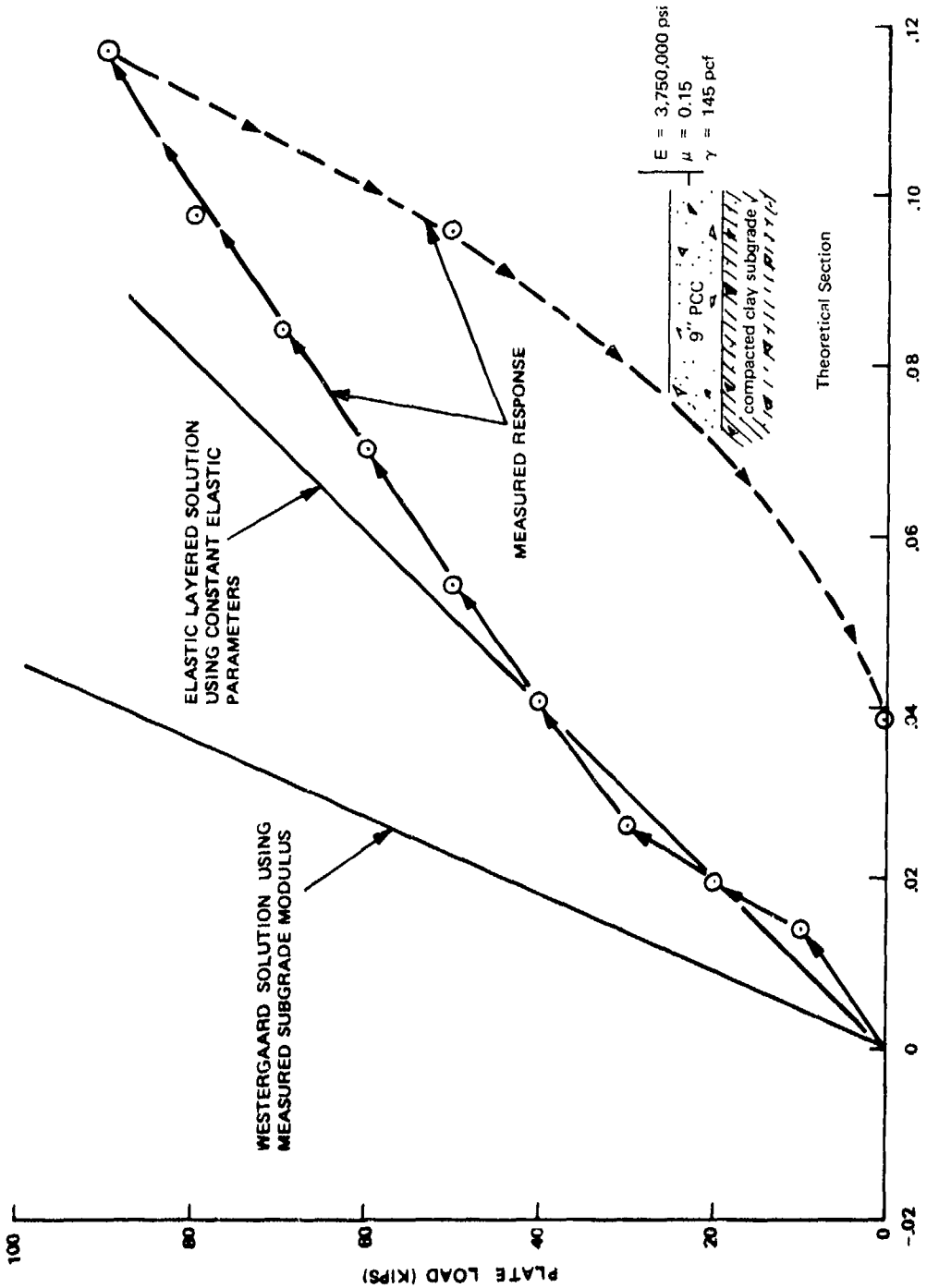

Figure 27. Measured Versus Calculated Deflections for Section B-1

Also shown on Figures 26 and 27 are settlement curves based upon Westergaard solutions (as presented in Reference 1) using the measured values of subgrade modulus, see Figures 24 and 25. It is evident that for both the sand and compacted clay subgrades, the Westergaard deflections using measured values of subgrade modulus underestimate the actual measured deflections. Based upon this limited data it is apparent that the Westergaard analysis overestimates the stiffness of a concrete surfacing over a homogeneous subgrade.

Because constant elastic parameters were used in this case, i.e., the influence of plate load on the soil parameters is not considered, the conclusions are applicable to all load ranges.

The stress functionals calculated by the ELAST program indicate required subgrade moduli of 269 and 63 psi per inch for the sand and clay subgrades, respectively in order to provide Westergaard deflections matching the elastic layer calculations. Thus even if the lower values of "uncorrected" measured subgrade moduli were used, the Westergaard analysis would still predict smaller surface deflection than actually occurs.

For this case, where only the influence of static load on the pavement material parameters is considered, the subgrade moduli calculated by elastic layered theory for the sand and clay subgrades is 641 and 198 respectively. These values are 106 and 71 percent, respectively, of the actual measured subgrade values for the sand and clay. This would indicate that as long as there is a fairly stiff surface layer to distribute the load, ignoring the effects of applied (live) loading in calculating an equivalent subgrade modulus by elastic layer theory is reasonably accurate. This is in contrast with the situation in Figures 24 and 25 where no stiff surface layer exists and there is a major influence of live load on the subgrade material parameters. The foregoing observations are in agreement with Reference 1 which noted Westergaard theory underpredicting elastic layer settlement by about 70 percent.

The foregoing considerations dealt only with deflection criteria, however consideration of maximum tensile stress might be more significant. Maximum tensile stress, or more correctly the resulting strain is perhaps the most broadly accepted criterion for concrete distress. For the comparisons carried out herein, since the concrete strain values have been measured directly, calculated strains rather than the calculated stresses are used. Figure 28 shows measured and calculated tensile strains for the slab in Section A1. The measured tensile strains show much more nonlinear yielding at least for the first loading cycle than that calculated by the two analytical methods. The strains predicted by the elastic layered analysis and the Westergaard analysis are somewhat less than the measured values, particularly at higher load levels. This might be due to selection of elastic parameter values that are too stiff, i.e., a modulus value of 3.75×10^6 psi, and an equivalent Poisson's ratio of 0.15, or to slight errors in strain measurement.

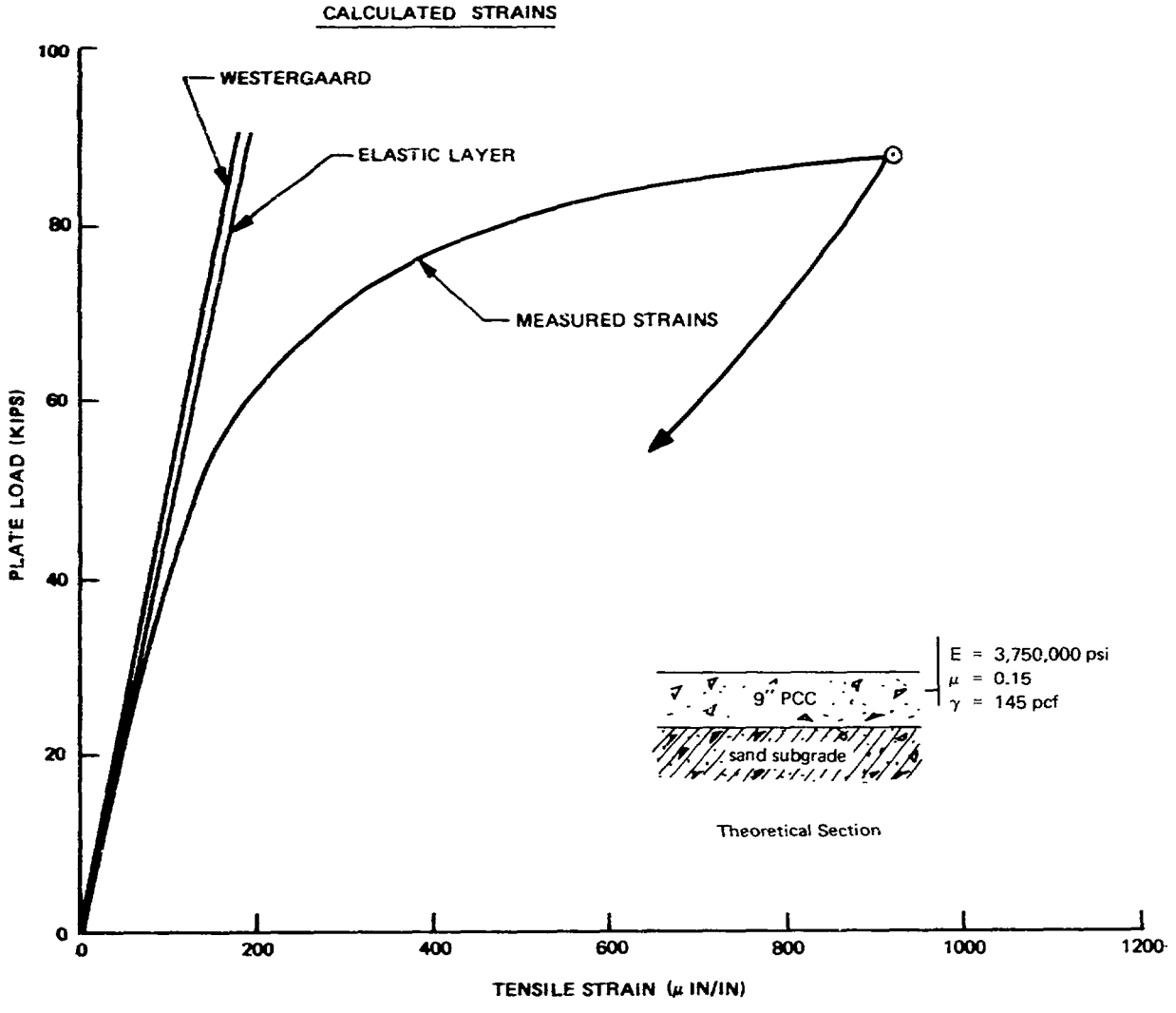

Figure 28. Measured Versus Calculated Concrete Tensile Strains for Section A-1

Nevertheless the Westergaard and elastic layer solutions are noted to give similar calculated strain levels (the Westergaard solution here predicts slightly smaller strains). Thus the Westergaard analysis for this simplified case of a plate on a relatively homogeneous foundation, although underconservative from a deflection standpoint appears to be compatible with elastic layered theory with regard to maximum tensile stress.

This agrees with the conclusions of Reference 1 in that peak tensile strain in the concrete slab is relatively insensitive to subgrade modulus, and can be expected to vary from the elastic layer solution by only about 10 percent. Thus for the two simplified situations studied above, realistic material characterizations permit realistic, compatible designs by either the elastic layer or Westergaard theory, as long as maximum tensile stress is adopted as the controlling criterion. It is noted that, based upon these measurements, both analytical methods are underconservative in the higher loading ranges. This could be expected, since in the very high loading regions the concrete is no longer performing elastically.

In order to investigate the applicability of not only elastic layered theory but particularly Westergaard theory in situations for which the Westergaard idealogy does not strictly apply, plate load tests were conducted on the more complex pavement systems A-2 (see Figure 12) and B-2 (see Figure 15). Figures 29 and 30 show a comparison of measured and calculated plate deflections for pavement Sections A-2 and B-2, respectively. The Westergaard solutions, using the values of subgrade modulus measured upon the asphaltic base of Section A-2 (see Figure B-31) and the stabilized clay base of Section B-2 (see Figure B-70) respectively, again show smaller deflections than either those predicted by elastic layered theory or the directly measured values. The elastic layered theory predicts the deflections of Section A-2 very closely but gives Section B-2 deflections that are slightly high. This could imply that the stabilized clay is slightly stiffer than is represented by the response parameter values selected for use in the analysis. This slight discrepancy could also be explained in terms of errors introduced by neglecting the influence of live load on the response parameters of the base material.

The ratios of subgrade values predicted by the elastic layer solutions to the measured subgrade values for the asphalt base of Section A-2 and the stabilized clay base of Section B-2 are 86 and 75 percent, respectively. Thus, for the two different test sections, considered herein, the elastic layer theory predicts values of subgrade reaction that are less than 25 percent below those that would be measured by a plate bearing test conducted on the different base courses.

The Westergaard solution is again observed to be underconservative, with respect to deflections criteria. This agrees with the observations upon the simpler test Sections, A-1 and B-1 and with the conclusions of Reference 1.

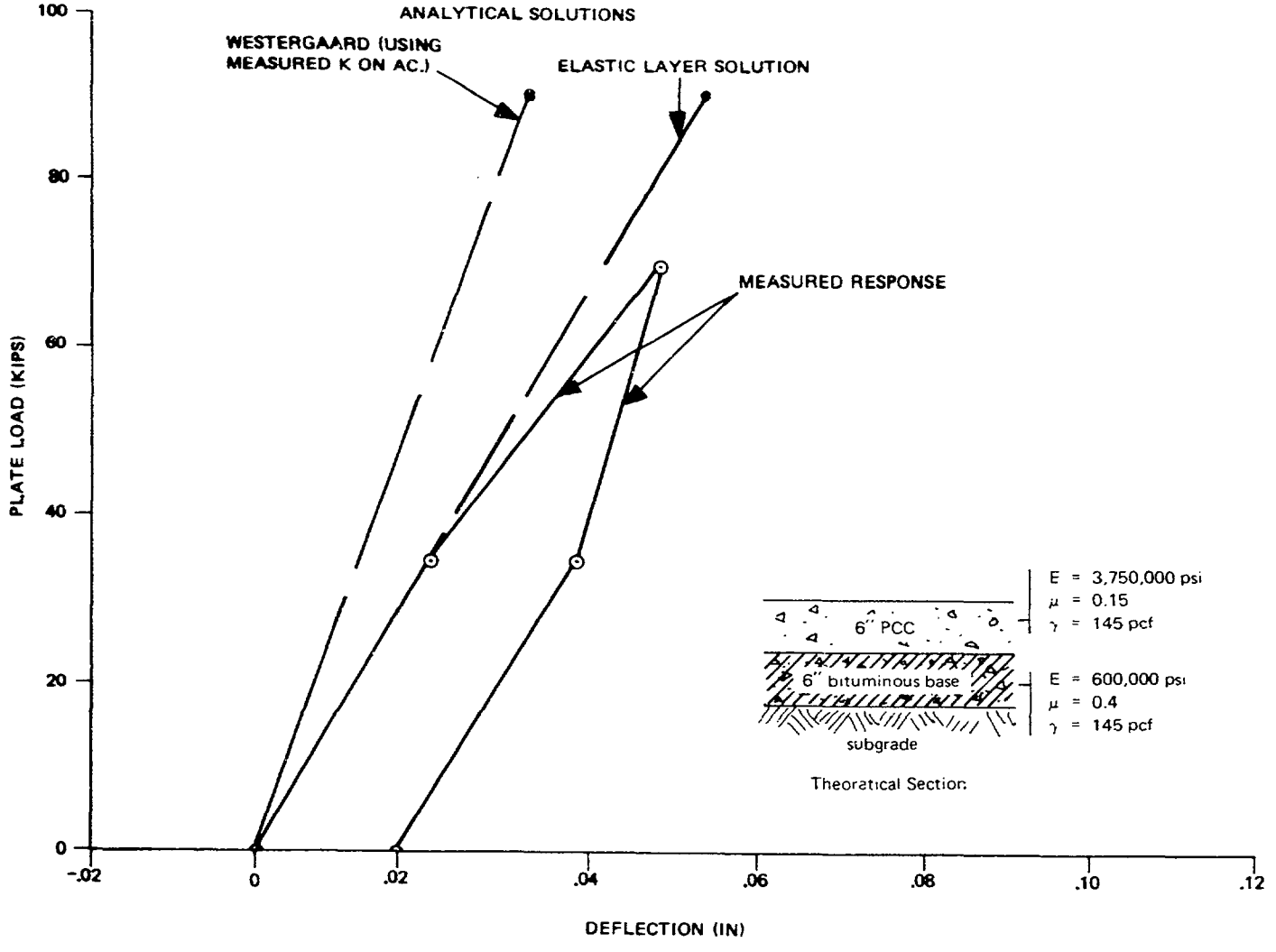

Figure 29. Measured Versus Calculated Deflections for Section A-2

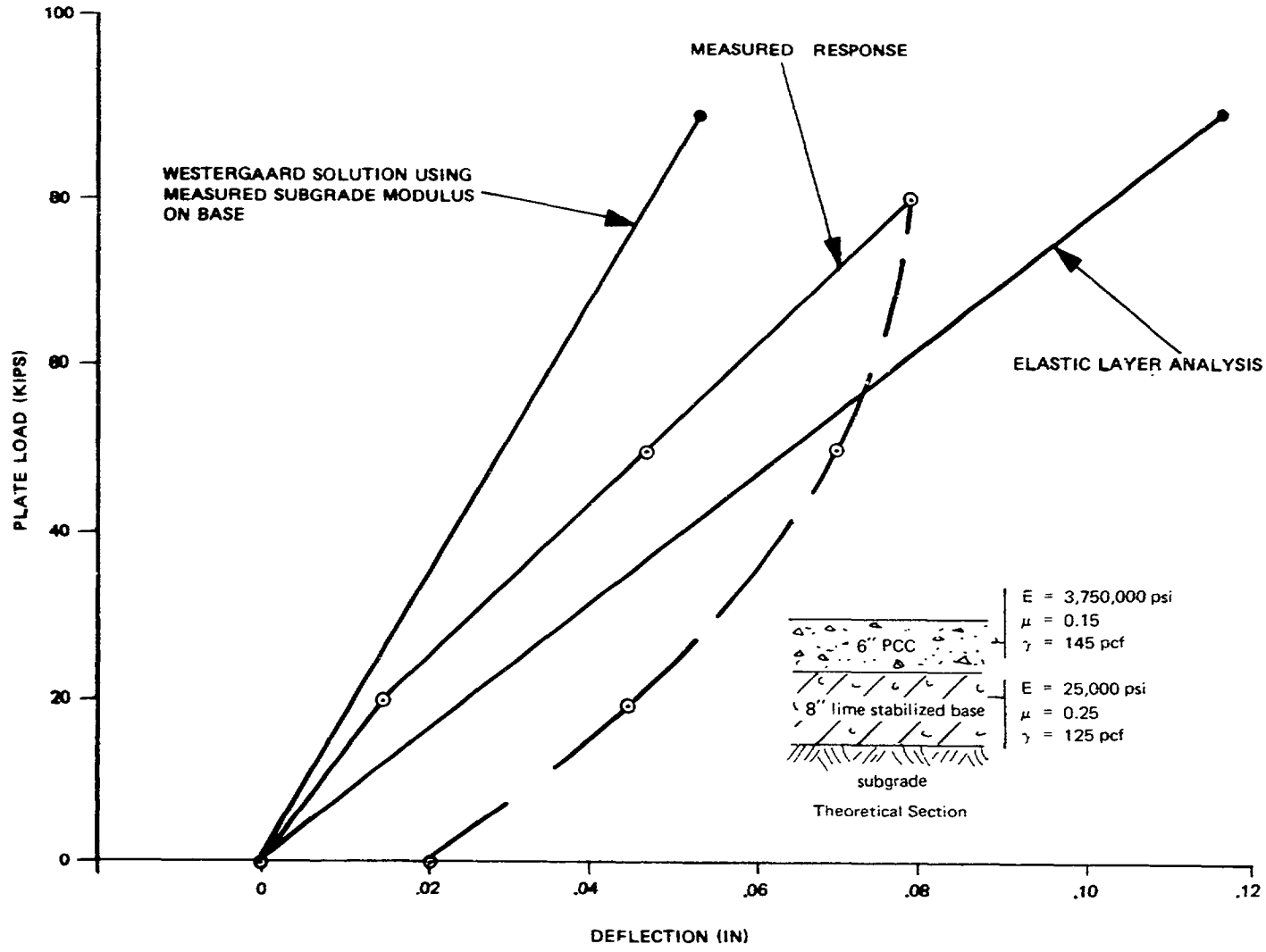

Figure 30. Measured Versus Calculated Deflections for Section B-2

Figures 31 and 32 show calculated and measured maximum tensile strains for test sections A-2 and B-2 respectively. It is noted that, particularly for test Section A-2 that the strains predicted by either analytical method are considerably below those measured. For the case of Section A-2, comparison of Figures 28 and 31 suggest that either the bituminous base material is yielding considerably, and that the "elastic" stiffness parameters selected for analysis herein are inaccurate, or that some difficulty in strain measurement was encountered. Alternatively the formation of cracks at high stress levels could be expected to introduce a discrepancy of this kind, but this would suggest a crack existed under the plate in the test on Section A-2 from a very early stage of loading. This latter interpretation is supported by the concrete strain measurement recorded under the edge of the slab and shown as a dashed line in Figure 32.

Nevertheless, the Westergaard and elastic layer stresses are again very similar except that for these more complex pavement sections, the Westergaard approach is slightly more conservative than the elastic layer analysis. The conclusions to be drawn from the analysis of these more complex test sections is compatible with those from the simpler test sections B-1 and B-2. If the pavement materials can be realistically characterized, both elastic layered analysis and Westergaard provide reasonable and roughly equivalent approaches to the design of concrete pavement based upon allowable tensile stress criteria. It must be emphasized however, that these conclusions can only be expected to apply to pavement situations similar to those investigated herein, and are dependent upon valid material parameter input.

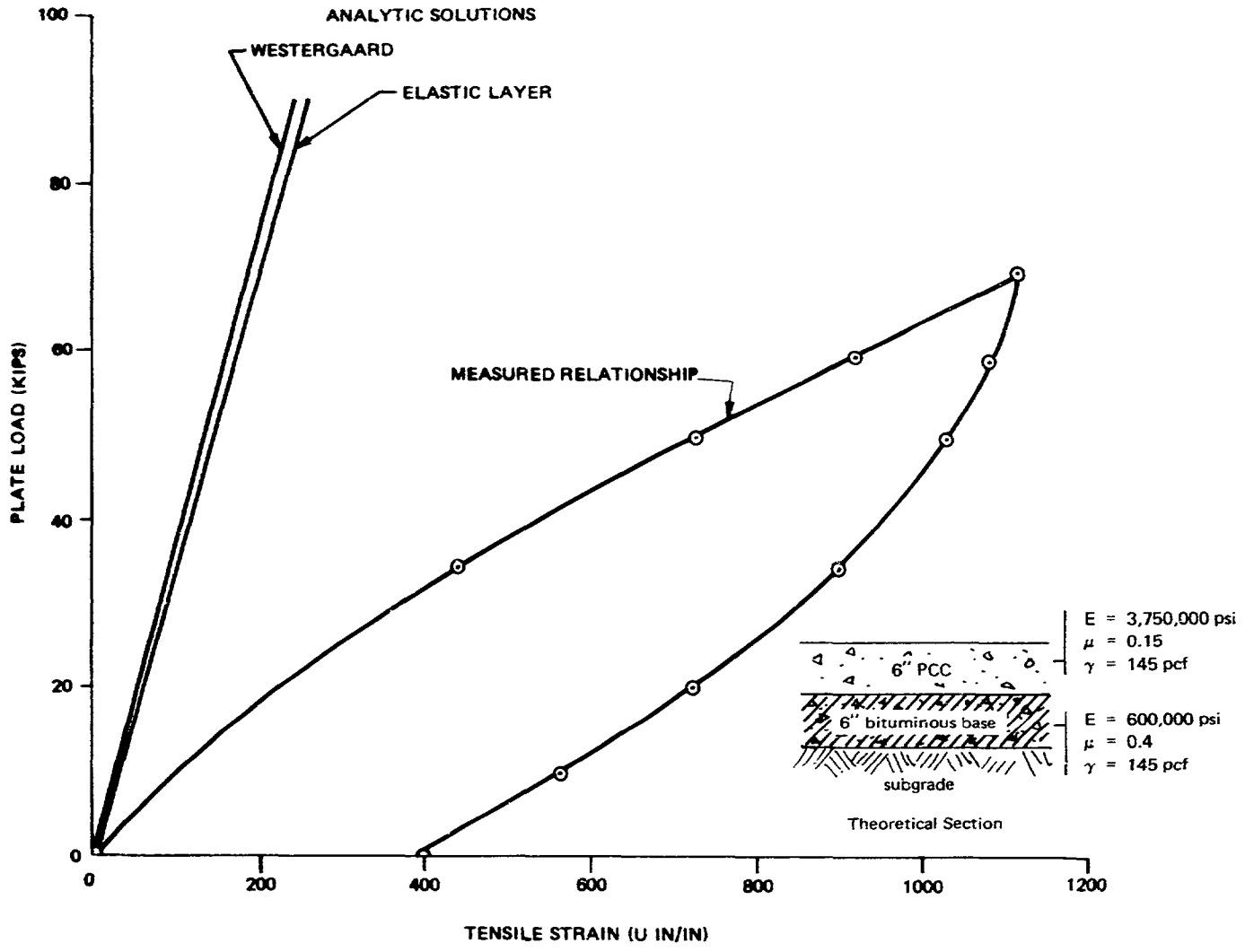

Figure 31. Measured Versus Calculated Concrete Tensile Strains for Section A-2

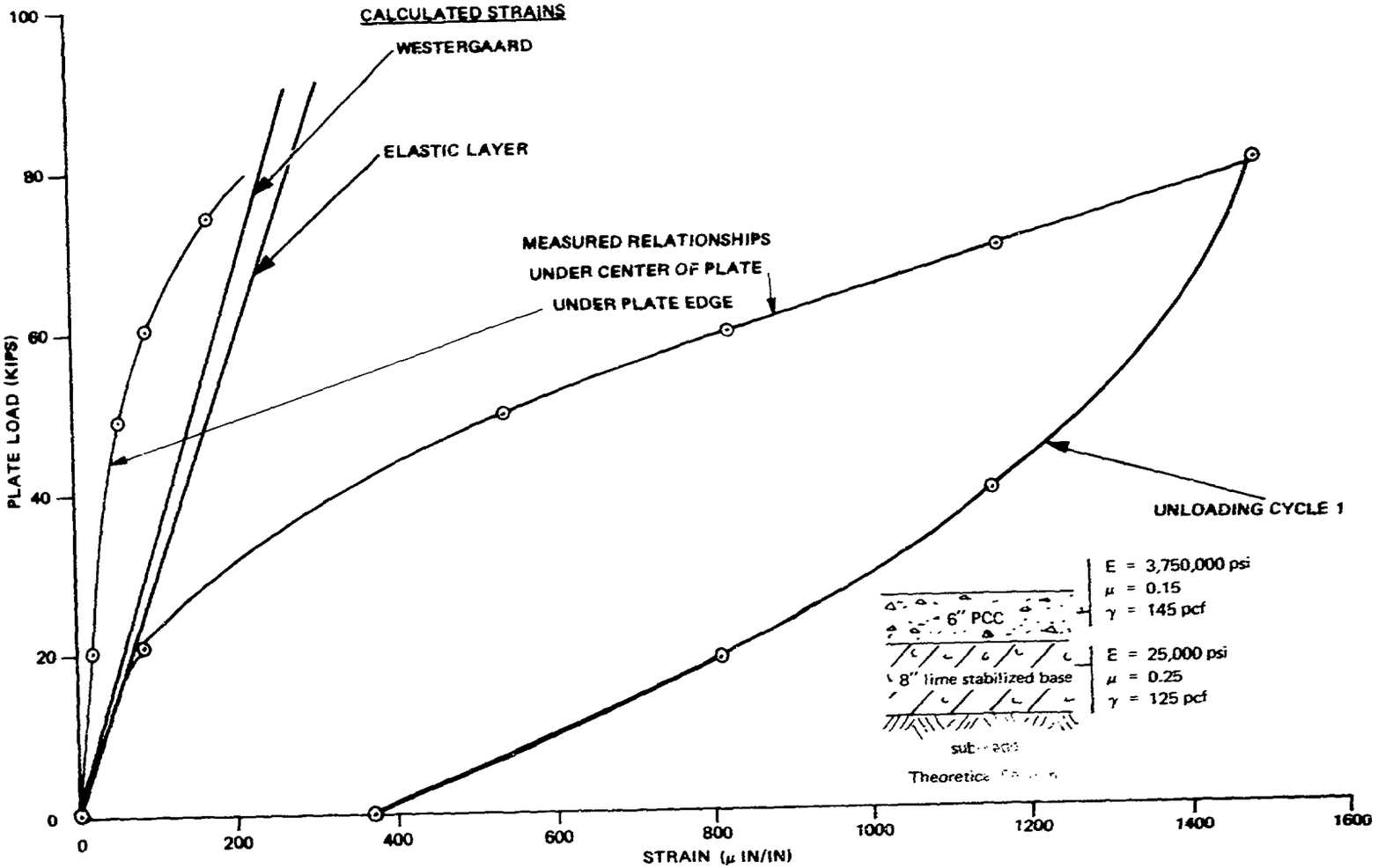

Figure 32. Measured Versus Calculated Concrete Tensile Strains for Section B-2

CONCLUSIONS AND RECOMMENDATIONS

CONCLUSIONS

By means of precisely controlled, large scale field tests and extensive material characterizations, analytical relationships relating Westergaard analysis and elastic layered analysis of rigid pavements have been compared. The comparisions between the analytic treatments and the field measurements of controlled test sections tend to support the general conclusions of Reference 1, in which the analytical treatments were presented. In addition, the following specific conclusions are made:

1. By using the material model developments presented herein and supported by adequate experimental data, it is possible to predict both deflections and maximum tensile stresses in typical rigid pavement sections by means of elastic layered theory.

2. Westergaard theory based upon measured values of subgrade modulus is found to be underconservative with regard to pavement design criteria based upon deflection.

3. Both Westergaard theory and elastic layered theory for the cases treated herein provided similar results with regard to design criteria based upon allowable tensile strain in the slab. However, both methods were found to be somewhat underconservative, compared with measured pavement response.

4. To evaluate the response of loads placed directly upon nonlinear pavement components such as subgrades, by elastic analysis, the influence of the live load on the material response parameters must be included. Thus solutions must be of an iterative nature, with initial estimates of stress and strain states made and then corroborated by the final solution.

5. For the two subgrade materials involved in this study, i.e., a dense sand and a compacted clay, the stress state which appeared to be representative of the average state for the subgrade was that located at a depth of one plate radius beneath the center of the load. The representative strain state, for use in modifying the subgrade stiffness parameters appeared to be that located at a depth of one plate radius beneath the edge of the plate.

6. For the normal range of loadings on rigid pavements it is not necessary to consider the change in stiffness values with applied load. Thus initial elastic parametric values may be selected, based upon initial static stress state, and used throughout the normal loading range.

7. For this investigation the incorporation of additional pavement layers (i.e., the bituminous base and the stabilized clay) did not markedly affect the results of the Westergaard analysis as compared to the elastic layered analysis as long as the subgrade value measured on the second layer was used. However, this conclusion may not be valid for loaded areas greater than that of the 30 inch plate with which the subgrade modulus was measured. The reason for this is that larger loaded areas may transmit significant stresses in material at greater depths whose response is not represented in the results of the subgrade modulus test.

8. Although a knowledge of basic soil index properties has appeared to be sufficient to formulate a valid material model for granular soils, for very complex materials such as compacted clays, model fitting must be based upon actual experimental data acquired within the pertinent stress and strain regions.

RECOMMENDATIONS

Pavement field testing, material characterizations and analytical treatments of pavements all represent significant areas of endeavor by themselves. The attempt herein to tie all of them into a relatively modest program was very ambitious. Since extensive efforts could not be made in all the different aspects, the experimental field testing was given priority. It was felt that the detailed, high precision field data must be obtained, while the opportunity existed, and if necessary, material characterization and analytical treatments could be substantiated at a later date.

For this reason, although the objectives of this work unit were met, a great wealth of experimental data, reported in the Appendices, has not been fully utilized. A wide range of soil strain and displacement data that has no direct significance with respect to Westergaard analysis has been obtained during the performance of the field tests. This was largely because of the difficulty to be encountered in obtaining such data and because it could not be acquired at a later date. The very precisely controlled and monitored field tests provided herein could be used to achieve intensive in-depth understanding of pavement response and a rigorous evaluation of various pavement models. These few very well defined situations, could be used to validate such techniques as use of a mechanical subgrade to extend our understanding of pavement sections to various other pavement situations.

APPENDIX A

CONSTRUCTION SPECIFICATIONS FOR EARTHWORK, CONCRETE, BITUMINOUS BASE COURSE AND LIME STABILIZED CLAY

The information contained in these specifications provides the standards used for the construction of the CEL pavement testing facility. These specifications are written to comply as closely as feasible with FAA standards for airport construction (References 2, 26). Construction standards are presented for earthwork, concrete, bituminous base course, and lime stabilized subgrades.

GENERAL PROVISIONS

Definition of Terms. Whenever the following terms are used in these specifications, the intent and meaning shall be as follows:

ASTM	The American Society for Testing and Materials
Embankment/Berm	The earth embankment containing the test subgrades.
Contractor	The Naval Construction Battalion responsible for the acceptable performance of the work.
Engineer	The individual authorized by the Laboratory to be responsible for engineering supervision of the contract work. The engineer may act directly or through an authorized representative.
FAA	The Federal Aviation Administration of the U. S. Department of Transportation.
Laboratory	The Civil Engineering Laboratory of the U.S. Navy.
Pavement	The combined surface course and subbase course, if any, considered as a single unit.
Subgrade	One of two pits of backfilled earth which form the test pavement foundation. The subgrade is contained by the embankment.

1. EARTHWORK

1.01 General. The embankment, subgrade, and subbase soils shall be placed where designated on the plans or as directed by the engineer. The materials shall be shaped and thoroughly compacted within the tolerances specified.

All equipment necessary for the proper construction of this work shall be on the project, shall be in first-class working condition, and

shall have been approved by the engineer before construction is permitted to start. Provision shall be made by the contractor for furnishing water at the site of the work using equipment of ample capacity and design to assure uniform application.

1.02 Grade and Line Control. The embankment shall be cut to the elevation specified on the print for the bottom of the subgrade; after compaction, the bottom surface of the cut shall not have a vertical deviation in excess of 0.1 foot from the specified elevation. After each subgrade is completely compacted and brought to grade the surface shall be tested for smoothness and accuracy of grade; any portion found to lack the required smoothness or to fail in accuracy of grade shall be scarified, reshaped, recompacted, and otherwise manipulated as the engineer may direct until the required smoothness and accuracy are obtained. The finished subgrade surface shall not vary more than 1/2 inch when tested with a 10 foot straight edge. At no point on the subgrade surface shall finished elevation deviate more than 0.1 foot from the specified elevation. Deviations from horizontal dimensions shall not exceed 6 inches for the subgrades.

1.03 Mixing of Clay Soil. The clay subgrade material shall be deposited in a designated mixing area and spread evenly to a uniform thickness and width. Water in the amount and as directed by the engineer shall be uniformly applied to the clay prior to and during the mixing operations, if necessary, to maintain the water content to within 14 to 17 percent of dry weight. Water shall be thoroughly mixed with the clay soil using a rotary speed mixer until a uniformity of moisture content is achieved. If necessary to achieve moisture dispersion, the engineer shall direct that the blended soil be allowed to cure followed by additional blending with the rotary speed mixer. When the mixing and blending have been completed, the material shall be deposited on the clay subgrade and spread in a uniform layer which, when compacted, will meet the requirements of thickness.

1.04 Sand Subgrade Moisture Control. The unwashed fill sand shall be deposited in the sand subgrade area and spread evenly to a uniform thickness and width. Water in the amount and as directed by the engineer shall be uniformly applied to the sand during placement, to maintain sufficient moisture content for compaction.

1.05 General Method for Placing. Soil courses shall be constructed in layers. Any layer shall not be less than 3 inches nor more than 8 inches of compacted thickness unless approved by the engineer. The material, as spread, shall be of uniform gradation with no pockets of fine or coarse materials. Each layer shall be checked for density requirements and approved by the engineer before proceeding to the next

layer. During the placing and spreading, sufficient caution shall be exercised to prevent the incorporation of berm or foreign material in the subgrades.

1.06 Finishing and Compacting. After spreading or mixing, the subgrade, subbase or berm materials shall be thoroughly compacted by rolling and resprinkling, when necessary. Rolling shall progress from one side toward previously placed material by lapping uniformly each preceding track by at least 12 inches. The rolling shall continue until the material is thoroughly set and stable, and the materials have been compacted to not less than the following percentages of maximum density as determined by the compaction control test specified in AASHO: T180, Method A (Reference 8).

Item	Percent of Maximum Dry Density
Clay Subgrade	90
Sand Subgrade	100
Lime Stabilized Clay Subbase	93
Embankment	90

2. PLAIN PORTLAND CEMENT CONCRETE PAVEMENT

2.01. General. This work shall consist of a pavement composed of portland cement concrete, without reinforcement, constructed on a prepared subgrade or subbase course in accordance with these specifications and shall conform to the thicknesses and typical cross sections shown on the plans and with lines and grades established by the engineer.

2.02 Aggregates. Aggregates shall meet the gradation requirements of Tables A-1 and A-2.

2.03 Mix Design. The concrete mix shall be designed on the basis of a predetermined cement content. The concrete shall have an admixture added to insure 3,000 psi compressive strength in 7 days. Maximum net water content shall not exceed 6 gallons per bag and the slump shall not be greater than 3 inches.

2.04 Field and Laboratory Tests. For each pavement slab placed, one set each of six, 6 inch by 12 inch cylinders shall be molded in accordance with ASTM C31 (Reference 27). Ultimate compressive strength of three cylinders shall be determined by ASTM C34 (Reference 10) on the day field testing of the slab is accomplished. The remaining cylinders shall be tested upon the discretion of the engineer. All specimens shall be field cured under conditions similar to those experienced by the slab. Tests for entrained air and flexural strength shall not be performed.

Table A-1. Gradation for Fine Aggregate

Sieve	Percentage by Weight Passing Sieves
3/8 in.	100
No. 4	95-100
No. 16	45-80
No. 30	25-55
No. 50	10-30
No. 100	2-10

Table A-2. Gradation for Coarse Aggregate (1 1/2 in. to No. 4)

	Percentage by weight passing sieves						
Sieve	2 inch	1 1/2 inch	1 inch	3/4 inch	3/8 inch	No. 4	No. 8
1 1/2 to 3/4 inch	100	90-100	20-55	0-15	0-5	-	-
3/4 inch to No. 4	-	100	94-97	60-70	4-11	0-1.5	-

2.05 Forms and Form Setting. Forms shall have a depth equal to the prescribed edge thickness of the concrete and shall be provided with adequate devices for secure settings so that when in place they will withstand the vibration and impact attendant to concrete placement. Forms with battered top surfaces, and bent, twisted, or broken forms shall be removed from the work. The top face of the form shall not vary from a true plane more than 1/8 inch in 10 feet. The forms shall contain provisions for locking the ends of abutting sections together tightly for secure setting.

After the forms have been set to correct grade, the grade shall be thoroughly tamped, either mechanically or by hand, at both the inside and outside edges of the form base. Forms shall be staked into place with not less than 5 pins for each 8 foot section. A pin shall be placed at each side of every joint. Form sections shall be tightly locked and shall be free from play or movement in any direction. The diameter of the circular slab formed shall not deviate from specified length by more than 3/4 inch at any point.

The alignment and grade elevations of the forms shall be checked and corrections made by the contractor immediately before placing the concrete. When any form has been disturbed or any grade has become unstable, the form shall be reset and rechecked.

2.06 Mixing Concrete. The time elapsing from the time water is added to the mix at the batch plant until the concrete is deposited in place at the work site shall not exceed 60 minutes. Retempering concrete by adding water or by other means will not be permitted, except if accomplished within 45 minutes after the initial mixing operation. Concrete that is not within the specified slump limits at time of placement shall not be used.

2.07 Placing Concrete. The concrete shall be deposited on the thoroughly moistened grade in such a manner as to require as little rehandling as possible. Necessary hand spreading shall be done with shovels, not rakes. Workmen shall not be allowed to walk in the freshly mixed concrete with boots or shoes coated with earth or foreign substances.

Concrete shall be thoroughly consolidated against and along the faces of all forms and along the full length and on both sides of all joint assemblies by means of vibrators inserted in the concrete. Vibrators shall not be permitted to come into contact with a joint assembly, the grade, or a side form. In no case shall the vibrator be operated longer than 15 seconds in any one location.

Should any concrete materials fall on or be worked into the surface of a completed slab, they shall be removed immediately by approved methods.

2.08 Strike-Off, Consolidation, and Finishing. The sequence of operations shall be the strike-off and consolidation, floating and removal of laitance, straight edging, and final surface finish. The addition of superficial water to the surface of the concrete to assist in finishing operations will not be permitted unless the water is applied to the surface as a fog spray by means of approved spray equipment.

Hand finishing shall be permitted. Concrete, as soon as placed, shall be struck-off and screeded to conform to the cross section shown on the plans and to an elevation such that when the concrete is properly consolidated and finished, the surface of the pavement shall be at the elevation shown on the plans. An approved portable screed shall be used.

The screed shall be at least 2 feet longer than the maximum width of the slab to be struck-off. It shall be of approved design and shall be sufficiently rigid to retain its shape.

Consolidation shall be attained by use of a suitable vibrator or other approved equipment.

After the concrete has been struck-off and consolidated, it shall be further smoothed, trued, and consolidated by means of a float. The float shall be worked with a sawing motion, while held in a floating position parallel to the slab centerline and passing gradually from one side of the pavement to the other. Forward movement shall be in successive advances of not more than one-half the length of the float. Any excess water or soupy material shall be wasted over the side forms on each pass.

After the floating has been completed and the excess water removed, but while the concrete is still plastic, the concrete surface shall be tested for trueness with a 10 foot straight edge. The straight edge shall be held in contact with the surface in successive positions parallel to the centerline and the whole area gone over from one side of the slab to the other, as necessary. Any depressions shall be immediately filled with freshly mixed concrete, struck-off, consolidated and refinished. High areas shall be cut down and refinished. Straight edge testing and surface corrections shall be continued until the entire surface is found to be free from observable departures from the straight edge and until the slab conforms to the required grade and cross section.

The surface of the slab shall be finished with a steel trowel finish. After the final finish, but before the concrete has taken its initial set, the edges of the slab shall be worked and rounded to a radius of 1/4 inch. A well-defined and continuous radius shall be produced and a smooth, dense, mortar finish obtained. The surface of the slab shall not be unduly disturbed by tilting of the tool during use. Any tool marks appearing on the slab adjacent to the joint shall be eliminated. In doing this, the rounding of the edge shall not be disturbed. All concrete on top of the joint filler shall be completely removed.

2.09 Curing. Immediately after the finishing operations have been completed and marring of the concrete will not occur, the entire surface of the newly placed concrete shall be cured by entirely covering the top surface and sides of the slab with polyethylene sheeting. The units used shall be lapped at least 18 inches. The sheeting shall be placed and weighted to remain in intimate contact with the surface covered. The sheeting, as placed, shall extend beyond the slab edges at least twice the slab thickness. The covering shall remain in place for 3 days after he concrete has been placed.

2.10 Removing Forms. Forms shall not be removed from freshly placed concrete until it has set for at least 24 hours. Forms shall be removed carefully to avoid damage to the pavement.

3. BITUMINOUS BASE COURSE

3.01 General. This item shall consist of a base course composed of mineral aggregate and bituminous material, mixed in a central mixing plant and placed on a prepared course in accordance with these specifications and in conformity with the dimensions shown on the plans and with lines and grades established by the engineer.

3.02 Composition of Mixture. The mineral aggregate for the base course shall be of such size that the percentage composition by weight will conform to the following:

Sieve Designation	Percentage by Weight Passing Sieves
1 inch	100
3/4 inch	82-100
1/2 inch	70-90
3/8 inch	60-82
No. 4	42-70
No. 10	30-60
No. 40	15-40
No. 80	8-26
No. 200	3-8

Asphalt Cement: 4.5-6.5 percent

3.03 Spreading and Laying. The base course shall be constructed in lifts not to exceed three inches in thickness. The mixture shall be dumped on the subgrade and distributed into place using hot shovels. It shall be spread with hot rakes in a uniformly loose layer to the full width required and of such depth that, when the work is completed, it will have the required thickness and will conform to the grade and surface contour

shown on the plans. Grade control may be accomplished with wood forms staked in lanes parallel to the pavement centerline. Forms shall be removed prior to rolling.

3.04 Compaction. After spreading, the mixture shall be thoroughly and uniformly compacted with power rollers. Rolling of the mixture shall begin as soon after spreading as it will bear the roller without undue displacement or hair checking. Successive trips of the roller shall overlap. The speed of the roller shall be slow to avoid displacement of the hot mixture.

Rolling shall continue until all roller marks are eliminated and the surface is of uniform texture and is true to grade and cross section. Field density tests shall be made on the completed base course.

3.05 Surface Tests. The finished surface shall not vary more then 3/8 inch when tested with a 10 foot straight edge applied parallel with, or at right angles to, the centerline.

4. LIME TREATED SUBGRADE

4.01 General. This item shall consist of constructing one course of clay soil, lime and water in accordance with this specification, and in conformity with the lines, grades and thicknesses established by the engineer.

Hydrated lime shall be used and shall conform to the requirements of ASTM C-206, Type S (Reference 29). Water used for mixing or curing shall be of potable quality. The soil for this work shall consist of a fat clay (CH) and shall be uniform in quality and shall be free of roots, sod, weeds, and stones larger than 2-1/2 inches.

At final compaction, the lime and water content shall conform to the following tolerances:

Lime	$\pm$0.5%
Water	+2%, -0%

4.02 Mixing. Clay soil shall be pulverized prior to mixing such that 80 percent of clods will pass a 1-1/2 inch sieve. Clay, lime and water shall be batched in measured quantities in a mixing machine approved by the engineer. After batching, the stabilized clay shall be deposited on the subgrade and water content shall be maintained at above optimum moisture for a minimum of 48 hours. After curing, the material shall be mixed by rototiller so that a minimum of 100 percent of clods will pass a 1-1/2 inch sieve and a minimum of 60% of clods will pass a No. 4 sieve.

4.03 Compaction. Compaction shall begin immediately after final mixing and shall continue until the entire depth of mixture is uniformly compacted to a density of at least 93% of maximum density at optimum moisture as determined by ASSHO T180 (Reference 8). After compaction it shall be trimmed with a motor grader to the grade specified by the engineer. The completed section shall be finished by rolling with a light roller. The finished subgrade surface shall not vary more than 1/2 inch when tested with a 10 foot straight edge.

APPENDIX B

FIELD TEST DATA

PART B-1

TEST SECTION MEASUREMENTS AS CONSTRUCTED

The Civil Engineering Laboratory's Pavement Test Facility contains two test sites, A and B. Site A contains a sand subgrade (SW, E-1) having the properties shown in Table B-1 and Figures B-1 and B-2. Site B contains a clay subgrade (CH, E-10) having the properties shown in Tables B-2 and B-3 and Figures B-3 and B-4.

Test results on the portland cement concrete pavements are given in Table B-4.

Table B-1. Sand Subgrade, Construction Data Summary

Elevation (ft)	Depth, z (ft)	W (%)	γ_{dry} (pcf)	γ_{wet} (pcf)	Void Ratio, e	Saturation, S (%)	Remarks
14.07	-7.51	6.6	115.6	123.2	0.43	40.5	Bottom Pit A
14.18	-7.40	10.7	109.8	121.5	0.51	55.8	lift no. 1
14.47	-7.11	7.4	114.7	123.2	0.44	44.5	lift no. 2
14.88	-6.70	6.1	115.5	122.5	0.43	37.2	lift no. 3
15.14	-6.44	7.2	119.1	127.7	0.39	49.3	lift no. 4
15.88	-5.70	7.1	115.7	123.9	0.43	43.8	lift no. 5
16.37	-5.21	7.1	124.4	133.2	0.33	56.9	lift no. 6
16.67	-4.91	9.5	119.3	130.6	0.39	65.0	lift no. 7
17.23	-4.35	6.5	116.6	124.2	0.42	41.3	lift no. 8
17.45	-4.13	8.3	118.5	128.3	0.40	55.4	lift no. 9
17.83	-3.75	9.2	118.1	129.0	0.40	61.1	lift no. 10
18.17	-3.41	8.0	114.7	123.9	0.44	48.1	lift no. 11
18.65	-2.93	10.0	123.9	136.3	0.34	79.3	lift no. 12
19.26	-2.32	7.1	122.3	131.0	0.35	53.5	lift no. 13
20.21	-1.37	7.1	124.4	133.2	0.33	56.9	lift no. 14
20.96	-0.62	6.9	118.8	127.0	0.39	46.7	lift no. 15
21.58	0.00	7.0	123.3	131.9	0.34	54.2	lift no. 16, top of subgrade

Note: 1. Depth, z, computed from subgrade finish surface elevation.
2. G_s for fill sand estimated to be 2.65.

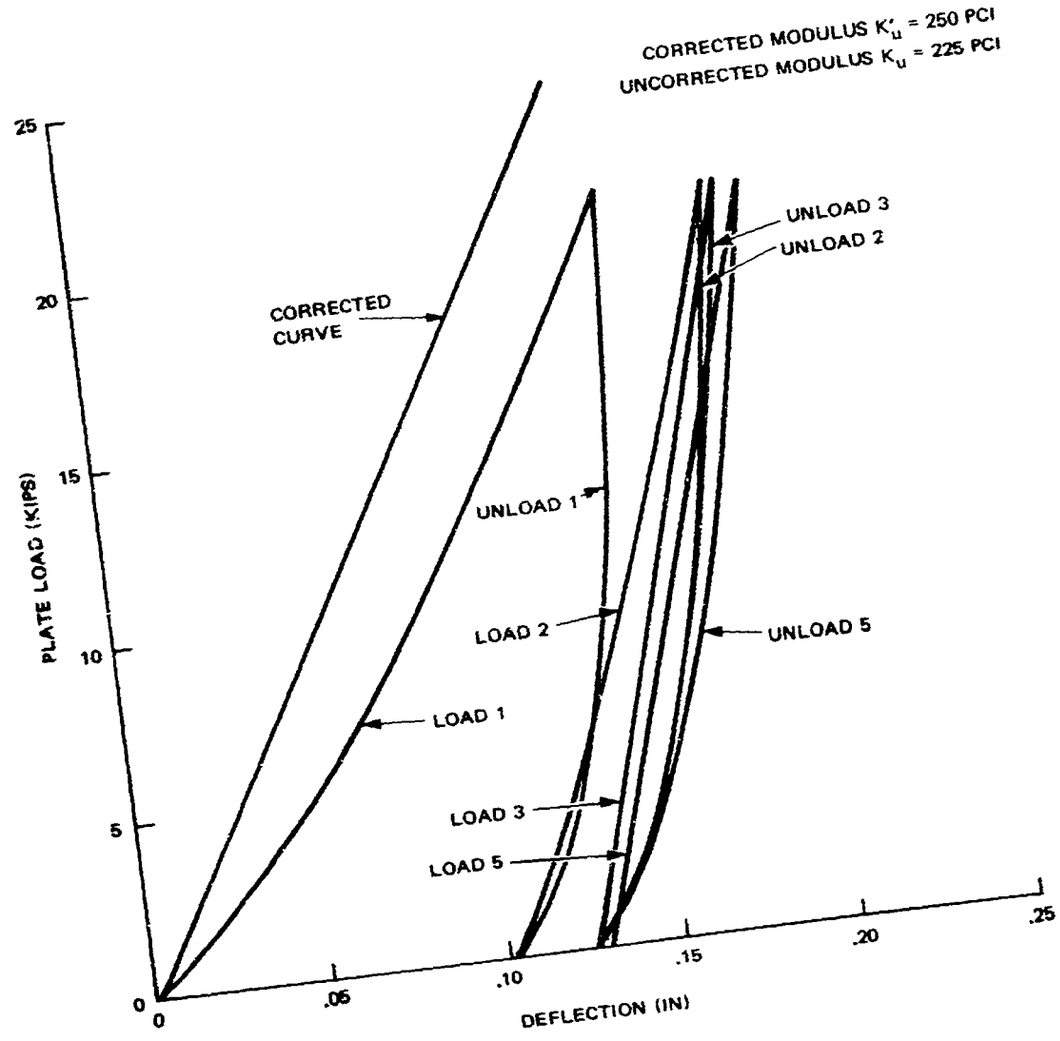

Figure B-1. Plate Load Versus Deflection at Bottom of Sand Subgrade, Elevation 13.94

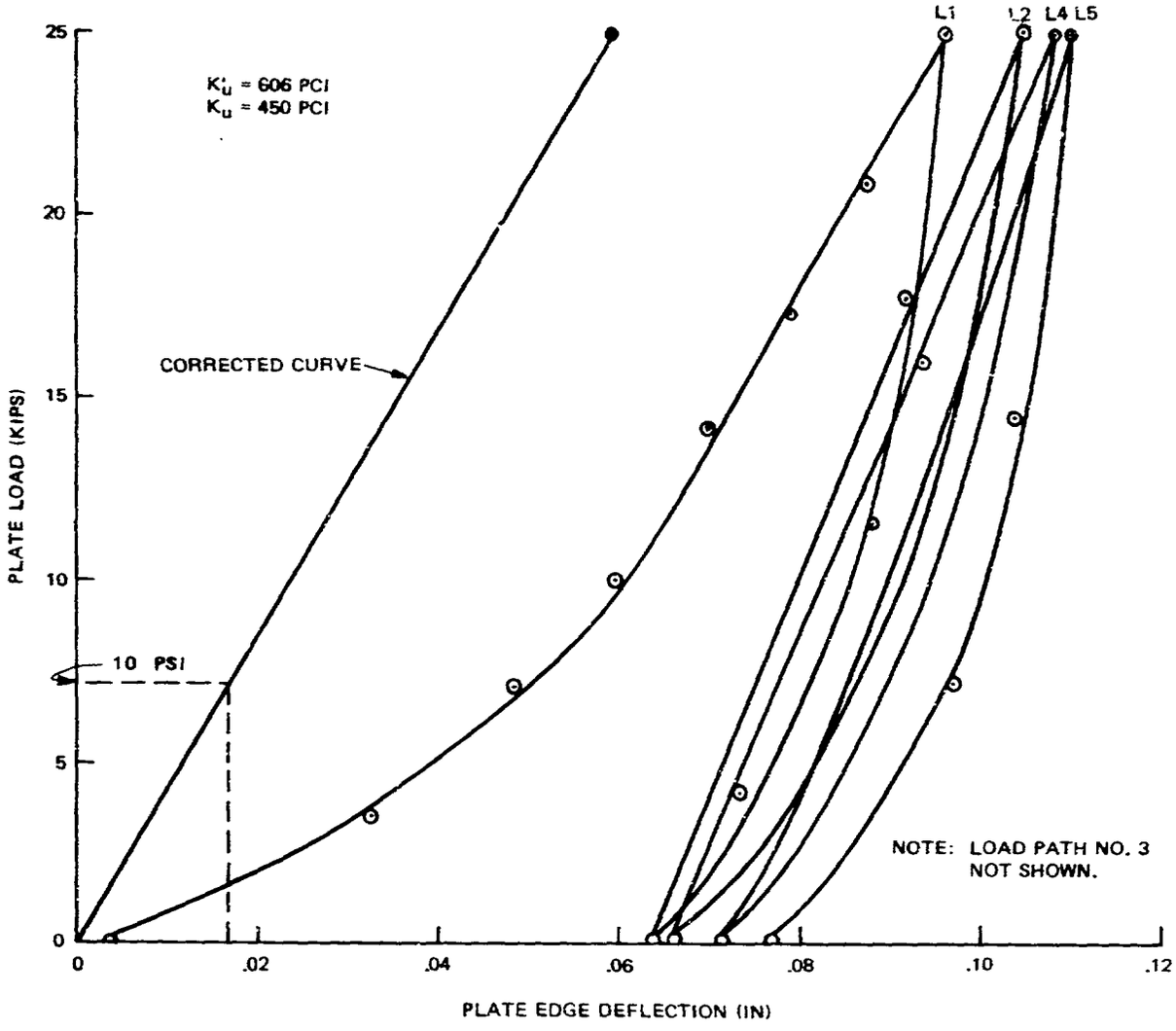

Figure B-2. Plate Load Versus Deflection at Surface of Sand Subgrade, Elevation 21.58

Table B-2. Clay Subgrade, Construction Data Summary

Elevation (ft)	Depth, z (ft)	W (%)	γ_{dry} (pcf)	γ_{wet} (pcf)	Void Ratio, e	Saturation, S (%)	Remarks
12.23	-8.32	6.6	117.9	125.7	0.40	43.6	Subgrade Bottom Unwashed Fill Sand
12.98	-7.57	14.6	94.6	108.2	0.79	49.2	2nd lift
14.39	-6.16	14.6	97.3	111.5	0.74	53.3	5th lift
14.66	-5.89	14.8	92.8	106.6	0.83	48.8	6th lift
15.22	-5.33	15.6	96.4	111.5	0.76	56.0	7th lift
15.83	-4.72	16.9	92.9	108.6	0.83	55.6	8th lift
16.60	-3.95	16.9	95.6	111.7	0.78	59.1	9th lift
17.06	-3.49	17.5	96.3	113.2	0.76	62.5	10th lift
17.57	-2.98	16.5	96.1	112.0	0.77	58.7	11th lift
18.22	-2.33	16.3	98.9	115.0	0.72	61.8	12th lift
18.81	-1.74	15.8	97.0	112.3	0.75	57.2	13th lift
19.41	-1.14	16.4	98.1	114.2	0.73	61.2	14th lift
20.01	-0.54	14.4	101.0	115.5	0.68	57.4	15th lift
20.55	0.00	15.4	100.0	115.4	0.70	60.1	16th lift Finish elevation
20.55	0.00	15.0	99.0	113.8	0.71	56.9	Location of Plate Test on Clay Surface

Note: 1. $G_s = 2.72$ (clay)
2. Depth, z, computed from clay finish surface elevation.

Table B-3. Clay Subgrade Boundary, Construction Data Summary

Elevation (ft)	Depth, z (ft)	W (%)	γ_{dry} (pcf)	γ_{wet} (pcf)	Void Ratio, e	Saturation, S (%)
14.66	-5.89	8.5	102.9	111.6	0.61	36.9
15.13	-5.42	6.9	106.6	114.0	0.55	33.4
16.60	-3.95	11.4	94.3	105.0	0.75	39.9
17.57	-2.98	5.6	107.7	113.7	0.75	27.6
18.22	-2.33	6.4	110.8	117.9	0.49	34.5
18.91	-1.74	6.2	106.6	113.2	0.55	29.8
19.41	-1.14	5.3	115.8	121.9	0.43	32.6
20.01	-0.54	5.1	107.0	113.1	0.55	27.7

Note: 1. Depth z, computed from clay finish surface elevation.
2. Specific gravity of solids estimated to be 2.65.
3. Boundary material was unwashed fill sand.

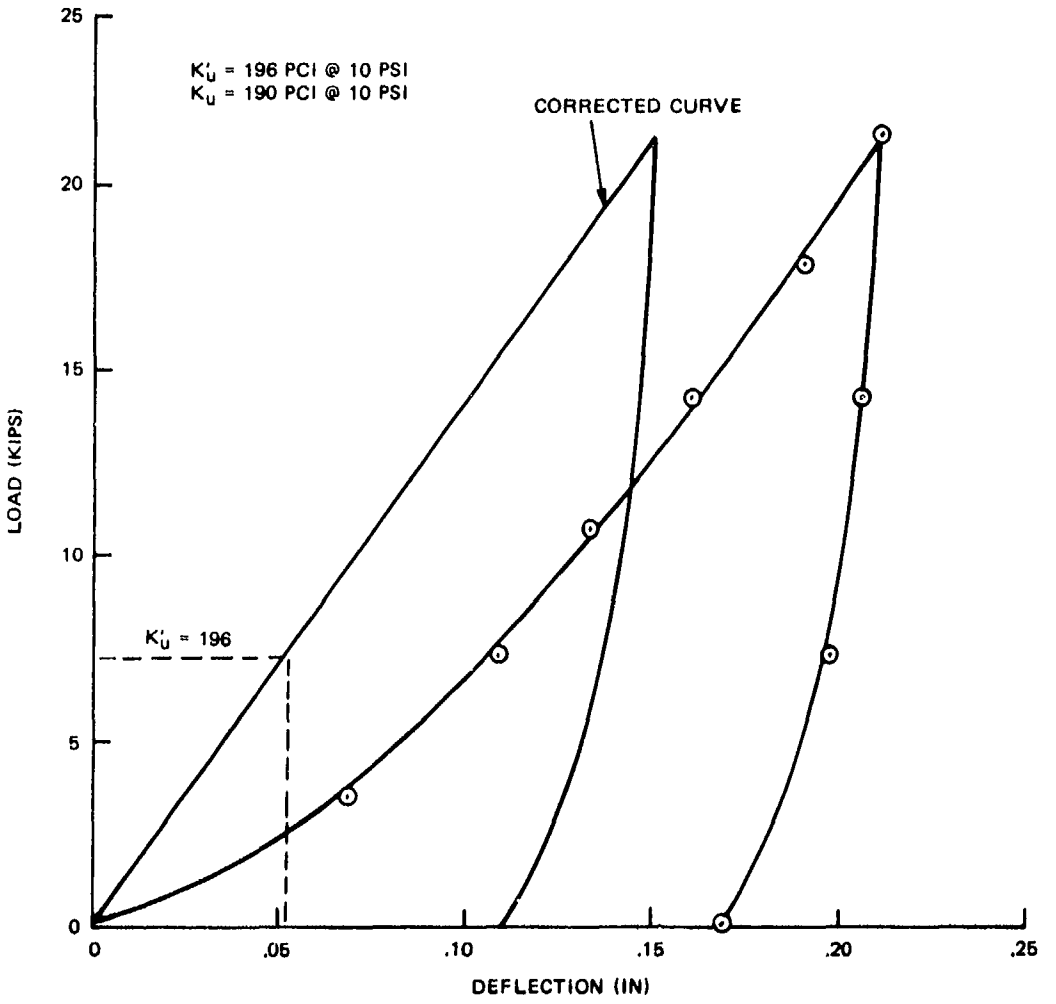

Figure B-3. Plate Load Versus Deflection at Bottom of Clay Subgrade, Elevation 12.23

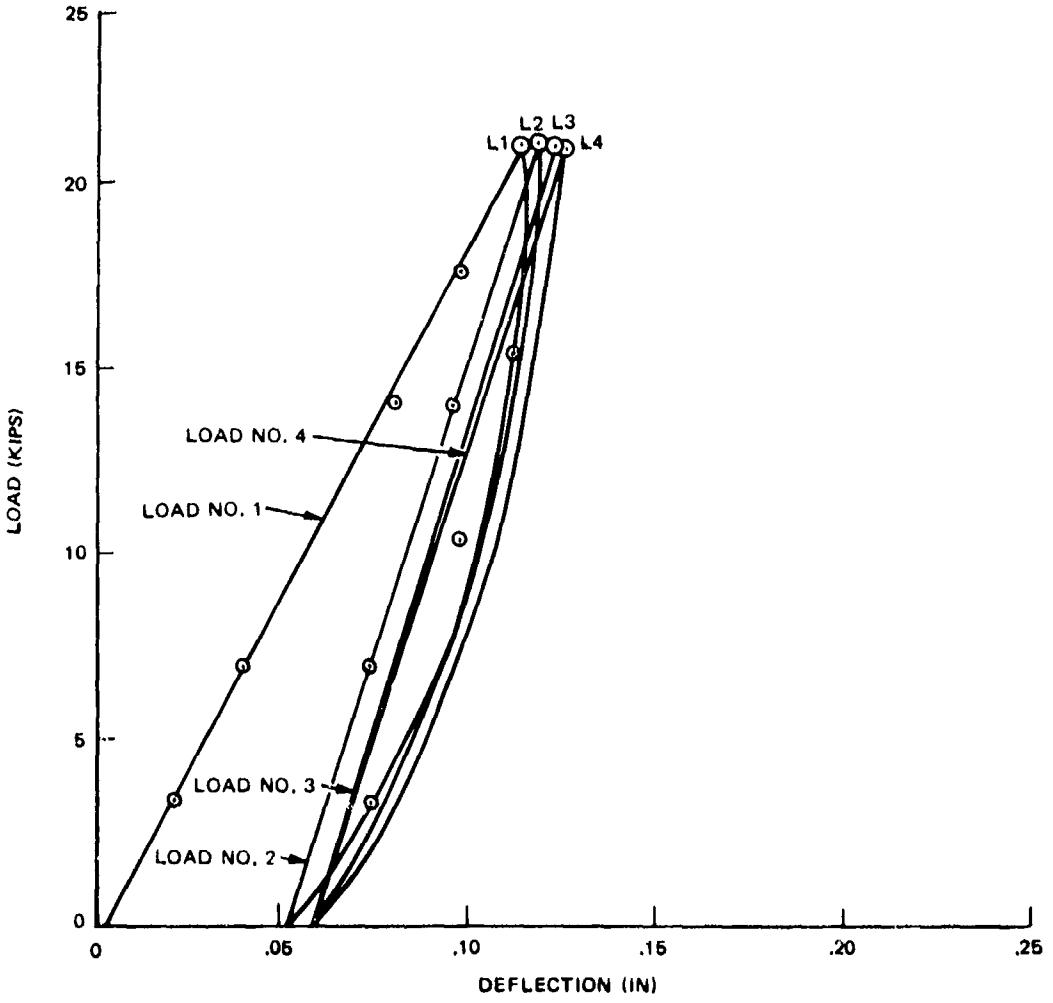

Figure B-4. Plate Load Versus Deflection at Surface of Clay Subgrade, Elevation 20.55

Table B-4. Concrete Pavement Cylinder Data

Test Section	Ultimate Compressive Strength (psi)	Unit Weight (pcf)
A-1	4,130	-
A-2	4,650	145.1
B-1 (cycle 1) (cycle 2) (cycle 3)	3,277 3,640 4,330	- - -
B-2	5,290	145.7

PART B-2

LOAD TEST DATA FOR PAVEMENT SECTION A1

Table B-5. Concrete Strain[a] Gage Data for Test A1

Cycles 1 and 2								
Gage Location	Load Level in KIPS							
	0[b]	30	60	90	45	0	90	0
C1	0	21	78	32	38	47	-	23
C2	0	71	169	1111	775	239	-	-
C3	0	48	74	-18	-09	06	-	-
Cycles 3 and 4								
Gage Location	Load Level in KIPS							
	0[b]	90	0	90	0			
C1	0	-08	11	-09	10			
C2	0	923	25	993	34			
C3	0	-24	17	-15	16			

[a]All strains are given in microinches. Positive strain is tension.

[b]At the beginning of each day's testing, all gages were zeroed.

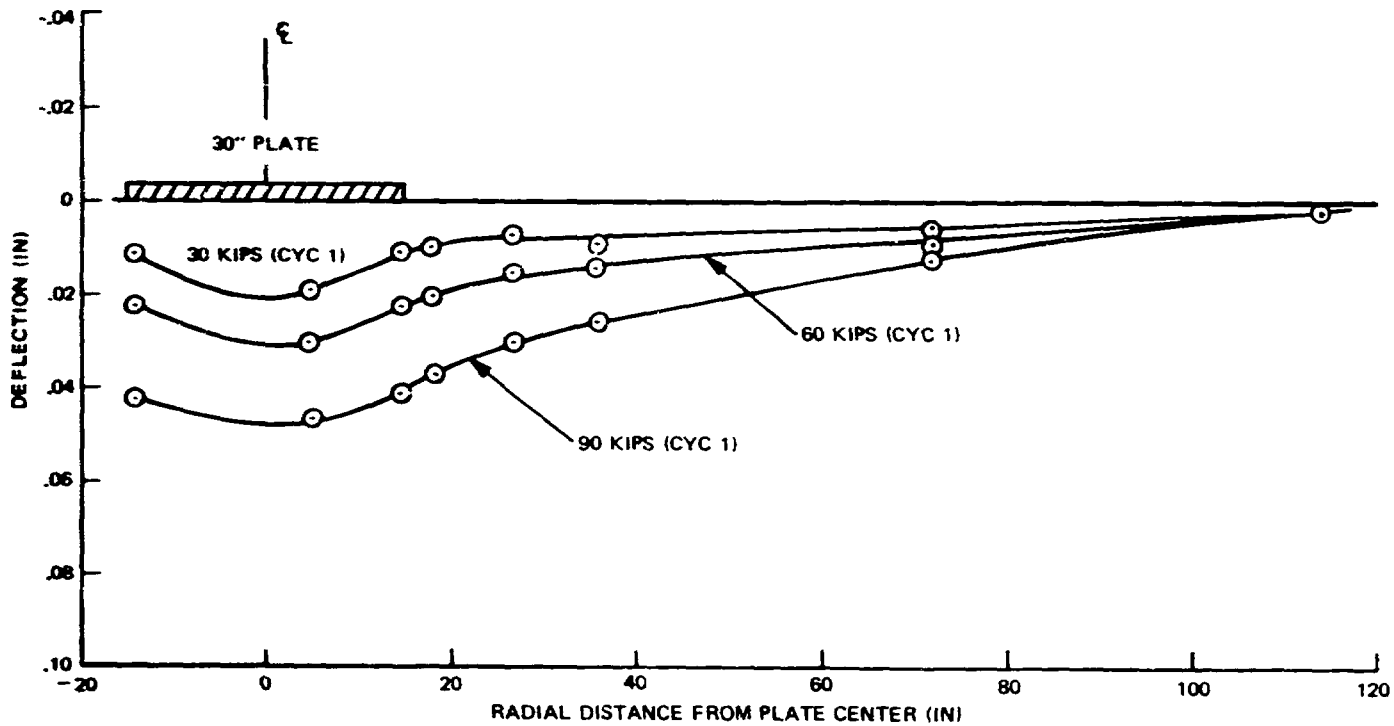

Figure B-5. Deflection Versus Radial Distance, Test A1, Cycle 1

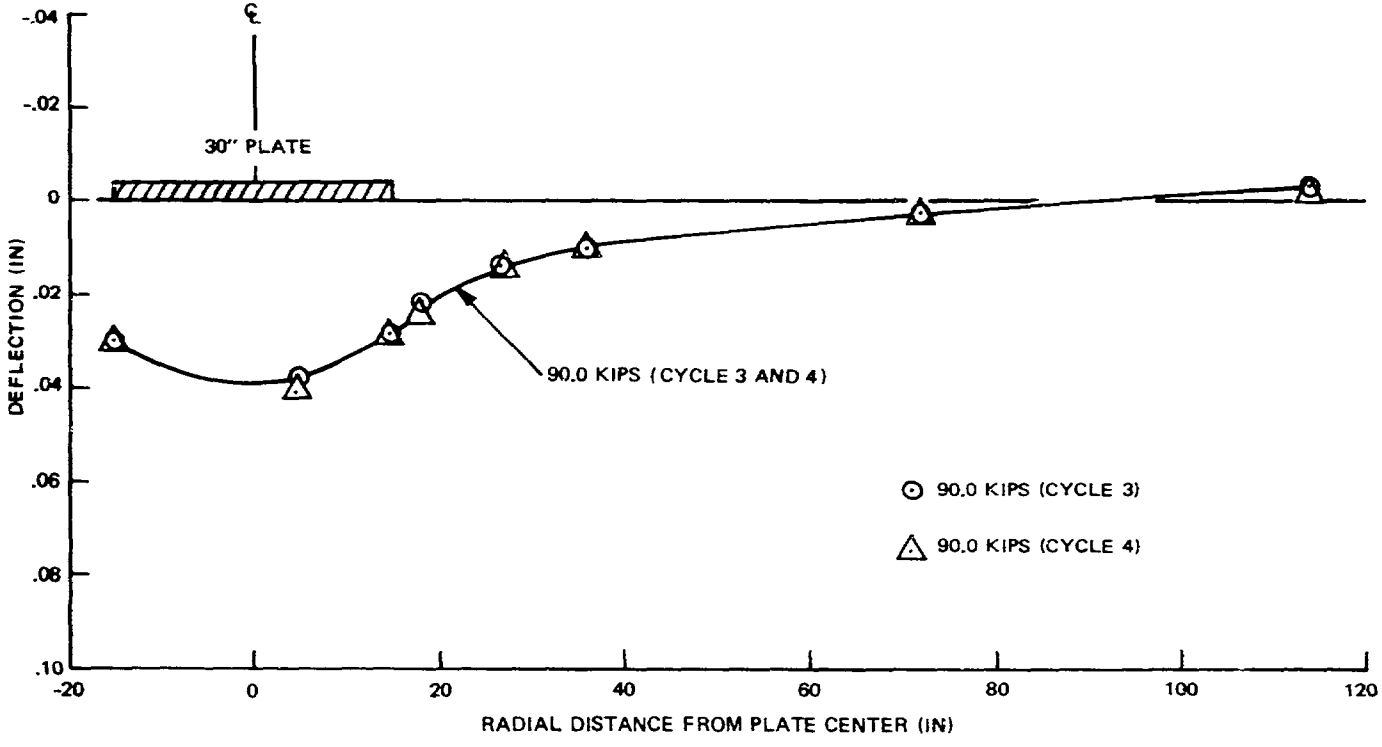

Figure B-6. Radial Distance Versus Deflection, Test A1, Cycles 3 and 4

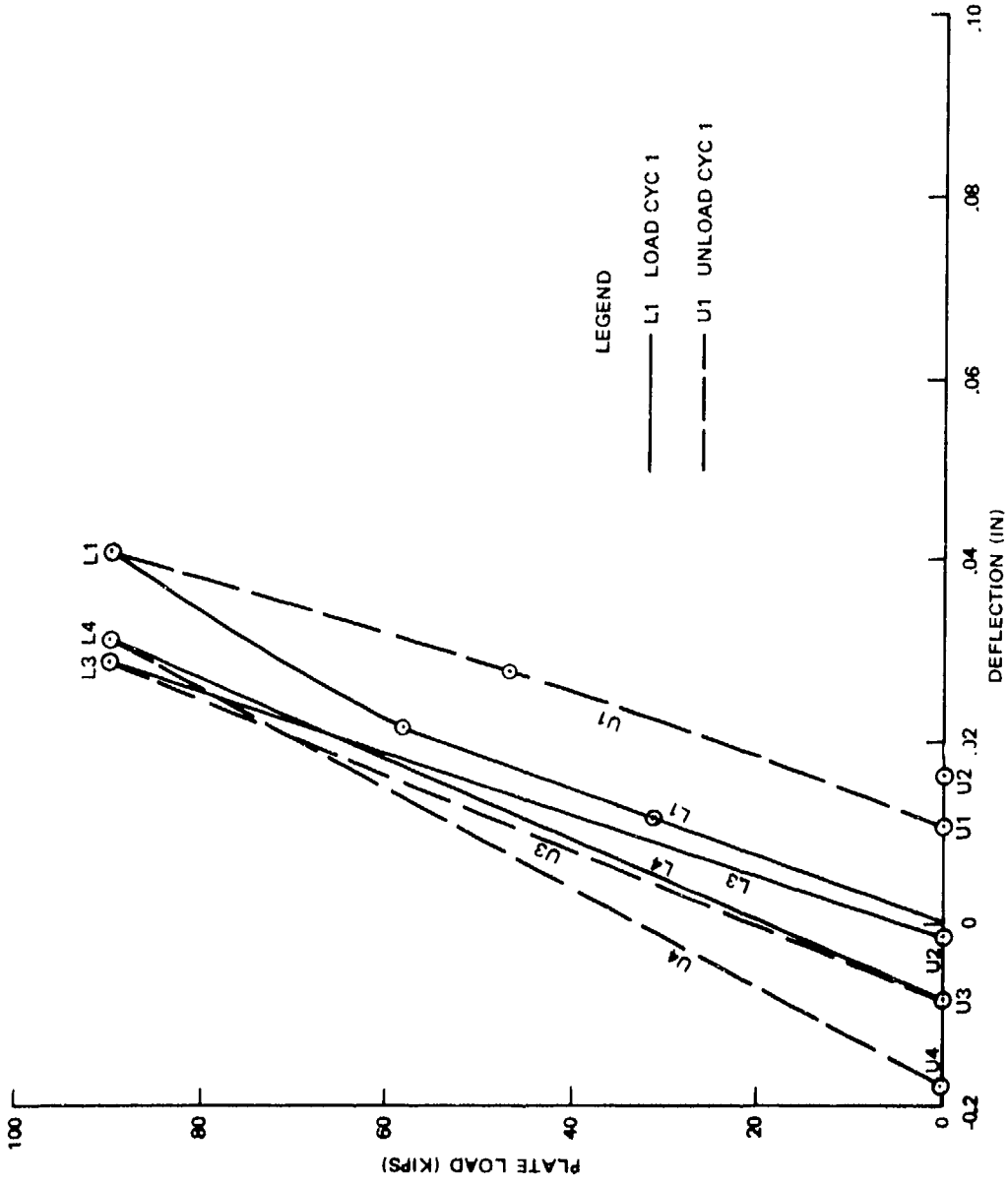

Figure B-7. Average Plate Edge Deflections Versus Plate Load, Test A1, Cycles 1 through 4

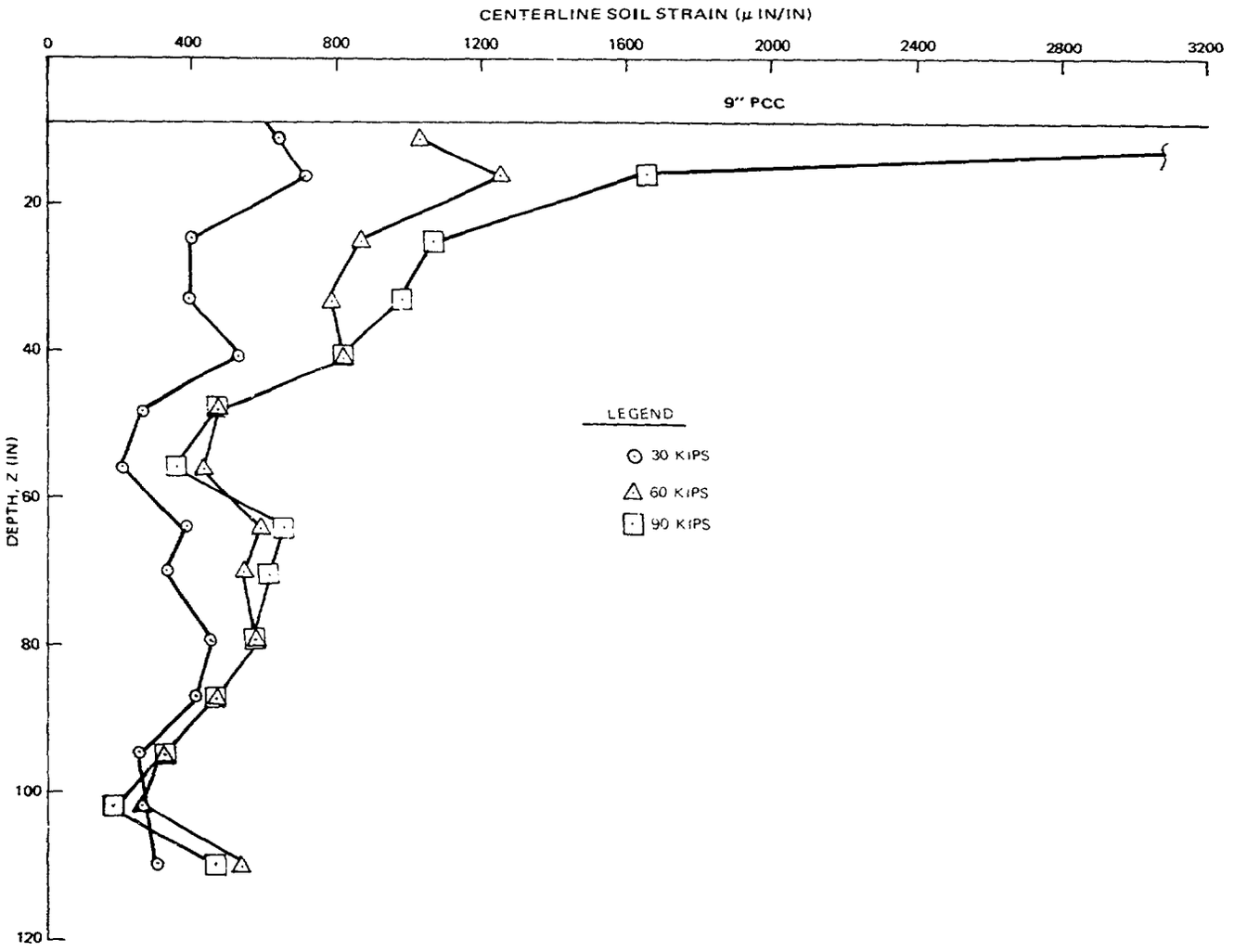

Figure B-8. Centerline Soil Strain Versus Depth, Test A1, Cycle 1

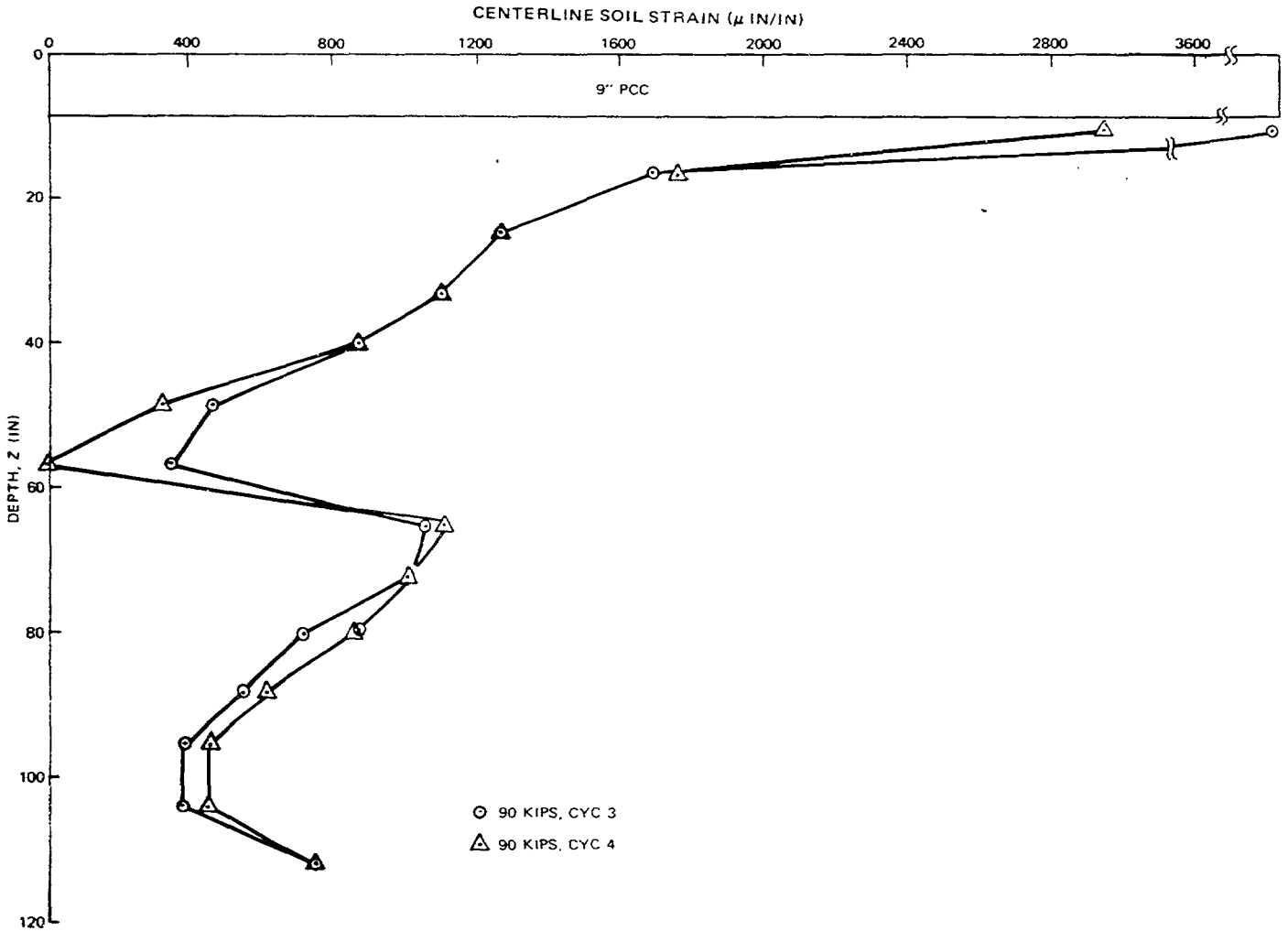

Figure B-9. Centerline Soil Strain Versus Depth, Test A1, Cycles 3 and 4

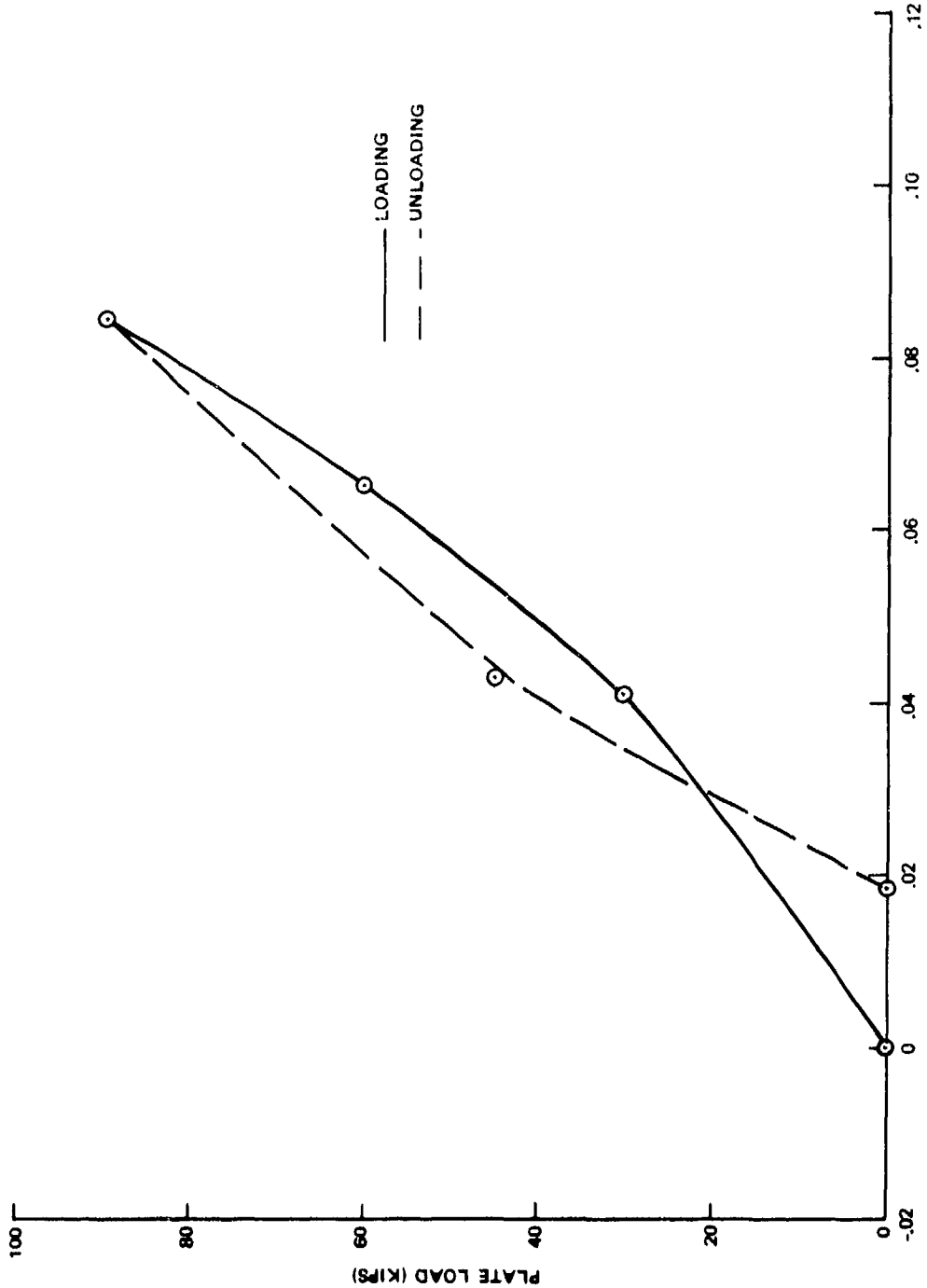

Figure B-10. Summation Centerline Bison Gage Relative Deflections Versus Plate Load, Test A1, Cycle 1

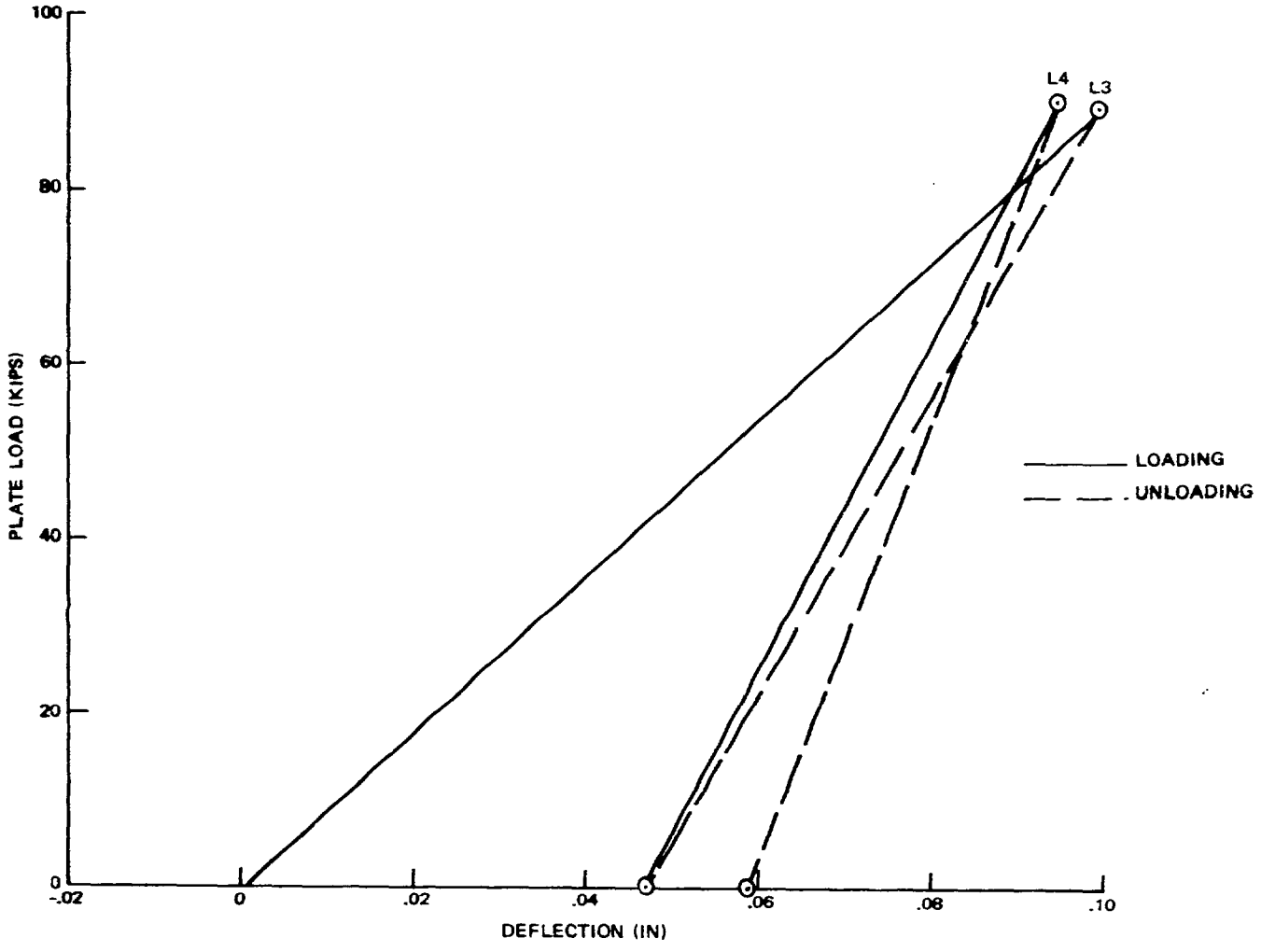

Figure B-11. Summation Centerline Bison Gage Relative Deflections Versus Plate Load, Test A1, Cycles 3 and 4

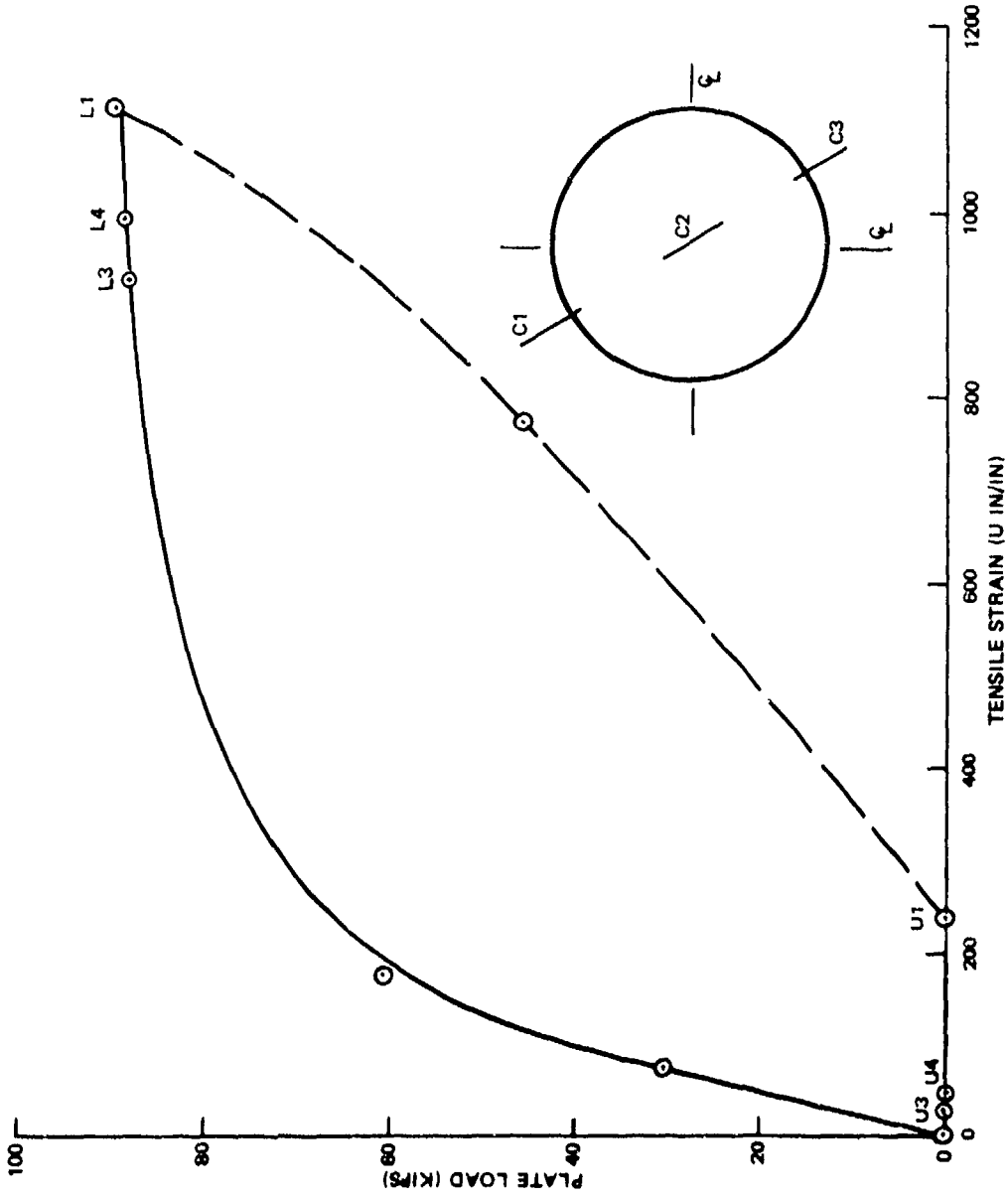

Figure B-12. Concrete Tensile Strain Versus Plate Load, Test A1, Cycles 1, 3, and 4, Gage C2

PART B-3

LOAD TEST DATA FOR PAVEMENT SECTION A2

Table B-6. Concrete Strain[a] Gage Data for Test A2

Cycle 1												
Gage Location	Load Level in KIPS											
	10[b]	45	60	70	80	70	60	45	30	20	10	0
C1	000	604	1025	1302	1687	1623	1517	1316	1052	792	543	299
C2	000	440	729	921	1121	1069	1037	902	727	568	396	206
C3	000	-11	-38	-55	-68	-67	-64	-60	-39	-30	-19	-16
C4	000	16	-1	-24	-30	-30	-40	-42	-26	-21	-15	-17

Cycles 2 and 3						
Gage Location	Load Level in KIPS					
	10[b]	80	10	80	10	
C1	000	1463	262	1607	338	
C2	000	908	165	986	209	
C3	000	-68	-10	-66	-8	

[a]All strains are given in microinches. Positive strain is tension.

[b]At the beginning of each day's testing, all gages were zeroed under a 10 KIP load.

Table B-6. Continued

Gage Location	Cycles 4 and 5								
	Load Level in KIPS								
	10[b]	45	80	45	10	80	10	0	
C1	000	700	1436	1079	299	1536	326	86	
C2	000	442	879	651	183	949	196	68	
C3	000	-35	-67	-65	-14	-71	-13	-7	
C4	000	-13	-24	-28	-3	-30	-4	-8	

[b]At the beginning of each day's testing, all gages were zeroed under a 10 KIP load.

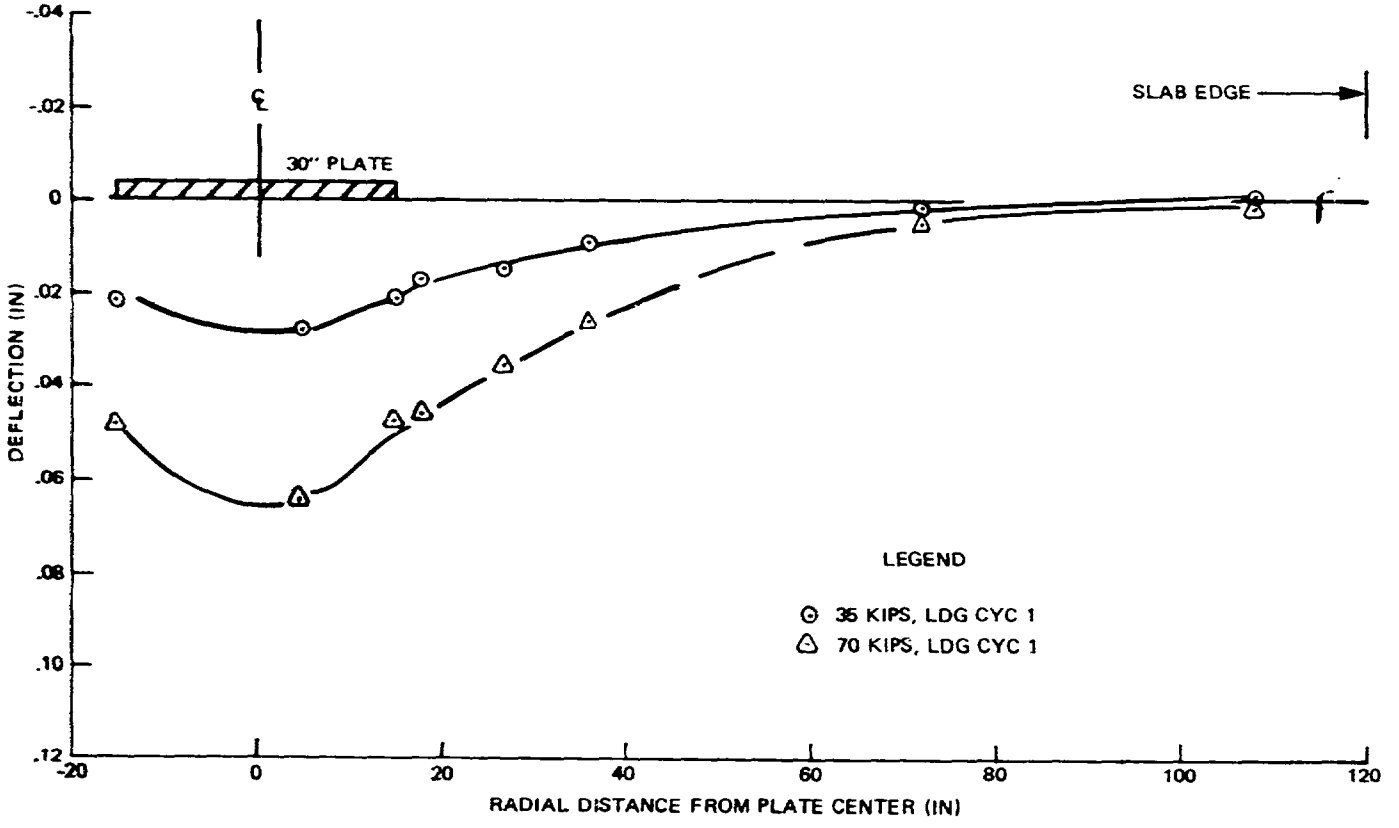

Figure B-13. Radial Distance Versus Deflection, Test A2, 6 Inch AC + 6 Inch PCC, Cycle 1

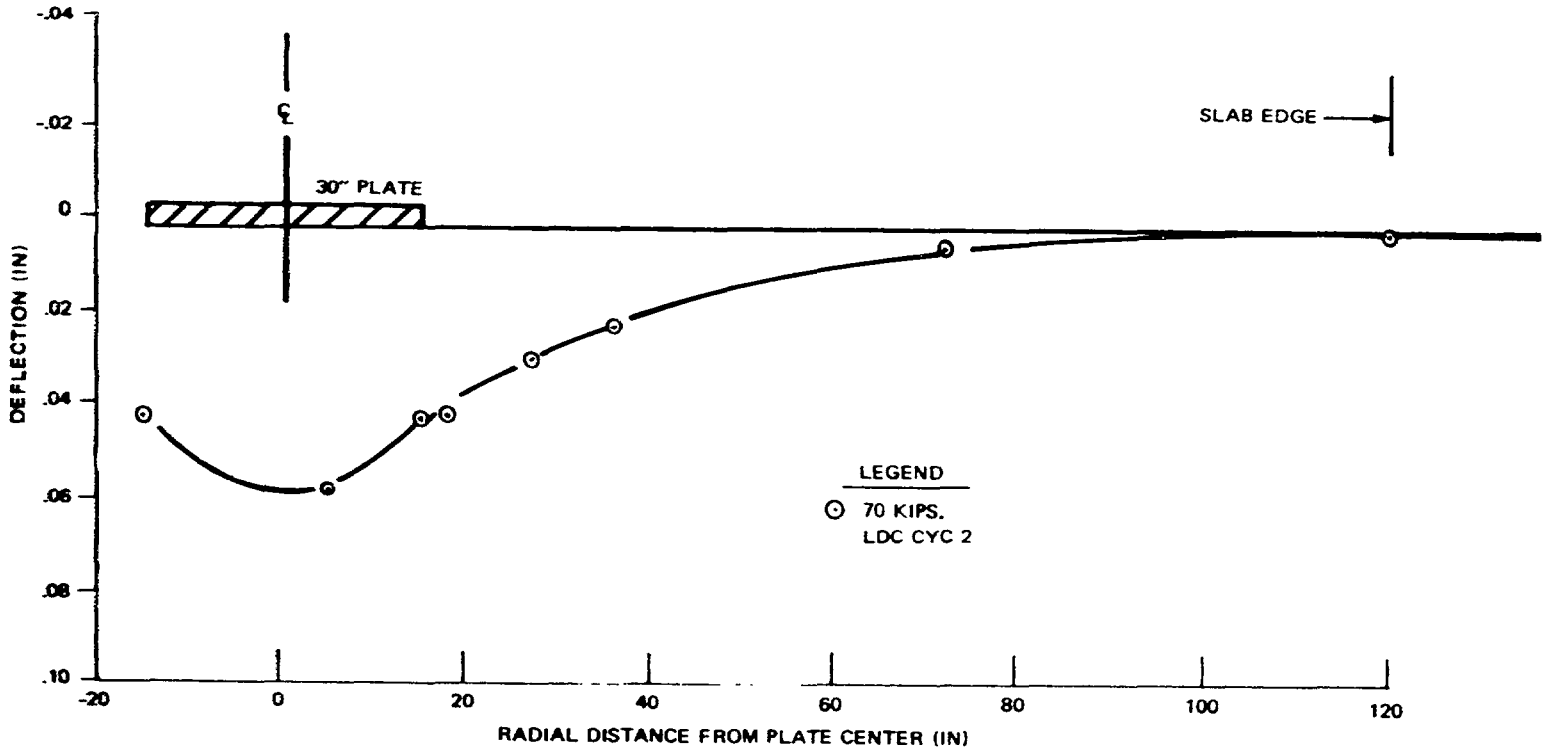

Figure B-14. Radial Distance Versus Deflection, Test A2, 6 Inch AC + 6 Inch PCC, Cycles 2 and 3

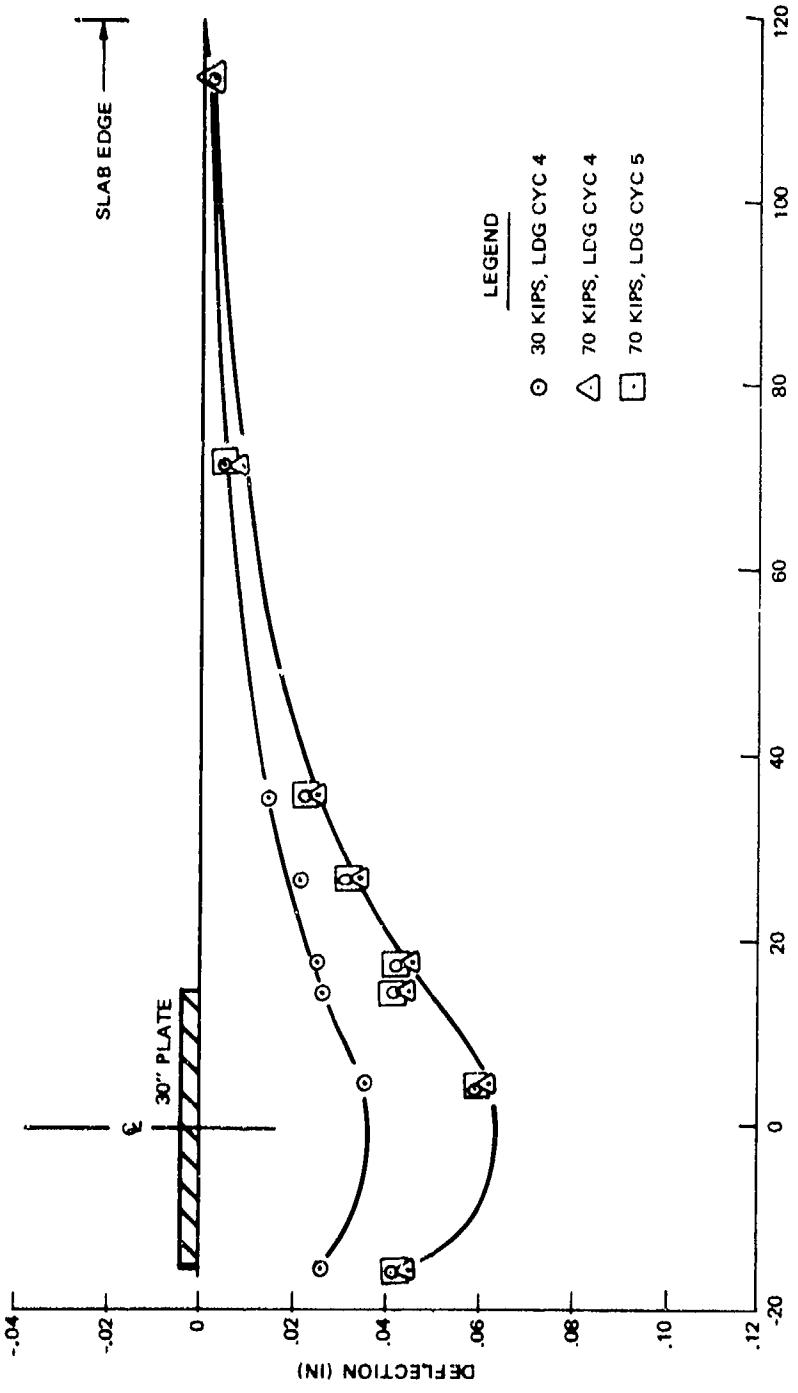

Figure B-15. Radial Distance Versus Deflection, Test A2, 6 Inch AC + 6 Inch PCC, Cycles 4 and 5

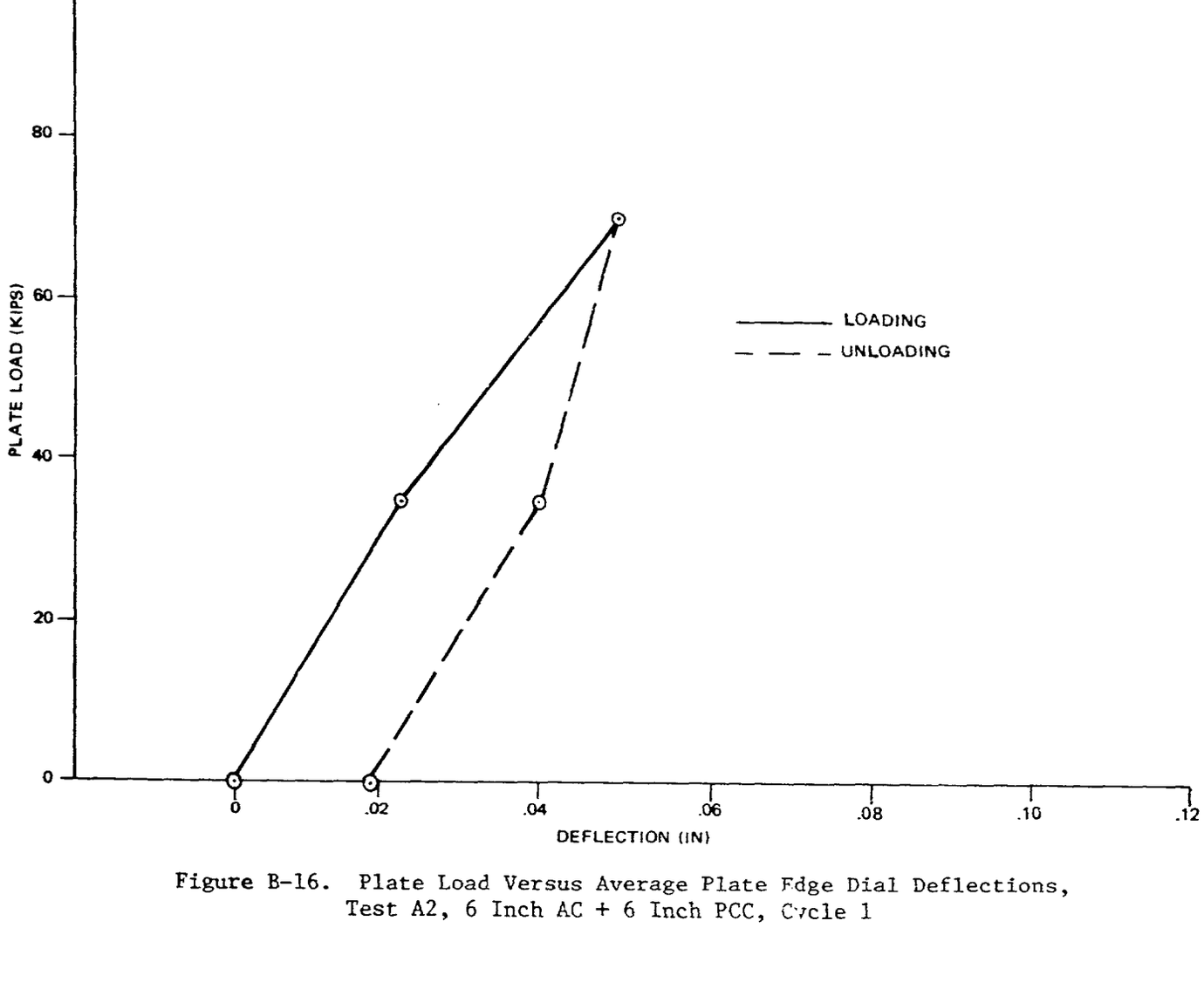

Figure B-16. Plate Load Versus Average Plate Edge Dial Deflections, Test A2, 6 Inch AC + 6 Inch PCC, Cycle 1

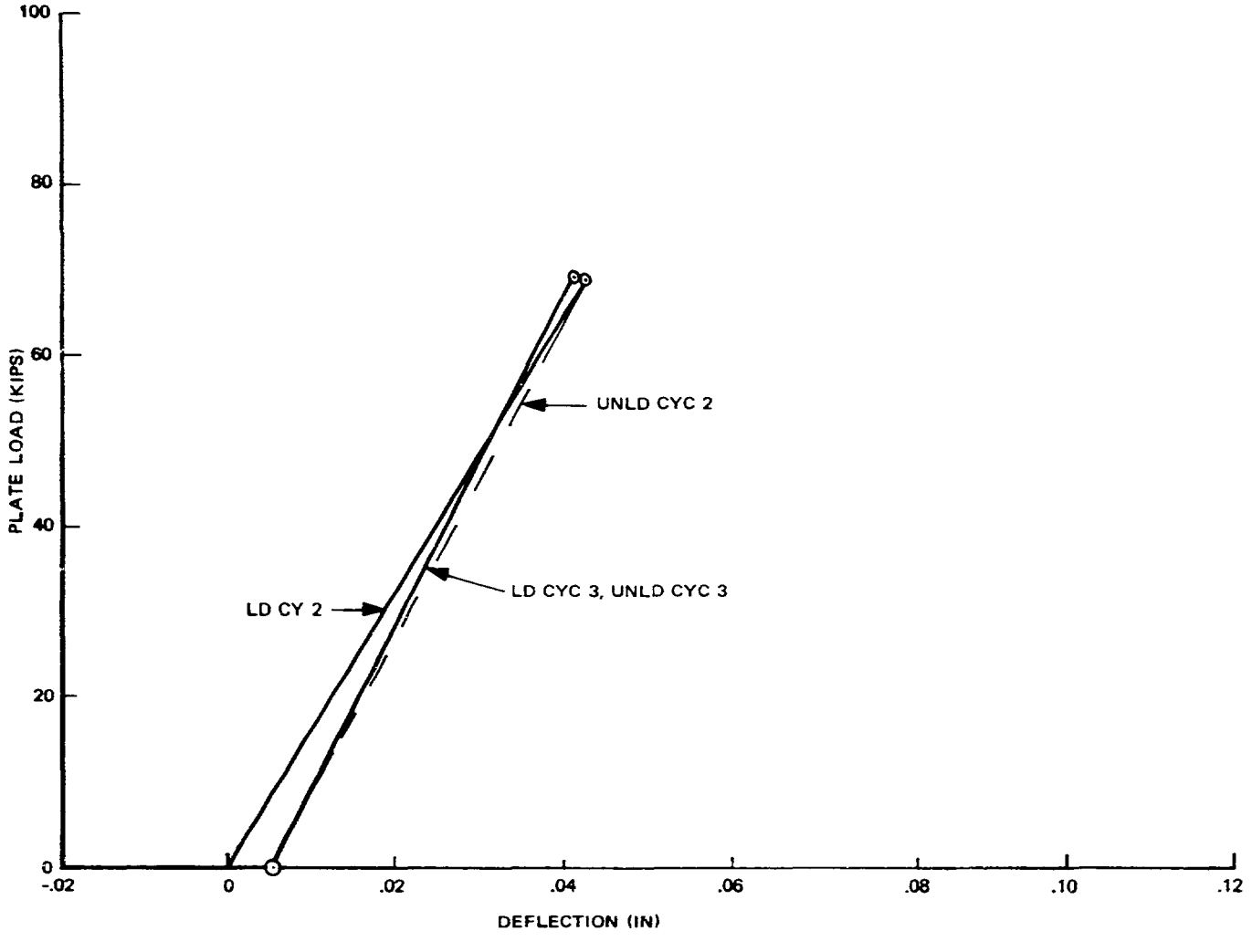

Figure B-17. Plate Load Versus Average Plate Edge Deflections, Test A2, 6 Inch AC + 6 Inch PCC, Cycles 2 and 3

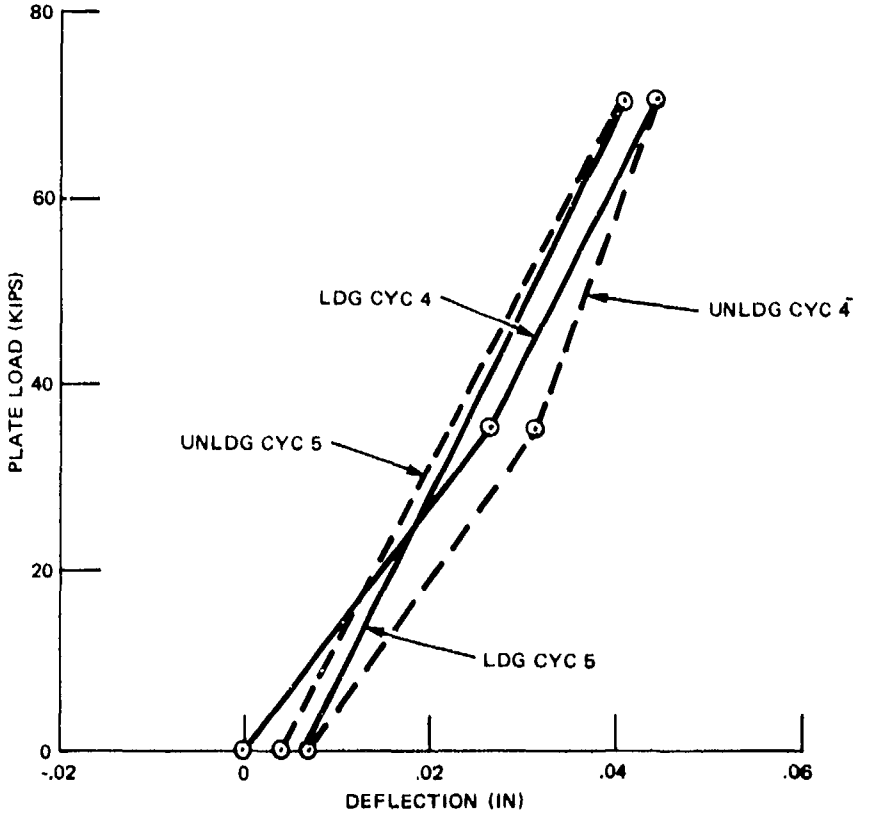

Figure B-18. Average Plate Edge Deflections Versus Plate Load, Test A2, 6 Inch AC + 6 Inch PCC, Cycles 4 and 5

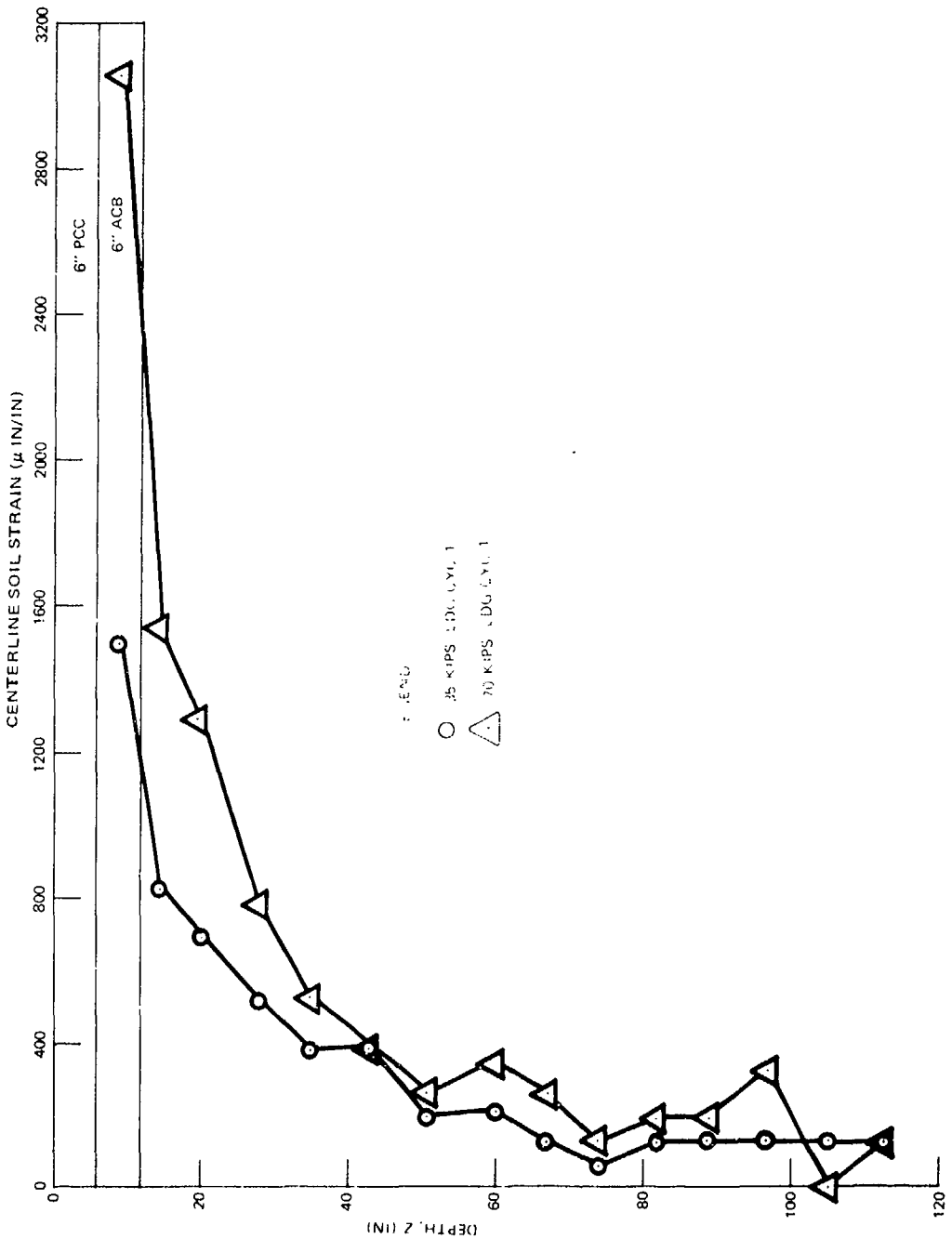

Figure B-19. Centerline Soil Strain Versus Depth, Test A2, 6 Inch AC + 6 Inch PCC, Cycle 1

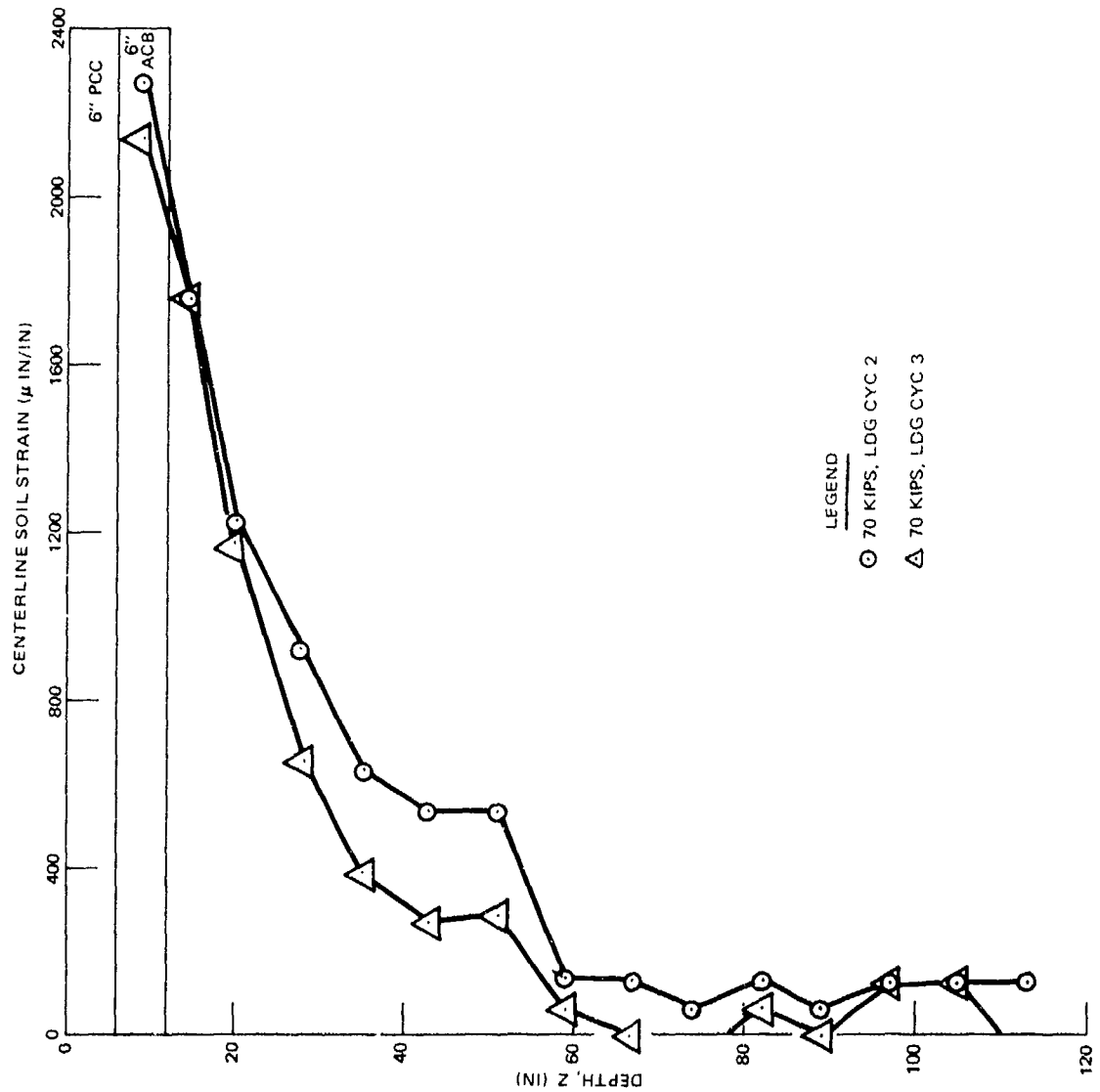

Figure B-20. Centerline Soil Strain Versus Depth, Test A2, 6 Inch AC + 6 Inch PCC, Cycles 2 and 3

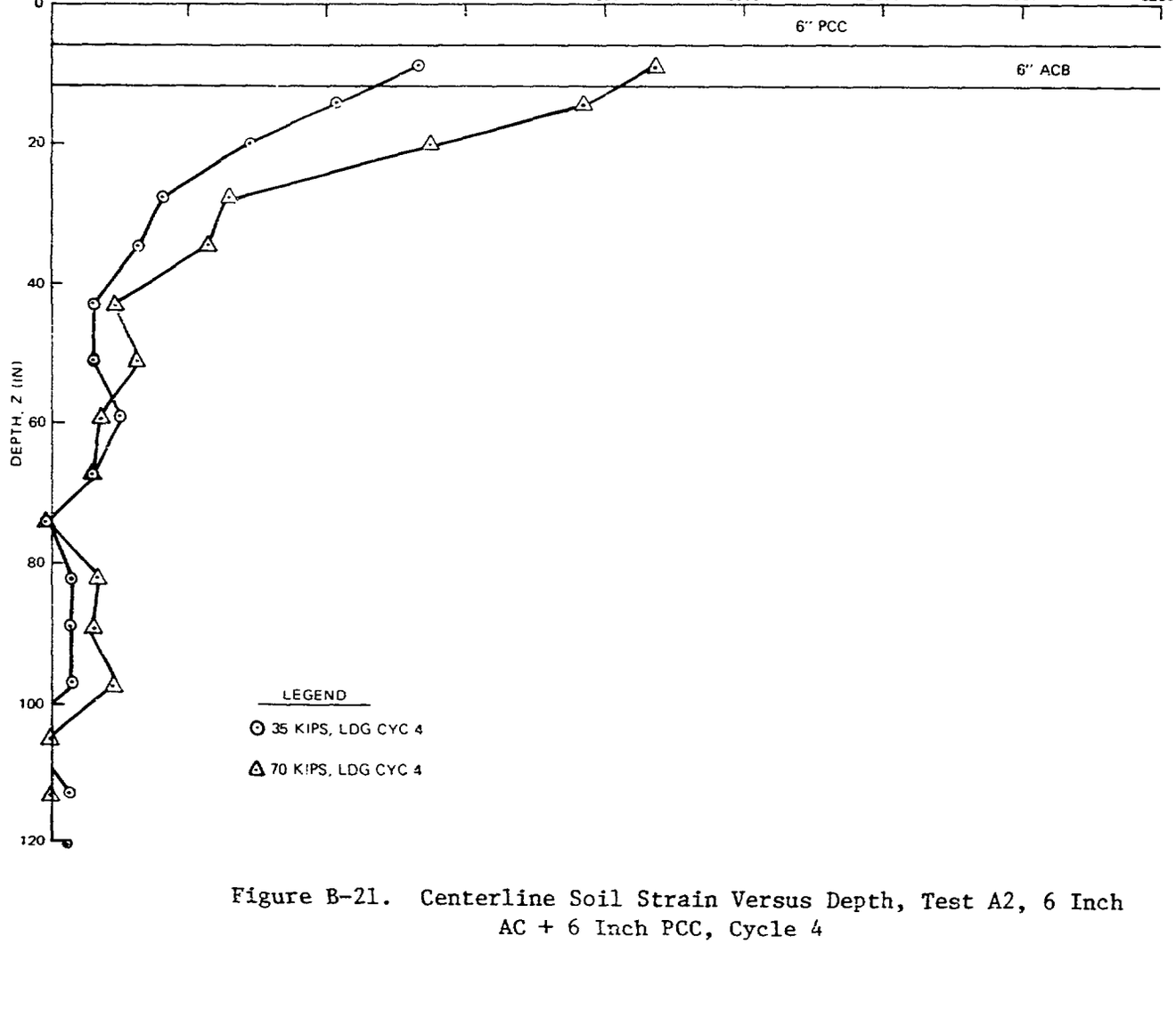

Figure B-21. Centerline Soil Strain Versus Depth, Test A2, 6 Inch AC + 6 Inch PCC, Cycle 4

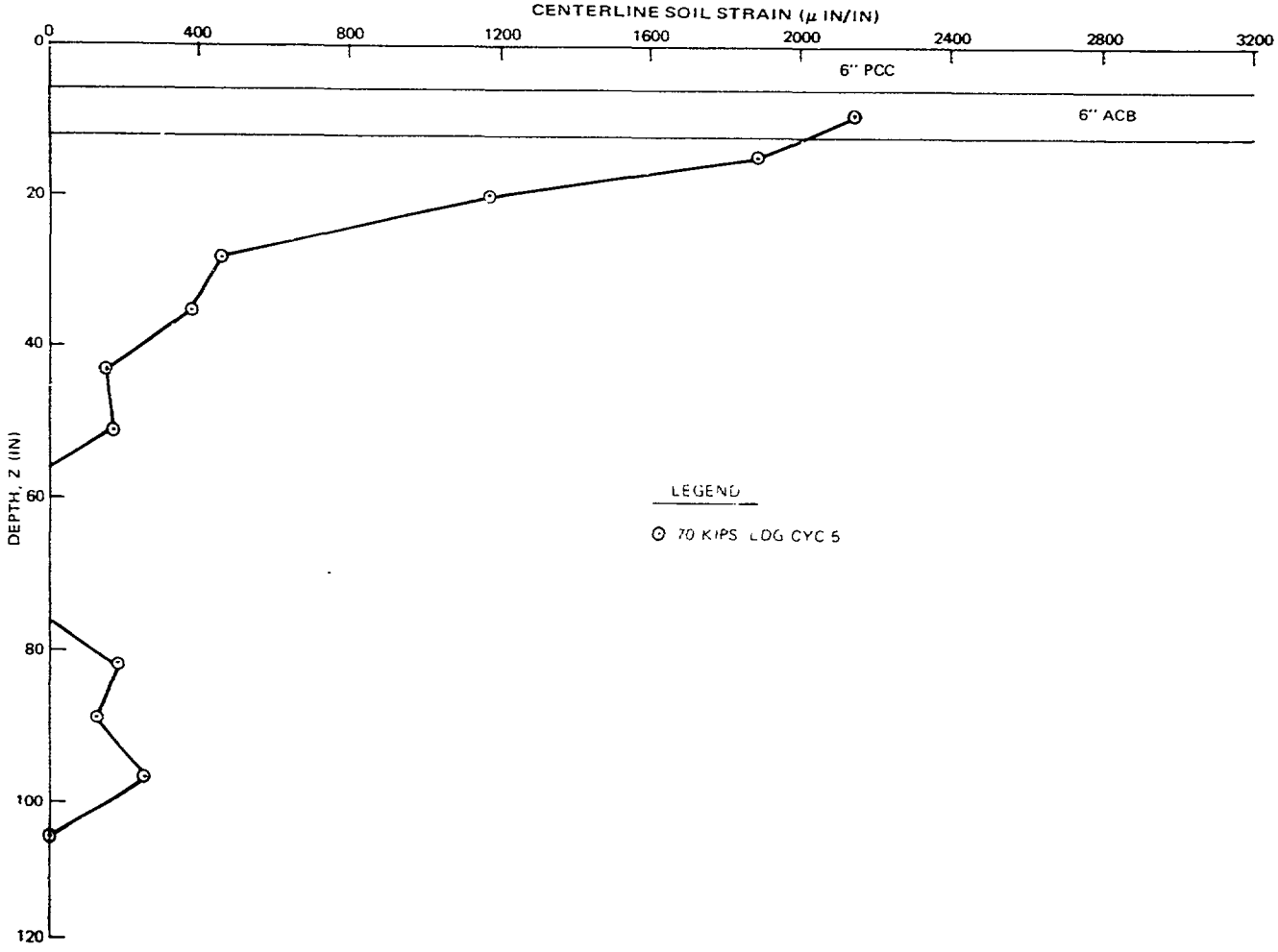

Figure B-22. Centerline Soil Strain Versus Depth, Test A2, 6 Inch AC + 6 Inch PCC, Cycle 5

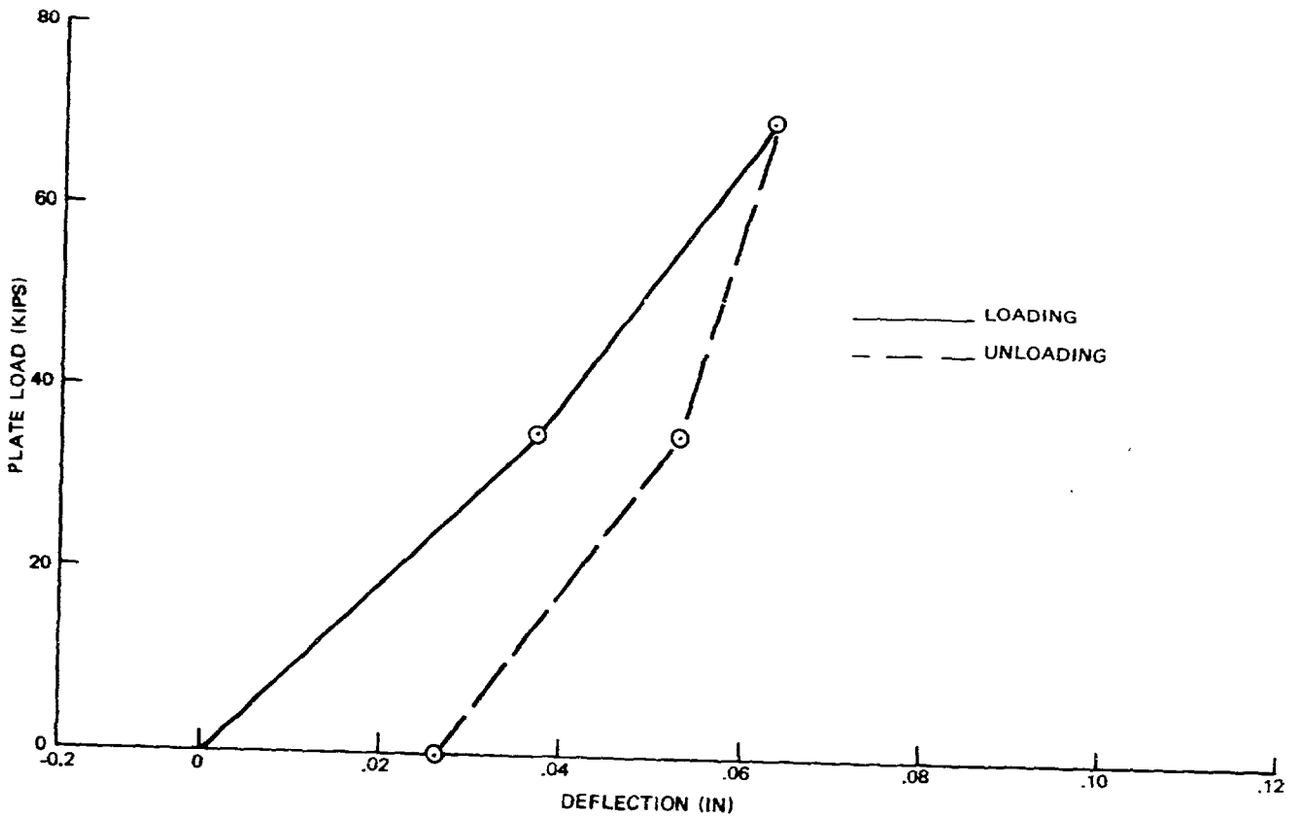

Figure B-23. Plate Load Versus Summation Centerline Bison Gage Relative Deflections, Test A2, 6 Inch AC + 6 Inch PCC, Cycle I

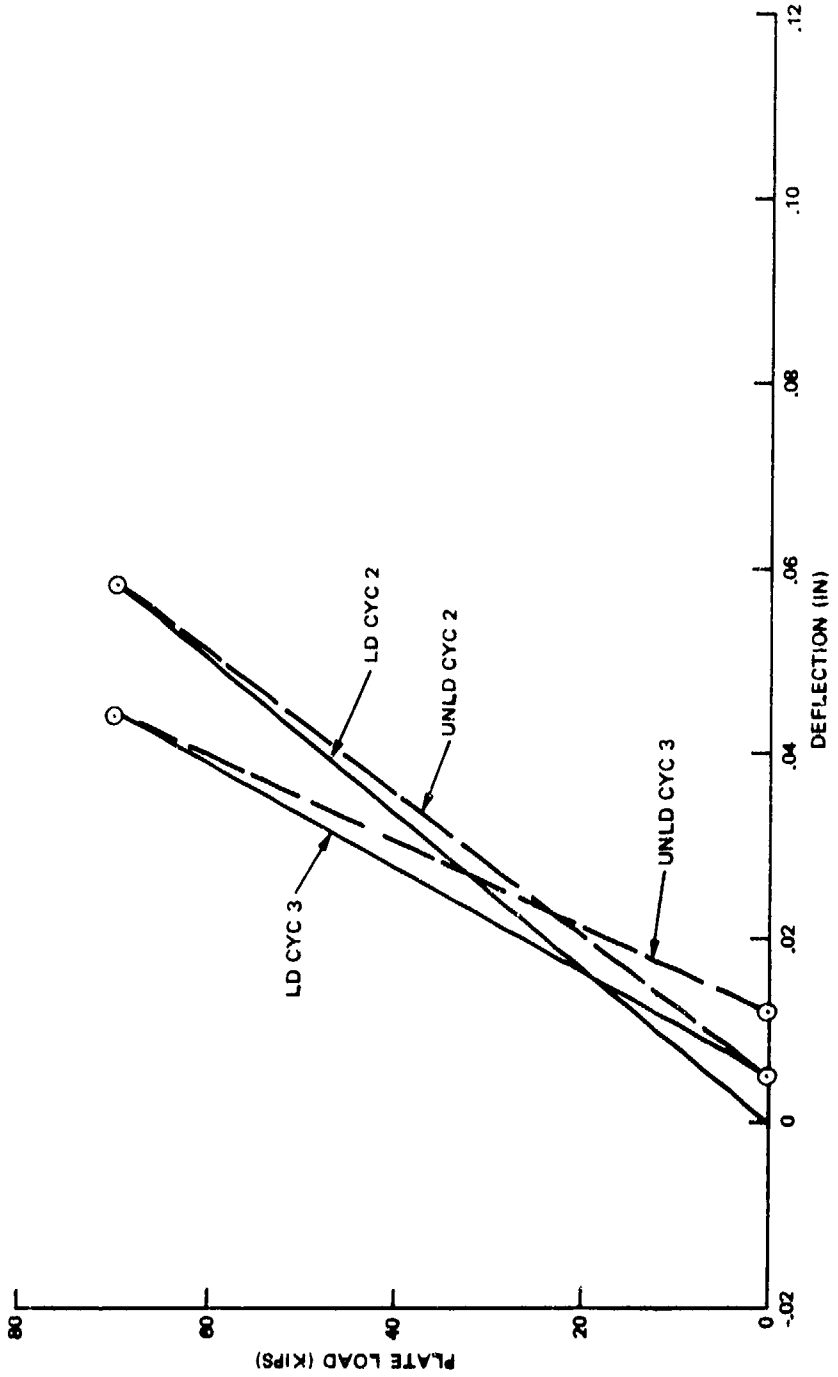

Figure B-24. Plate Load Versus Summation Centerline Bison Gage Relative Deflections, Test A2, 6 Inch AC + 6 Inch PCC, Cycles 2 and 3

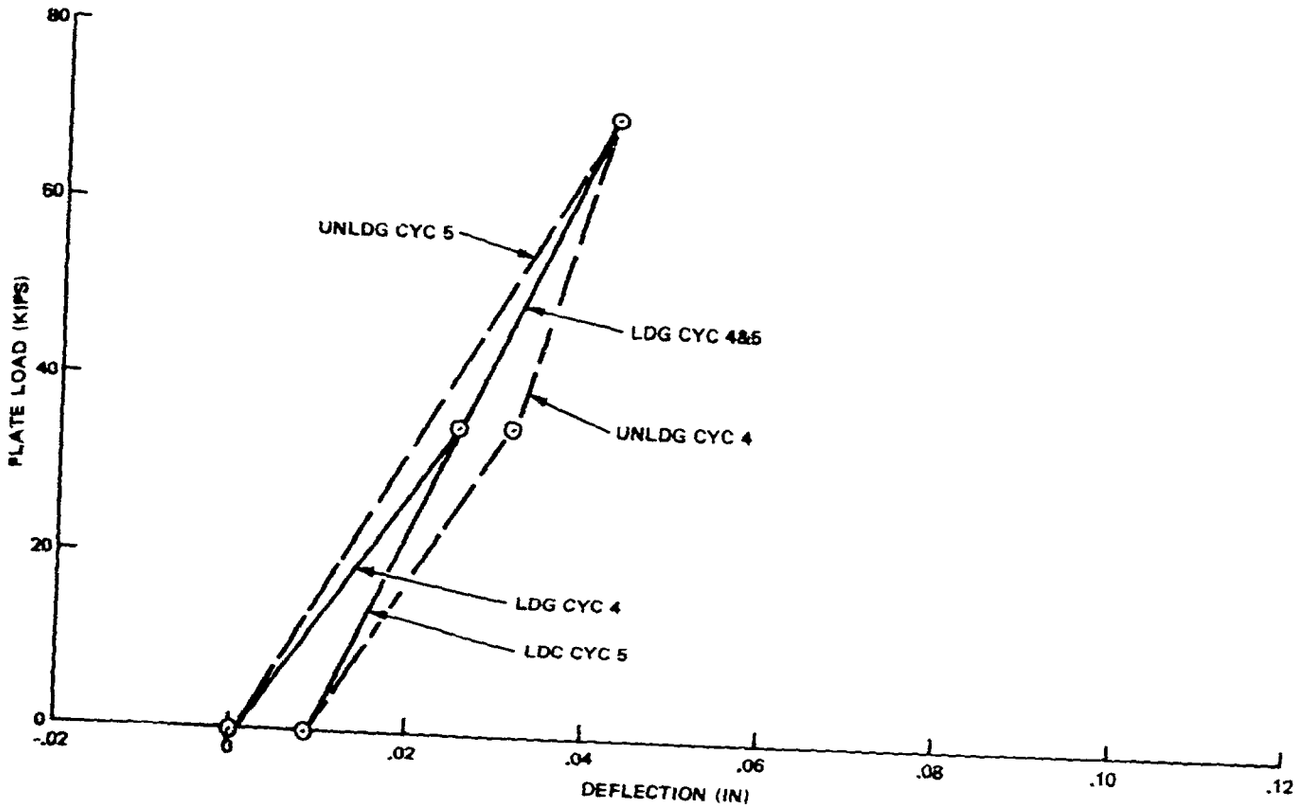

Figure B-25. Summation Centerline Bison Gage Relative Deflections Versus Plate Load, Test A2, 6 Inch AC + 6 Inch PCC, Cycles 4 and 5

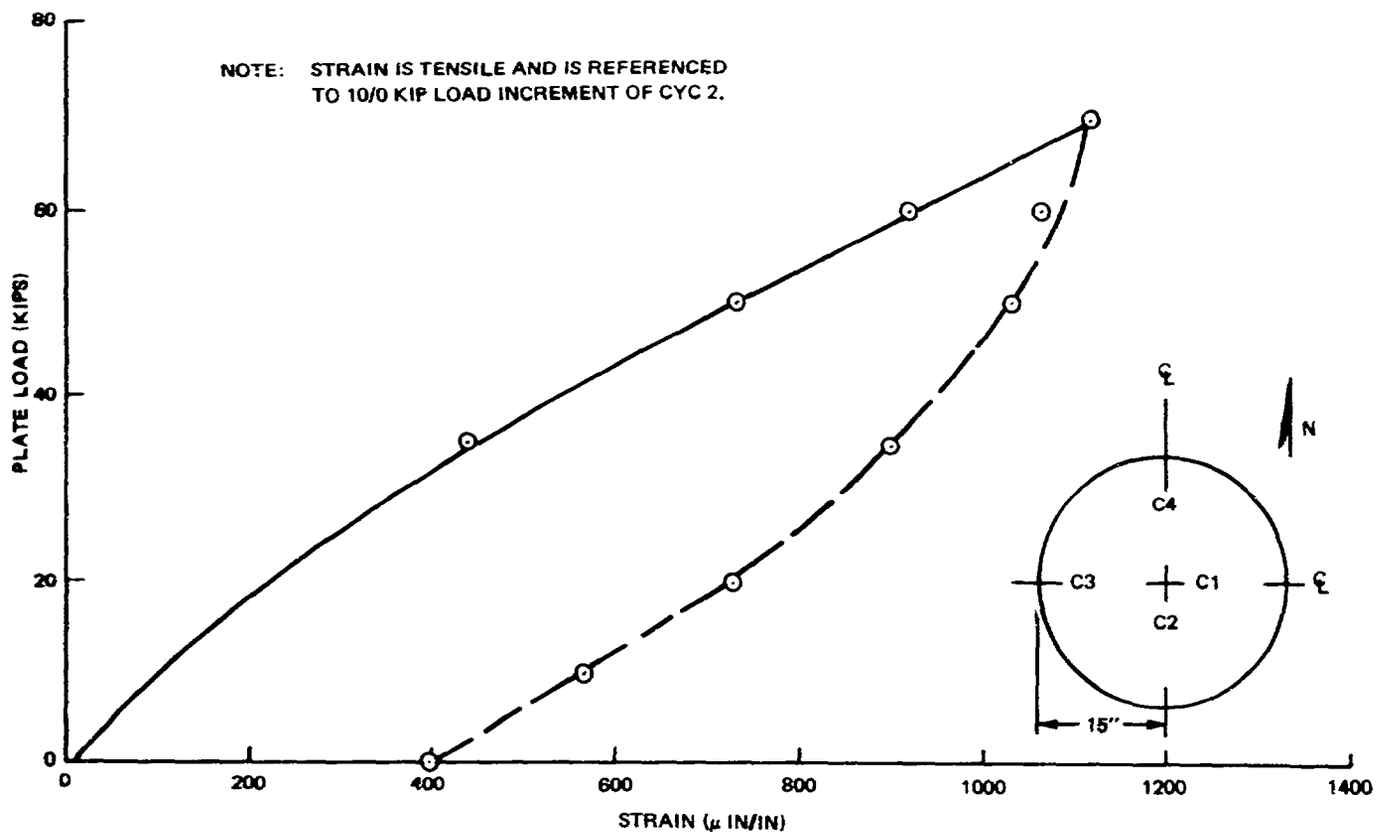

Figure B-26. Concrete Strain Versus Plate Load, Test A2, 6 Inch AC + 6 Inch PCC, Cycle 1, Gage C2

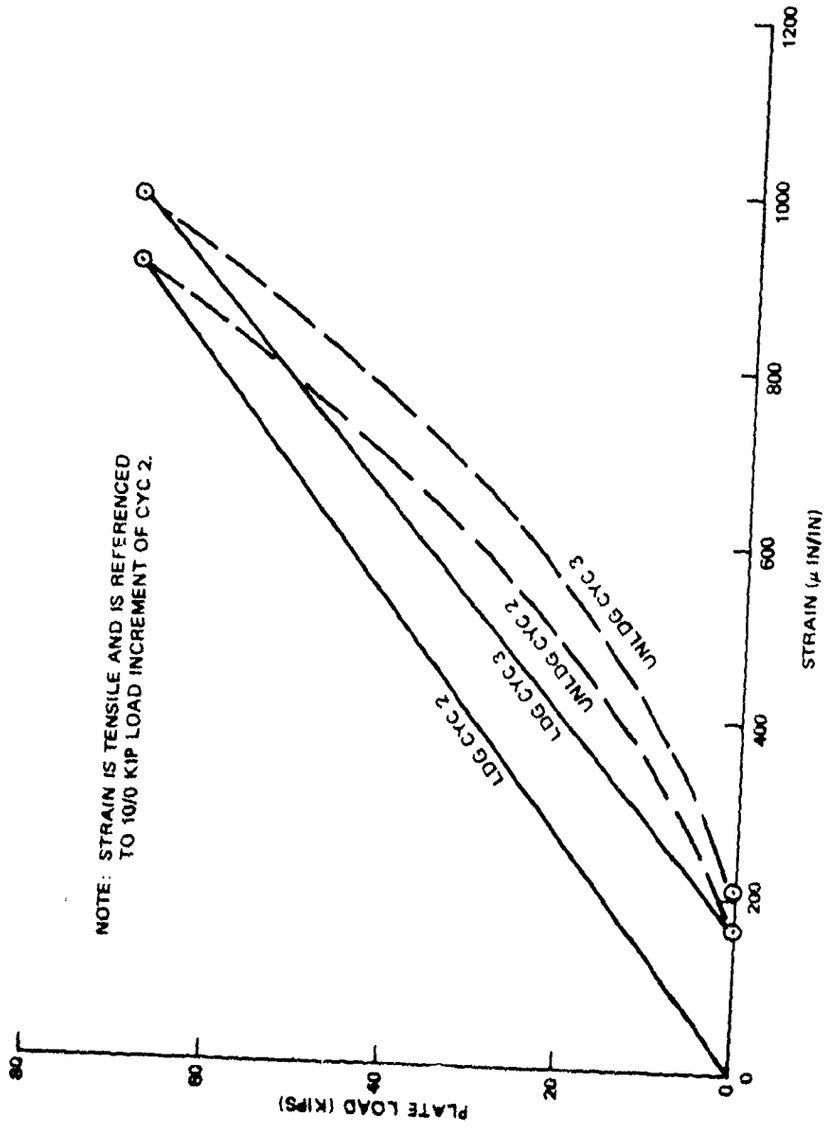

Figure B-27. Concrete Strain Versus Plate Load, Test A2, 6 Inch AC + 6 Inch PCC, Cycles 2 and 3, Gage C2

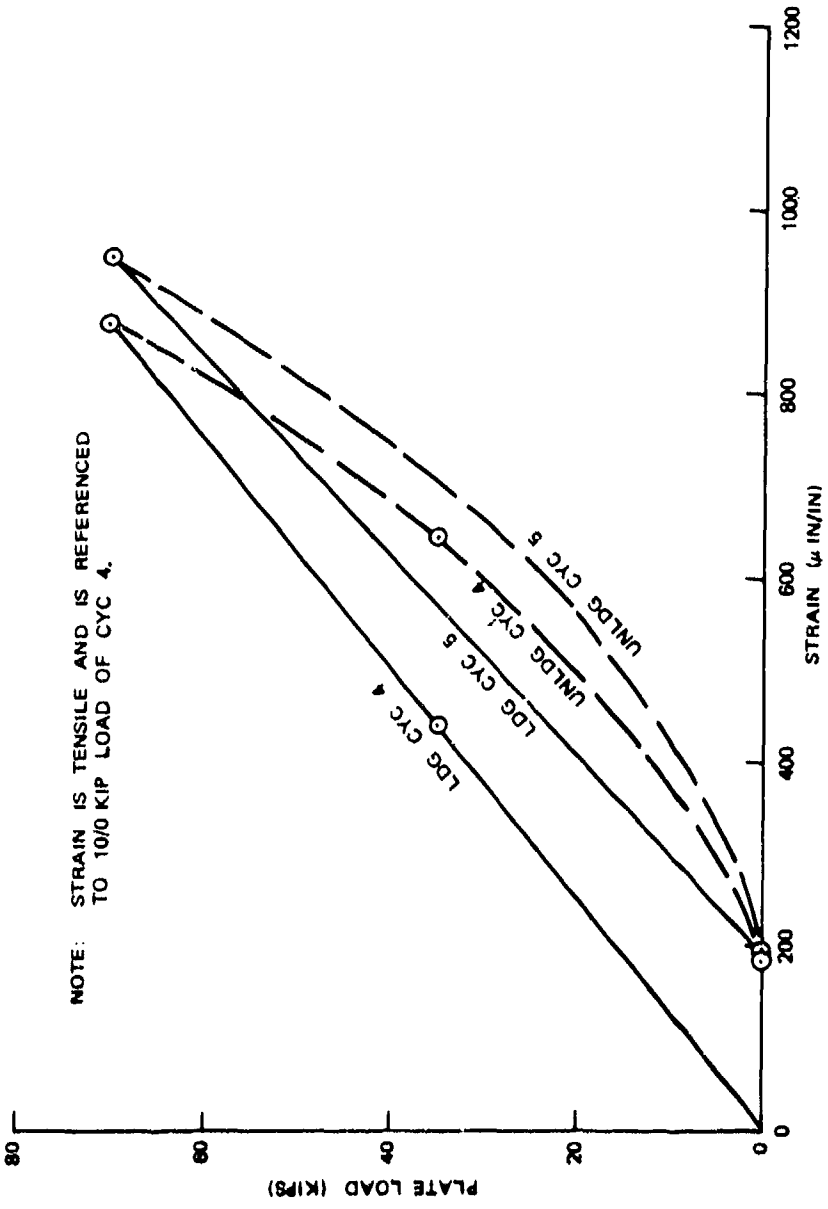

Figure B-28. Concrete Strain Versus Plate Load, Test A2, 6 Inch AC + 6 Inch PCC, Cycles 4 and 5, Gage C2

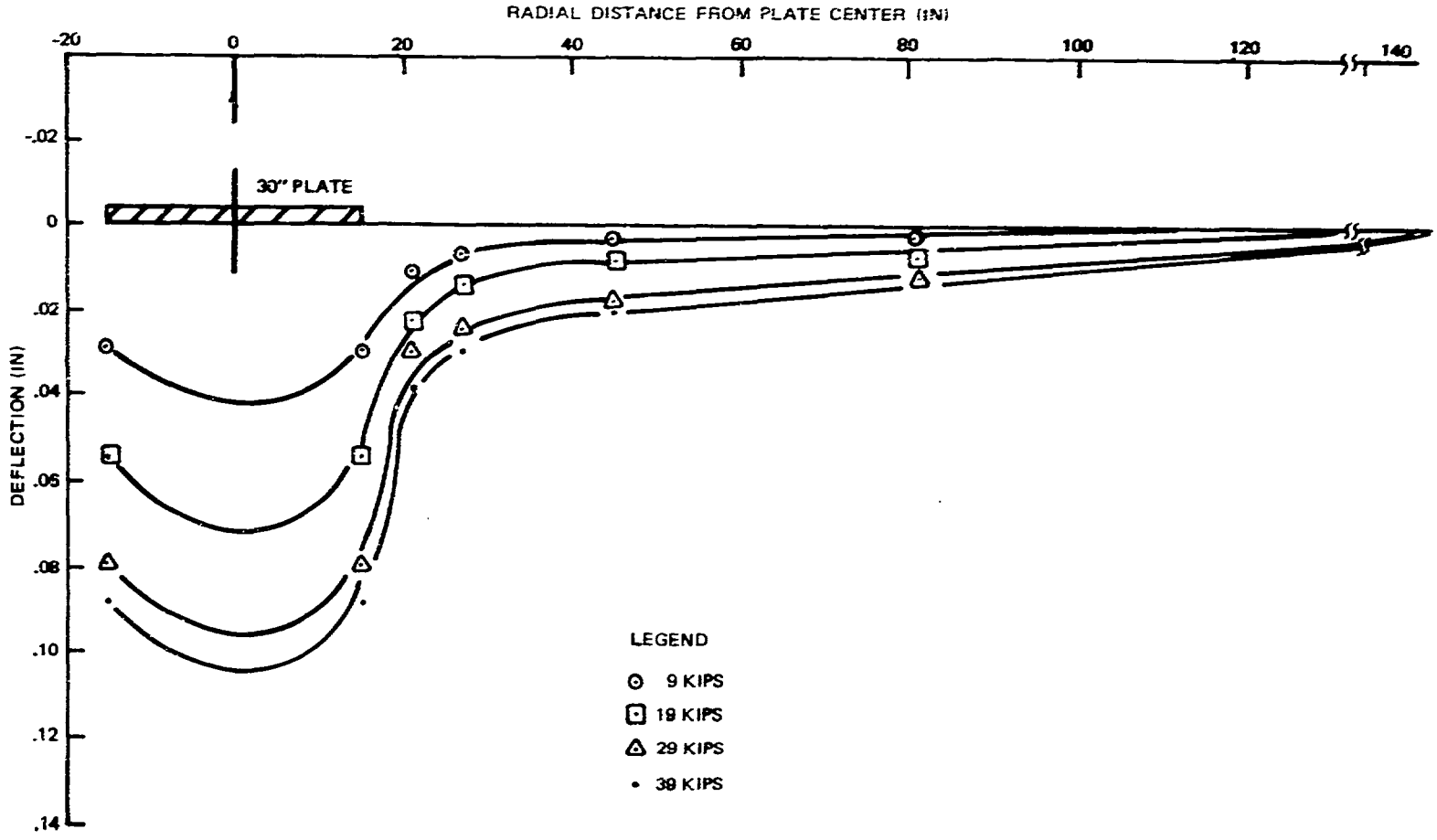

Figure B-29. Radial Distance Versus Deflection, Test A2, 6 Inch AC Base, Cycle 1

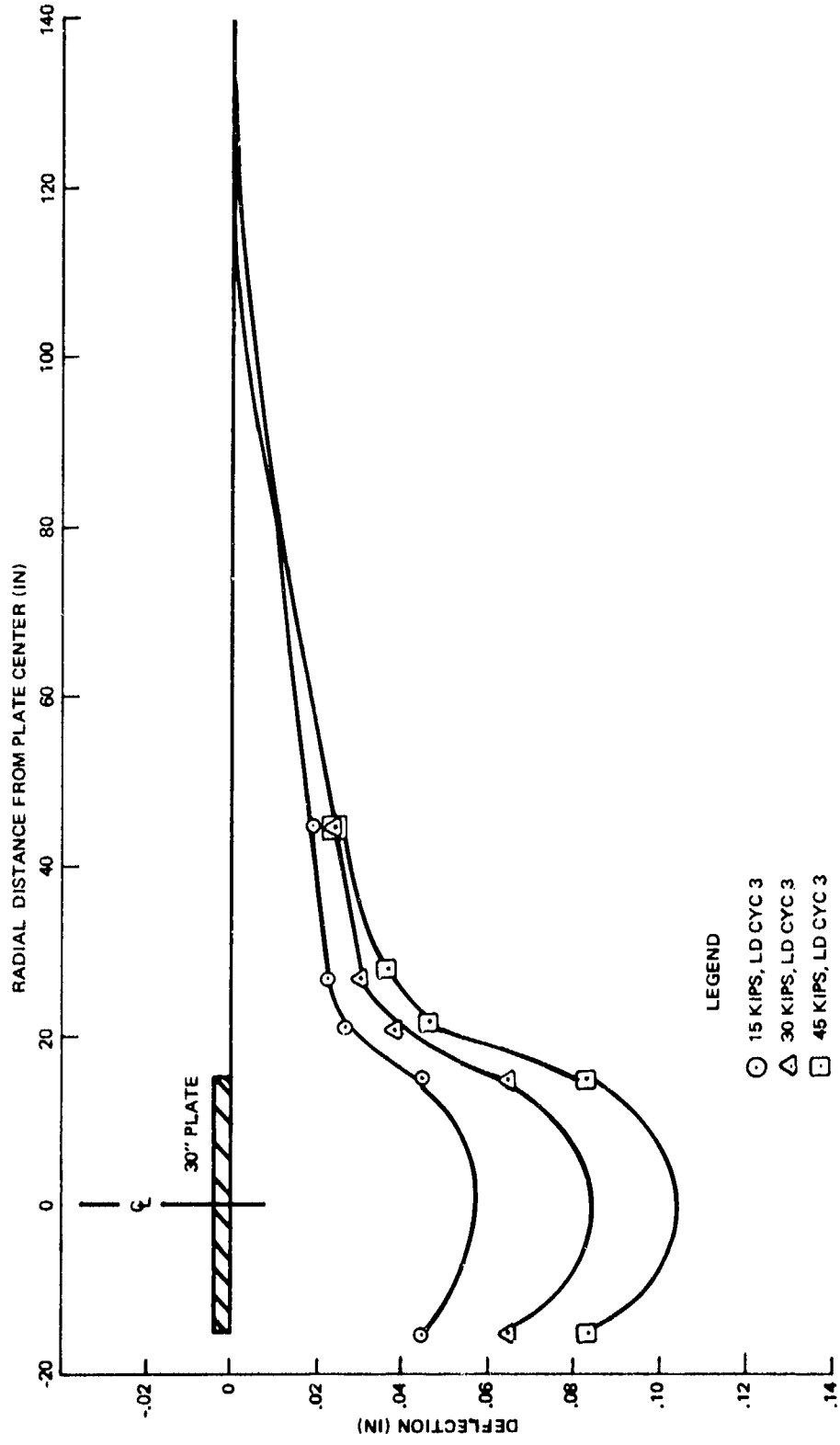

Figure B-30. Radial Distance Versus Deflection, Test A2, 6 Inch AC Base, Cycle 3

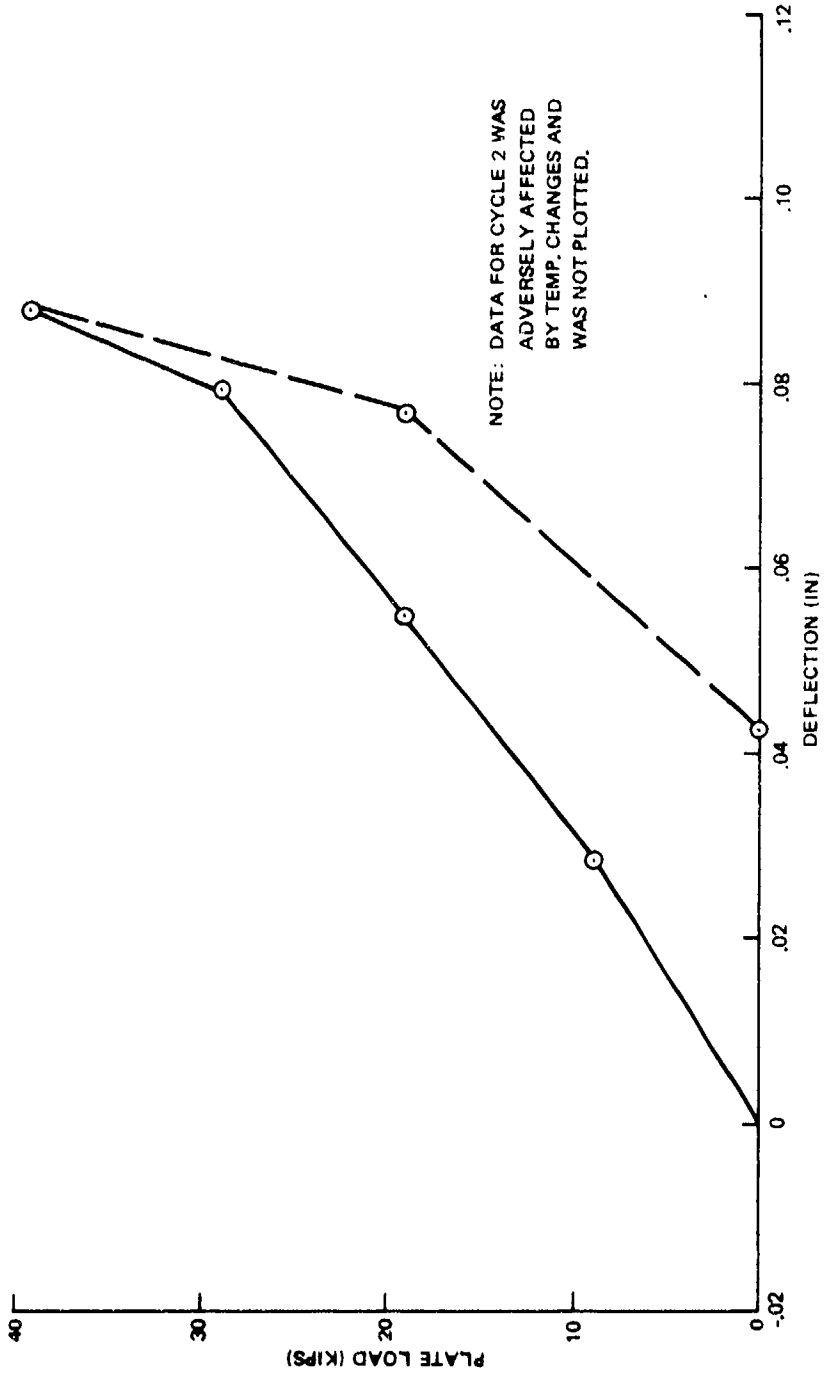

Figure B-31. Average Plate Edge Deflections Versus Plate Load, Test A2, 6 Inch AC Base, Cycle 1

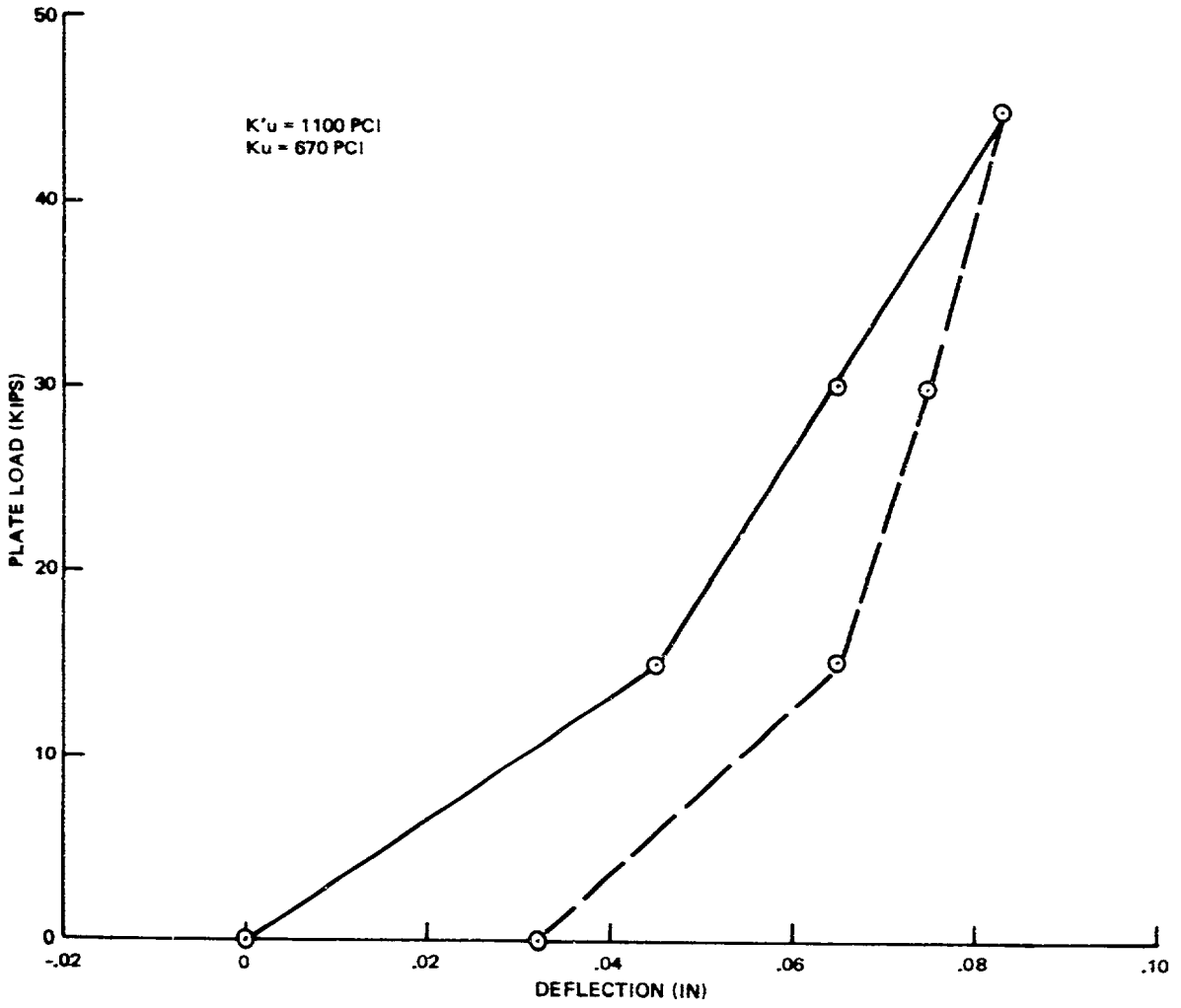

Figure B-32. Average Plate Edge Deflections Versus Plate Load, Test A2, 6 Inch AC Base, Cycle 3

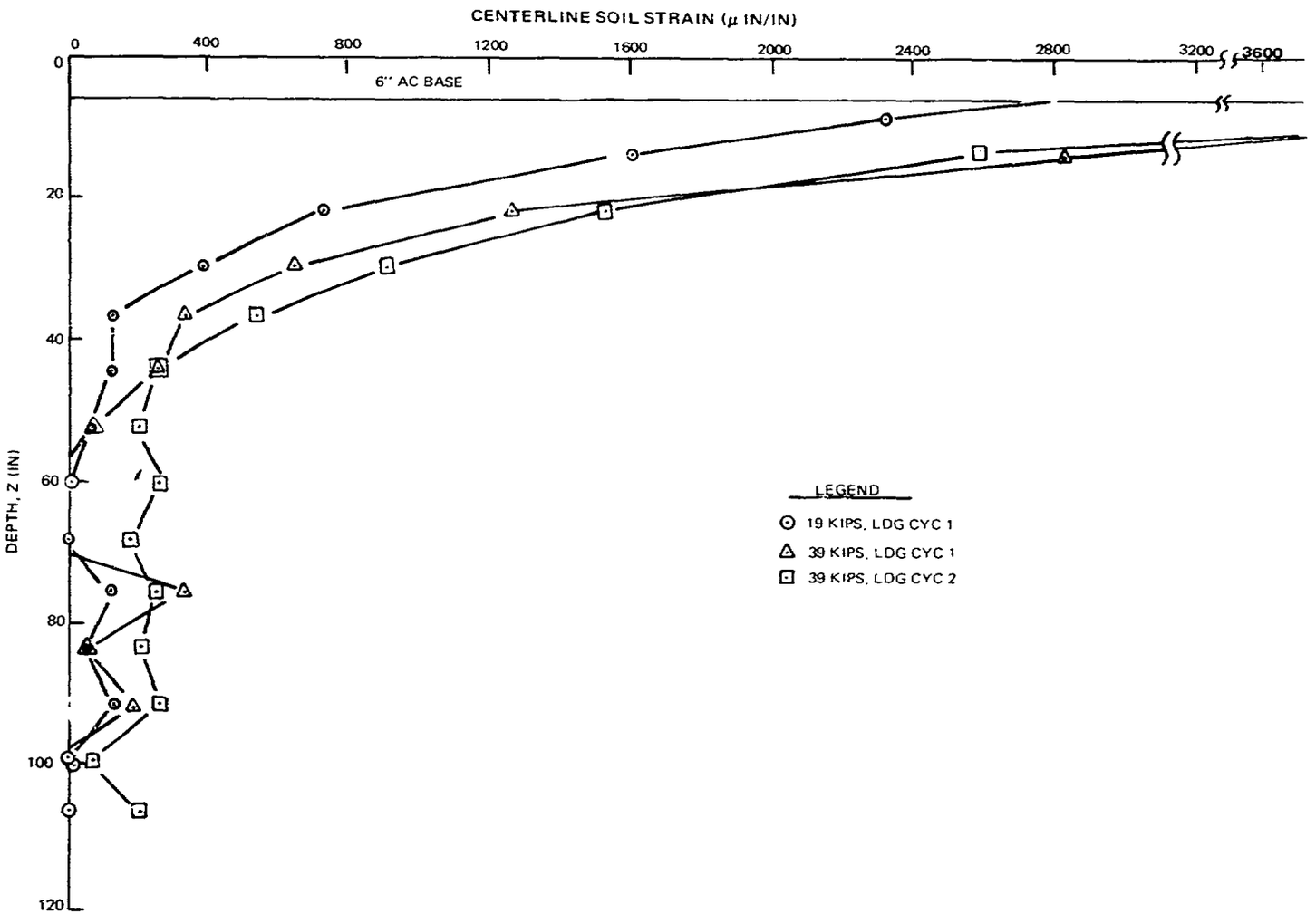

Figure B-33. Centerline Soil Strain Versus Depth, Test A2, 6 Inch AC Base, Cycles 1 and 2

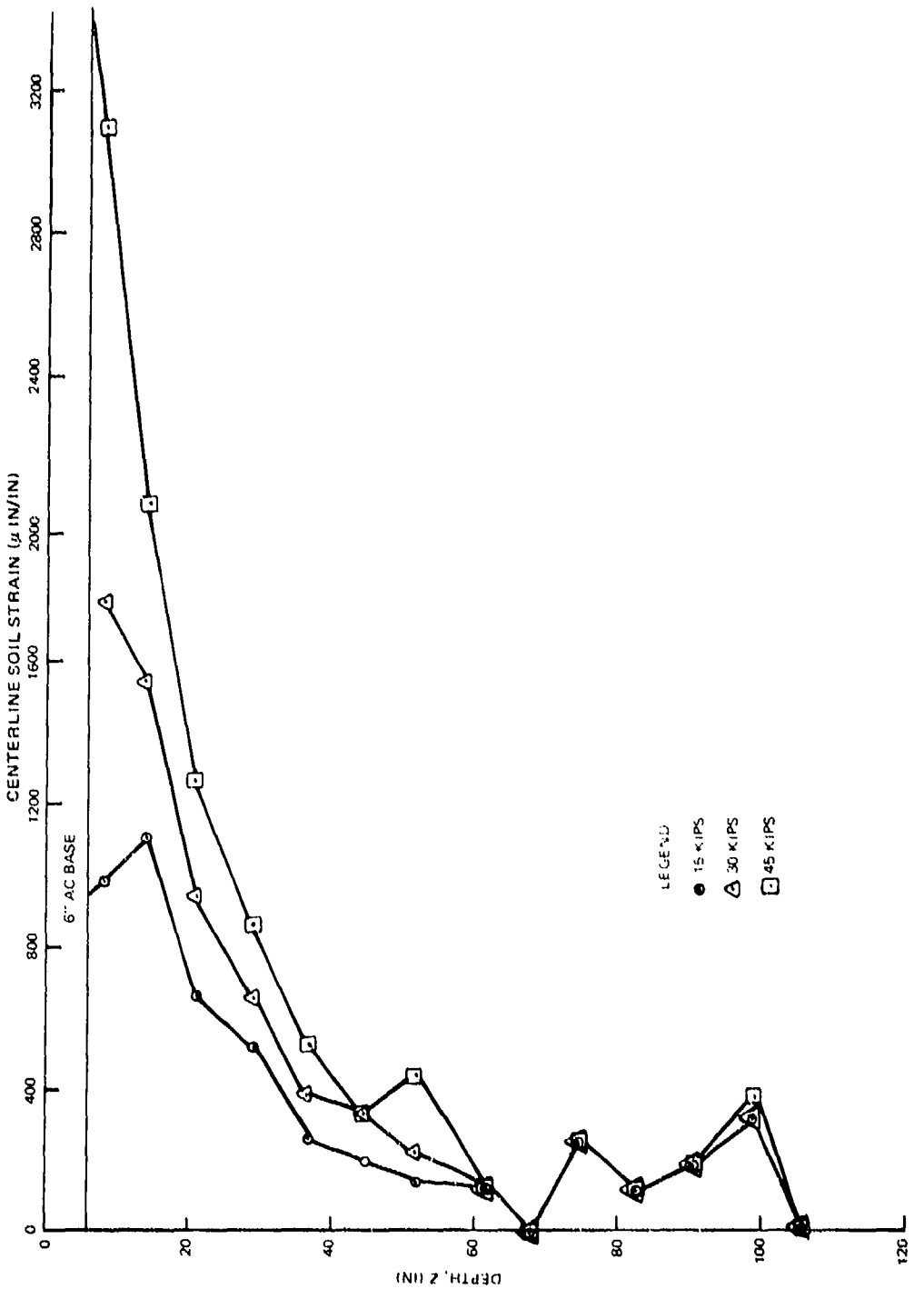

Figure B-34. Centerline Soil Strain Versus Depth, Test A2, 6 Inch AC Base, Cycle 3

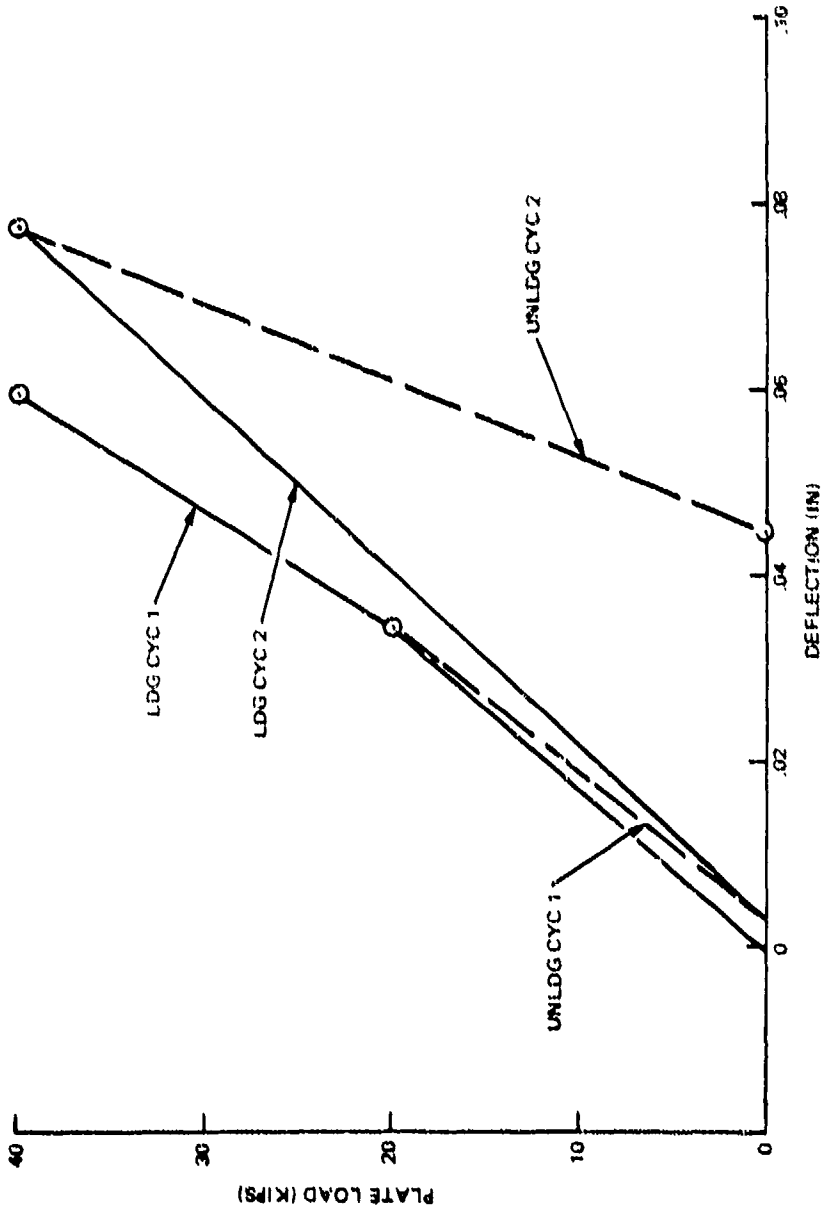

Figure B-35. Summation Centerline Bison Gage Relative Deflections Versus Plate Load, Test A2, 6 Inch AC Base, Cycles 1 and 2

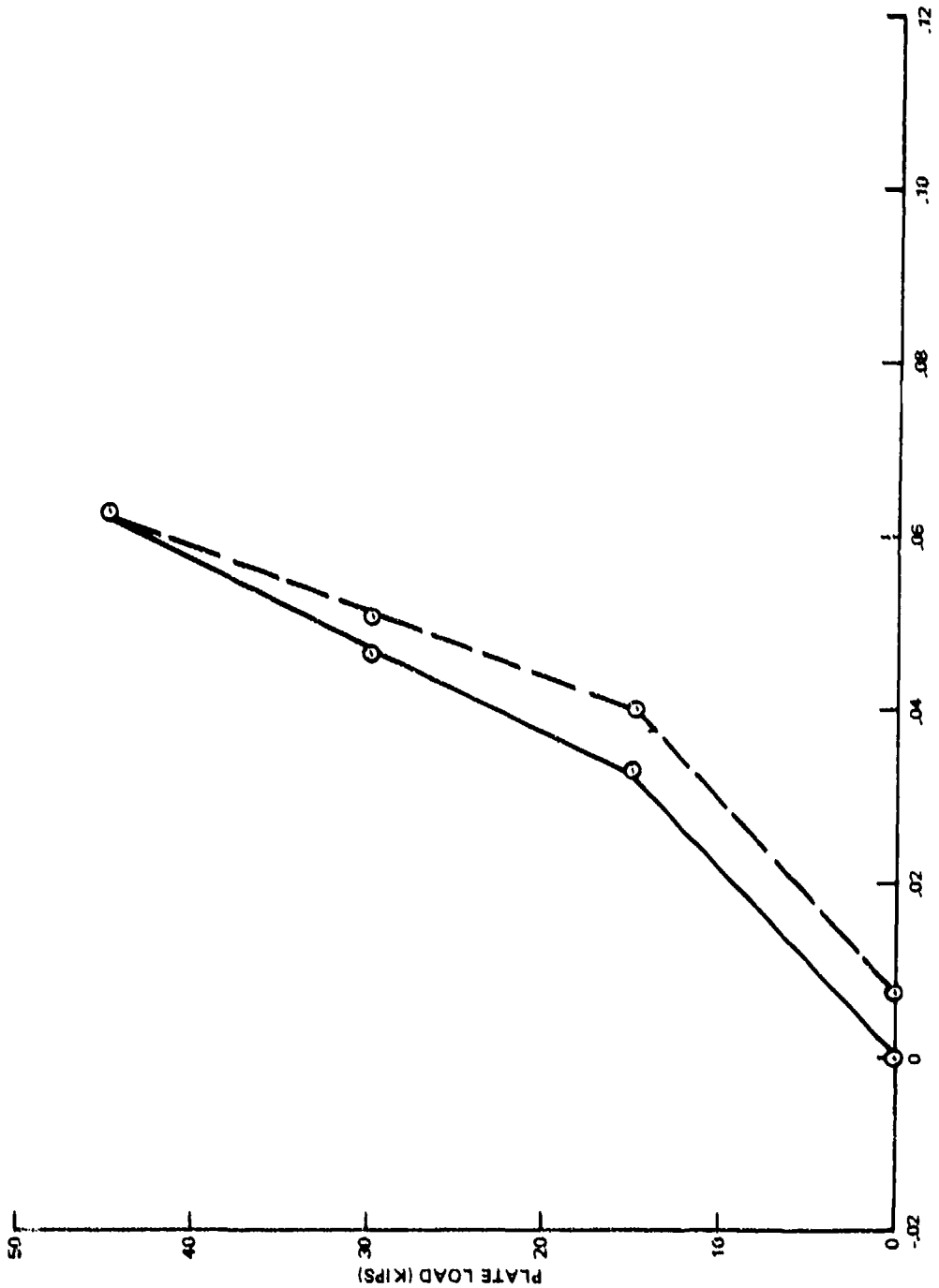

Figure B-36. Summation Centerline Bison Cage Relative Deflections Versus Plate Load, Test A2, 6 Inch AC Base, Cycle 3

PART B-4

LOAD TEST DATA FOR PAVEMENT SECTION B1

Table B-7. Concrete Strain[a] Gage Data for Test B1

Cycle 1													
Gage Location	Load Level in KIPS												
	0[b]	10.1	20.1	30.1	40.3	50.3	60.3	70.3	80.3	90.1	70	50	0
C1	00	08	15	21	04	00[c]	15	19	-21	-24	-18	-08	13
C2	00	05	15	27	14	-03	01	-03	-17	-18	-19	-18	-08

Cycles 2 and 3										
Gage Location	Load Level in KIPS									
	0[b]	30.3	49.7	69.8	90	30	0	90	0	
C1	00	003	001	-011	-026	-014	-007	-034	-008	
C2	00	-019	-030	-047	-059	-035	-020	-057	-013	

[a] All strains are given in microinches. Positive strain is tension.

[b] At the beginning of each day's testing, all gages were zeroed.

[c] Gage rezeroed.

Table B-8. Concrete Strain[a] Gage Data for Test B2

Gage Location	Cycle 1											
	Load Level in KIPS											
	10[b]	30	60	70	80	90	60	50	40	30	10	0
C1	0	9	-12	-16	-26	-40	-31	-20	-11	-3	10	15
C2	0	62	546	829	1171	1495	1285	1159	1005	812	383	233
C3	0	17	62	97	145	208	180	168	151	136	96	72
C4	0	50	39	42	42	39	33	43	43	38	26	17

Gage Location	Cycles 2 and 3																
	Load Level in KIPS																
	10	20	30	40	50	60	70	80	70	60	50	40	30	20	10	80	10
C1	-3	-8	-9	-13	-18	-22	-24	-31	-31	-29	-26	-21	-15	-7	–	–	–
C2	209	400	549	729	917	1091	1270	1463	1439	1349	1233	1093	913	684	440	1529	553
C3	38	58	74	97	114	133	157	188	184	173	159	144	130	113	88	218	102
C4	7	4	9	16	20	23	26	31	28	26	23	22	16	13	5	28	11

Gage Location	Cycles 4 and 5								
	Load Level in KIPS								
	10	30	60	80	60	30	10	80	10
C1	-17	-14	-31	-36	-28	-13	7	-23	17
C2	198	525	1102	1463	1312	832	365	1449	364
C3	29	59	124	167	145	90	69	178	74
C4	4	15	27	29	35	22	24	49	35

Gage Location	Cycles 6 and 7								
	Load Level in KIPS								
	10	30	60	80	60	30	10	80	10
C1	9	9	-13	-25	-20	-3	9	-17	9
C2	148	510	1096	1445	1282	816	365	1456	371
C3	56	71	131	181	148	101	69	189	68
C4	42	17	49	42	42	32	24	48	27

[a]All strains are given in microinches. Positive strain is tension.

[b]Strain referenced to load cycle 1, 10/0 kip load.

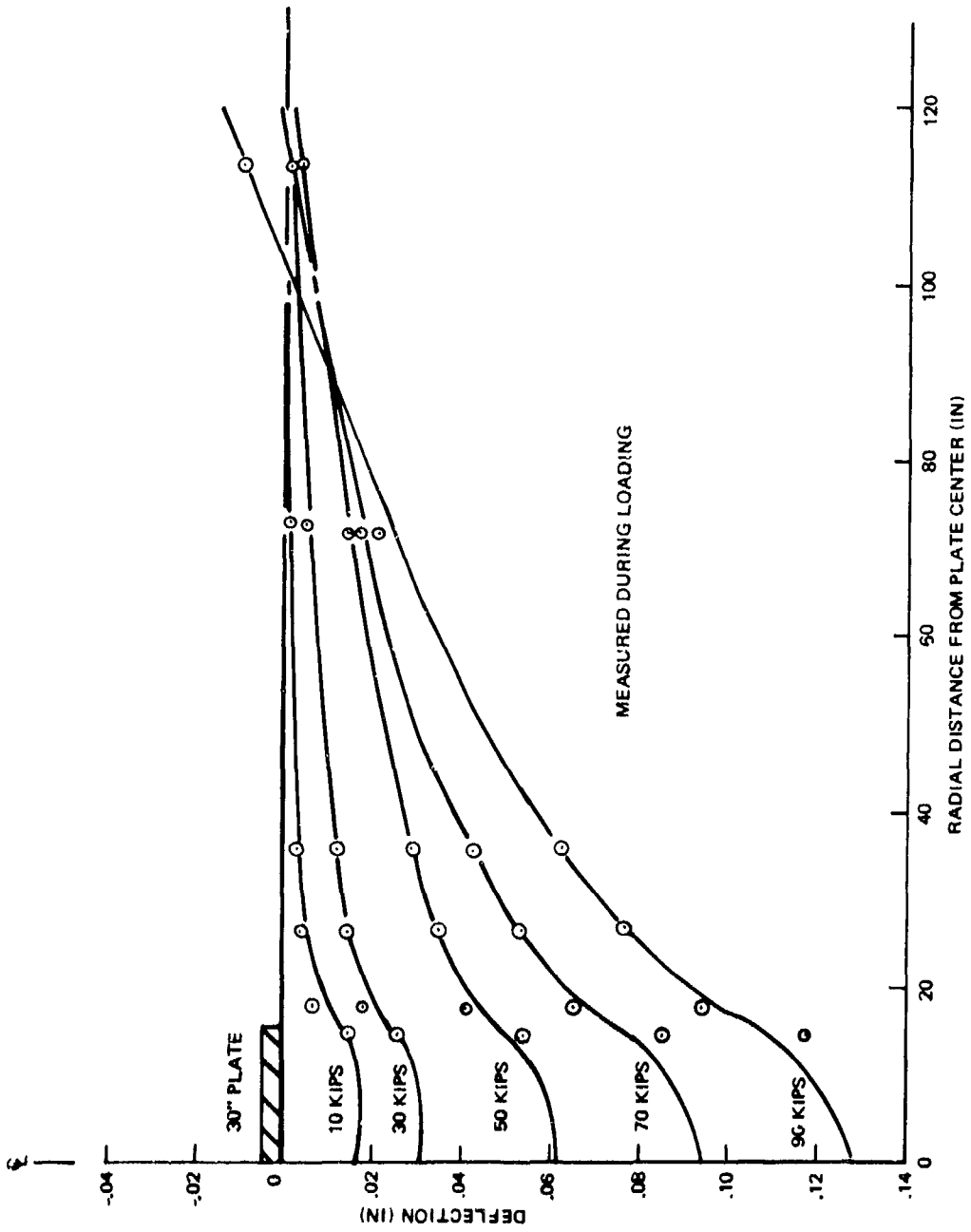

Figure B-37. Radial Distance Versus Deflection, Test B1, Cycle 1

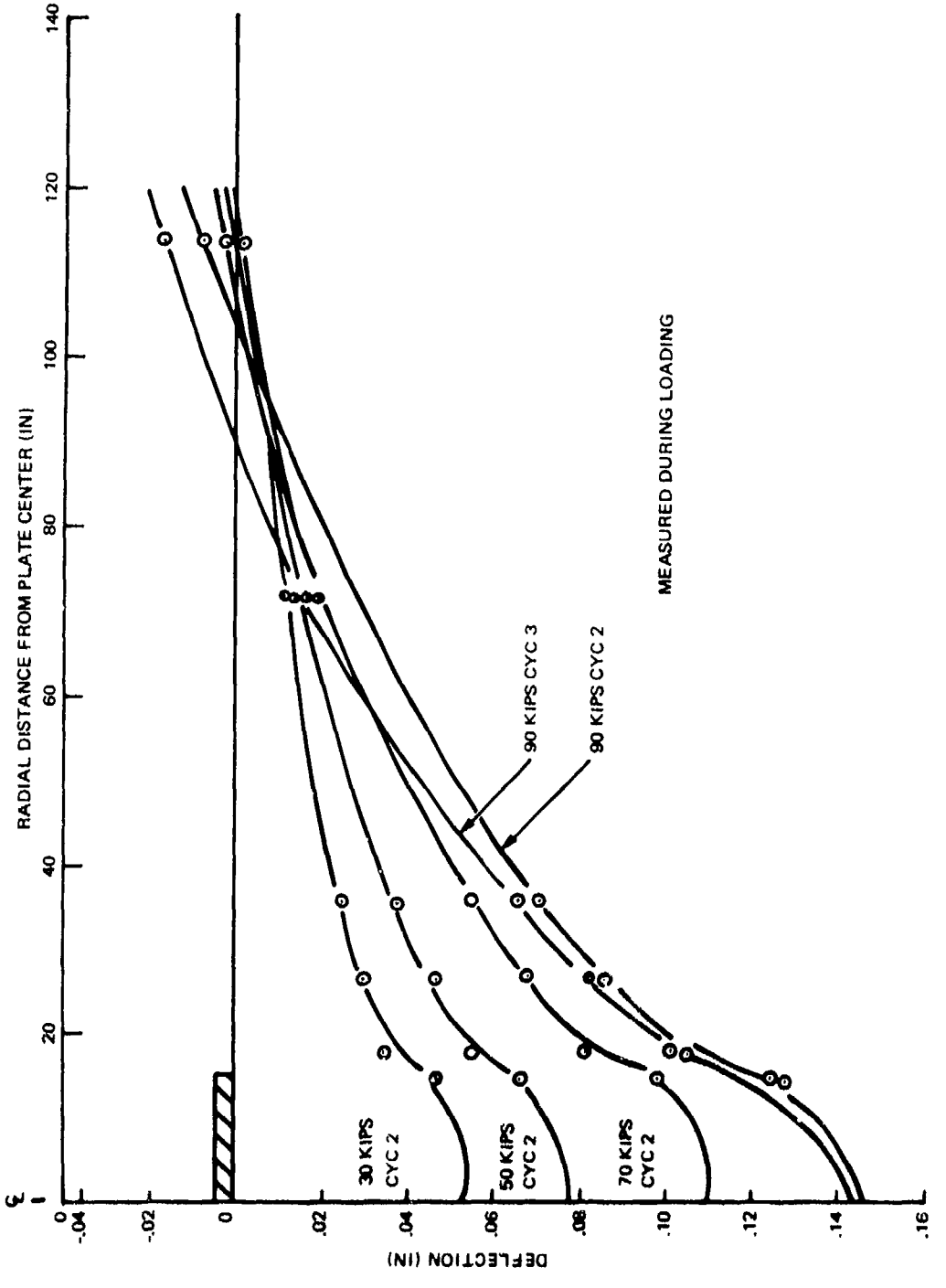

Figure B-38. Radial Distance Versus Deflection, Test B1, Cycles 2 and 3

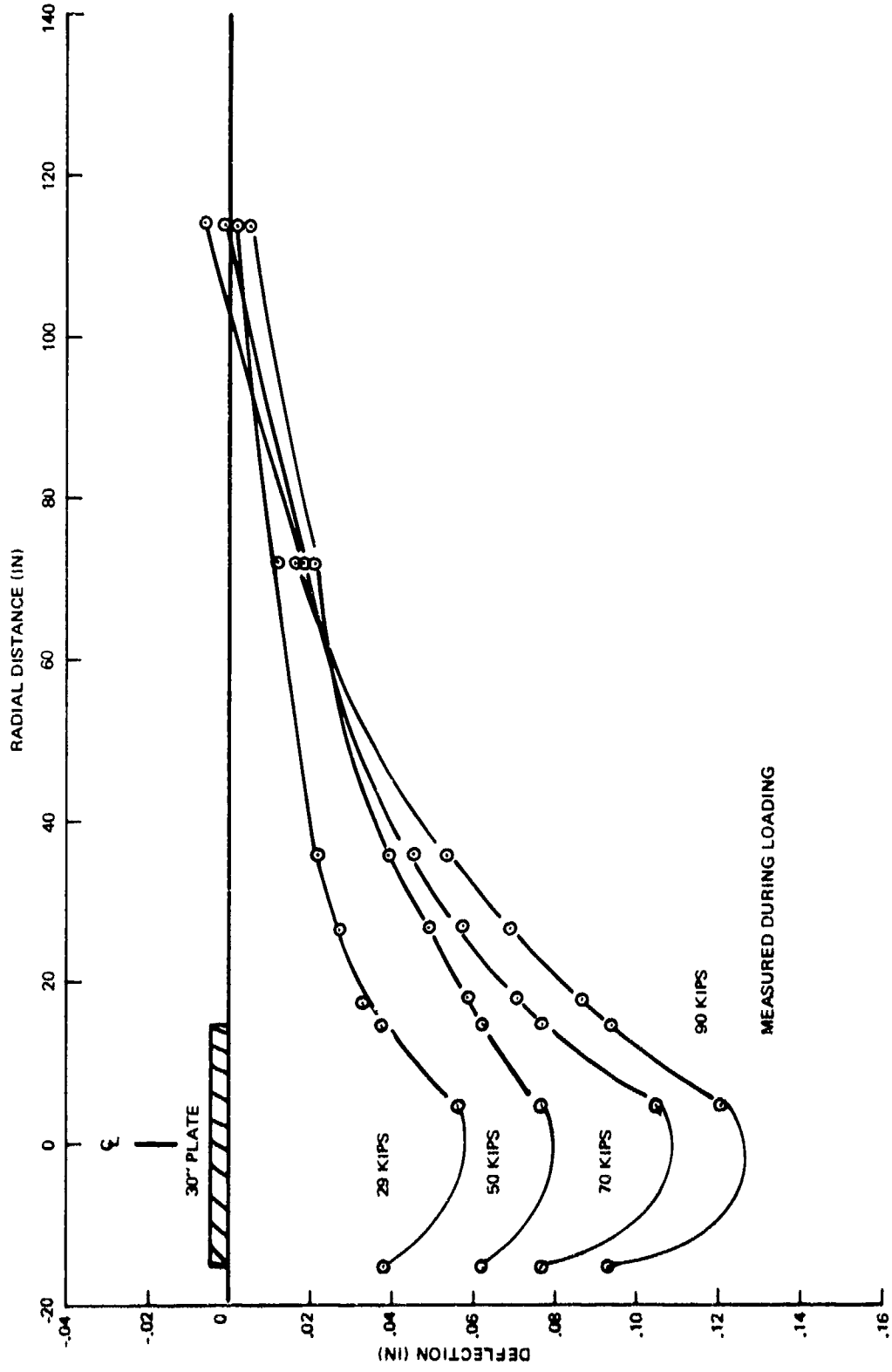

Figure B-3[illegible]. Deflection Versus Radial Distance, Test B1, Cycle 4

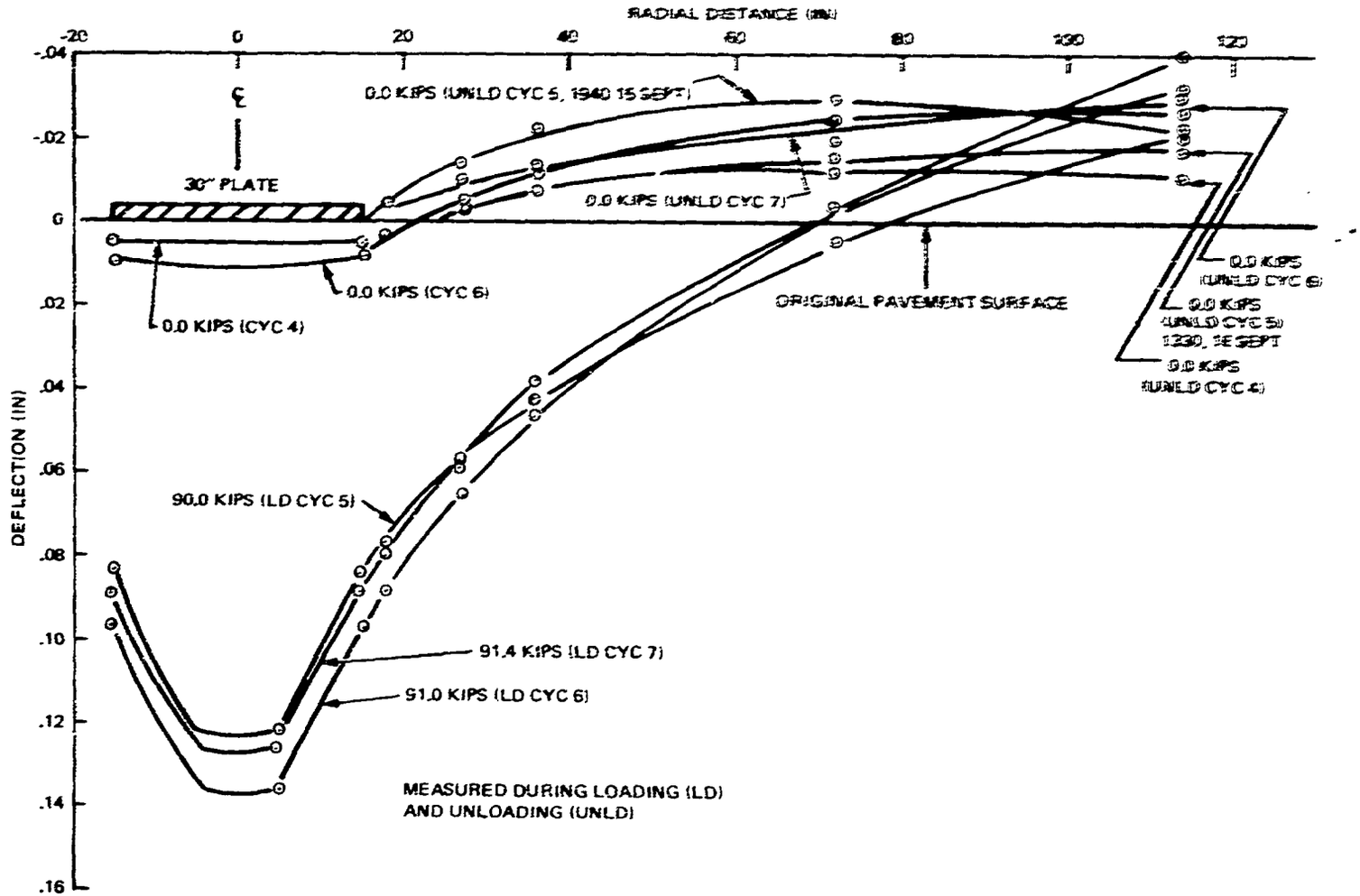

Figure B-40. Deflection Versus Radial Distance, Test B1, Cycles 5 through 7

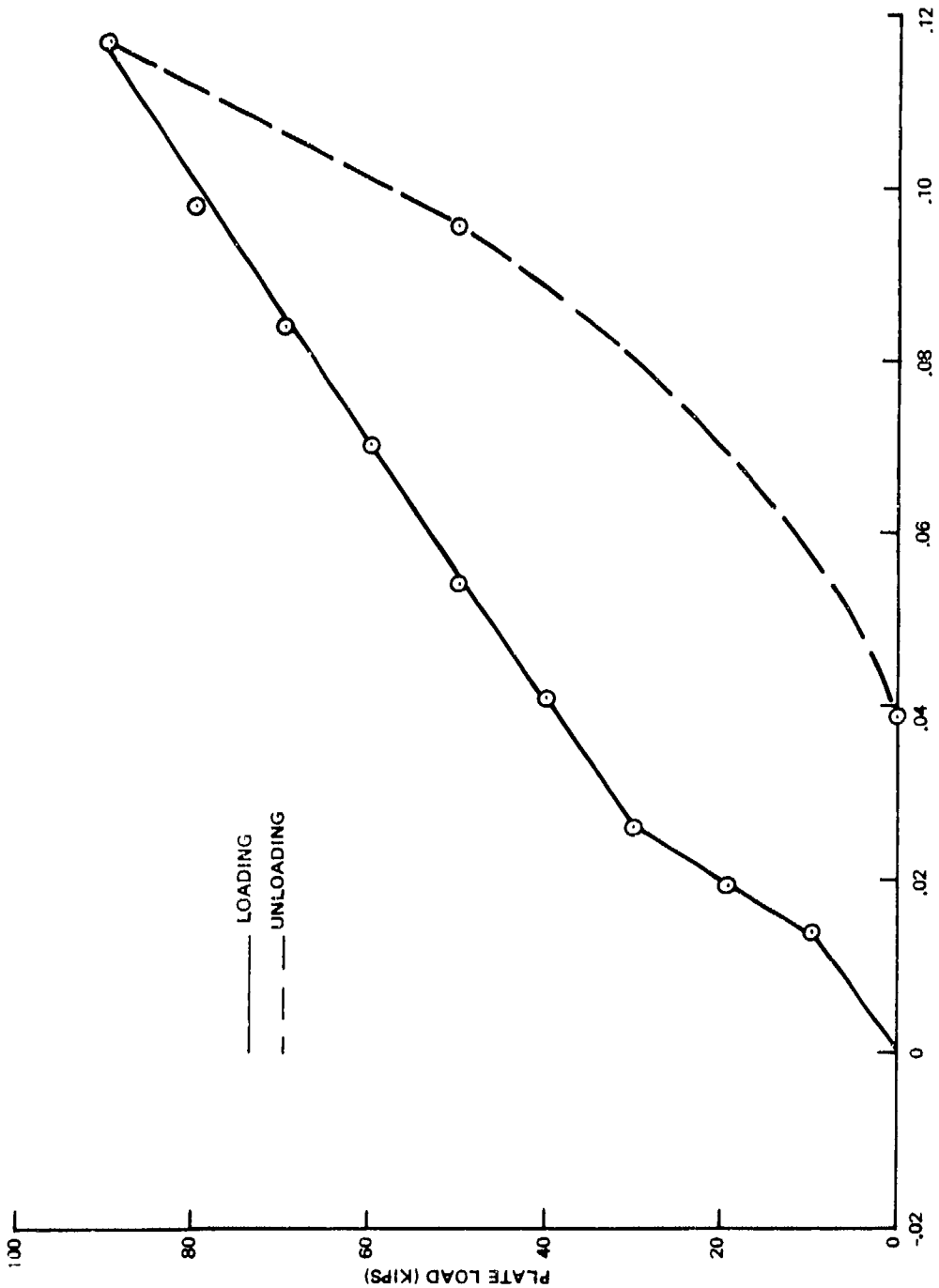

Figure B-41. Average Plate Edge Deflections Versus Plate Load, Test B1, Cycle 1

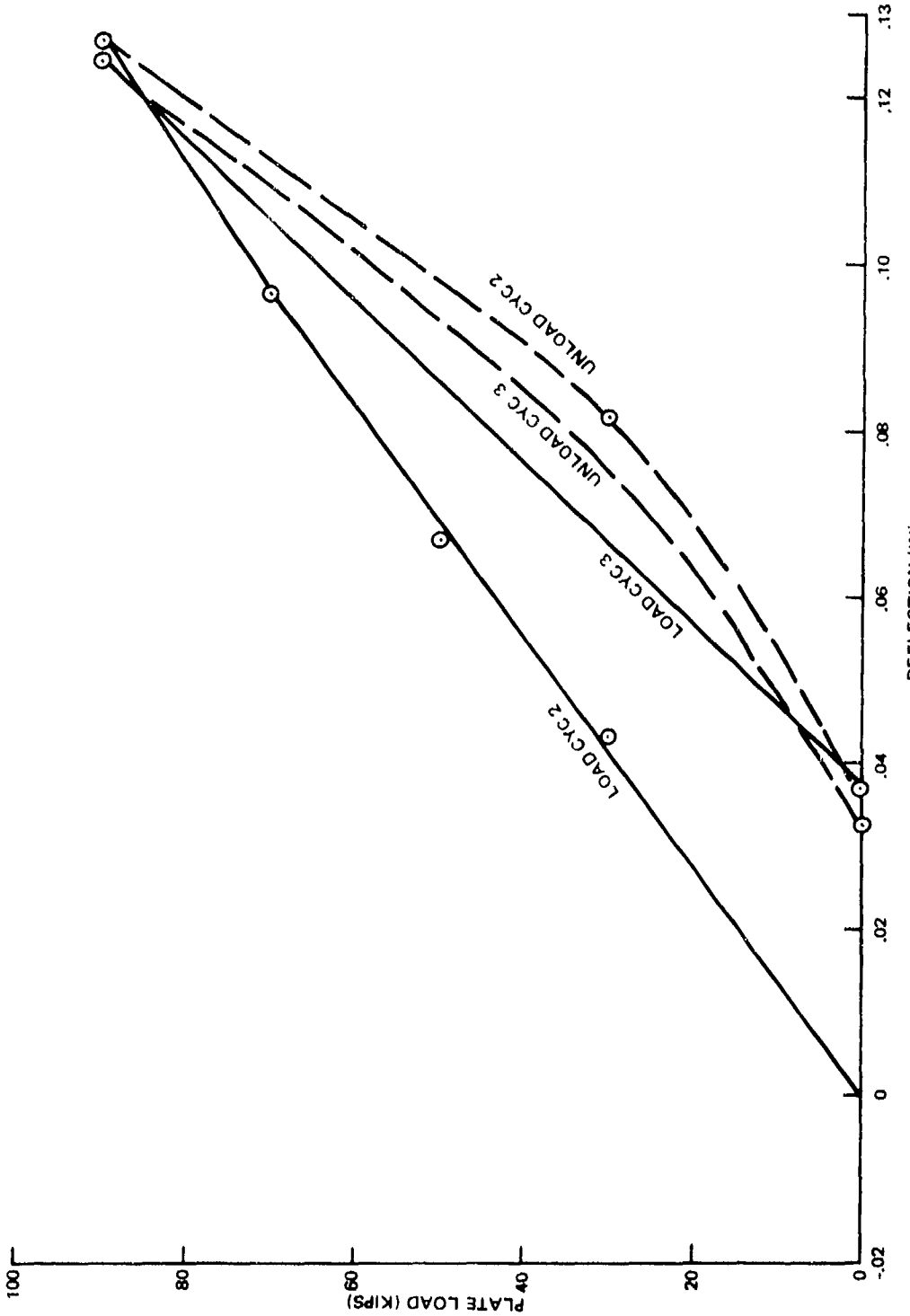

Figure B-42. Average Plate Edge Deflections Versus Plate Load, Test B1, Cycles 2 and 3

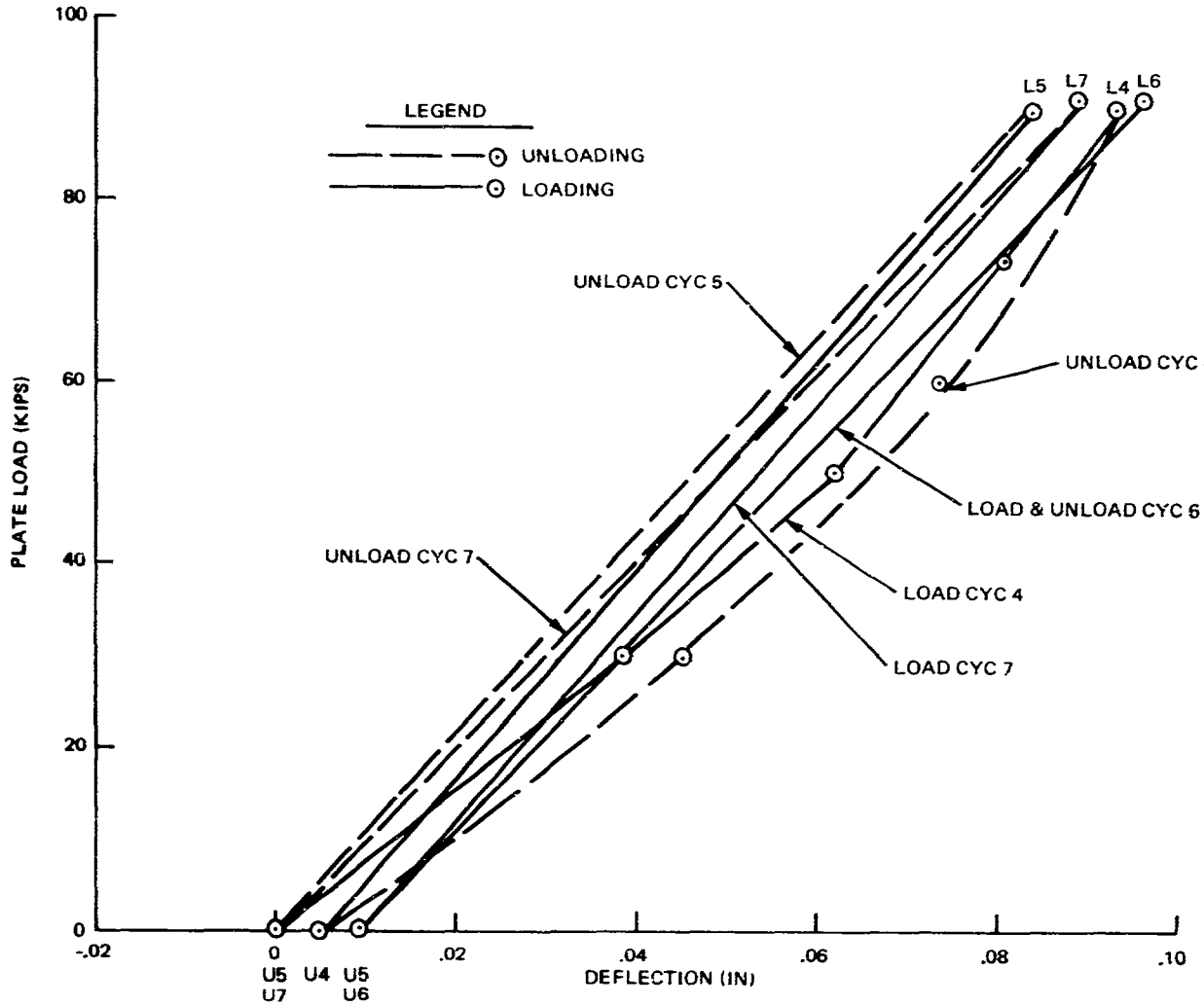

Figure B-43. Average Plate Edge Deflections Versus Plate Load, Test B1, Cycles 4 through 7

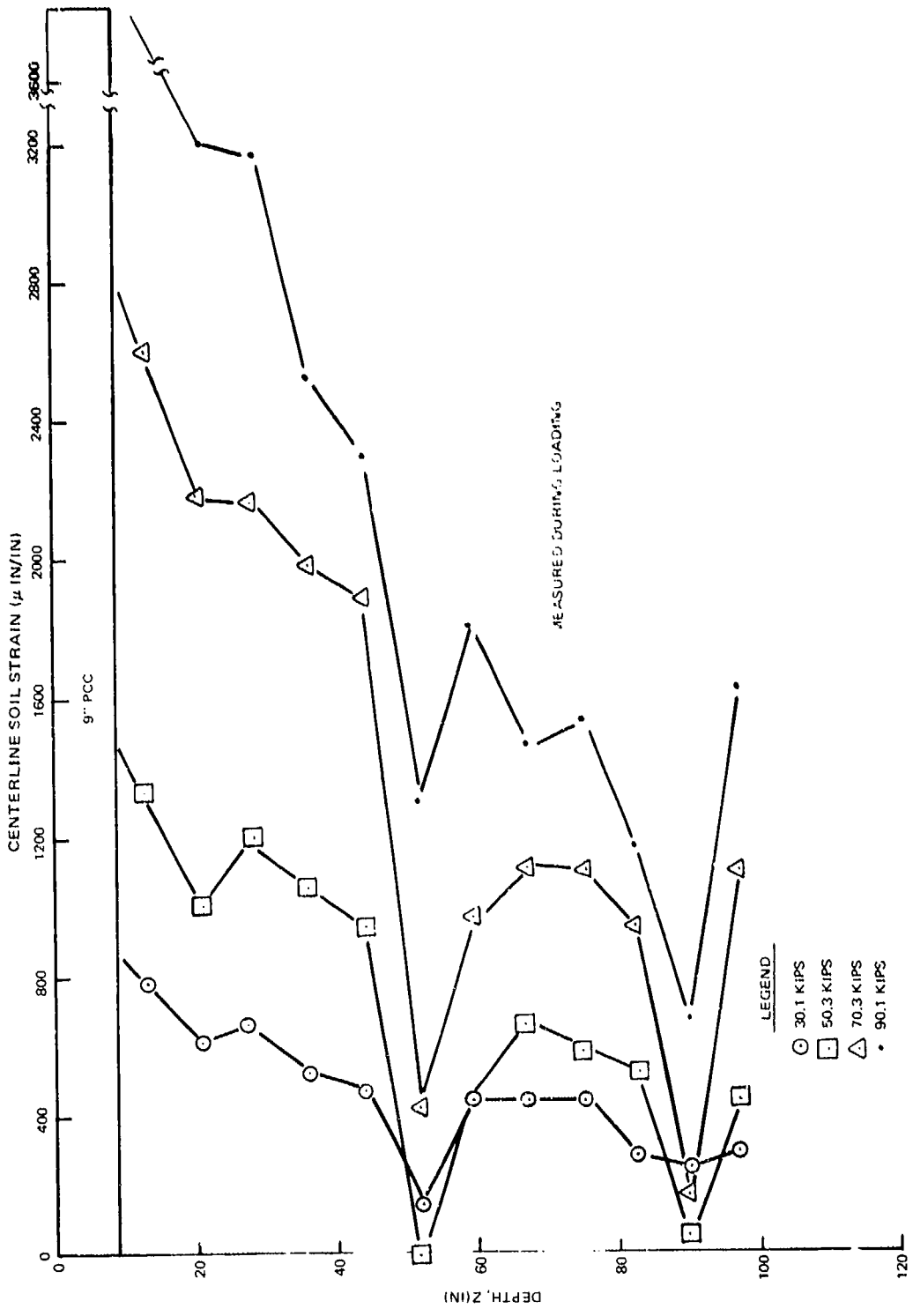

Figure B-44. Centerline Soil Strain Versus Depth, Test B1, Cycle 1

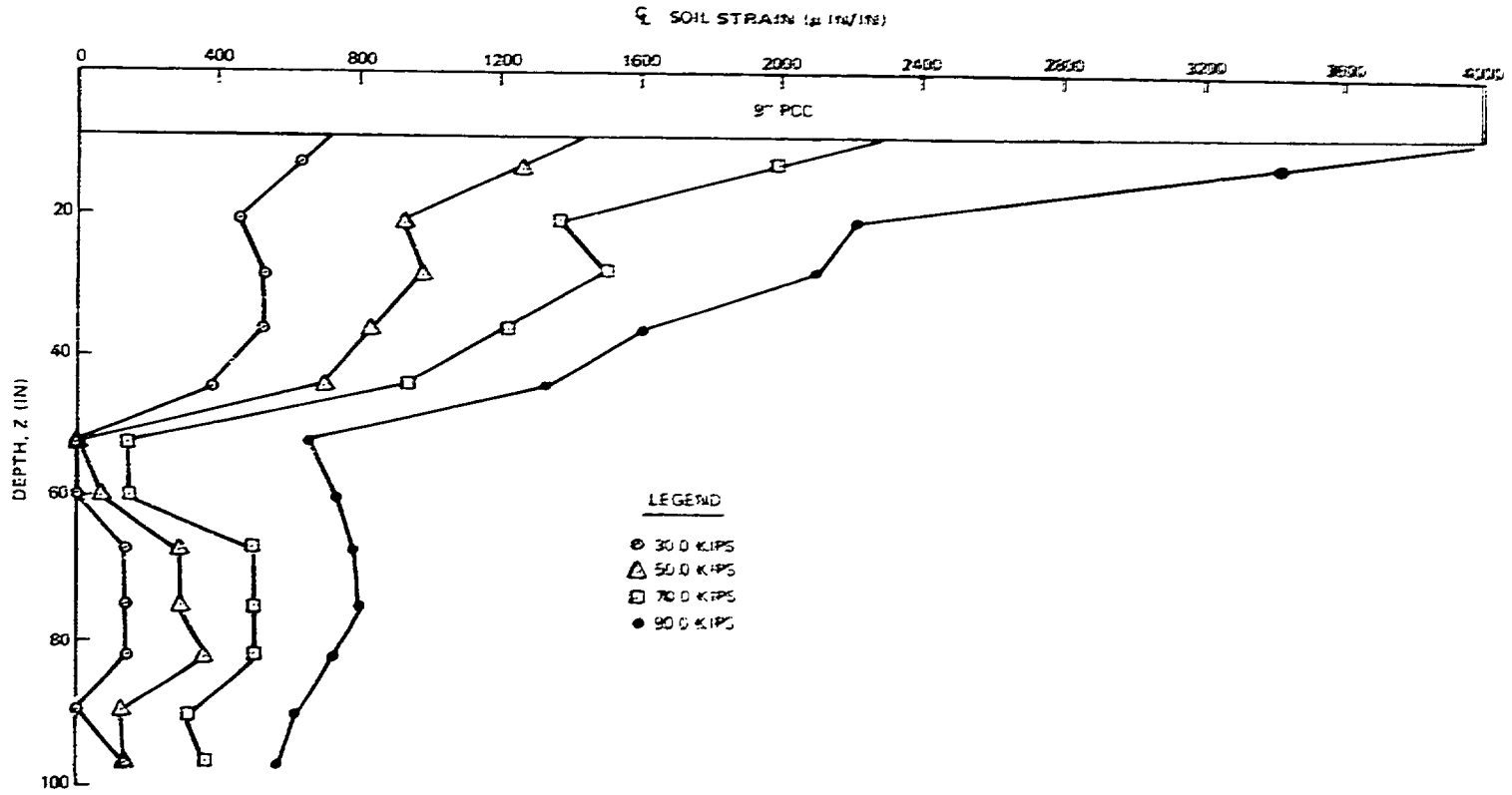

Figure B-45. Centerline Soil Strain Versus Depth, Test B1, Cycle 2

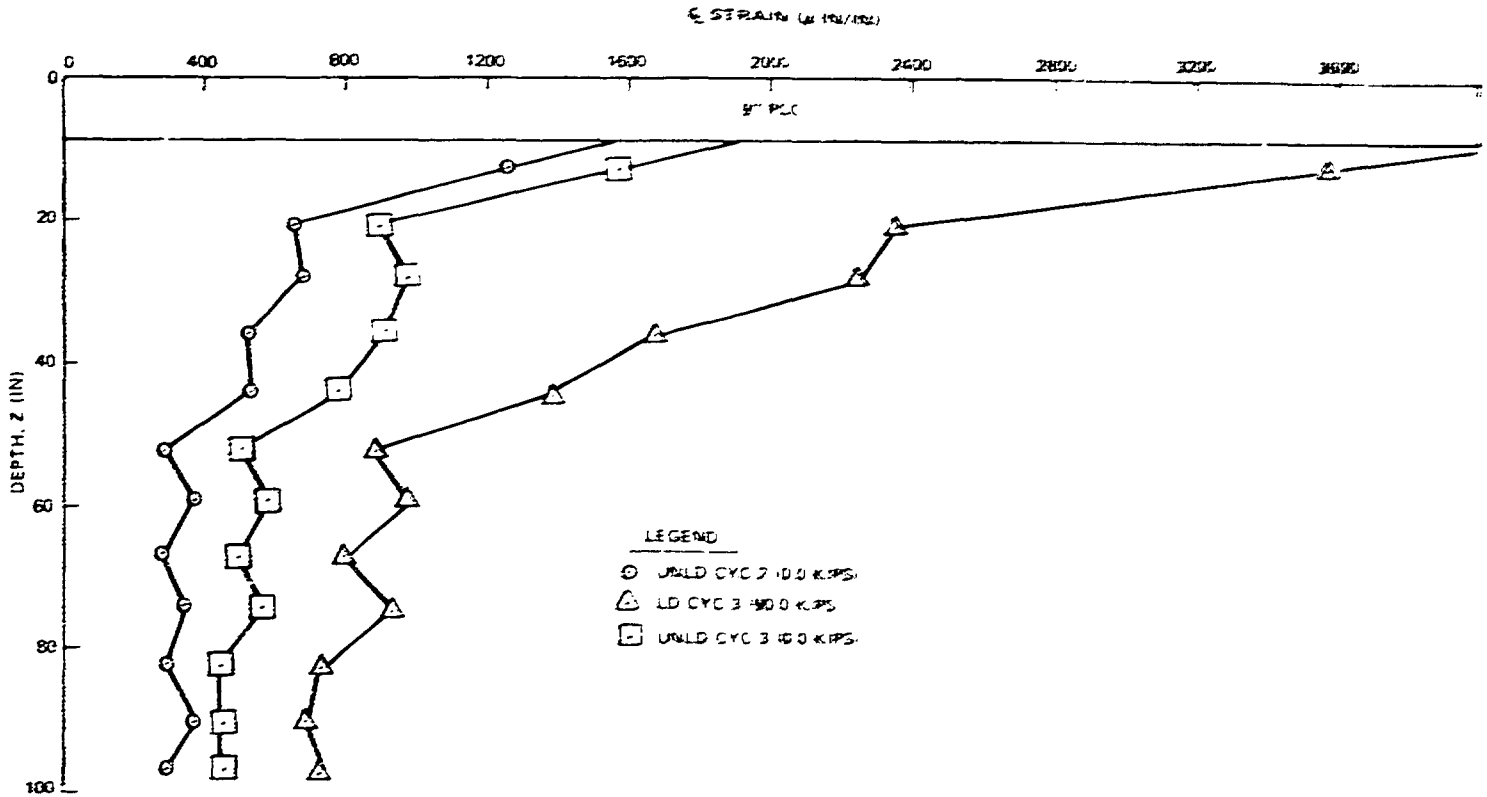

Figure B-46. Centerline Soil Strain Versus Depth, Test B1, Cycles 2 and 3

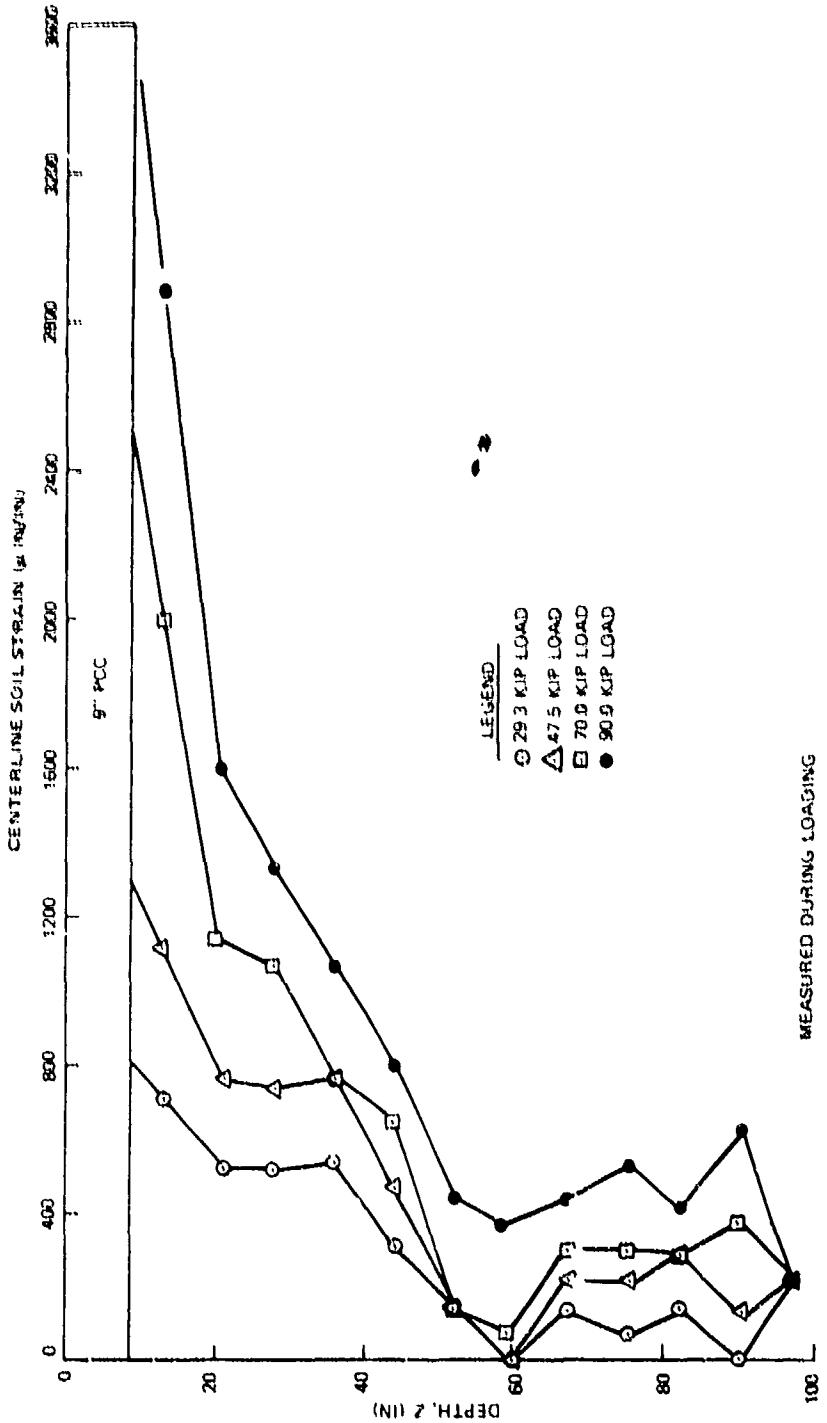

Figure B-47. Centerline Soil Strain Versus Depth, Test E1, Cycle 4

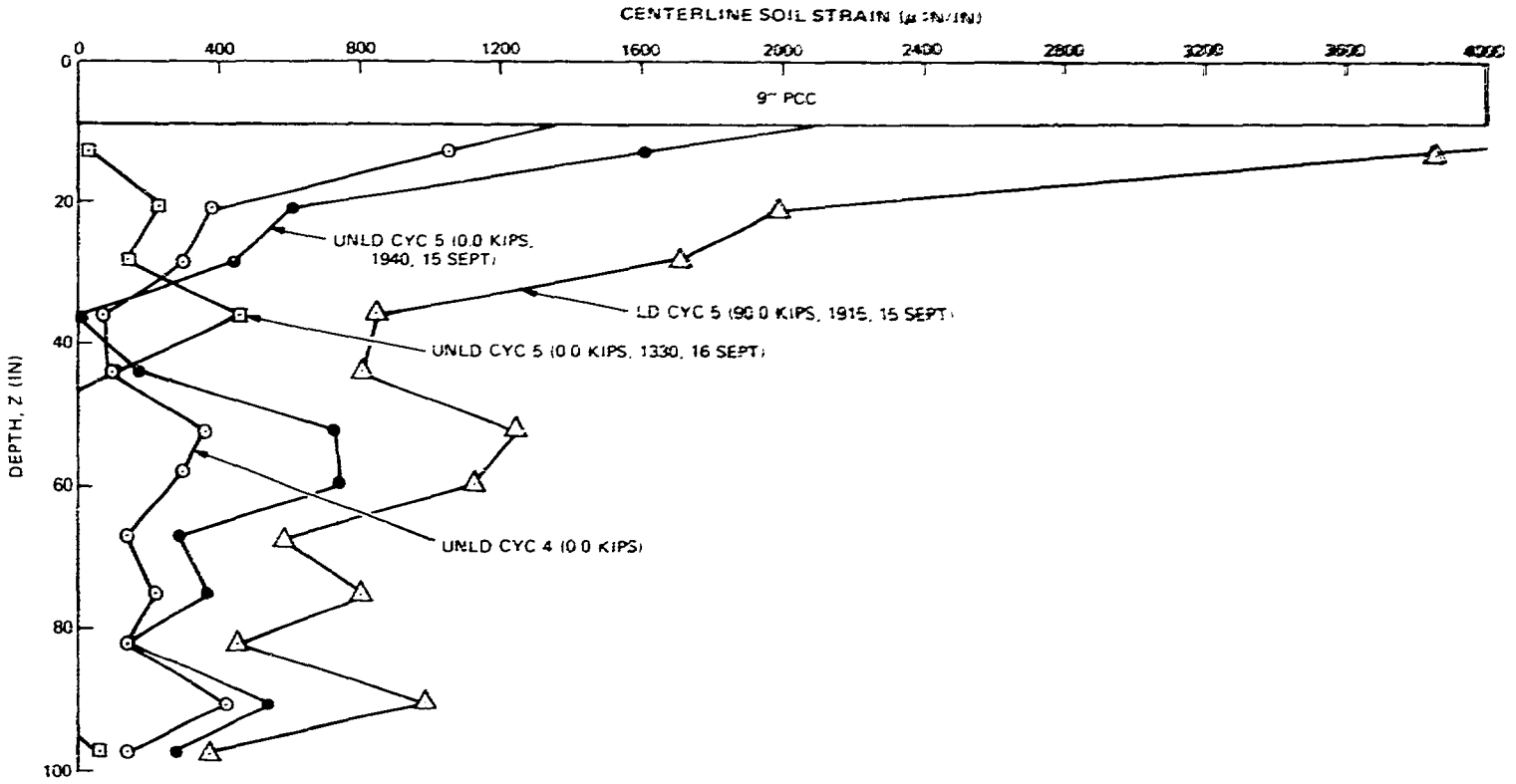

Figure B-48. Centerline Soil Strain Versus Depth, Test B1, Cycles 4 and 5

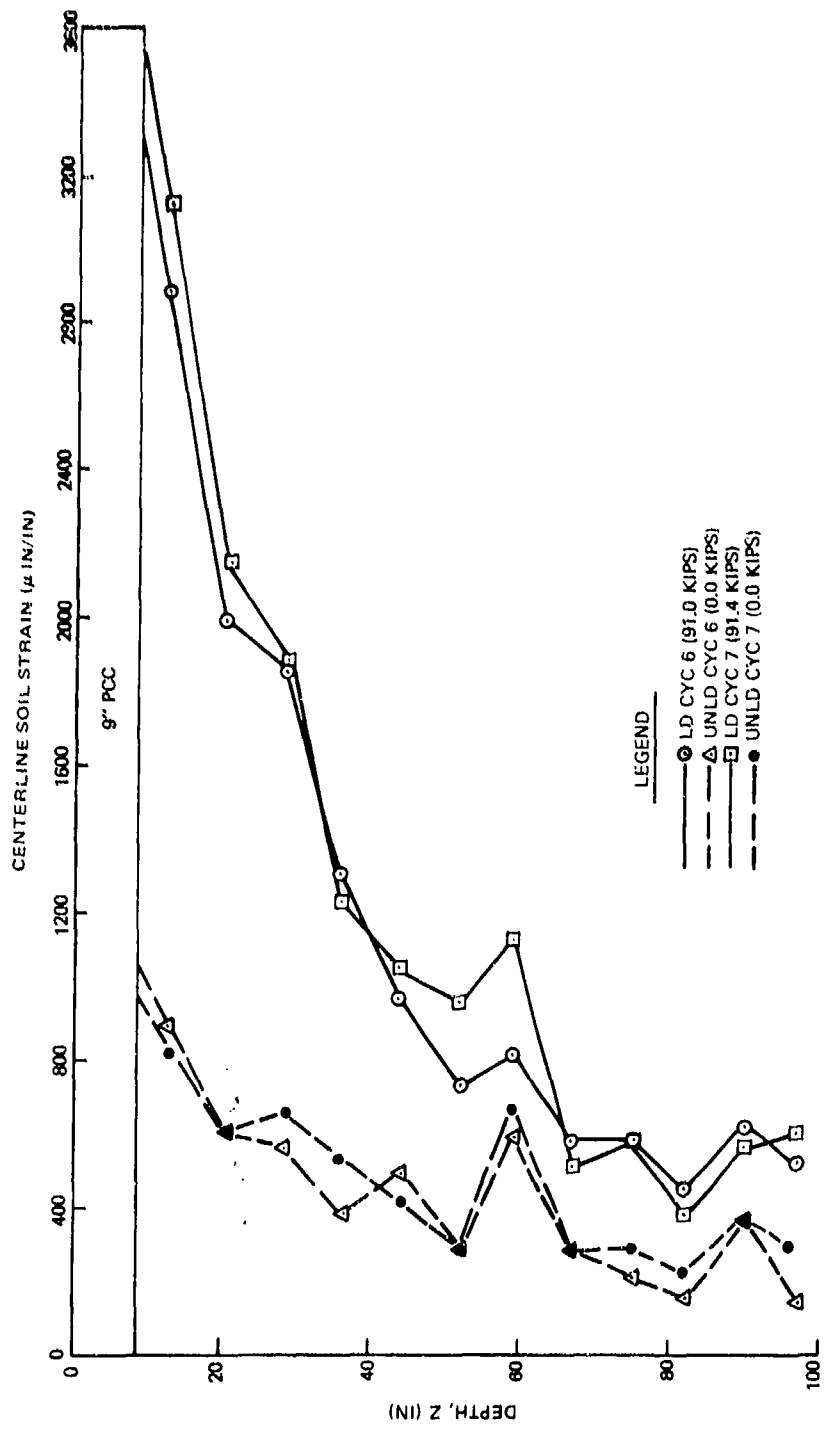

Figure B-49. Centerline Soil Strain Versus Depth, Test B1, Cycles 6 and 7

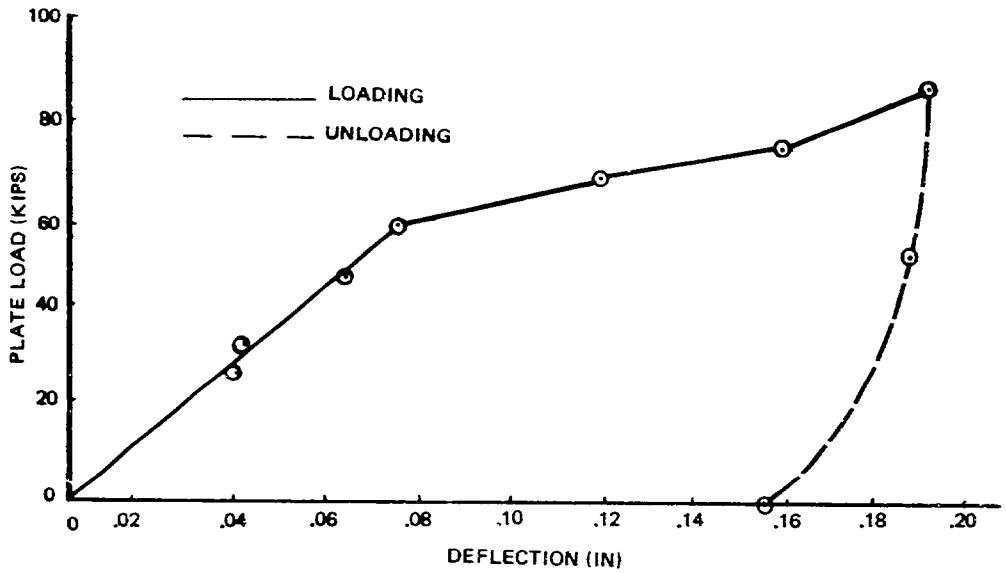

Figure B-50. Summation Centerline Bison Gage Relative Deflections Versus Plate Load, Test B1, Cycle 1

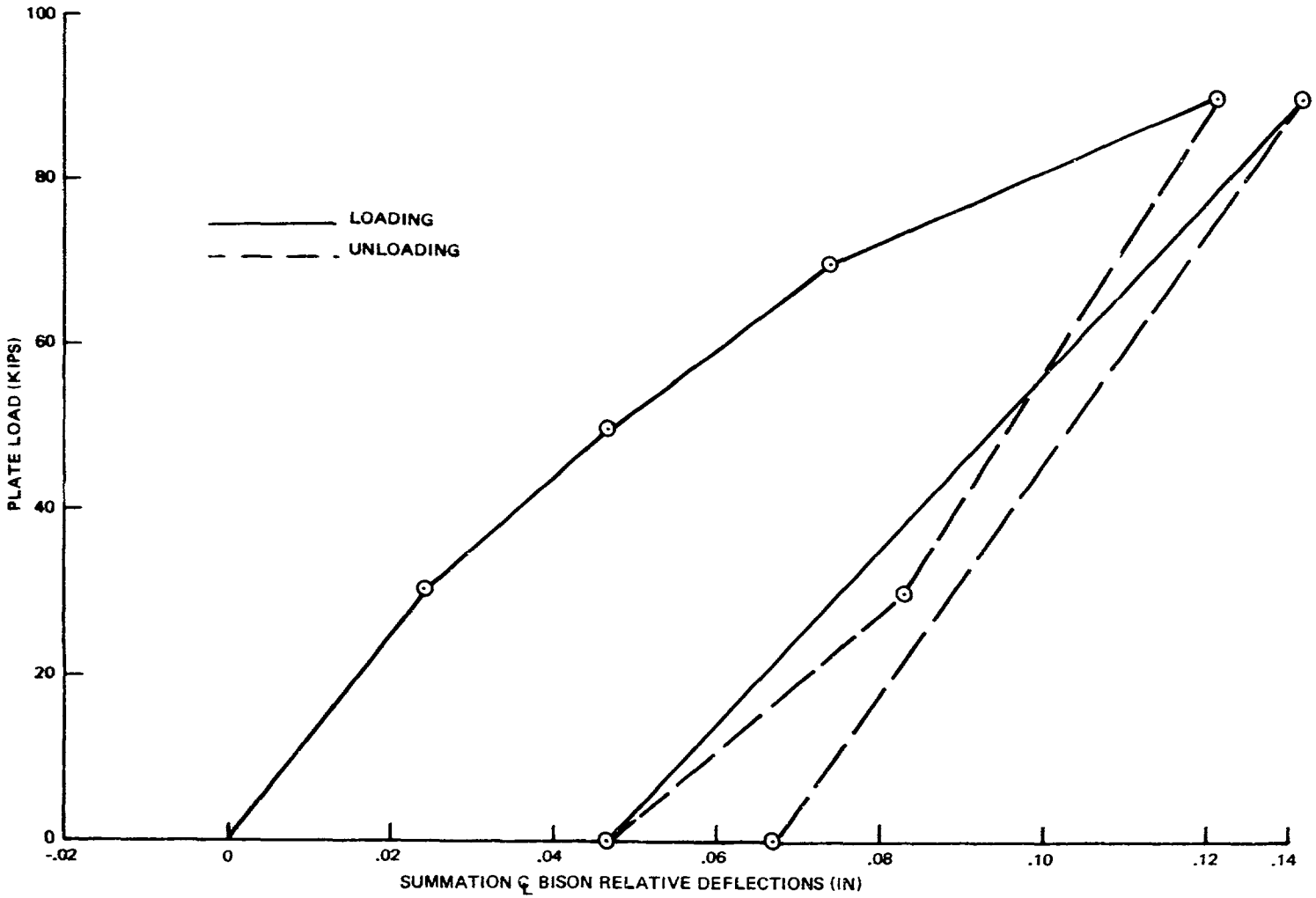

Figure B-51. Plate Load Versus Summation Centerline Bison Gage Relative Deflections, Test B1, Cycles 2 and 3

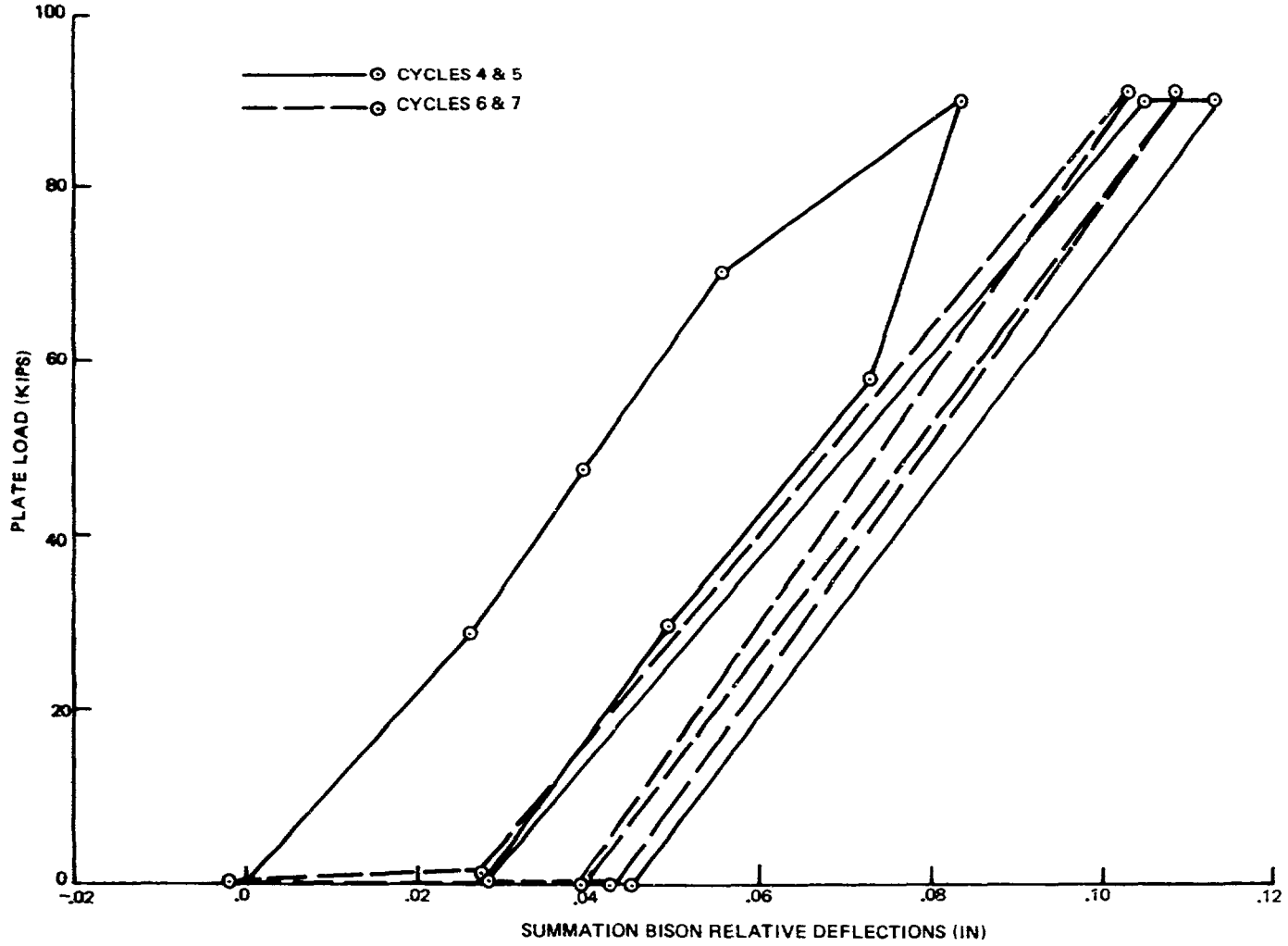

Figure B-52. Plate Load Versus Summation Centerline Bison Gage Relative Deflections, Test B1, Cycles 4 through 7

PART B-5

LOAD TEST DATA FOR PAVEMENT SECTION B2

Pavement section B2 consists of 6 inch PCC, supported by a 8.5 inch lime stabilized clay, and placed on the clay subgrade of Site B, Figure 15. The results of the load tests conducted on this section follow. Also shown in Figure B-70 is the stiffness of the stabilized base. An outline of the tests conducted is shown in Table 1 and their description is given in Section III.4.

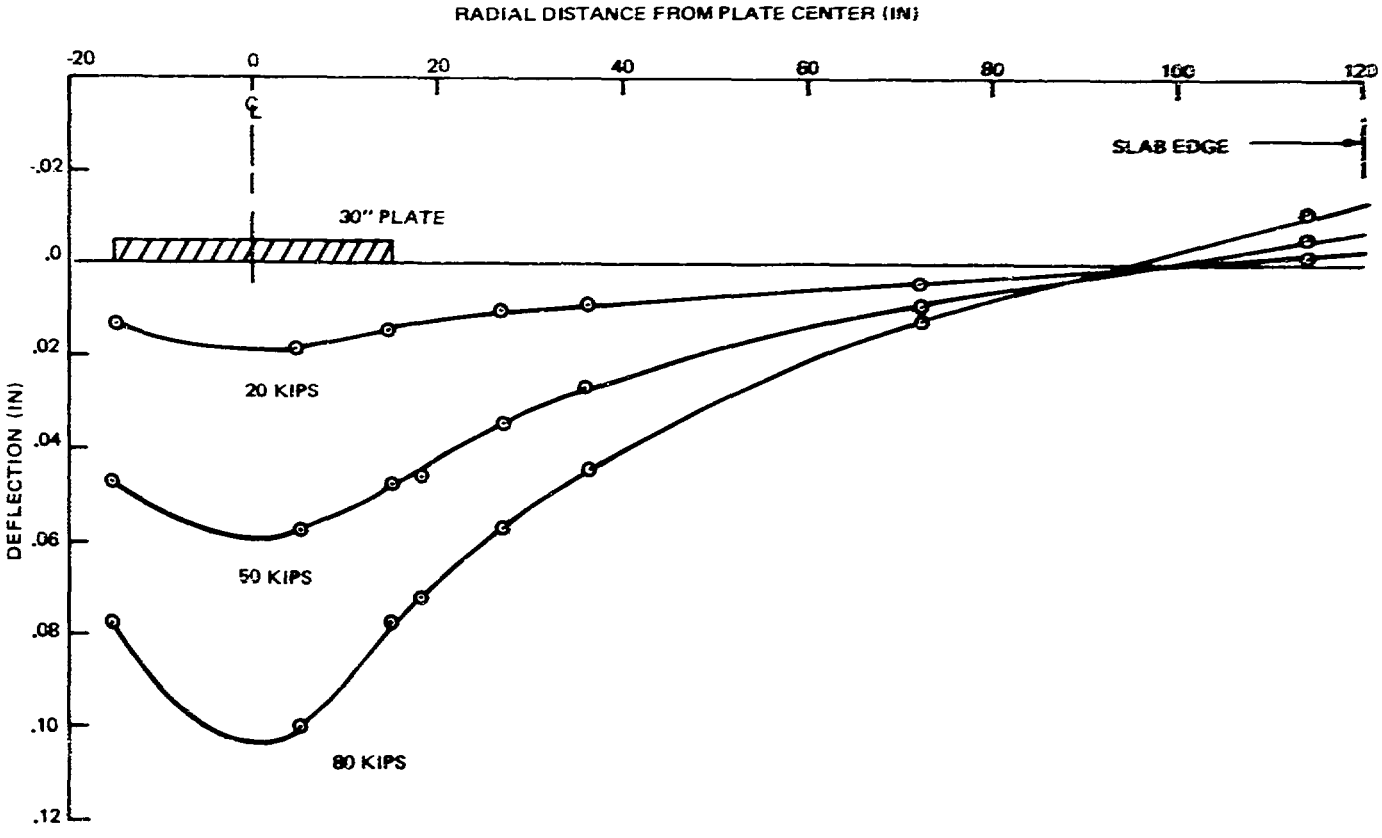

Figure B-53. Radial Distance Versus Deflection, Test B2, Cycle 1

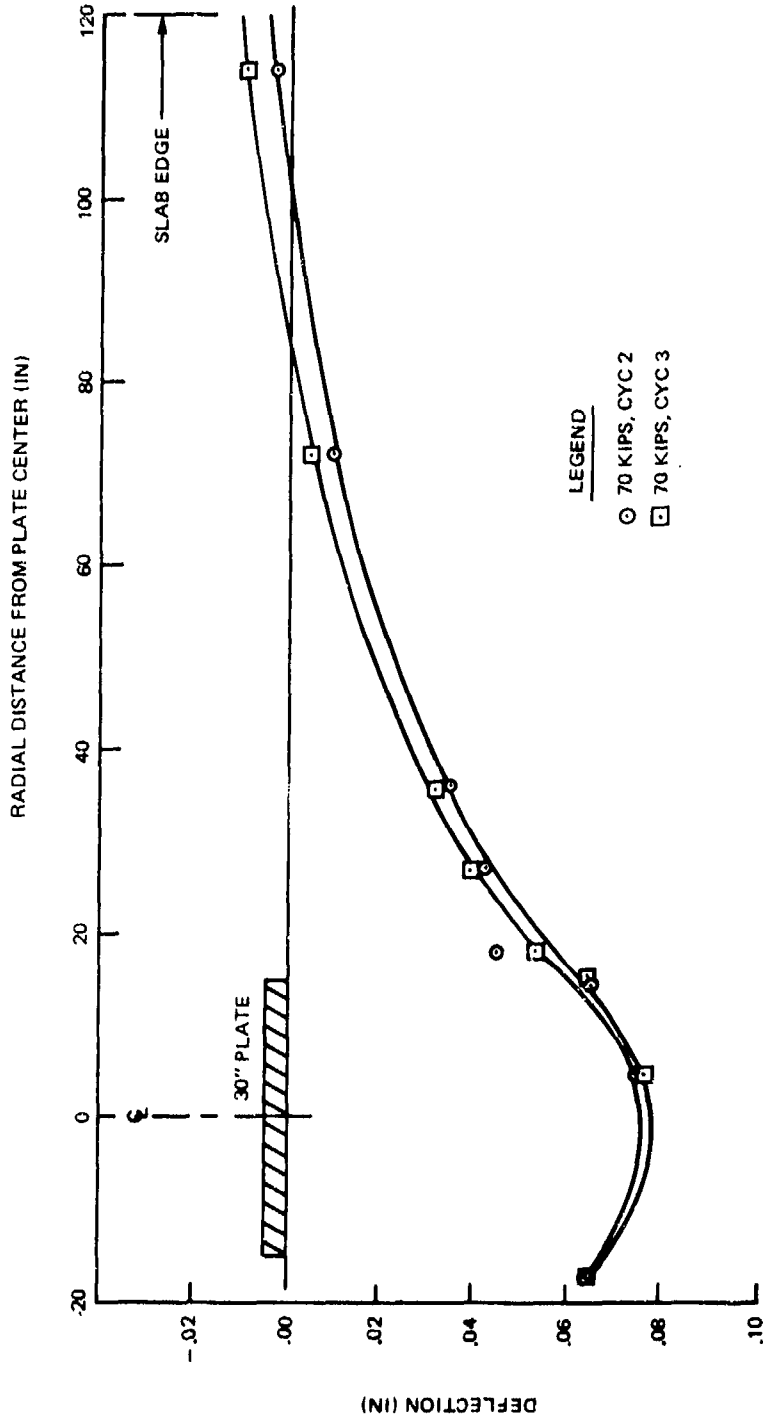

Figure B-54. Radial Distance Versus Deflection, Test B2, Cycles 2 and 3

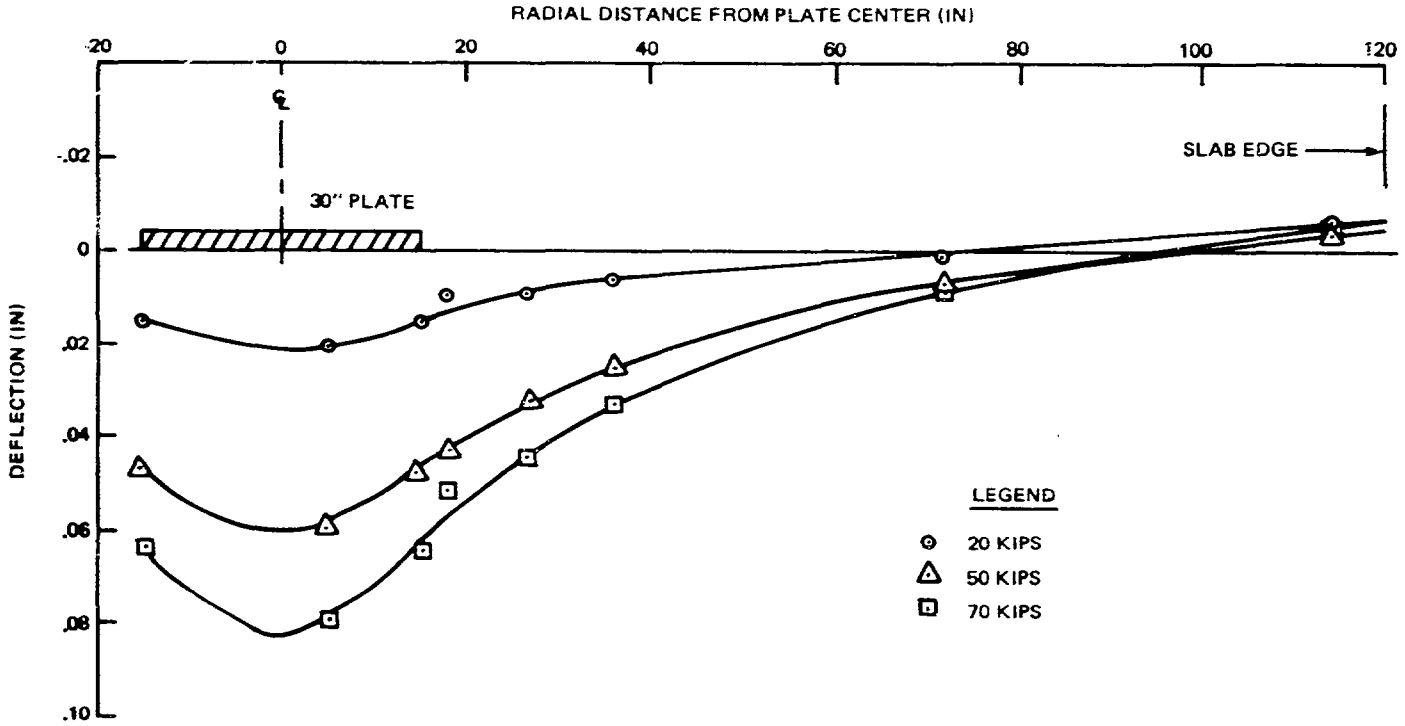

Figure B-55. Radial Distance Versus Deflection, Test B2, Cycle 4

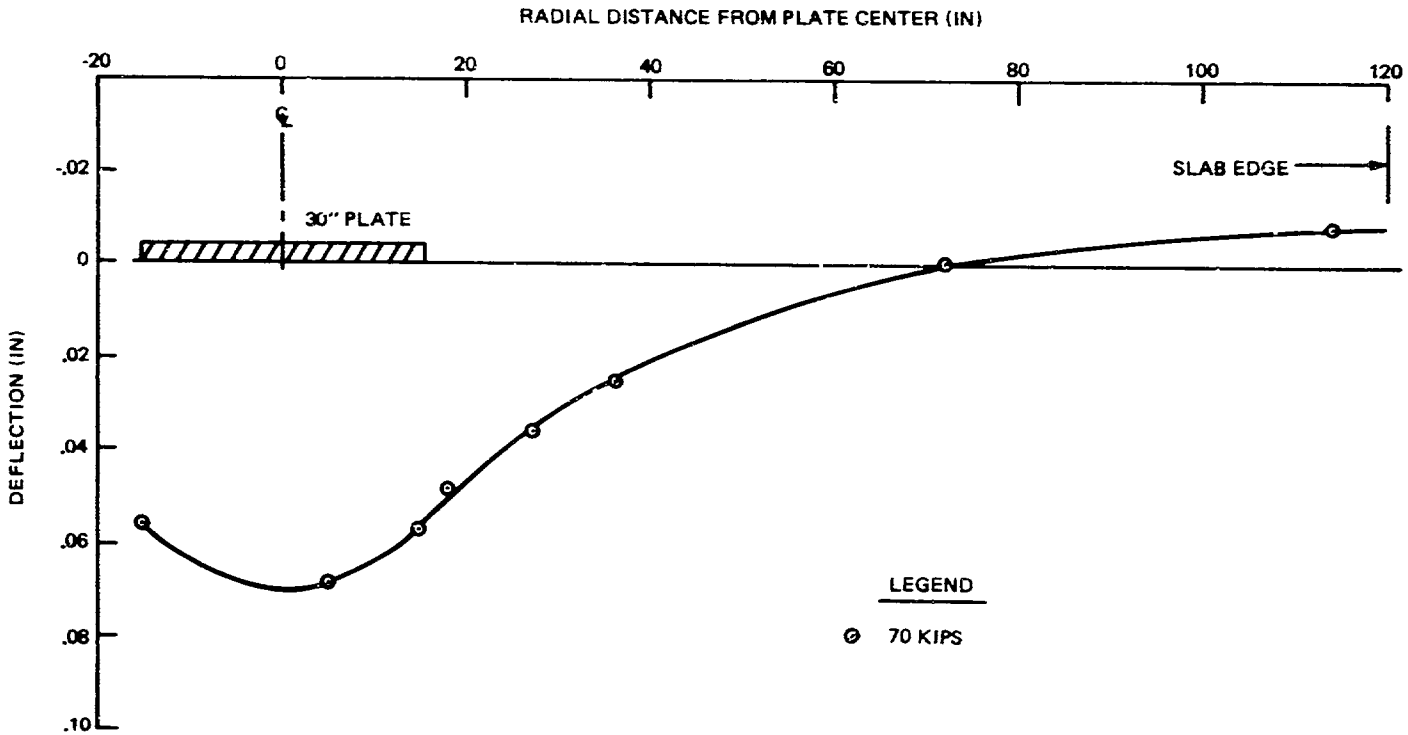

Figure B-56. Radial Distance Versus Deflection, Test B2, Cycle 5

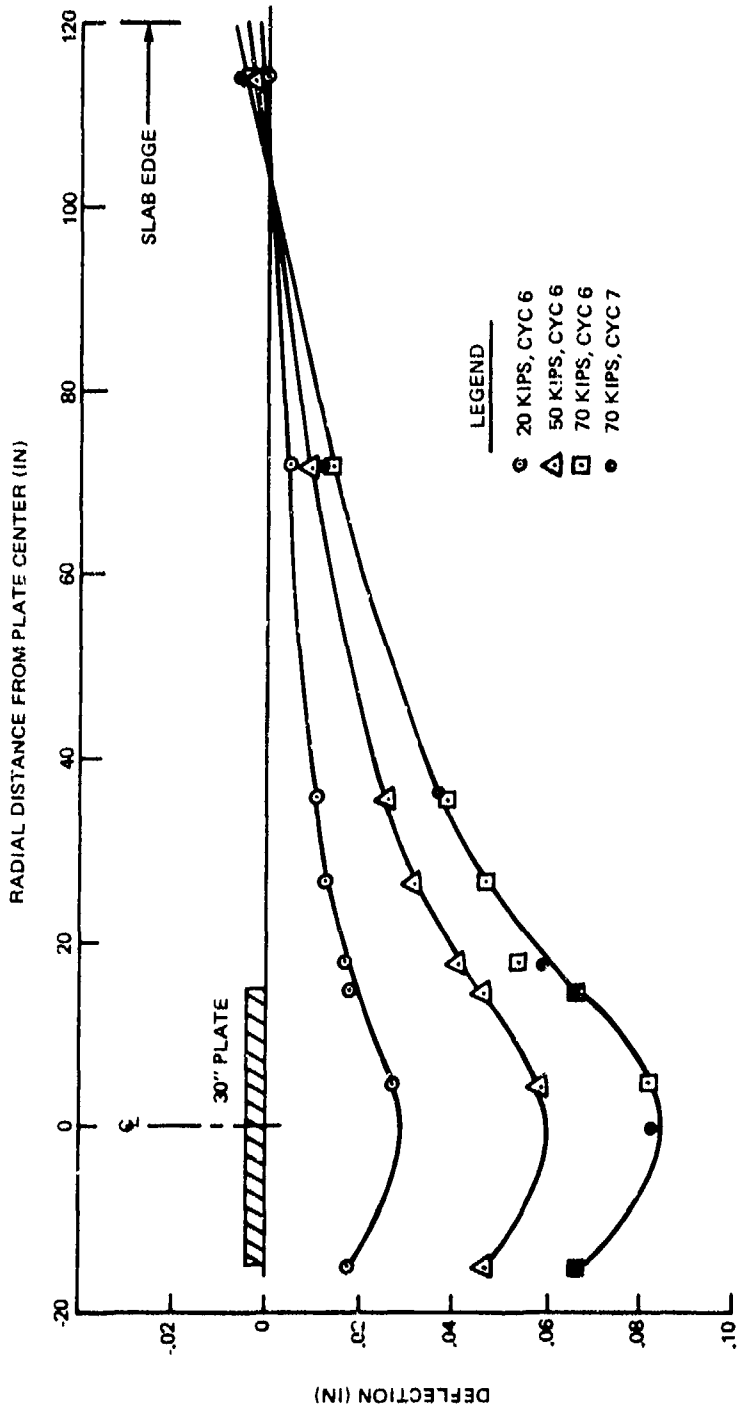

Figure B-57. Radial Distance Versus Deflection, Test B2, Cycles 6 and 7

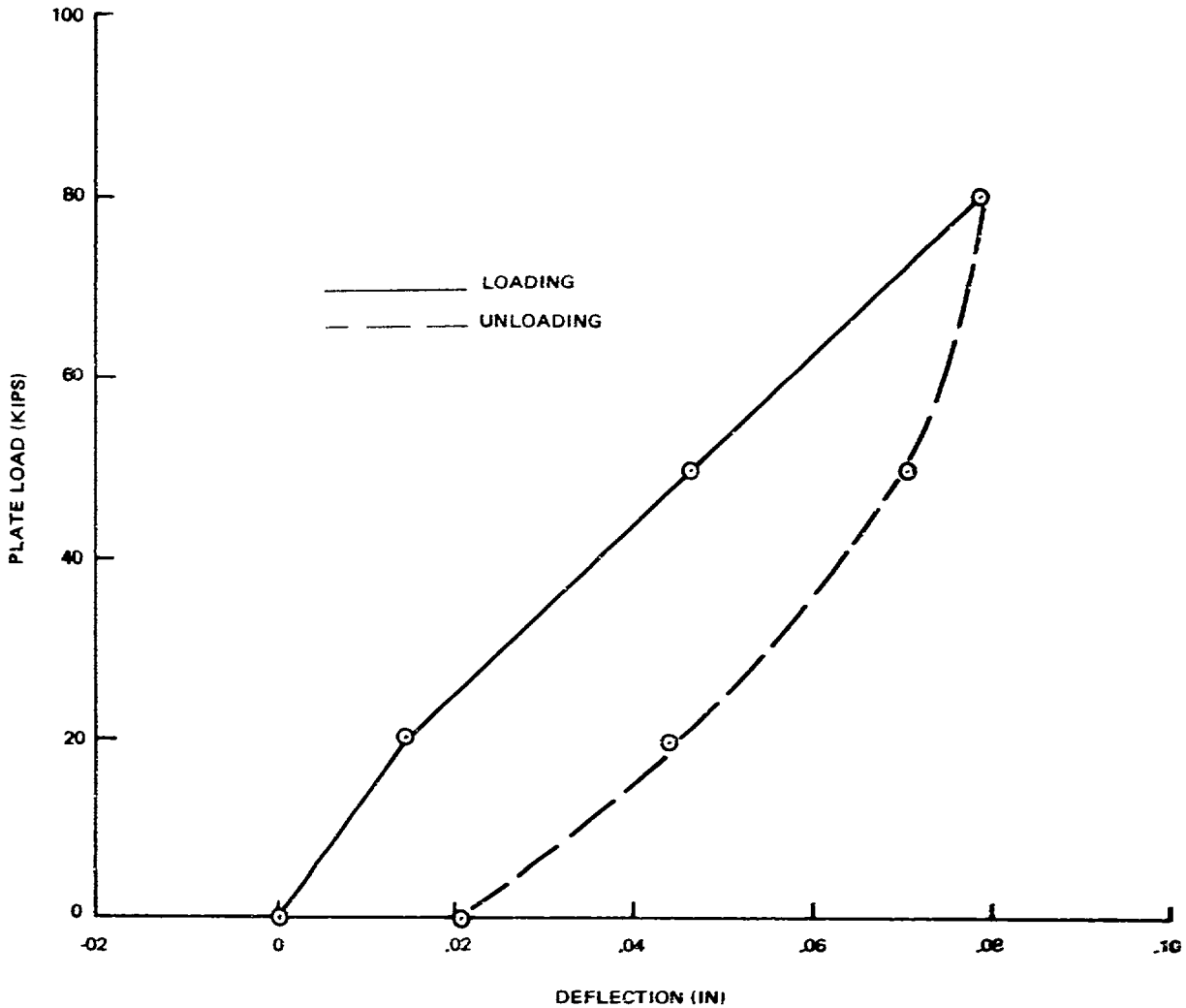

Figure B-58. Average Plate Edge Deflections Versus Plate Load, Test B2, Cycle 1

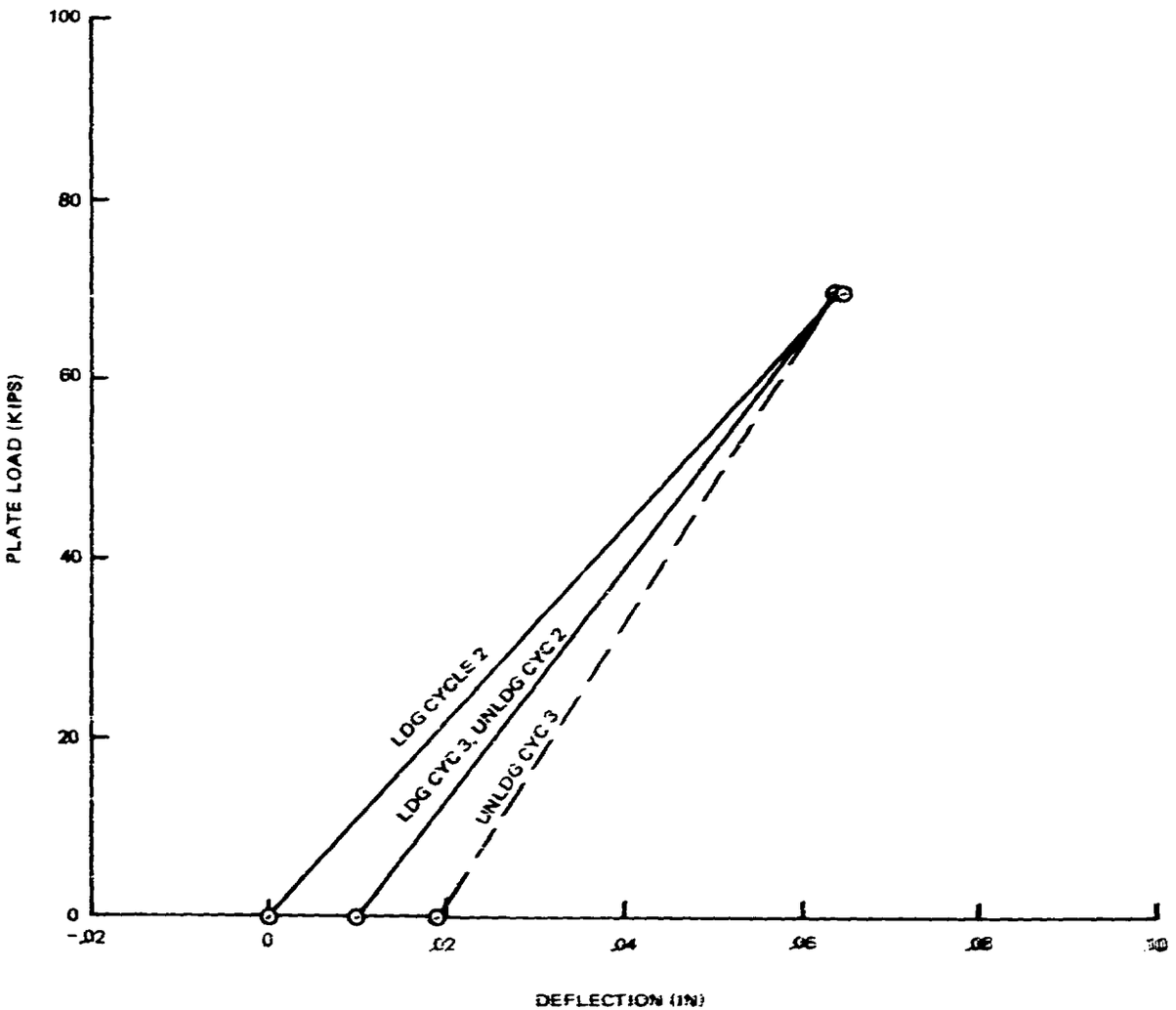

Figure B-59. Average Plate Edge Deflections Versus Plate Load, Test B2, Cycles 2 and 3

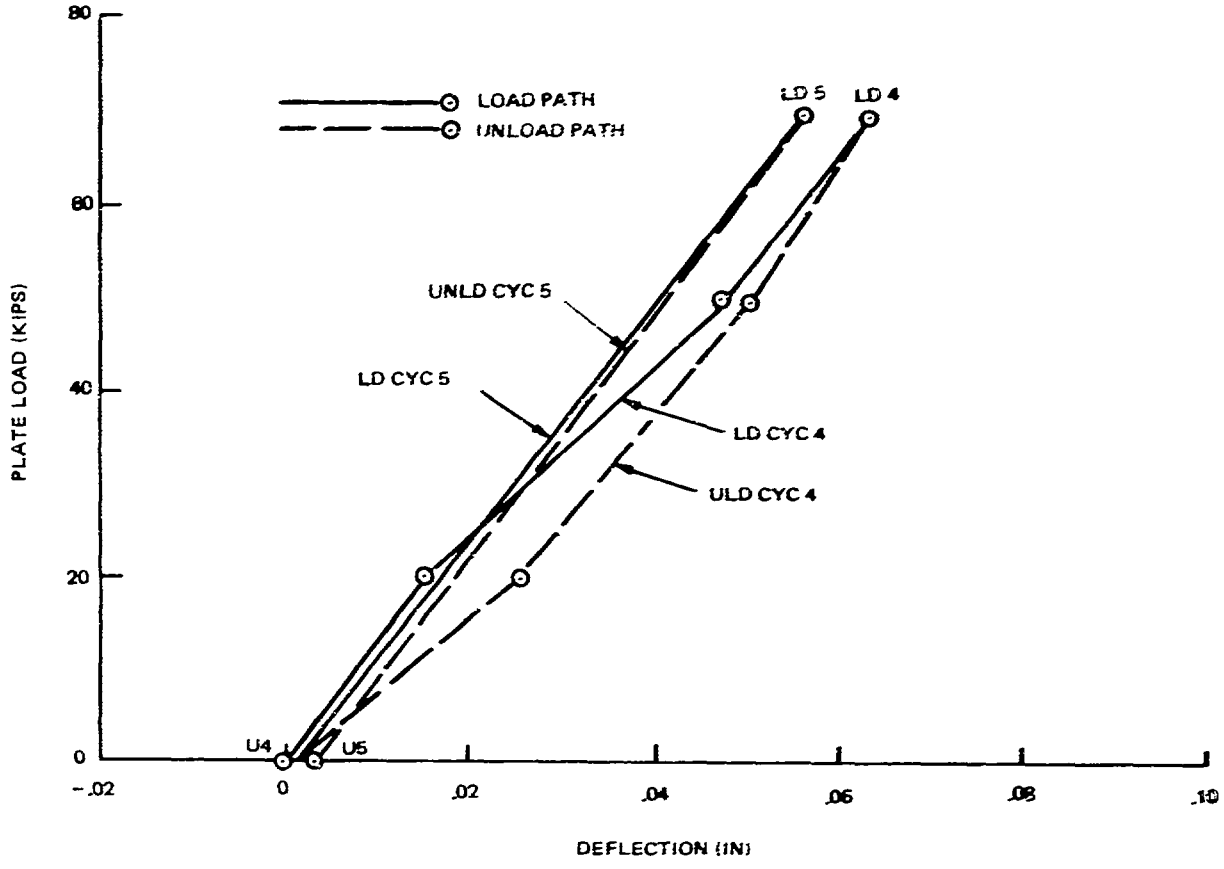

Figure B-60. Average Plate Edge Deflection Versus Plate Load, Test B2, Cycles 4 and 5

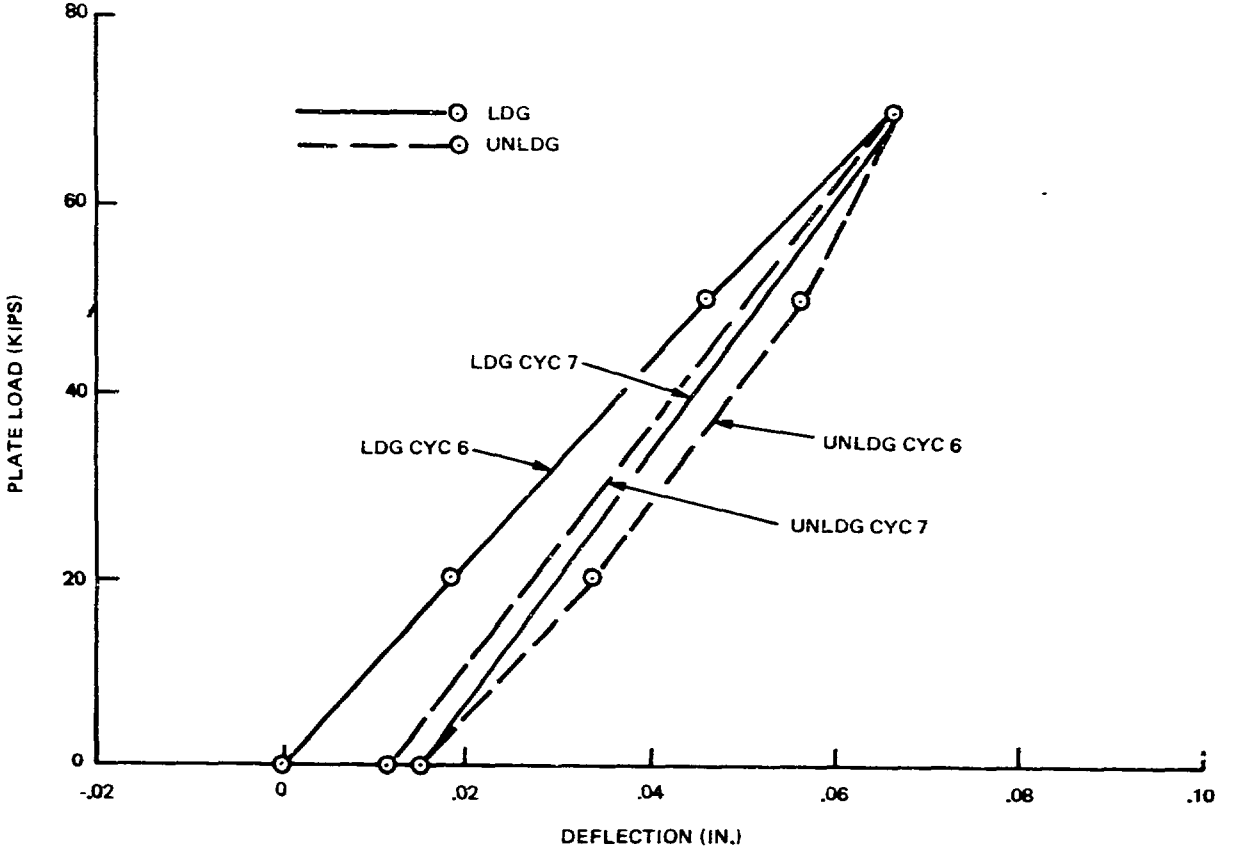

Figure B-61. Average Plate Edge Deflection Versus Plate Load, Test B2, Cycles 6 and 7

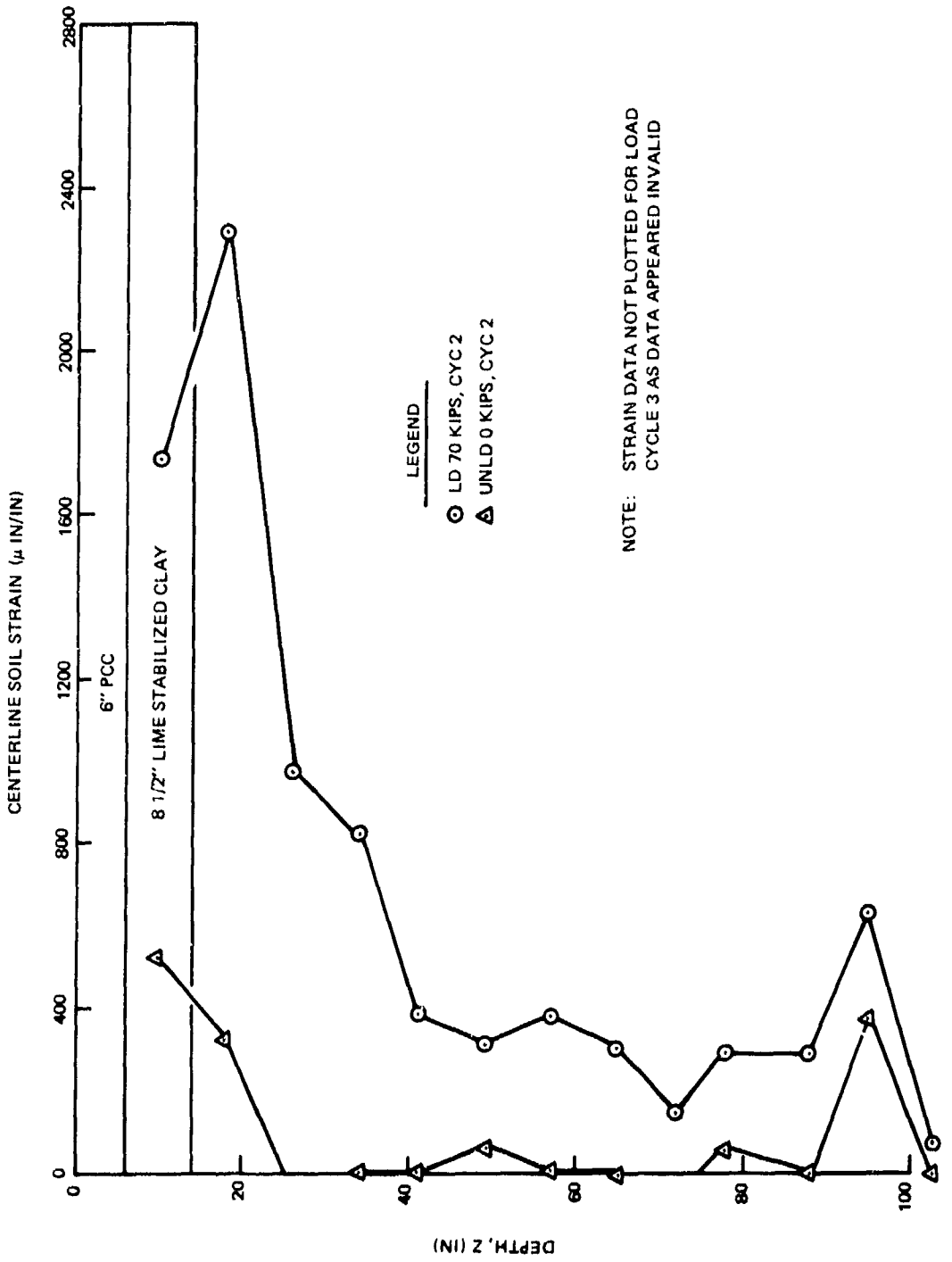

Figure B-62. Centerline Soil Strain Versus Depth, Test B2, Cycle 2

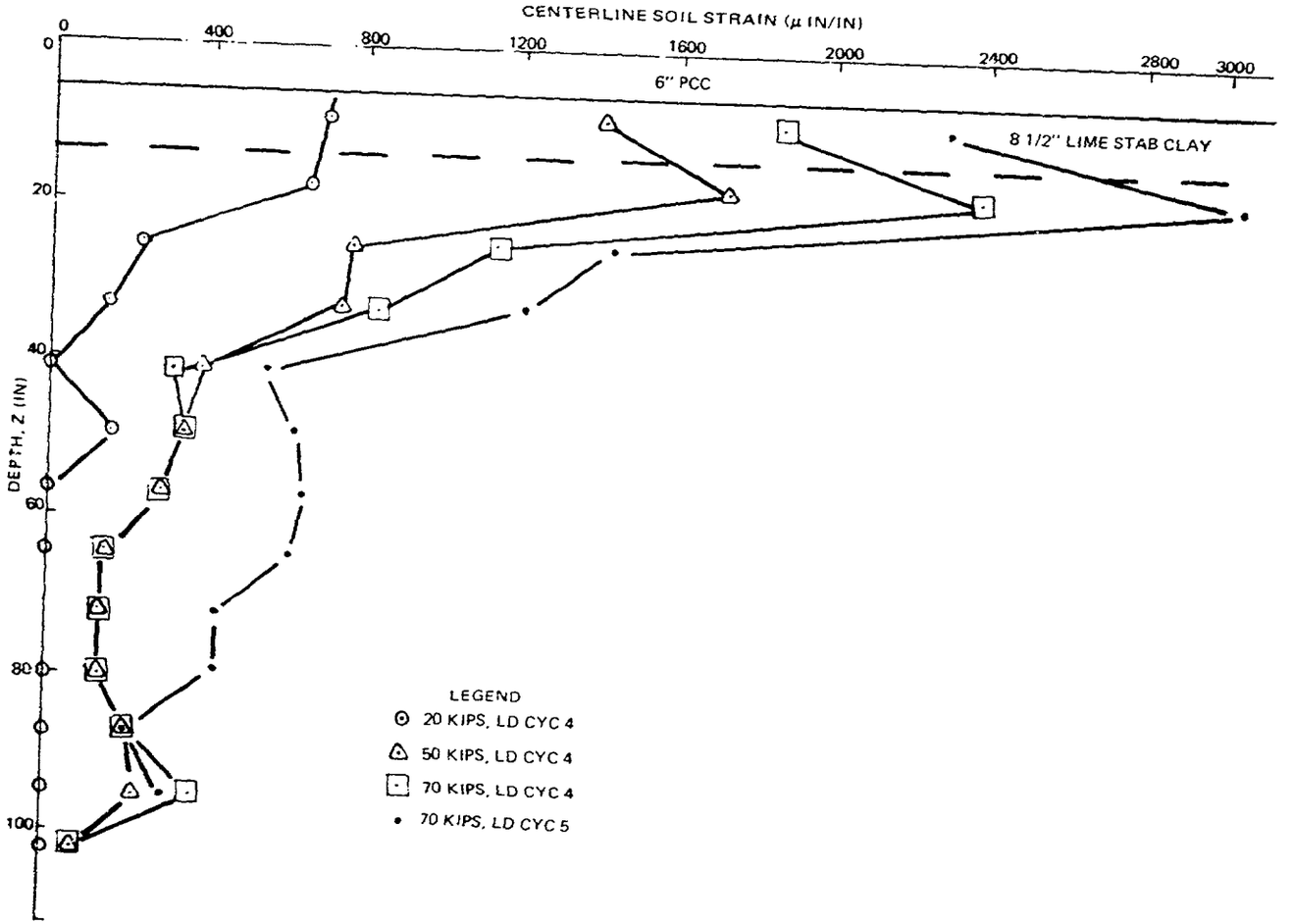

Figure B-63. Centerline Soil Strain Versus Depth, Test B2, Cycles 4 and 5

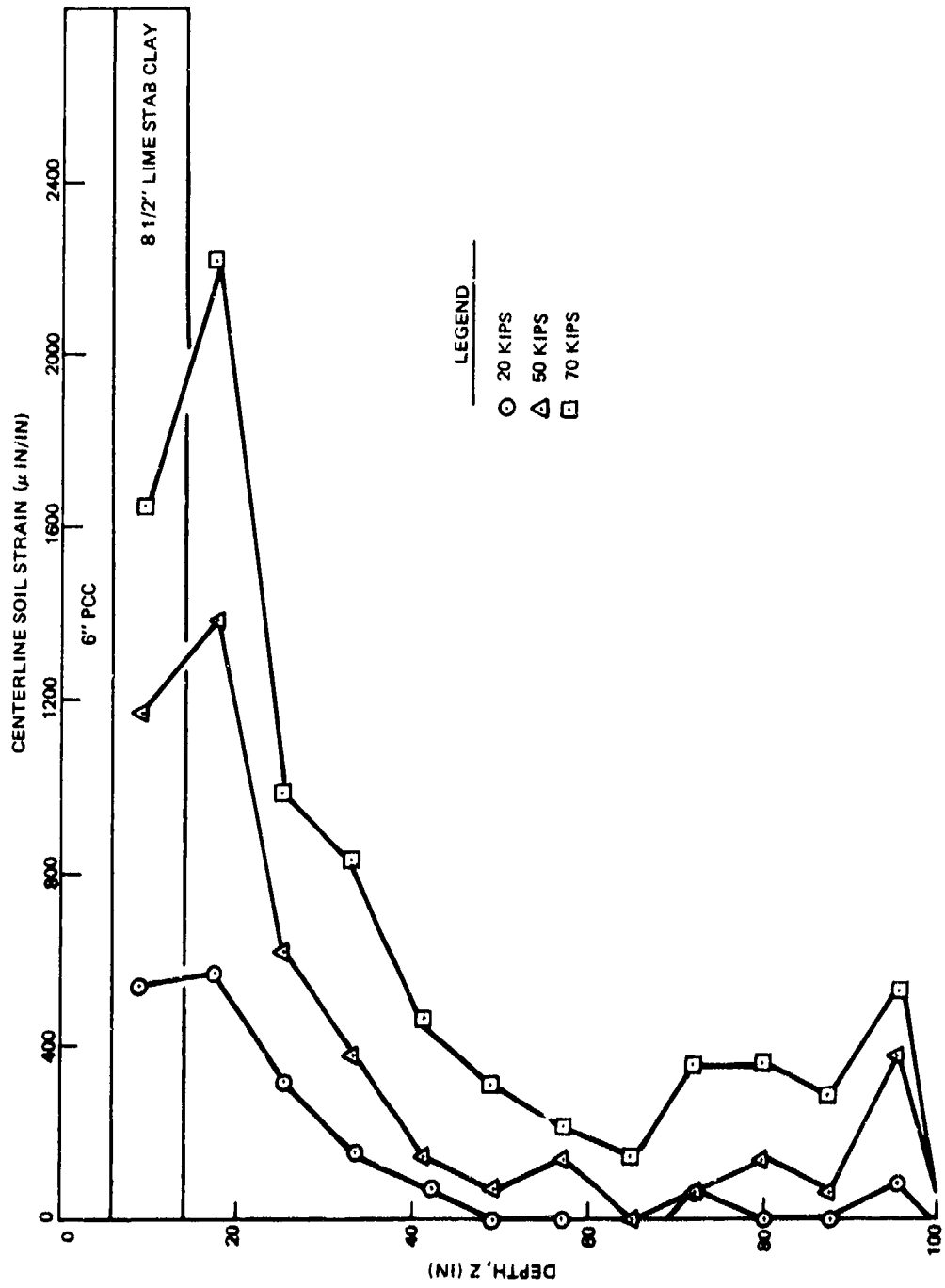

Figure B-64. Centerline Soil Strain Versus Depth, Test B2, Cycle 6

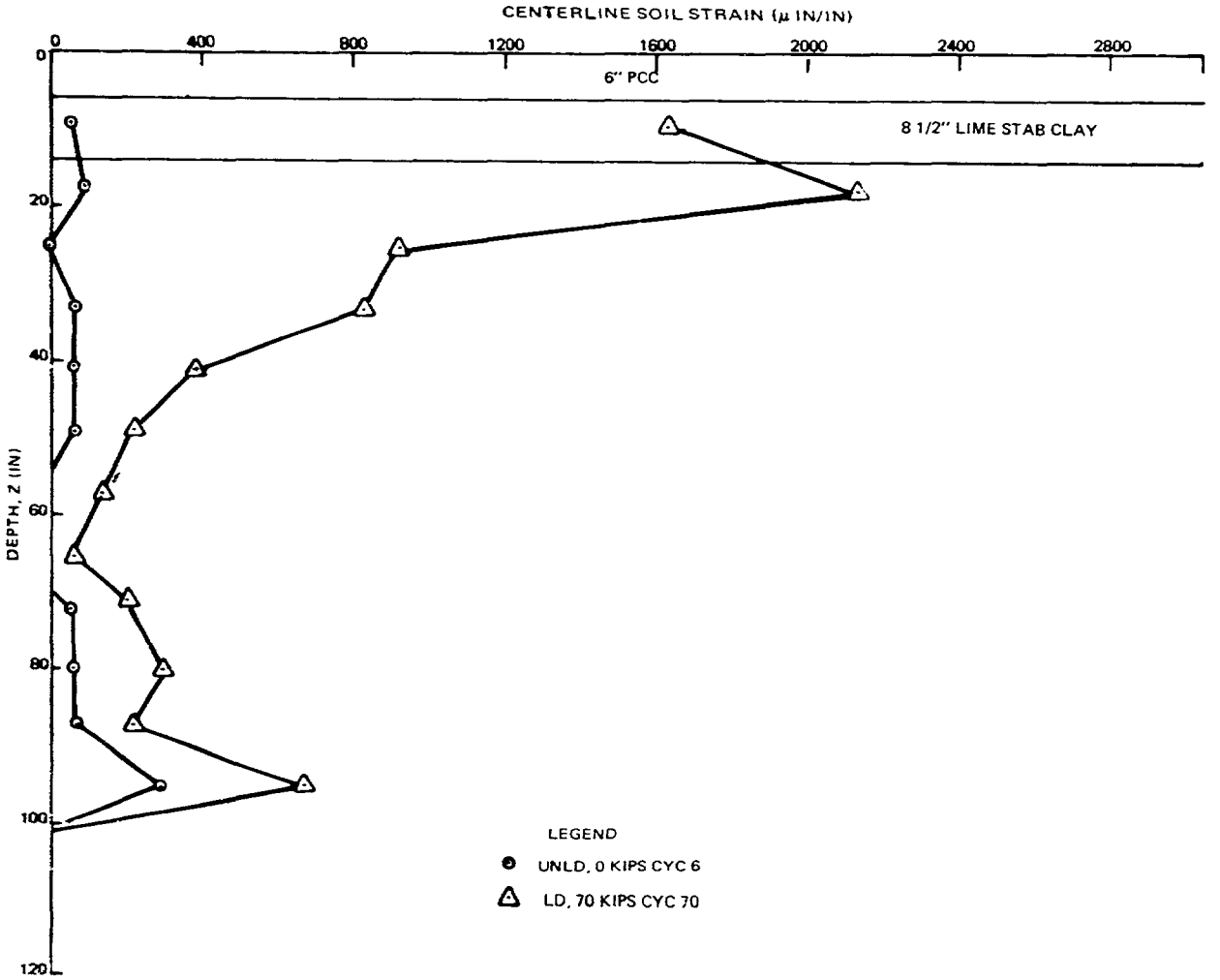

Figure B-65. Centerline Soil Strain Versus Depth, Test B2, Cycles 6 and 7

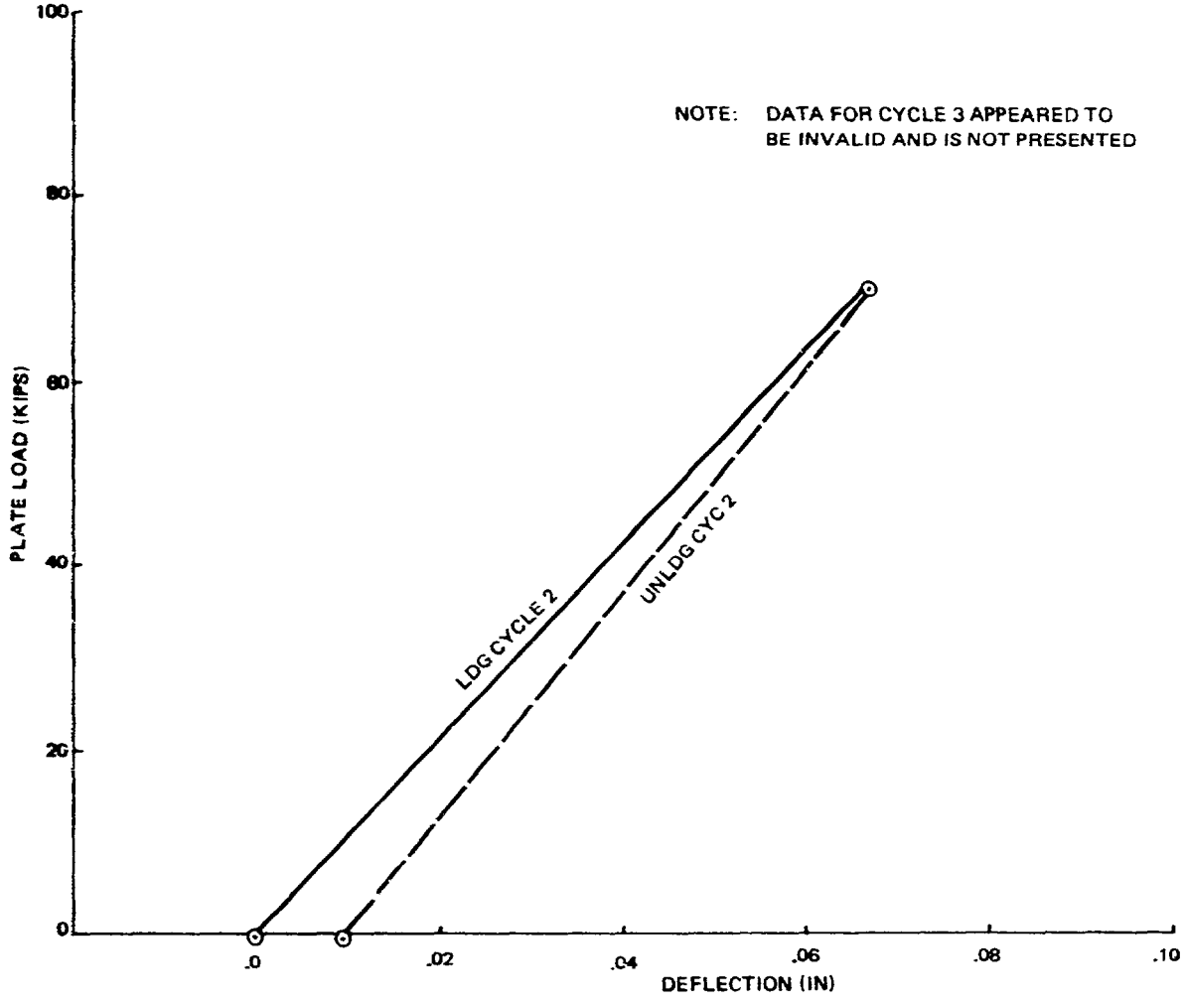

Figure B-66. Summation of Centerline Bison Gage Relative Deflections, Test B2, Cycle 2

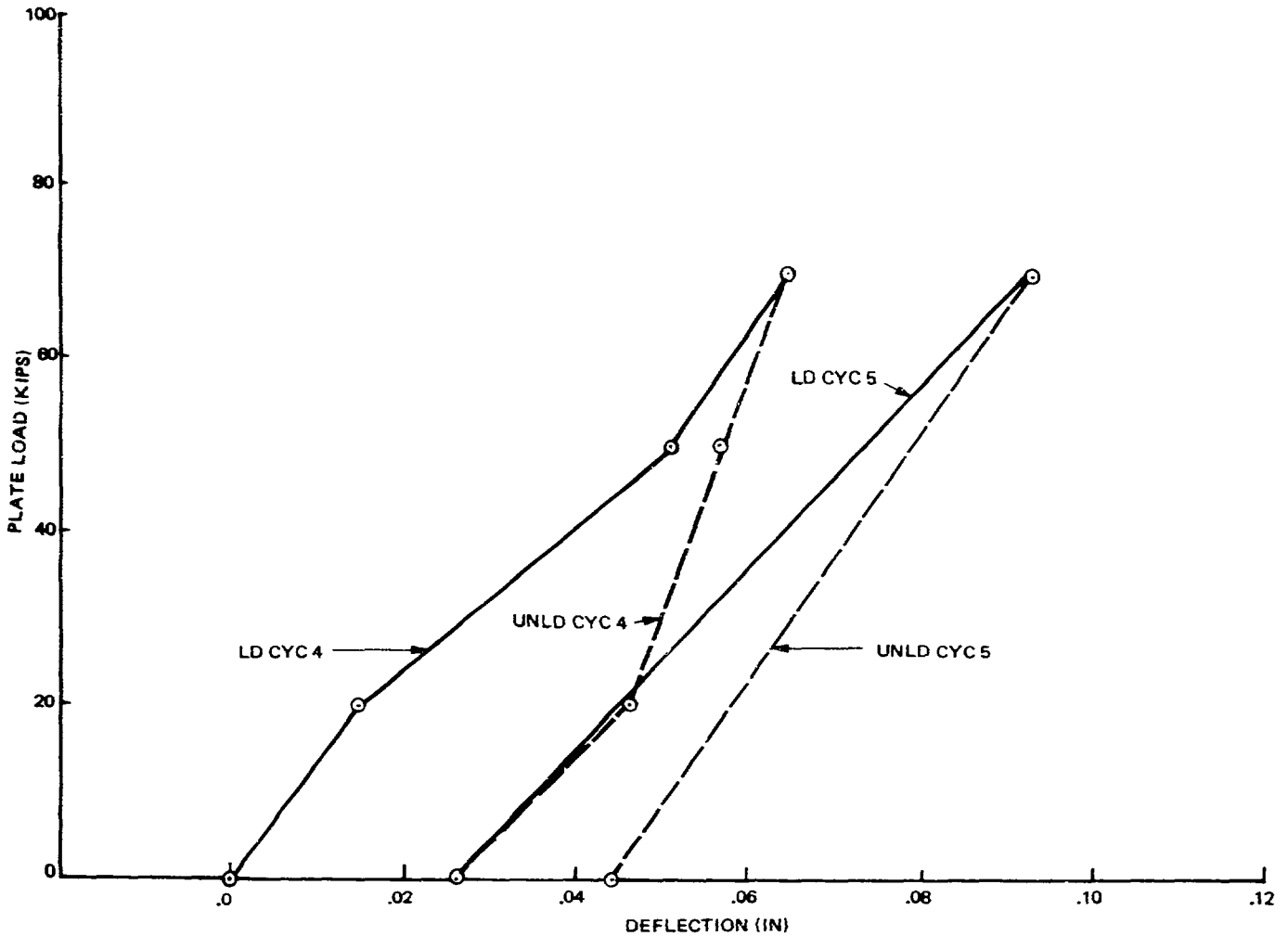

Figure B-67. Summation Centerline Bison Gage Relative Deflections, Test B2, Cycles 4 and 5

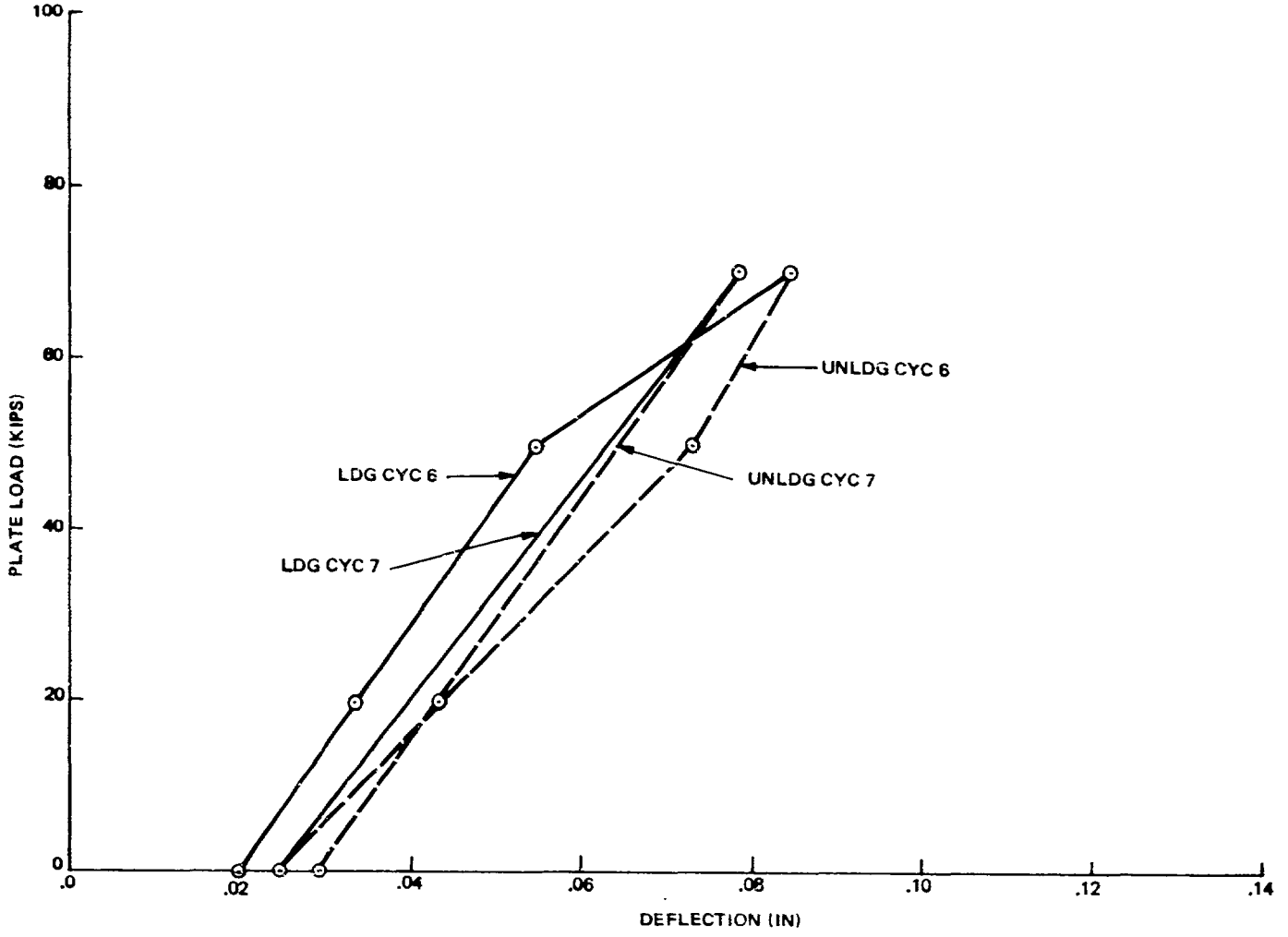

Figure B-68. Summation Centerline Bison Gage Relative Deflections, Test B-2, Cycles 6 and 7

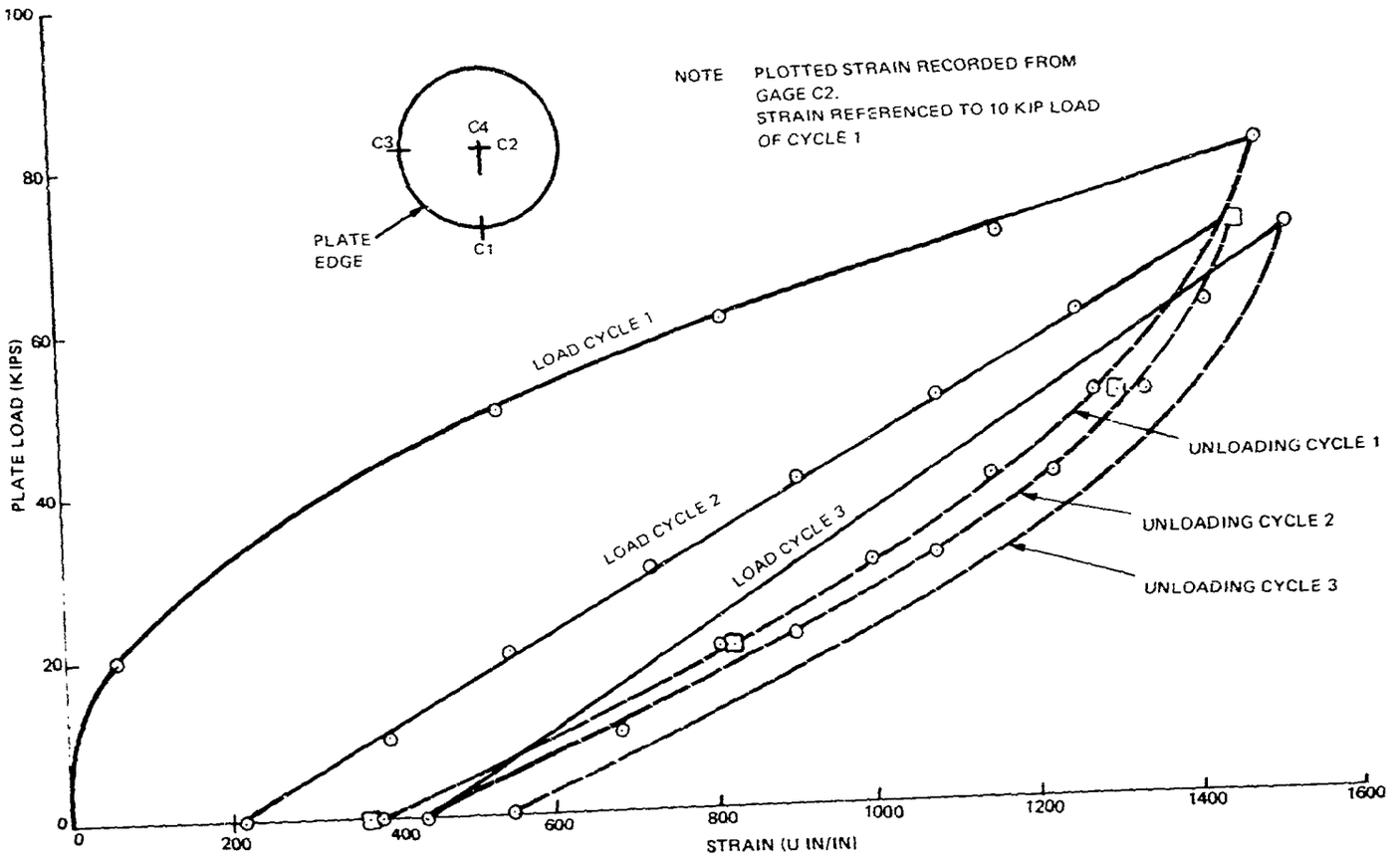

Figure B-69. Concrete Strain Versus Plate Load, Test B-2, Cycles 1 - 3

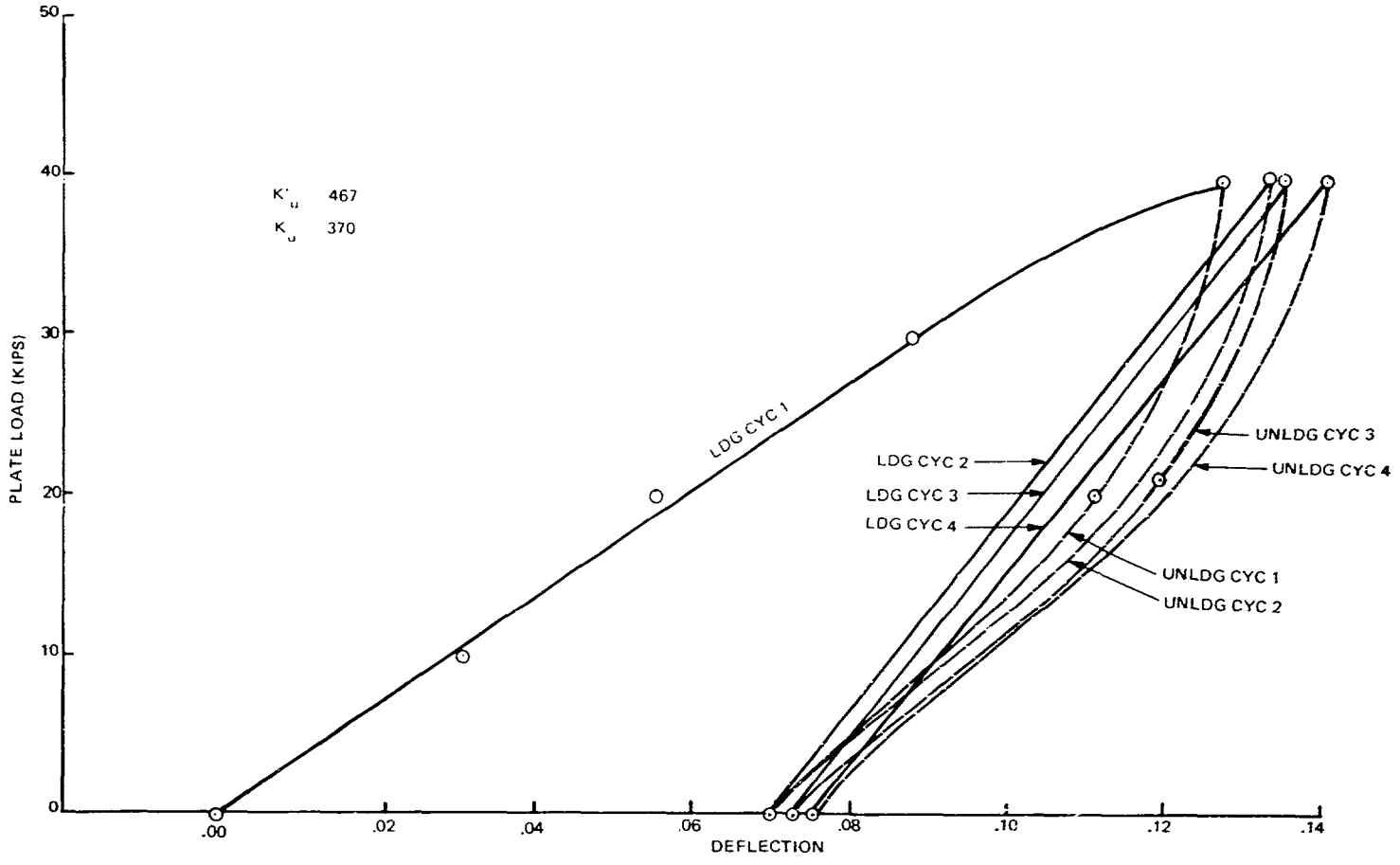

Figure B-70. Plate Load Versus Deflection on Surface of Stabilized Clay

APPENDIX C

MATERIAL TEST DATA

This Appendix contains experimental data obtained on specimens of the various airfield pavement component materials. Considerable experimental data was secured for the improved subgrade material, so much in fact that the large bulk of electronically recorded output for the compacted clay had to be compressed into the form of charts to permit publication. On the other hand, for the more conventional pavement materials, such as the portland cement concrete and the asphalt base, only a minimum of identifying tests were possible.

PART C-1

LABORATORY DATA ON COOK'S BAYOU SAND

Table C-1. Summary of Tests for Cook's Bayou Sand

Test Type	Test Numbers	Tabular Test Data (Table Nos.)
Hydrostatic	1,2	3,4
One-Dimensional Constrained Compression (K_o)	3,4	5,6
Triaxial Compression	5,6,7,8,9	7,8,9,10,11

Table C-2. Abbreviations Used in Data Tables

Term	Definition
RADI STRE	Radial stress - psi
STRES DIFF	Axial stress - Radial stress
AX STRESS	Axial stress - psi
MEAN STRE	$\frac{2 \text{ radial stress} + \text{axial stress}}{3}$
AXIAL STRAIN	inch/inch
RADIAL STRAIN	inch/inch
VOLUME STRAIN	$\frac{\text{Change in volume}}{\text{total volume}} = \text{axial strain} + 2 \text{ radial strain}$
STRAIN DIFF	Axial strain - Radial strain

Table C-3. Tabular Data from Hydrostatic Test of Cook's Bayou Sand (Test 1)

DIAMETER = 2.735 HEIGHT = 4.250 CROSS SECTION L AREA = 5.861

Dry Density = 112.06 lbs/ft^3

RADI STRE	STRE DIFF	AX STRE	MEAN STRE	AXIAL STRAIN	RADIAL STRAIN	VOLUME STRAIN	STRAIN DIFF
5	0.00	5.00	5.00	0.00000	0.00000	0.00000	0.00000
10	0.00	10.00	10.00	0.00019	0.00011	0.00041	0.00008
20	0.00	20.00	20.00	0.00040	0.00033	0.00106	0.00007
30	0.00	30.00	30.00	0.00059	0.00055	0.00169	0.00004
40	0.00	40.00	40.00	0.00073	0.00073	0.00219	-.00000
50	0.00	50.00	50.00	0.00089	0.00091	0.00272	-.00002
40	0.00	40.00	40.00	0.00068	0.00080	0.00229	-.00012
30	0.00	30.00	30.00	0.00052	0.00069	0.00191	-.00018
20	0.00	20.00	20.00	0.00038	0.00055	0.00147	-.00017
10	0.00	10.00	10.00	0.00019	0.00033	0.00085	-.00014
5	0.00	5.00	5.00	0.00009	0.00022	0.00053	-.00013
25	0.00	25.00	25.00	0.00061	0.00062	0.00185	-.00001
50	0.00	50.00	50.00	0.00094	0.00099	0.00292	-.00005
75	0.00	75.00	75.00	0.00122	0.00128	0.00378	-.00006
100	0.00	100.00	100.00	0.00146	0.00154	0.00453	-.00008
75	0.00	75.00	75.00	0.00108	0.00135	0.00379	-.00027
50	0.00	50.00	50.00	0.00080	0.00110	0.00299	-.00030
25	0.00	25.00	25.00	0.00052	0.00080	0.00213	-.00029
5	0.00	5.00	5.00	0.00021	0.00037	0.00094	-.00015
25	0.00	25.00	25.00	0.00075	0.00077	0.00229	-.00001
50	0.00	50.00	50.00	0.00108	0.00113	0.00335	-.00005
75	0.00	75.00	75.00	0.00134	0.00139	0.00412	-.00005
100	0.00	100.00	100.00	0.00155	0.00161	0.00477	-.00006
125	0.00	125.00	125.00	0.00179	0.00183	0.00544	-.00004
150	0.00	150.00	150.00	0.00198	0.00201	0.00600	-.00003
125	0.00	125.00	125.00	0.00165	0.00186	0.00538	-.00022
100	0.00	100.00	100.00	0.00144	0.00172	0.00487	-.00028
75	0.00	75.00	75.00	0.00120	0 00150	0.00420	-.00030
50	0.00	50.00	50.00	0.00101	0.00128	0.00357	-.00027
25	0.00	25.00	25.00	0.00071	0.00095	0.00261	-.00024
5	0.00	5.00	5.00	0.00031	0.00048	0.00126	-.00017
50	0.00	50.00	50.00	0.00139	0.00124	0.00387	0.00015
100	0.00	100.00	100.00	0.00179	0.00168	0.00515	0.00011
150	0.00	150.00	150.00	0.00207	0.00208	0.00624	-.00001
175	0.00	175.00	175.00	0.00226	0.00223	0.00672	0.00003
200	0.00	200.00	200.00	0.00240	0.00241	0.00723	-.00001

Table C-3. Continued

DIAMETER = 2.735 HEIGHT = 4.250 CROSS SECTIONAL AREA = 5.861

Dry Density = 112.06 lbs/ft^3

RADI STRE	STRE DIFF	AX STRE	MEAN STRE	AXIAL STRAIN	RADIAL STRAIN	VOLUME STRAIN	STRAIN DIFF
150	0.00	150.00	150.00	0.00200	0.00216	0.00631	-.00016
100	0.00	100.00	100.00	0.00165	0.00186	0.00538	-.00022
50	0.00	50.00	50.00	0.00125	0.00143	0.00410	-.00018
5	0.00	5.00	5.00	0.00056	0.00062	0.00181	-.00006
50	0.00	50.00	50.00		0.00139	0.00	
100	0.00	100.00	100.00	0.00205	0.00186	0.00578	0.00018
150	0.00	150.00	150.00	0.00240	0.00219	0.00679	0.00021
200	0.00	200.00	200.00	0.00273	0.00249	0.00770	0.00024
225	0.00	225.00	225.00	0.00296	0.00263	0.00823	0.00033
250	0.00	250.00	250.00	0.00304	0.00274	0.00852	0.00029
200	0.00	200.00	200.00	0.00264	0.00256	0.00775	0.00008
150	0.00	150.00	150.00	0.00231	0.00230	0.00691	0.00000
100	0.00	100.00	100.00	0.00195	0.00201	0.00597	-.00006
50	0.00	50.00	50.00	0.00148	0.00154	0.00455	-.00005
5	0.00	5.00	5.00	0.00071	0.00084	0.00239	-.00014

Table C-4. Tabular Data from Hydrostatic Test of Cook's Bayou Sand - Test 2

DIAMETER = 2.722 HEIGHT = 4.250 CROSS SECTIONAL AREA = 5.810

Dry Density = 111.50 lbs/ft^3

RADI STRE	STRE DIFF	AX STRE	MEAN STRE	AXIAL STRAIN	RADIAL STRAIN	VOLUME STRAIN	STRAIN DIFF
0	0.00	0.00	0.00	0.00000	0.00000	0.00000	0.00000
25	0.00	25.00	25.00	0.00059	0.00051	0.00162	0.00007
50	0.00	50.00	50.00	0.00096	0.00088	0.00273	0.00008
75	0.00	75.00	75.00		0.00118		
100	0.00	100.00	100.00	0.00162	0.00143	0.00449	0.00019
125	0.00	125.00	125.00	0.00188	0.00162	0.00512	0.00027
150	0.00	150.00	150.00	0.00207	0.00180	0.00567	0.00027
175	0.00	175.00	175.00	0.00226	0.00198	0.00623	0.00027
200	0.00	200.00	200.00	0.00240	0.00213	0.00666	0.00027
225	0.00	225.00	225.00	0.00256	0.00228	0.00712	0.00029
250	0.00	250.00	250.00	0.00268	0.00242	0.00753	0.00026
225	0.00	225.00	225.00	0.00240	0.00235	0.00710	0.00005
200	0.00	200.00	200.00	0.00224	0.00228	0.00679	-.00004
175	0.00	175.00	175.00	0.00209	0.00217	0.00643	-.00007
150	0.00	150.00	150.00	0.00193	0.00206	0.00604	-.00013
125	0.00	125.00	125.00	0.00179	0.00191	0.00561	-.00012
100	0.00	100.00	100.00	0.00162	0.00176	0.00515	-.00014
75	0.00	75.00	75.00	0.00146	0.00158	0.00462	-.00012
50	0.00	50.00	50.00	0.00127	0.00136	0.00399	-.00009
25	0.00	25.00	25.00	0.00101	0.00107	0.00314	-.00005
5	0.00	5.00	5.00	0.00056	0.00059	0.00174	-.00002

END OF RUN 21

RUNNING TIME: 2.6 SECS 1/O TIME: .7 SECS

READY

Table C-5. Tabular Data from One-Dimensional Constrained Compression Test - Test 3

DIAMETER = 2.742 HEIGHT = 6.032 CROSS SECTIONAL AREA = 5.881

Dry Density = 111.87 lbs/ft^3

RADI STRE	STRE DIFF	AX STRE	MEAN STRE	AXIAL STRAIN	RADIAL STRAIN	VOLUME STRAIN	STRAIN DIFF
2	0.37	2.17	1.92	0.00000	0.00000	0.00000	0.00000
10	17.37	27.37	15.79	0.00136	0.00000	0.00136	0.00136
20	32.88	52.88	30.96	0.00225	0.00000	0.00225	0.00225
30	50.76	80.76	46.92	0.00315	0.00000	0.00315	0.00315
50	81.95	131.95	77.32	0.00431	0.00000	0.00431	0.00431
75	132.07	207.07	119.02	0.00572	0.00000	0.00572	0.00572
100	175.41	275.41	158.47	0.00680	0.00000	0.00680	0.00680
125	222.65	347.65	199.22	0.00789	0.00000	0.00789	0.00789
150	265.83	415.83	238.61	0.00879	0.00000	0.00879	0.00879
175	308.67	483.67	277.89	0.00965	0.00000	0.00965	0.00965
200	352.69	552.69	317.56	0.01044	0.00000	0.01044	0.01044
225	394.68	619.68	356.56	0.01114	0.00000	0.01114	0.01114
250	433.62	683.62	394.54	0.01179	0.00000	0.01179	0.01179
225	247.85	472.85	307.62	0.01061	0.00000	0.01061	0.01061
200	158.28	358.28	252.76	0.00995	0.00000	0.00995	0.00995
175	92.24	267.24	205.75	0.00925	0.00000	0.00925	0.00925
150	50.08	200.08	166.69	0.00849	0.00000	0.00849	0.00849
125	15.03	140.03	130.01	0.00781	0.00000	0.00781	0.00781
109	-5.14	104.26	107.69	0.00721	0.00000	0.00721	0.00721
109	-5.11	103.89	107.30	0.00721	0.00000	0.00721	0.00721
125	36.37	161.37	137.12	0.00771	0.00000	0.00771	0.00771
150	129.17	279.17	193.06	0.00850	0.00000	0.00850	0.00850
175	267.01	442.01	264.00	0.00927	0.00000	0.00927	0.00927
200	346.76	546.76	315.59	0.01003	0.00000	0.01003	0.01003
225	399.08	624.08	358.03	0.01063	0.00000	0.01063	0.01063
250	445.47	695.47	398.49	0.01126	0.00000	0.01126	0.01126
225	257.00	482.00	310.67	0.01043	0.00000	0.01043	0.01043
200	151.67	351.67	250.56	0.00962	0.00000	0.00962	0.00962
175	78.35	253.35	201.12	0.00892	0.00000	0.00892	0.00892
150	30.94	180.94	160.31	0.00806	0.00000	0.00806	0.00806
126	0.70	127.20	126.73	0.00731	0.00000	0.00731	0.00731

END OF RUN 31

RUNNING TIME: 2.6 SECS I/O TIME: .8 SECS

READY

Table C-6. Tabular Data from One-Dimensional Constrained Compression Test - Test 4

DIAMETER = 2.722 HEIGHT = 6.052 CROSS SECTIONAL AREA = 5.810

Dry Density = 111.44 lbs/ft^3

RADI STRE	STRE DIFF	AX STRE	MEAN STRE	AXIAL STRAIN	RADIAL STRAIN	VOLUME STRAIN	STRAIN DIFF
2	0.02	2.02	2.01	0.00000	0.00000	0.00000	0.00000
10	23.13	33.13	17.71	0.00106	0.00000	0.00106	0.00106
20	46.25	66.25	35.42	0.00200	0.00000	0.00200	0.00200
30	67.49	97.49	52.50	0.00291	0.00000	0.00291	0.00291
40	88.04	128.04	69.35	0.00370	0.00000	0.00370	0.00370
50	106.70	156.70	85.57	0.00446	0.00000	0.00446	0.00446
40	38.38	78.38	52.79	0.00347	0.00000	0.00347	0.00347
30	13.53	43.53	34.51	0.00281	0.00000	0.00281	0.00281
20	0.37	20.37	20.12	0.00218	0.00000	0.00218	0.00218
40	88.04	128.04	69.35	0.00406	0.00000	0.00406	0.00406
60	131.20	191.20	103.73	0.00520	0.00000	0.00520	0.00520
80	165.43	245.43	135.14	0.00625	0.00000	0.00625	0.00625
100	195.18	295.18	165.06	0.00725	0.00000	0.00725	0.00725
80	109.92	189.92	116.64	0.00596	0.00000	0.00596	0.00596
60	47.00	107.00	75.67	0.00497	0.00000	0.00497	0.00497
40	1.43	41.43	40.48	0.00392	0.00000	0.00392	0.00392
50	68.55	118.55	72.85	0.00507	0.00000	0.00507	0.00507
75	155.32	230.32	126.77	0.00648	0.00000	0.00648	0.00648
100	213.40	313.40	171.13	0.00745	0.00000	0.00745	0.00745
125	260.31	385.31	211.77	0.00834	0.00000	0.00834	0.00834
150	310.13	460.13	253.38	0.00919	0.00000	0.00919	0.00919
125	154.79	279.79	176.60	0.00815	0.00000	0.00815	0.00815
100	60.46	160.46	120.15	0.00707	0.00000	0.00707	0.00707
75	13.55	88.55	79.52	0.00580	0.00000	0.00580	0.00580
52	-.51	51.49	51.83	0.00347	0.00000	0.00347	0.00347
75	96.21	171.21	107.07	0.00659	0.00000	0.00659	0.00659
100	188.65	288.65	162.88	0.00791	0.00000	0.00791	0.00791
125	259.45	384.45	211.48	0.00881	0.00000	0.00881	0.00881
150	311.16	461.16	253.72	0.00958	0.00000	0.00958	0.00958
175	358.24	533.24	294.41	0.01041	0.00000	0.01041	0.01041
200	397.24	597.24	332.41	0.01110	0.00000	0.01110	0.01110
175	220.42	395.42	248.47	0.01021	0.00000	0.01021	0.01021
150	118.87	268.87	189.62	0.00920	0.00000	0.00920	0.00920
125	58.56	183.56	144.52	0.00669	0.00000	0.00669	0.00669
100	13.72	113.72	104.57	0.00725	0.00000	0.00725	0.00725
84	-.88	83.12	83.71	0.00610	0.00000	0.00610	0.00610
100	100.33	200.33	133.44	0.00796	0.00000	0.00796	0.00796
125	202.22	327.22	192.41	0.00912	0.00000	0.00912	0.00912

Table C-6. Continued

DIAMETER = 2.722 HEIGHT = 6.052 CROSS SECTIONAL AREA = 5.810

Dry Density = 111.44 lbs/ft^3

RADI STRE	STRE DIFF	AX STRE	MEAN STRE	AXIAL STRAIN	RADIAL STRAIN	VOLUME STRAIN	STRAIN DIFF
150	284.18	434.18	244.73	0.00998	0.00000	0.00998	0.00998
175	343.29	518.29	289.43	0.01074	0.00000	0.01074	0.01074
200	403.60	603.60	334.53	0.01140	0.00000	0.01140	0.01140
225	439.85	664.85	371.62	0.01208	0.00000	0.01208	0.01208
250	484.87	734.87	411.62	0.01272	0.00000	0.01272	0.01272
225	335.20	560.20	336.73	0.01216	0.00000	0.01216	0.01216
200	210.62	410.62	270.21	0.01130	0.00000	0.01130	0.01130
175	121.96	296.96	215.65	0.01046	0.00000	0.01046	0.01046
150	58.90	208.90	169.63	0.00796	0.00000	0.00796	0.00796
125	16.29	141.29	130.43	0.00869	0.00000	0.00869	0.00869
100	2.89	102.89	100.96	0.00724	0.00000	0.00724	0.00724

Table C-7. Tabular Data from Triaxial Test of Cook's Bayou Sand - Test 5 - Radial Pressure = 25 psi

TEST NUMBER: 5 Dry Density = 112.0 lbs/ft^3

MATERIAL DESCRIPTION: COOKS BAYOU SAND
TRIAXIAL TEST #5

DIAMETER = 2.736 HEIGHT = 6.041 CROSS SECTIONAL AREA = 5.861

Dry Density = 112.0 lbs/ft^3

RADI STRE	STRE DIFF	AX STRE	MEAN STRE	AXIAL STRAIN	RADIAL STRAIN	VOLUME STRAIN	STRAIN DIFF
25	0.33	25.33	25.11	0.00000	0.00000	0.00000	0.00000
25	6.63	31.63	27.21	0.00017	0.00000	0.00017	0.00017
25	15.13	40.13	30.04	0.00041	-.00004	0.00034	0.00045
25	23.63	48.63	32.88	0.00073	-.00011	0.00051	0.00084
25	32.13	57.13	35.71	0.00094	-.00018	0.00058	0.00113
25	40.62	65.62	38.54	0.00121	-.00029	0.00062	0.00150
25	49.11	74.11	41.37	0.00157	-.00040	0.00077	0.00197
25	57.59	82.59	44.20	0.00200	-.00058	0.00083	0.00259
25	66.05	91.05	47.02	0.00248	-.00080	0.00087	0.00329
25	4.50	99.50	49.83	0.00306	-.00110	0.00087	0.00416
25	82.91	107.91	52.64	0.00392	-.00154	0.00085	0.00546
25	91.27	116.27	55.42	0.00526	-.00219	0.00088	0.00746
25	99.51	124.51	58.17	0.00740	-.00333	0.00075	0.01073
25	107.56	132.56	60.85	0.01079	-.00519	0.00041	0.01598
25	111.17	136.17	62.06	0.01301	-.00640	0.00022	0.01941

END OF RUN 15

RUNNING TIME: 2.2 SECS I/O TIME: 9 SECS

Table C-8. Tabular Data from Triaxial Test of Cook's Bayou Sand - Test 6 - Radial Pressure = 50 psi

MATERIAL DESCRIPTION: COOKS BAYOU SAND TRIAXIAL TEST #6 Dry Density = 112.12 lbs/ft^3

DIAMETER = 2.734 HEIGHT = 6.041 CROSS SECTIONAL AREA = 5.861

Dry Density = 112.12 lbs/ft^3

RADI STRE	STRE DIFF	AX STRE	MEAN STRE	AXIAL STRAIN	RADIAL STRAIN	VOLUME STRAIN	STRAIN DIFF
50	0.16	50.16	50.05	0.00000	0.00000	0.00000	0.00000
50	4.75	54.75	51.58	0.00020	0.00000	0.00020	0.00020
50	13.27	63.27	54.42	0.00033	-.00004	0.00026	0.00037
50	21.78	71.78	57.26	0.00048	-.00007	0.00033	0.00055
50	30.30	80.30	60.10	0.00065	-.00011	0.00043	0.00076
50	47.32	97.32	65.77	0.00113	-.00022	0.00069	0.00135
50	64.33	114.33	71.44	0.00174	-.00037	0.00101	0.00210
50	81.31	131.31	77.10	0.00240	-.00062	0.00116	0.00302
50	98.26	148.26	82.75	0.00323	-.00091	0.00140	0.00414
50	115.15	165.15	88.38	0.00424	-.00139	0.00146	0.00563
50	132.01	182.01	94.00	0.00561	-.00187	0.00188	0.00748
50	148.60	198.60	99.53	0.00748	-.00315	0.00119	0.01063
50	164.98	214.98	104.99	0.01031	-.00483	0.00066	0.01514
50	180.89	230.89	110.30	0.01440	-.00750	-.00059	0.02190
50	196.14	246.14	115.38	0.02058	-.01145	-.00232	0.03202

END OF RUN 15

RUNNING TIME: 2.3 SECS I/O TIME: .7 SECS

READY

Table C-9. Tabular Data from Triaxial Test of Cook's Bayou Sand - Test 7 - Radial Pressure = 100 psi

MATERIAL DESCRIPTION: COOKS BAYOU SAND TRIAXIAL TEST #7 Dry Density = 111.75 lbs/ft^3

DIAMETER = 2.737 HEIGHT = 6.036 CROSS SECTIONAL AREA = 5.861

Dry Density = 111.75 lbs/ft^3

RADI STRE	STRE DIFF	AX STRE	MEAN STRE	AXIAL STRAIN	RADIAL STRAIN	VOLUME STRAIN	STRAIN DIFF
100	0.99	100.99	100.33	0.00000	0.00000	0.00000	0.00000
100	9.49	109.49	103.16	0.00023	0.00000	0.00023	0.00023
100	17.98	117.98	105.99	0.00043	-.00004	0.00036	0.00047
100	26.48	126.48	108.83	0.00063	-.00004	0.00056	0.00067
100	43.47	143.47	114.49	0.00099	-.00007	0.00085	0.00107
100	60.46	160.46	120.15	0.00146	-.00015	0.00117	0.00160
100	77.44	177.44	125.81	0.00191	-.00022	0.00147	0.00212
100	94.41	194.41	131.47	0.00237	-.00033	0.00171	0.00270
100	111.37	211.37	137.12	0.00283	-.00044	0.00196	0.00327
100	128.31	228.31	142.77	0.00333	-.00058	0.00216	0.00391
100	145.17	245.17	148.39	0.00384	-.00099	0.00187	0.00483
100	162.14	262.14	154.05	0.00441	-.00099	0.00243	0.00539
100	179.01	279.01	159.67	0.00504	-.00124	0.00255	0.00628
100	195.83	295.83	165.28	0.00568	-.00157	0.00254	0.00725
100	212.60	312.60	170.87	0.00644	-.00197	0.00250	0.00842
100	229.30	329.30	176.43	0.00731	-.00248	0.00234	0.00979
100	245.91	345.91	181.97	0.00827	-.00311	0.00206	0.01137
100	262.40	362.40	187.47	0.00941	-.00387	0.00166	0.01328
100	278.72	378.72	192.91	0.01075	-.00486	0.00103	0.01561
100	294.82	394.82	198.27	0.01231	-.00610	0.00011	0.01841
100	310.69	410.69	203.56	0.01445	-.00760	-.00075	0.02205
100	326.16	426.16	208.72	0.01708	-.00957	-.00206	0.02665
100	341.21	441.21	213.74	0.02029	-.01198	-.00367	0.03228
100	355.75	455.75	218.58	0.02417	-.01494	-.00572	0.03912
100	359.72	459.72	219.91	0.02621	-.01681	-.00740	0.04302

END OF RUN 25

RUNNING TIME: 2.4 SECS 1/O TIME: .9 SECS

Table C-10. Tabular Data from Triaxial Test of Cook's Bayou Sand - Test 8 - Radial Pressure = 150 psi

DIAMETER = 2.733 HEIGHT = 6.032 CROSS SECTIONAL AREA = 5.866

Dry Density = 112.0 lbs/ft^3

RADI STRE	STRE DIFF	AX STRE	MEAN STRE	AXIAL STRAIN	RADIAL STRAIN	VOLUME STRAIN	STRAIN DIFF
150	2.71	152.71	150.90	0.00000	0.00000	0.00000	0.00000
150	11.24	161.24	153.75	0.00083	0.00000	0.00083	0.00083
150	19.76	169.76	156.59	0.00133	-.00004	0.00125	0.00136
150	36.80	186.80	162.27	0.00199	-.00004	0.00192	0.00203
150	53.85	203.85	167.95	0.00232	-.00007	0.00217	0.00239
150	70.88	220.88	173.63	0.00249	-.00015	0.00219	0.00263
150	87.91	237.91	179.30	0.00282	-.00018	0.00245	0.00300
150	104.94	254.94	184.98	0.00315	-.00026	0.00264	0.00341
150	121.96	271.96	190.65	0.00365	-.00033	0.00299	0.00398
150	138.96	288.96	196.32	0.00398	-.00044	0.00310	0.00442
150	155.97	305.97	201.99	0.00431	-.00051	0.00329	0.00482
150	172.95	322.95	207.65	0.00481	-.00066	0.00349	0.00547
150	189.93	339.93	213.31	0.00531	-.00077	0.00377	0.00687
150	206.88	356.88	218.96	0.00580	-.00095	0.00390	0.00675
150	223.81	373.81	224.60	0.00680	-.00113	0.00403	0.00743
150	240.73	390.73	230.24	0.00680	-.00132	0.00416	0.00811
150	257.60	407.60	235.87	0.00729	-.00157	0.00415	0.00887
150	274.43	424.43	241.48	0.00796	-.00187	0.00423	0.00982
150	291.22	441.22	247.07	0.00862	-.00220	0.00423	0.01082
150	307.94	457.94	252.65	0.00945	-.00260	0.00425	0.01205
150	324.59	474.59	258.20	0.01028	-.00307	0.00413	0.01335
150	341.14	491.14	263.71	0.01127	-.00366	0.00396	0.01493
150	357.59	507.59	269.20	0.01227	-.00432	0.00363	0.01659
150	373.92	523.92	274.64	0.01359	-.00509	0.00342	0.01868
150	390.08	540.08	280.03	0.01492	-.00600	0.00292	0.02092
150	406.07	556.07	285.36	0.01641	-.00706	0.00229	0.02347
150	421.84	571.84	290.61	0.01807	-.00831	0.00146	0.02638
150	437.47	587.47	295.82	0.02006	-.00962	0.00081	0.02968
150	452.79	602.79	300.93	0.02221	-.01120	-.00018	0.03341
150	467.79	617.79	305.93	0.02470	-.01303	-.00135	0.03773
150	482.43	632.43	310.81	0.02752	-.01511	-.00270	0.04263
150	496.53	646.53	315.51	0.03100	-.01764	-.00427	0.04864

END OF RUN 32

RUNNING TIME: 3.2 SECS 1/O TIME: .7 SECS

READY

Table C-11. Tabular Data from Triaxial Test of Cook's Bayou Sand - Test 9 Radial Pressure = 250 psi

DIAMETER = 2.730 HEIGHT = 6.017 CROSS SECTIONAL AREA = 5.860

Dry Density = 112.0 lbs/ft^3

RADI STRE	STRE DIFF	AX STRE	MEAN STRE	AXIAL STRAIN	RADIAL STRAIN	VOLUME STRAIN	STRAIN DIFF
250	8.58	258.58	252.86	0.00000	0.00000	0.00000	0.00000
250	15.92	265.92	255.31	0.00008	-.00004	0.00001	0.00012
250	24.46	274.46	258.15	0.00017	-.00004	0.00009	0.00020
250	33.00	283.00	261.00	0.00025	-.00007	0.00010	0.00032
250	50.08	300.08	266.69	0.00042	-.00007	0.00027	0.00049
250	67.16	317.16	272.39	0.00058	-.00011	0.00036	0.00069
250	84.24	334.24	278.08	0.00075	-.00011	0.00053	0.00086
250	101.31	351.31	283.77	0.00091	-.00015	0.00062	0.00106
250	118.38	368.38	289.46	0.00108	-.00018	0.00071	0.00126
250	135.45	385.45	295.15	0.00125	-.00022	0.00081	0.00147
250	152.51	402.51	300.84	0.00141	-.00026	0.00090	0.00167
250	169.58	419.58	306.53	0.00158	-.00029	0.00099	0.00187
250	186.64	436.64	312.21	0.00191	-.00033	0.00125	0.00224
250	203.70	453.70	317.90	0.00208	-.00037	0.00134	0.00244
250	220.73	470.73	323.58	0.00224	-.00044	0.00136	0.00268
250	237.79	487.79	329.26	0.00258	-.00048	0.00162	0.00305
250	254.82	504.82	334.94	0.00274	-.00055	0.00164	0.00329
250	271.84	521.84	340.61	0.00307	-.00062	0.00183	0.00370
250	288.86	538.86	346.29	0.00324	-.00070	0.00185	0.00394
250	305.88	555.88	351.96	0.00357	-.00077	0.00203	0.00434
250	322.86	572.86	357.62	0.00391	-.00088	0.00215	0.00478
250	339.87	589.87	363.29	0.00424	-.00095	0.00233	0.00519
250	356.84	606.84	368.95	0.00440	-.00106	0.00228	0.00547
250	373.80	623.80	374.60	0.00474	-.00117	0.00239	0.00591
250	390.73	640.73	380.24	0.00507	-.00132	0.00243	0.00639
250	407.65	657.65	385.88	0.00557	-.00147	0.00264	0.00703
250	424.56	674.56	391.52	0.00590	-.00161	0.00268	0.00751
250	441.43	691.43	397.14	0.00623	-.00179	0.00264	0.00803
250	458.28	708.28	402.76	0.00673	-.00198	0.00277	0.00871
250	475.09	725.09	408.36	0.00723	-.00220	0.00283	0.00943
250	491.85	741.85	413.95	0.00773	-.00245	0.00282	0.01018
250	508.59	758.59	419.53	0.00823	-.00271	0.00281	0.01094
250	525.27	775.27	425.09	0.00889	-.00380	0.00288	0.01190
250	541.90	791.90	430.63	0.00939	-.00333	0.00272	0.01272
250	558.46	808.46	436.15	0.01022	-.00370	0.00282	0.01392
250	574.91	824.91	441.64	0.01089	-.00414	0.00261	0.01503
250	591.34	841.34	447.11	0.01172	-.00458	0.00256	0.01630
250	607.65	857.65	452.55	0.01255	-.00509	0.00236	0.01764

Table C-11. Continued

DIAMETER = 2.730 HEIGHT = 6.017 CROSS SECTIONAL AREA = 5.860

Dry Density = 112.0 lbs/ft^3

RADI STRE	STRE DIFF	AX STRE	MEAN STRE	AXIAL STRAIN	RADIAL STRAIN	VOLUME STRAIN	STRAIN DIFF
250	623.83	873.83	457.94	0.01354	-.00568	0.00219	0.01922
250	639.89	889.89	463.30	0.01471	-.00634	0.00203	0.02105
250	655.85	905.85	468.62	0.01587	-.00703	0.00181	0.02290
250	671.63	921.63	473.88	0.01720	-.00784	0.00152	0.02504
250	687.25	937.25	479.08	0.01853	-.00872	0.00109	0.02725
250	702.62	952.62	484.21	0.02019	-.00974	0.00071	0.02994
250	717.83	967.83	489.28	0.02202	-.01084	0.00034	0.03286
250	732.76	982.76	494.25	0.02402	-.01209	-.00016	0.03610
250	747.40	997.40	499.13	0.02634	-.01348	-.00062	0.03982
250	761.63	1011.63	503.88	0.02900	-.01509	-.00118	0.04409
250	775.56	1025.56	508.52	0.03199	-.01685	-.00171	0.04884
250	789.95	1039.95	513.32	0.03432	-.01824	-.00216	0.05256
250	802.56	1052.56	517.52	0.03864	-.02073	-.00282	0.05937
250	813.68	1063.68	521.23	0.04446	-.02410	-.00375	0.06856
250	821.97	1071.97	523.99	0.05393	-.02919	-.00446	0.08312

PART C-2

LABORATORY DATA SUMMARY ON COMPACTED CLAY

Table C-12. Composition Properties for Triaxial Tests on Clay

Test No.	Wet Density γ (g/cc)	Water Content w (percent)	Dry Density γ_d (g/cc)	Degree of Saturation S (percent)	Void Ratio e	Air Voids V_a (percent)
A.1	2.050	19.67	1.713	90.4	0.5939	3.57
A.2	2.039	20.47	1.692	91.2	0.6130	3.36
A.3	2.030	20.26	1.689	89.7	0.6164	3.92
A.4	2.033	20.11	1.693	89.6	0.6127	3.95
A.5	2.043	20.53	1.695	91.8	0.6107	3.12
A.6	2.028	21.38	1.671	92.1	0.6339	3.07
A.7	2.027	21.50	1.668	92.2	0.6366	3.03
A.8	2.025	20.40	1.682	89.4	0.6227	4.05
A.9	2.031	20.65	1.684	90.7	0.6215	3.56
A.10	Sample Lost Before Testing					
A.11	2.045	Sample Leaked				
A.12	2.065	20.74	1.710	94.9	0.5965	1.90
B.1	1.832	15.15	1.591	57.8	0.7157	17.61
B.2	1.846	15.19	1.603	59.0	0.7032	16.94
B.3	1.838	15.27	1.595	58.5	0.7121	17.24
B.4	1.839	15.20	1.596	58.4	0.7104	17.27
B.5	1.842	15.25	1.598	58.8	0.7080	17.08
B.6	1.833	15.25	1.590	58.1	0.7169	17.51
B.7	1.848	15.03	1.606	58.7	0.6994	17.01
B.8	1.852	15.03	1.610	59.0	0.6956	16.82
B.9	1.810	15.04	1.574	55.9	0.7349	18.69
B.10	1.900	14.99	1.653	62.8	0.6518	14.69
B.11	1.836	Sample Leaked				
B.12	1.871	15.40	1.621	61.5	0.6841	15.66
C.1	1.630	10.21	1.479	32.9	0.8462	30.74
C.2	1.682	10.12	1.528	35.1	0.7870	28.58
C.3	1.708	10.22	1.550	36.6	0.7613	27.38
C.4	1.684	10.11	1.530	35.2	0.7845	28.50
C.5	1.669	9.99	1.518	34.1	0.7987	29.24
C.6	1.641	10.22	1.489	33.5	0.8335	30.24

Table C-12. Continued

Test No.	Wet Density γ (g/cc)	Water Content w (percent)	Dry Density γ_d (g/cc)	Degree of Saturation S (percent)	Void Ratio e	Air Voids V_a (percent)
C.7	1.674	10.19	1.519	35.2	0.7912	28.88
C.8	1.668	10.02	1.516	34.2	0.8004	29.26
C.9	1.693	9.86	1.541	34.9	0.7717	28.37
C.10	1.656		Sample Leaked			
C.11	1.660		Sample Leaked			
C.12	1.639	10.92	1.478	35.2	0.8471	29.72

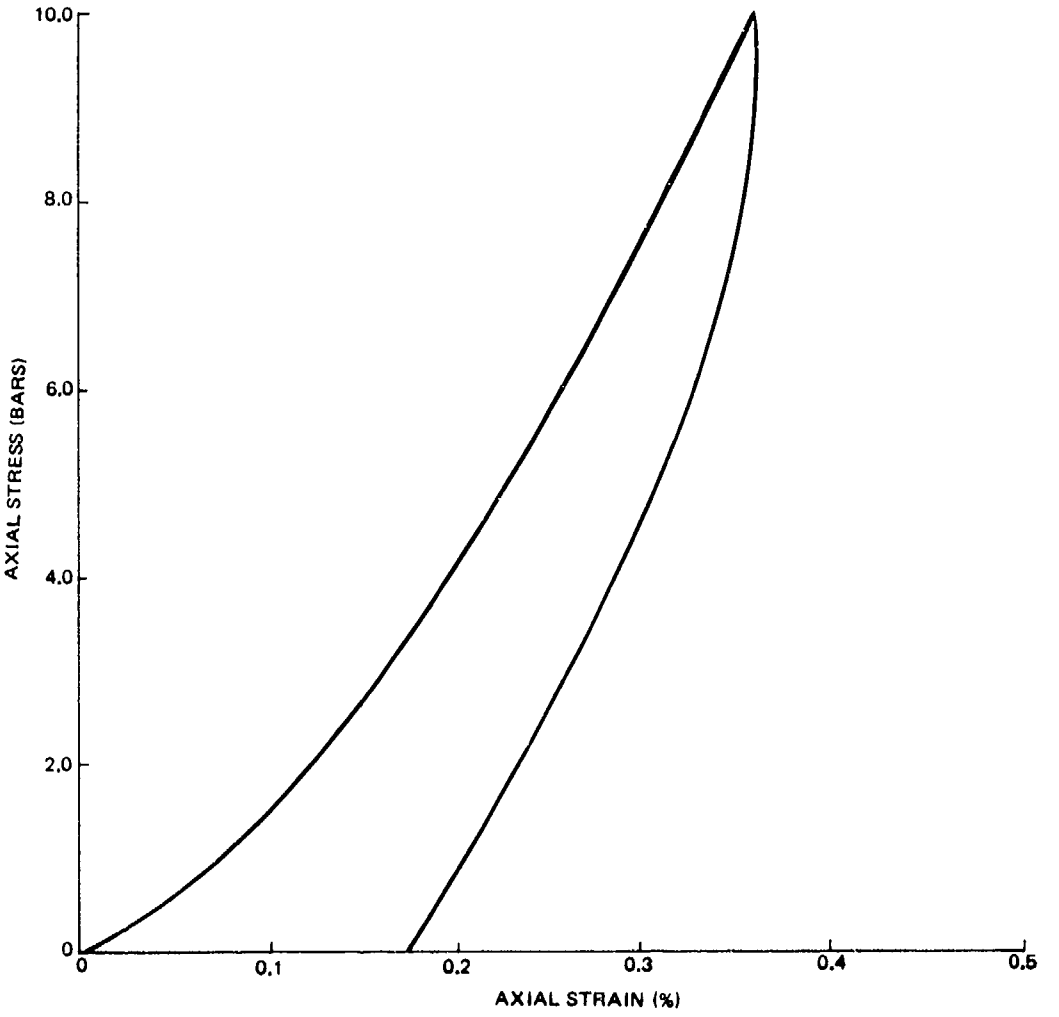

Figure C-1. Recommended Uniaxial Strain Relation for Clay at Wet Density of 2.060 g/cc

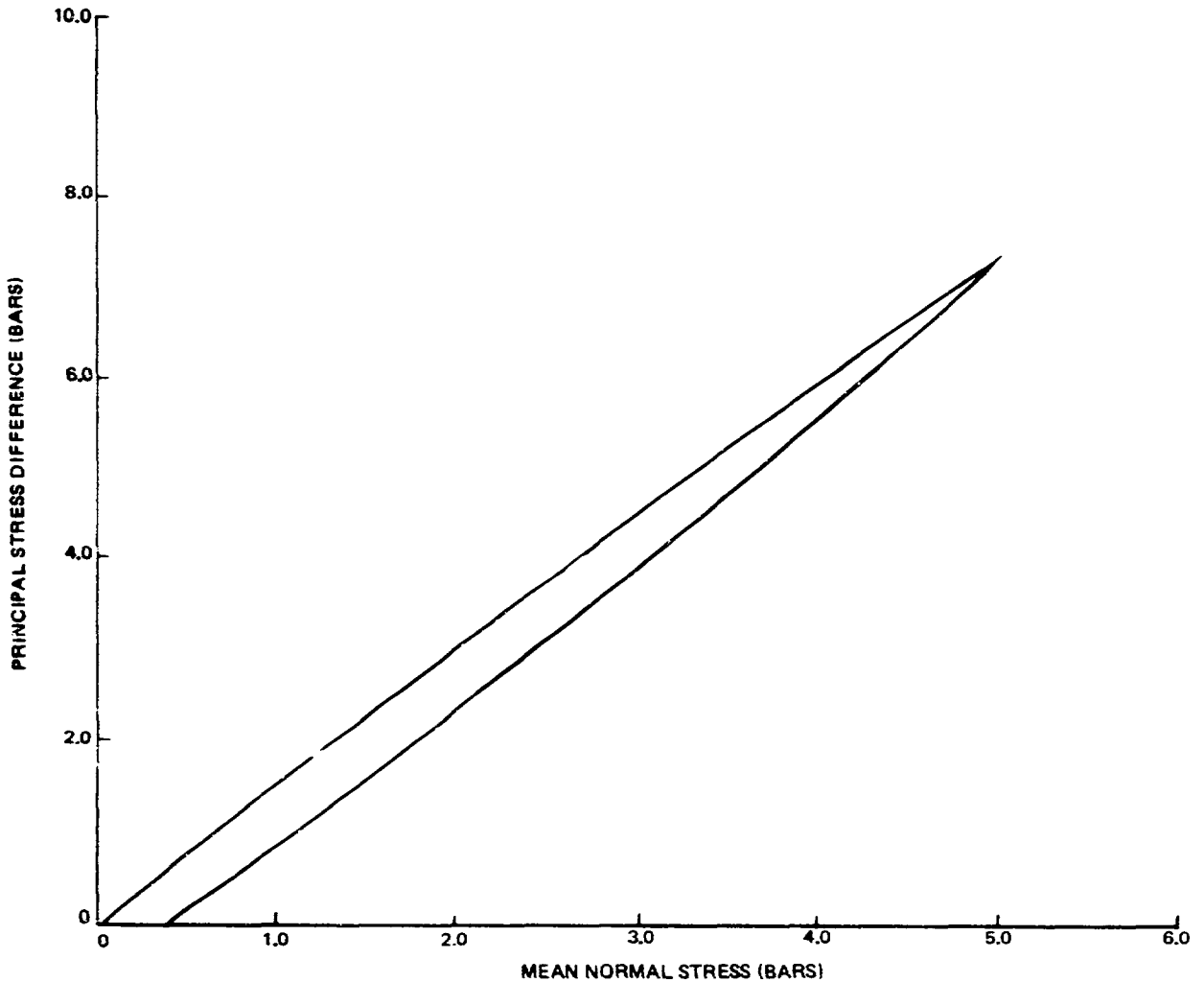

Figure C-2. Recommended Uniaxial Strain Stress Path for Clay at Wet Density of 2.060 g/cc

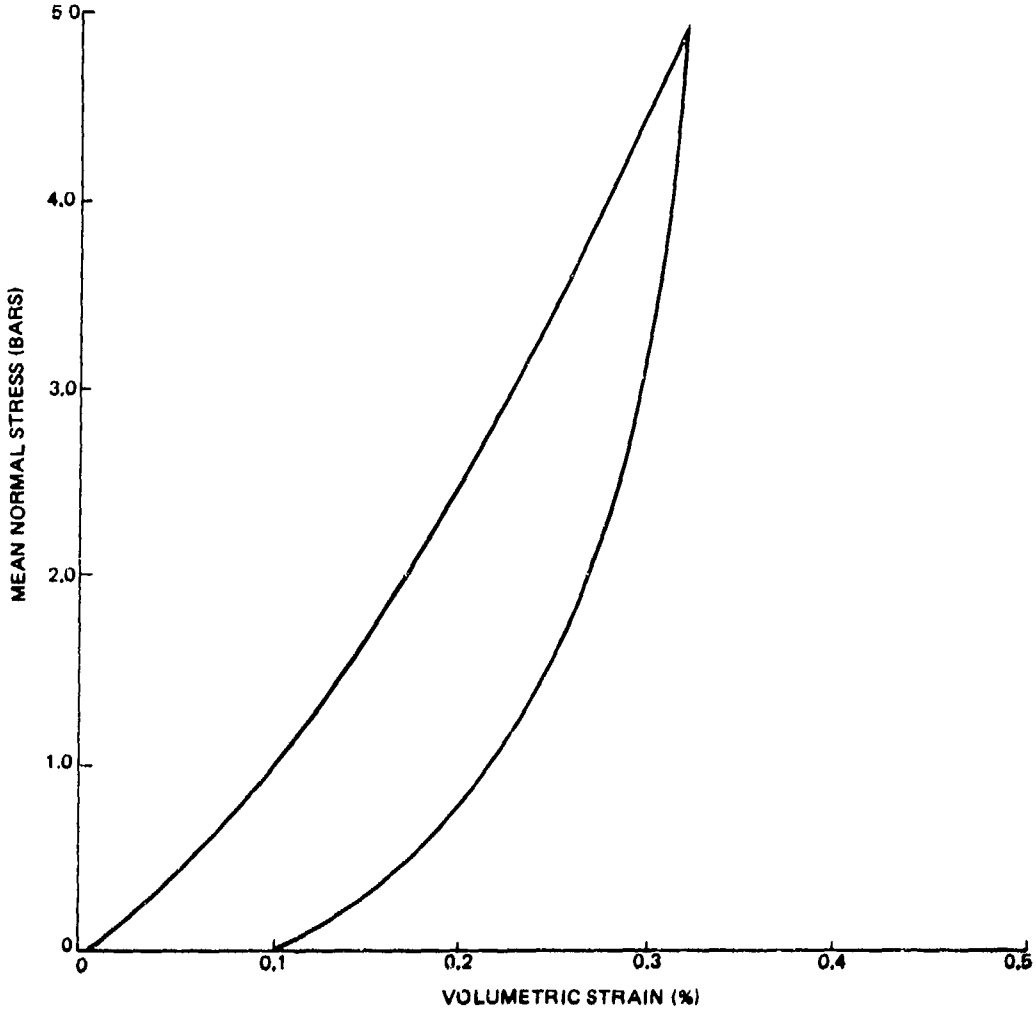

Figure C-3. Recommended Isotropic Compression Relation for Clay at Wet Density of 2.060 g/cc

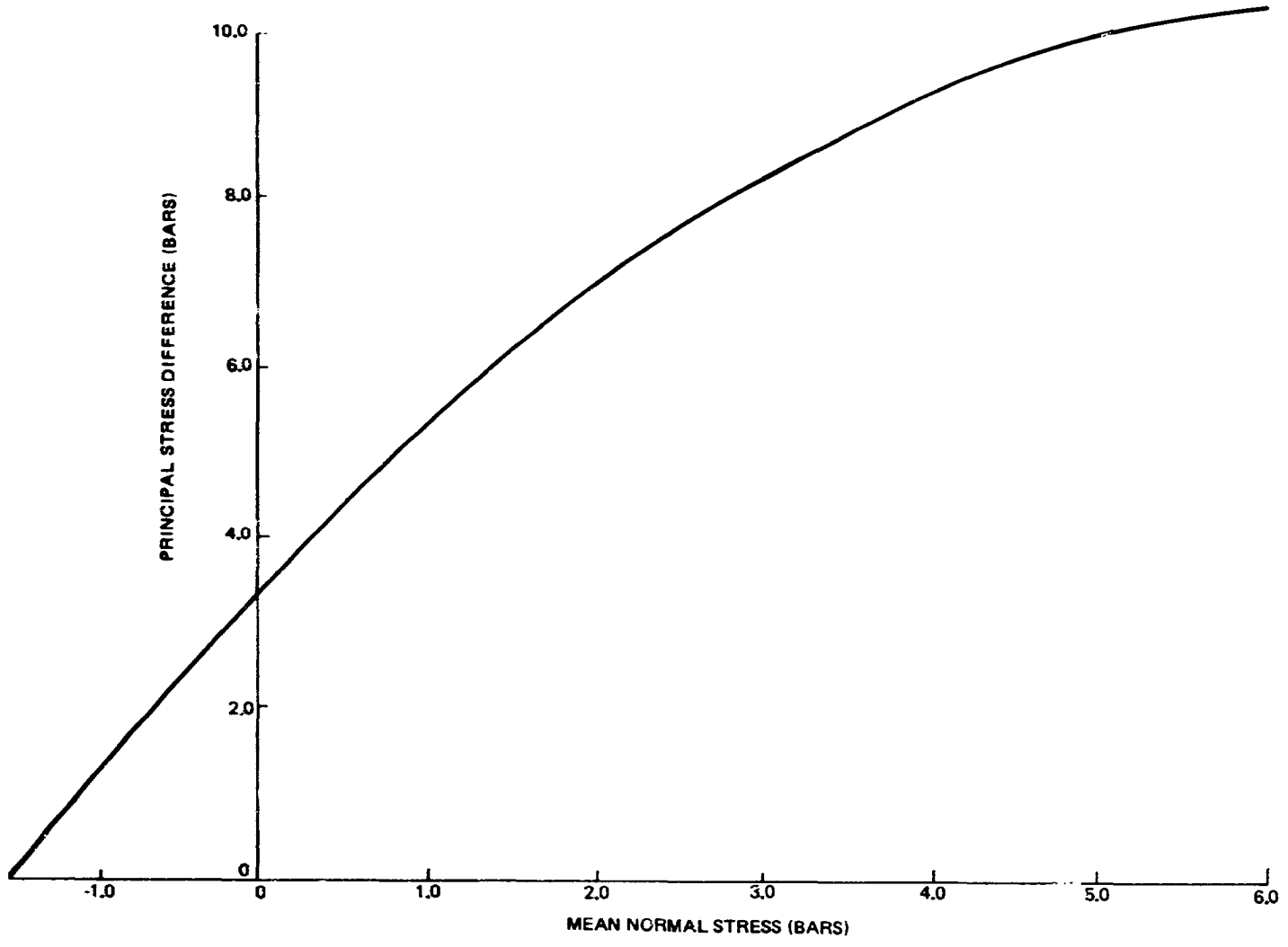

Figure C-4. Recommended Triaxial Failure Envelope for Clay at Wet Density of 2.060 g/cc

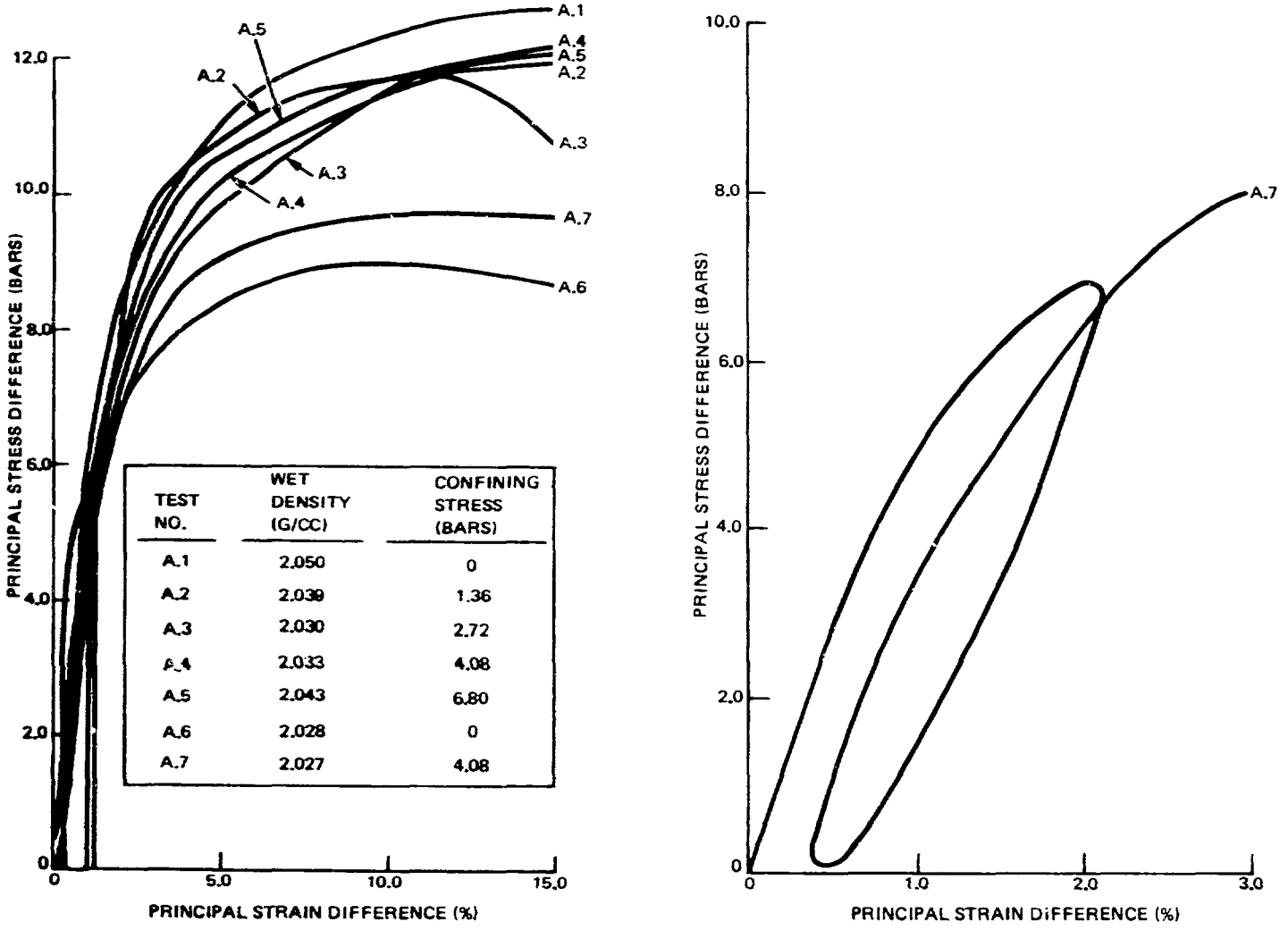

TEST NO.	WET DENSITY (G/CC)	CONFINING STRESS (BARS)
A.1	2.050	0
A.2	2.039	1.36
A.3	2.030	2.72
A.4	2.033	4.08
A.5	2.043	6.80
A.6	2.028	0
A.7	2.027	4.08

Figure C-5. Triaxial Shear Data for Tests Performed on Clay at a Nominal Wet Density of 2.060 g/cc

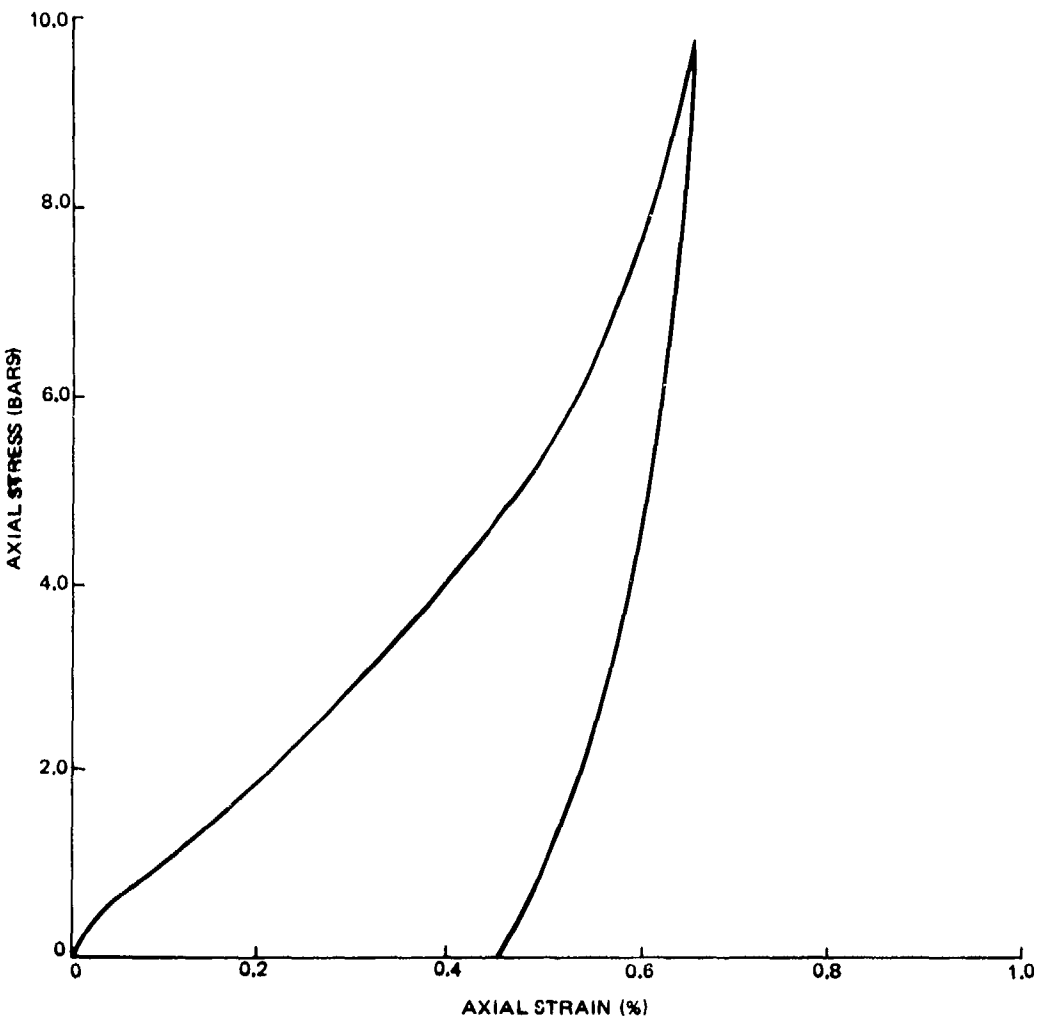

Figure C-6. Recommended Uniaxial Strain Relation for Clay at Wet Density of 1.866 g/cc

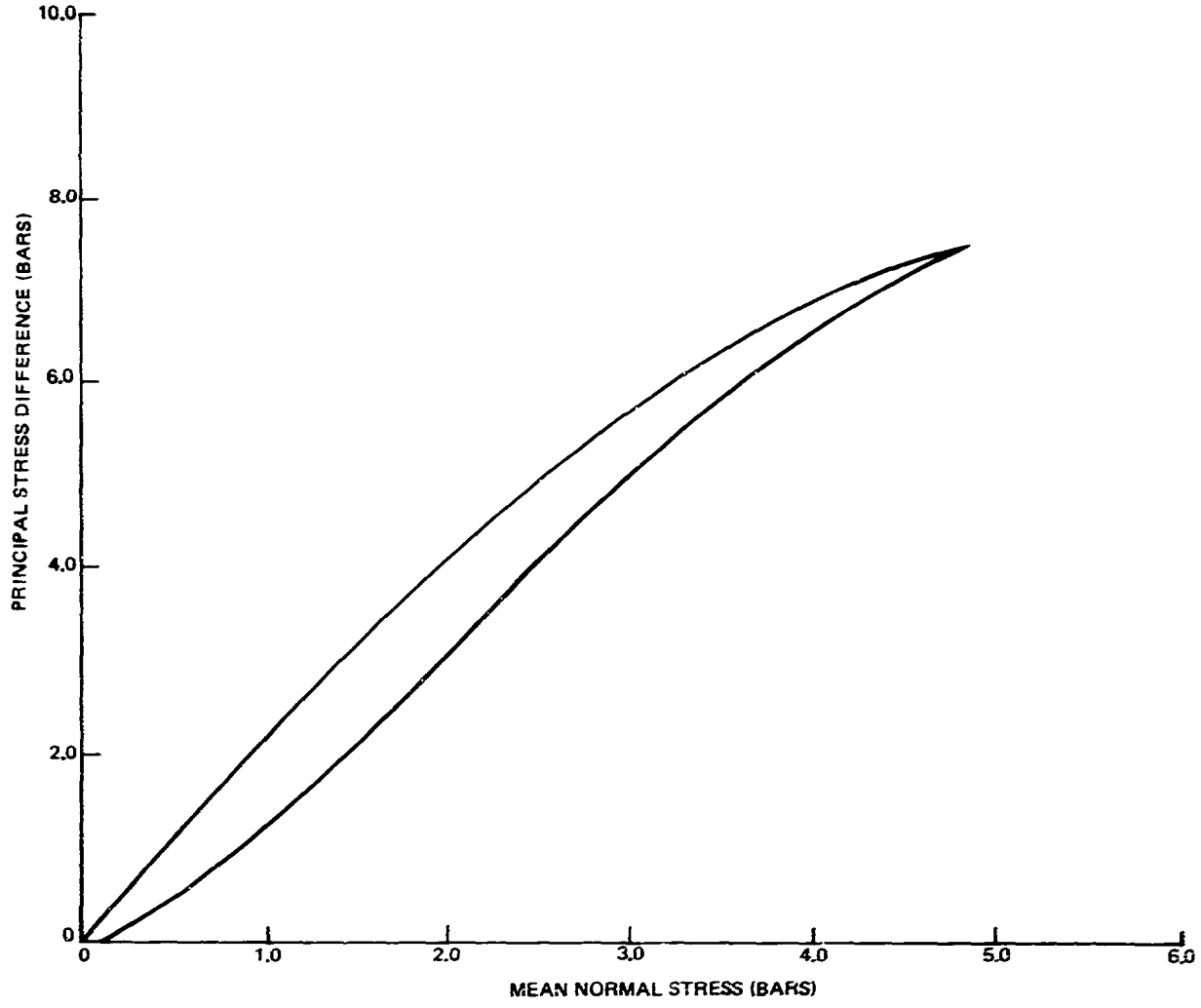

Figure C-7. Recommended Uniaxial Strain Stress Path for Clay at Wet Density of 1.866 g/cc

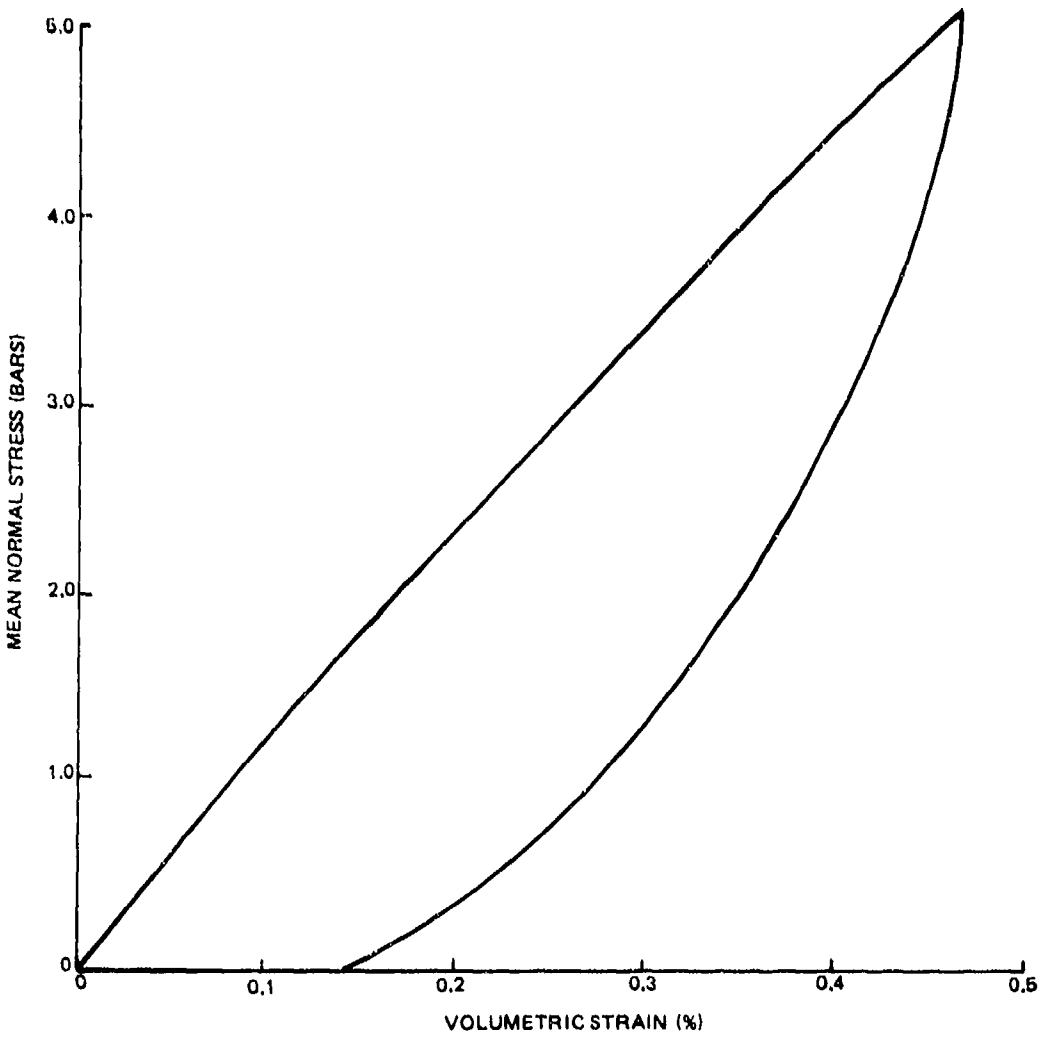

Figure C-8. Recommended Isotropic Compression Relation for Clay at Wet Density of 1.866 g/c

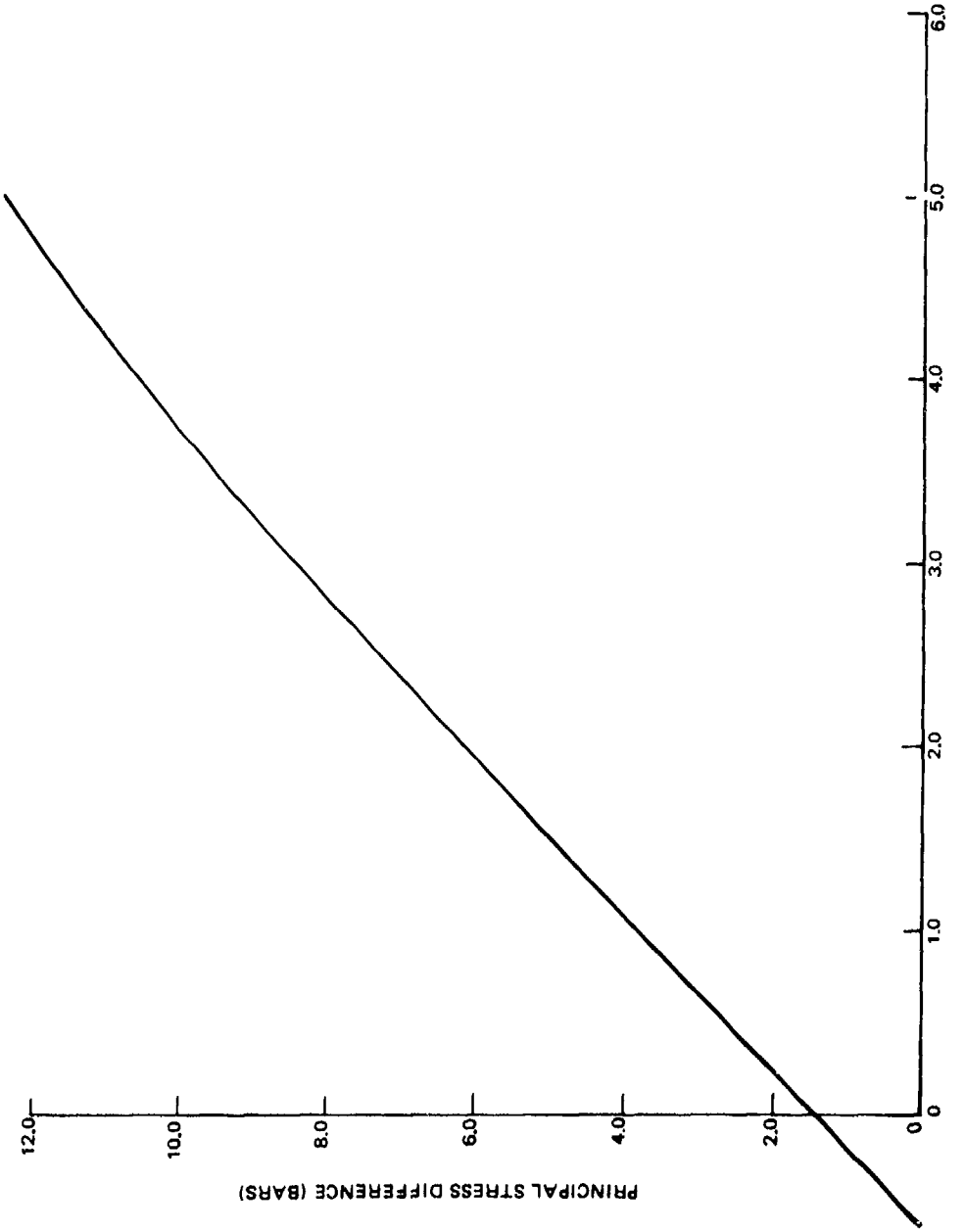

Figure C-9. Recommended Triaxial Failure Envelope for Clay at Wet Density of 1.866 g/cc

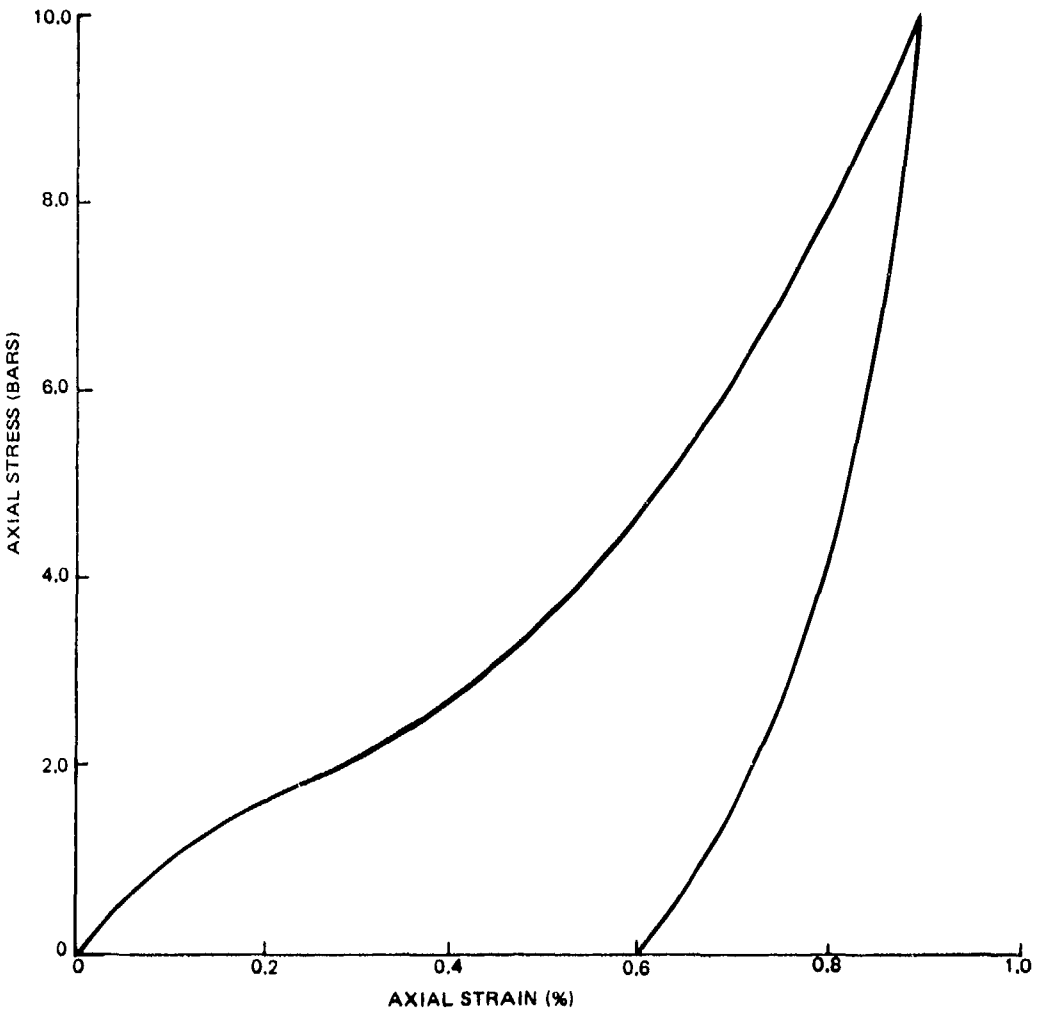

Figure C-10. Recommended Uniaxial Strain Relation for Clay at Wet Density of 1.685 g/cc

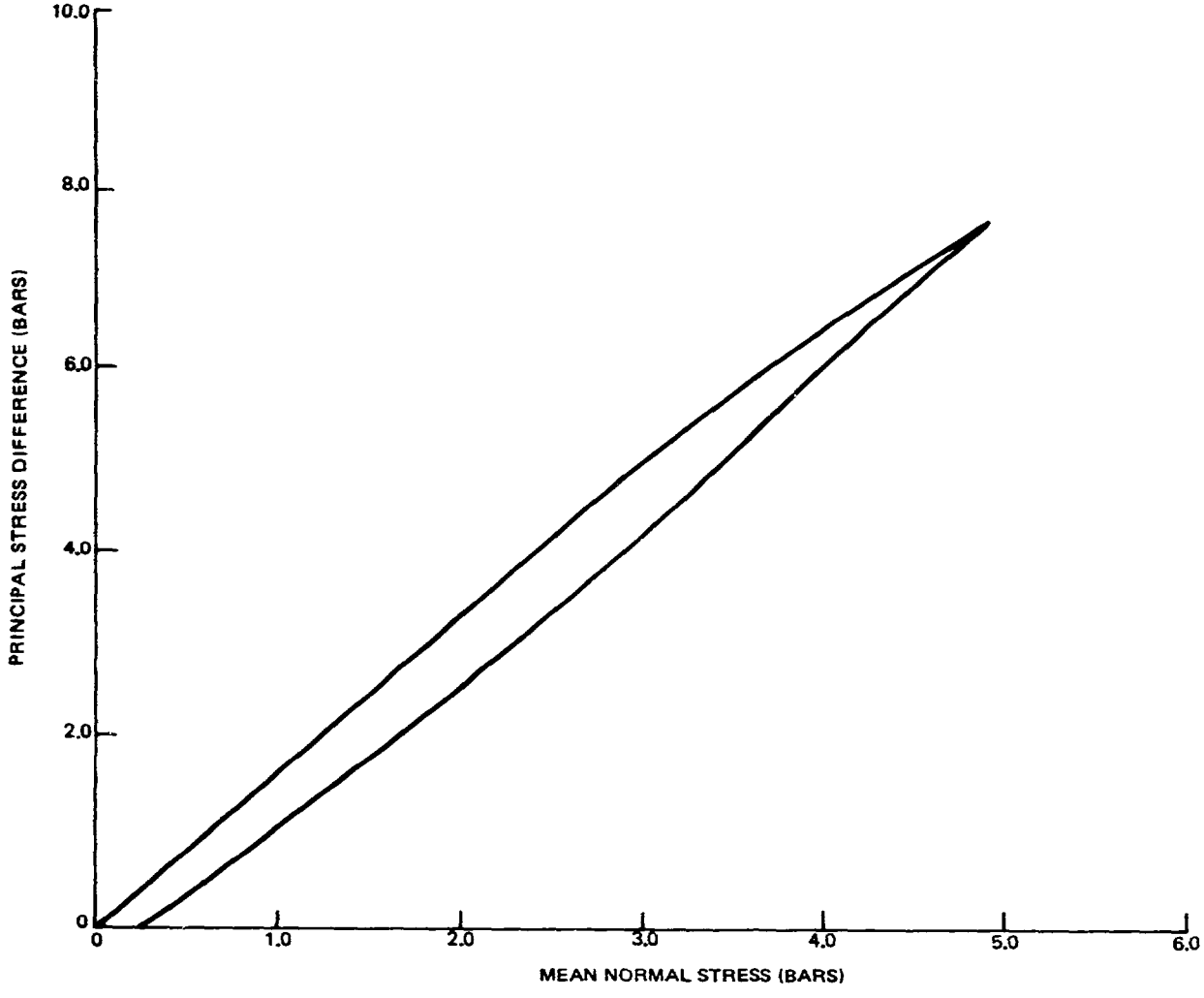

Figure C-11. Recommended Uniaxial Strain Stress Path for Clay at Wet Density of 1.685 g/cc

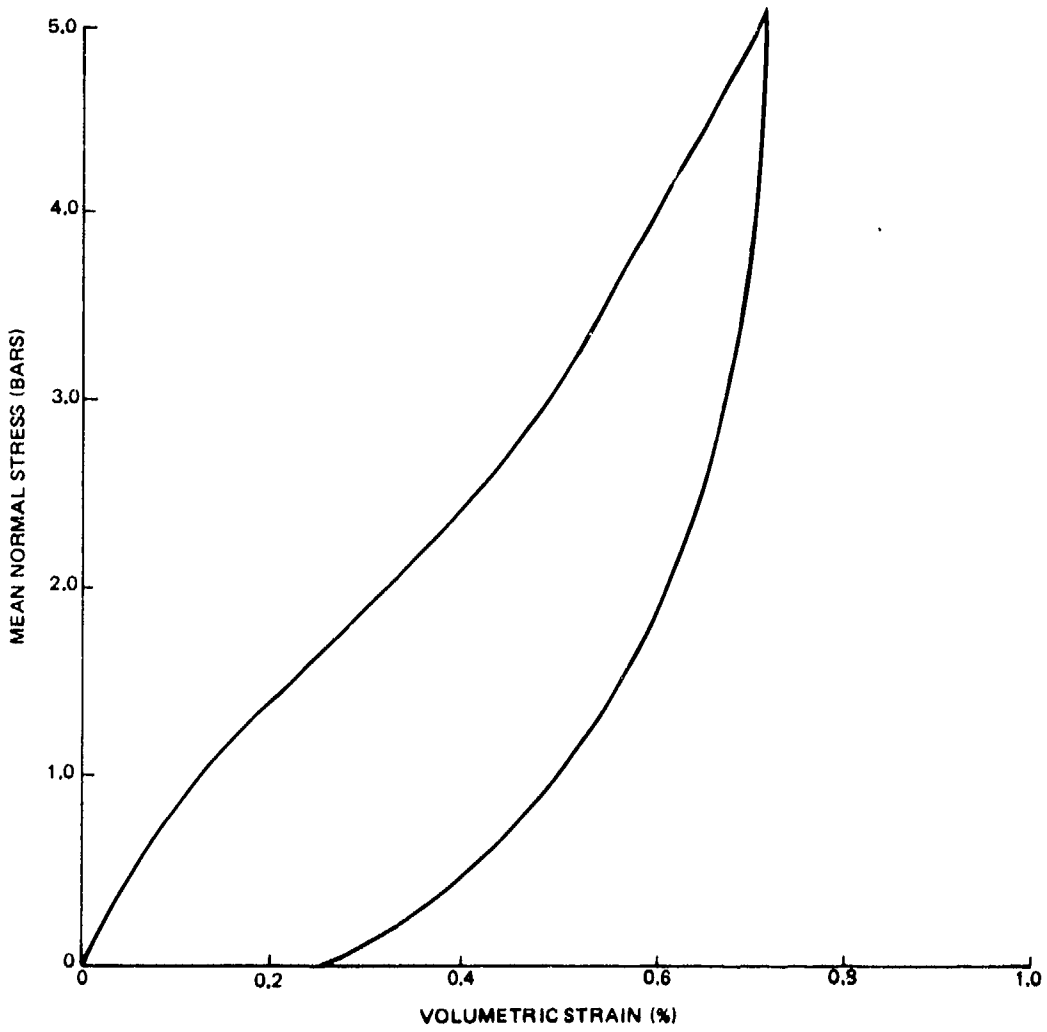

Figure C-12. Recommended Isotropic Compression Relation for Clay at Wet Density of 1.685 g/cc

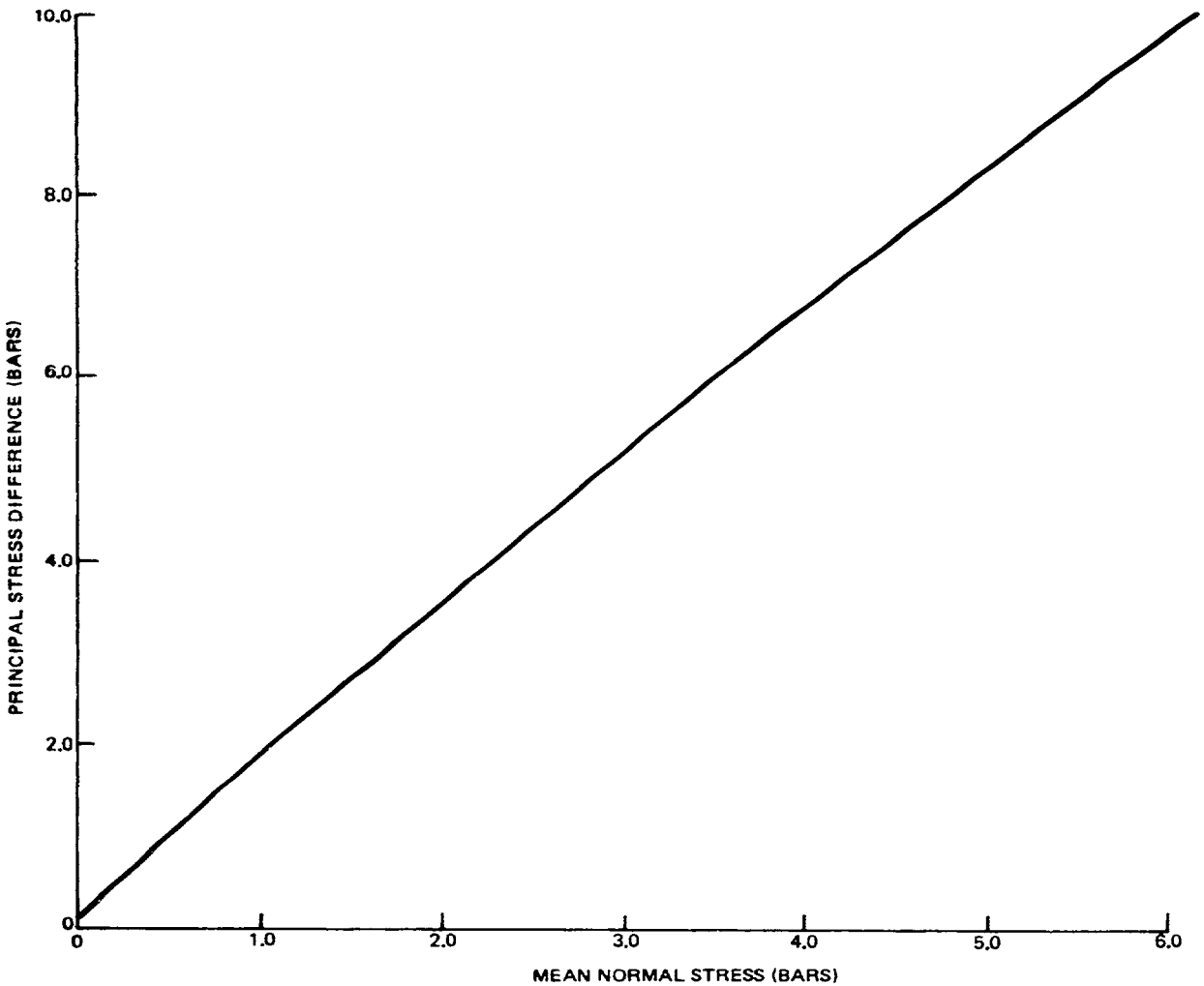

Figure C-13. Recommended Triaxial Failure Envelope for Clay at Wet Density of 1.685 g/cc

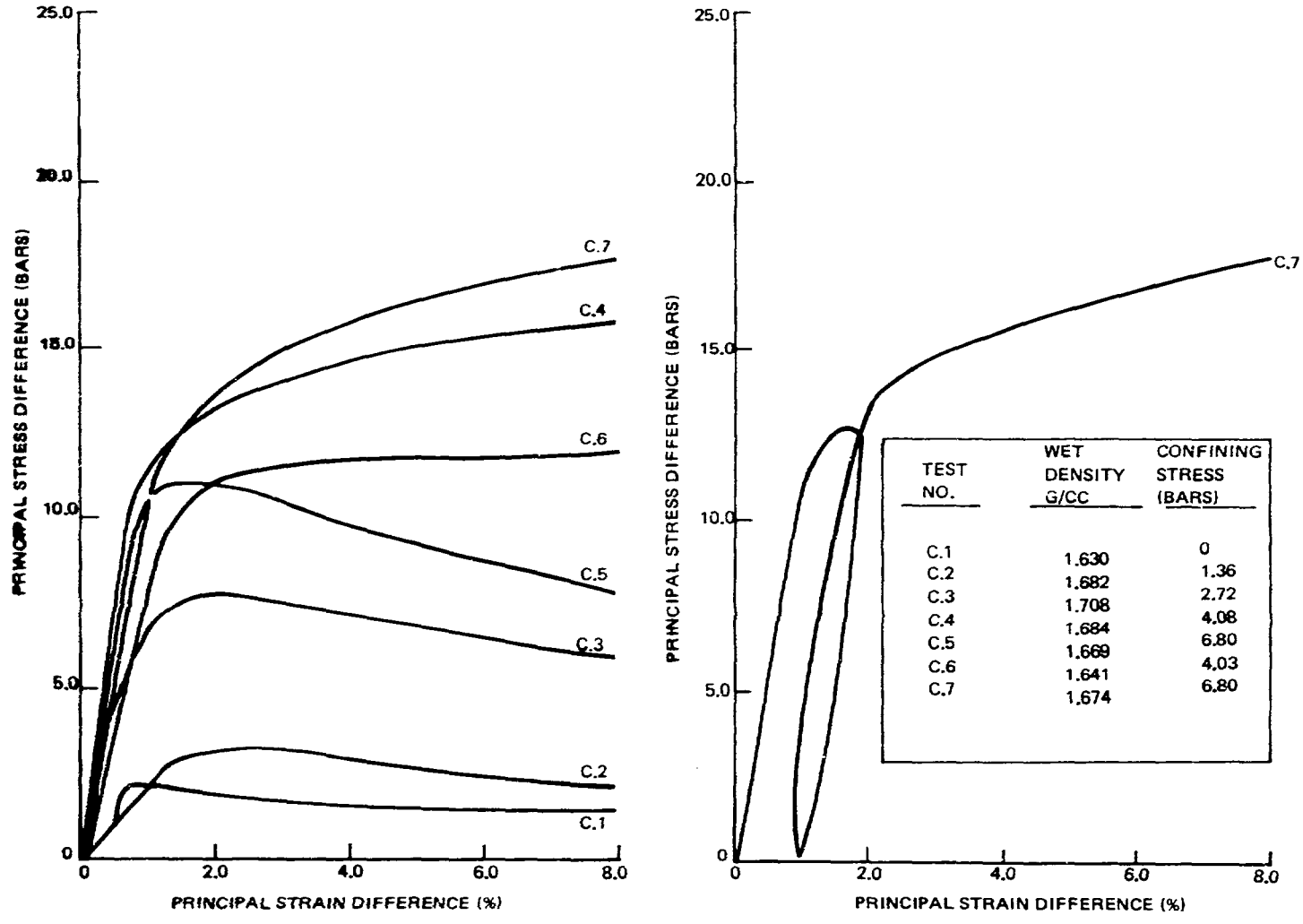

Figure C-14. Triaxial Shear Data for Tests Performed on Clay at a Nominal Wet Density of 1.685 g/cc

PART C-3

TEST DATA ON PAVEMENT COMPONENTS

C-3.1 PORTLAND CEMENT CONCRETE

Test data on the portland cement concrete test slabs are reported in conjunction with the field test data in Appendix B (see Table B-4).

C-3.2 BITUMINOUS BASE COURSE

The Bituminous base course material was purchased from Southern Pacific Milling Company, at El Rio, California, and met the specifications outlined in Appendix A. These specifications are in accord with FAA specifications (Reference 26). Asphalt cement was noted to vary between 6.0 and 6.4 percent. The aggregate was a crushed river gravel with a maximum size of 3/4 inch, and met the gradation requirements of Appendix A.

C-3.3 LIME STABILIZED BASE

The lime stabilized clay base material was constructed according to the specifications in Appendix A which are in accordance with FAA specifications, (Reference 21). After mixing 6 percent type S hydrated lime with the clay at the optimum moisture content (Figure C-15) in a batch plant, the material was permitted to cure for 48 hours in place. The stabilized material was then remixed in place with a rototiller and recompacted.

Characteristics of the material as placed are shown in Table C-1. A typical moisture - density curve has been presented in Figure C-13.

Table C-13. Properties of Lime Stabilized Clay

Measurements Taken 5 feet Distant from Center of Section in Direction	Wet Density γ_w	Dry Density γ_d	% Compaction	% Moisture
West	115.4	93.8	94.4	23.0
East	116.2	96.1	96.1	20.9
North	114.0	93.0	93.6	22.6
South	115.7	95.6	96.2	21.0
		Average	94.6	21.9

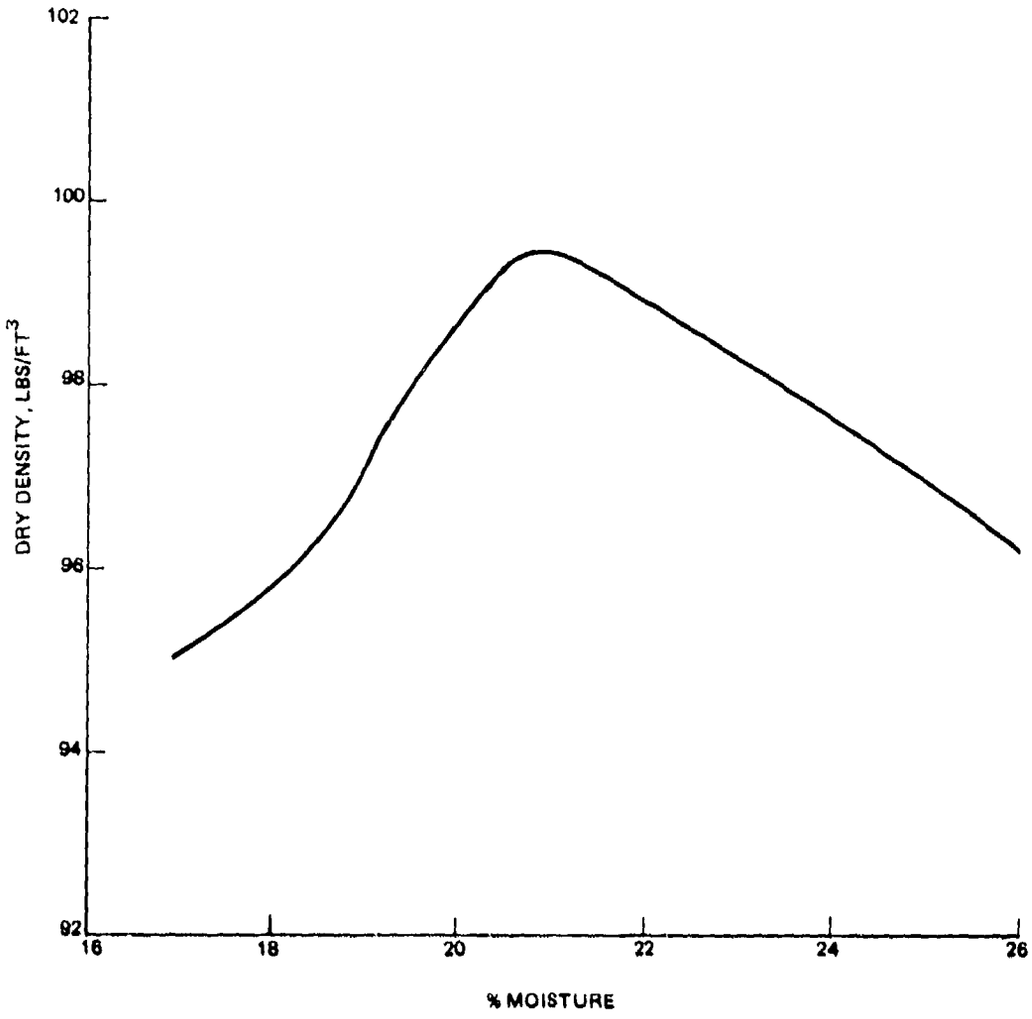

Figure C-15. Moisture Versus Density for Lime Stabilized Clay

APPENDIX D

DEVELOPMENT OF HARDIN SOIL MODEL

In this appendix the Hardin soil model (see References 12, 13, 30) will be presented and discussed. Although this appendix is devoted to the Hardin model, the authors do not imply that other soil models are not worthy of consideration. To the contrary, the purpose of presenting the Hardin model is to demonstrate the basic assumptions of a group of soil models based on a hyperbolic form and a variable modulus classification (References 12-15, 30-32).

The Hardin model is representative of this group, and like other hyperbolic models it has some good and some not-so-good characteristics which will be discussed in later sections. By and large, the authors believe the Hardin model is capable of correctly representing the non-linear behavior of soils (particularly granular and mixed soils) for conditions representative of pavement loadings (dead and live load). One of the features of the Hardin model is that if no triaxial soil data is available, a set of auxiliary equations can often be used to estimate parameters of the model based on fundamental properties such as soil classification, void ratio, plasticity index, and percent saturation.

The above notions are discussed and enlarged in the following sequence; (1) Hardin shear modulus development, (2) verification of shear modulus for granular soils, (3) extended Hardin model (i.e., inclusion of variable Poisson ratio), (4) verification of extended Hardin for granular soil, (5) verification of extended Hardin model for cohesive soils, and (6) parameter determination of extended Hardin model for all soils.

1. Hardin Shear Modulus Development

The Hardin relationship relates accumulated maximum shear stress to accumulated maximum shear strain by Equation D-1 and is shown graphically in Figure D-1.

$$\tau = G_s \gamma \qquad \text{(D-1)}$$

where τ = accumulated maximum shear stress

γ = accumulated maximum shear strain

G_s = secant shear modulus

The heart of Hardin's model is the relation for the secant shear modulus (G_s) expressed in a hyperbolic form as:

$$G_s = \frac{G_{max}}{1 + \gamma_h} \qquad \text{(D-2)}$$

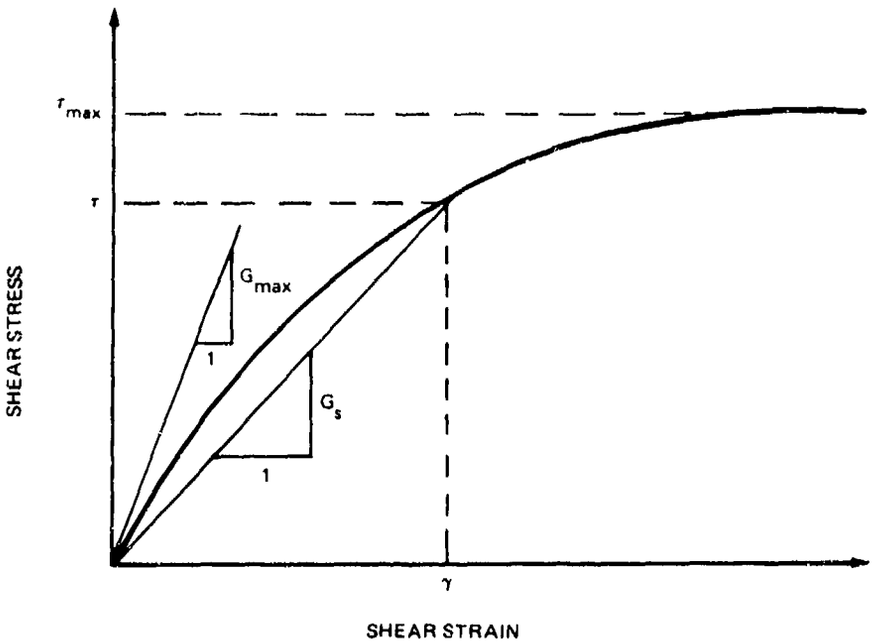

Figure D-1. Idealized Shear Stress/Strain Relation

G_{max} is the maximum value of the shear modulus, dependent on spherical stress, and γ_h is the so-called hyperbolic shear strain dependent on the ratio of shear strain to reference shear strain as defined below.

$$G_{max} = S_1 \sqrt{\sigma_m} \qquad \text{(D-3)*}$$

$$\gamma_h = \frac{\gamma}{\gamma_r} \left(1 + a/\exp \left(\frac{\gamma}{\gamma_r}\right)^{0.4}\right) \qquad \text{(D-4)}$$

$$\gamma_r = G_{max}/C_1 \qquad \text{(D-5)}$$

*Equation D-3 is not a fundamental element of Hardin's model. Its purpose is to provide a highly simplified form for G_{max}, which appears to work for granular soil. This form may not work for clays because of pore water affects and may require that G_{max} be expressed in a more complicated form.

where σ_m = spherical or average stress; i.e., $(\sigma_{11} + \sigma_{22} + \sigma_{33})/3$ (compressive only)

γ_r = reference shear strain

S_1 = soil parameter, (related to void ratio)

a = soil parameter, (related to soil type, and percent saturation)

C_1 = soil parameter, (related to void ratio percent saturation and plasticity index)

Equations D-1 through D-5 embody the general form of Hardin's soil model for shear modulus. To utilize the model for a particular soil, it only remains to specify values for the soil parameters, S_1, a, and C_1. One way of accomplishing this is to perform a series of triaxial tests and curve fit these parameters to the model. This approach is discussed at the end of the appendix. However, the beauty of Hardin's work is that he presents relationships for these parameters in terms of fundamental soil characteristics which are readily measurable or readily available: void ratio, plasticity index and percent saturation.

Below are the expressions for S_1, a, and C_1 for one cycle of loading at a slow loading rate, applicable for the inch-pound-second system of units.

$$S_1 = 1230F \qquad \text{(D-6)}$$

$$a = \begin{cases} 3.2 & \text{granular soil} \\ 2.54\ (1+0.02S) & \text{mixed soil} \\ 1.12\ (1+0.02S) & \text{cohesive soil} \end{cases} \qquad \text{(D-7)}$$

$$C_1 = F^2R^2/(0.6-0.25(PI/100)^{0.6})$$

where $F = (2.973-e)^2/(1+e)$

$$R = \begin{cases} 1100 & \text{granular soil} \\ 1100-6S & \text{mixed or cohesive soil} \end{cases}$$

e = void ratio

S = percent saturation $(0 < S < 100)$

PI = plasticity-index $(0<PI<100)$

With the additional equations D-6, D-7, and D-8 the Hardin model for the shear modulus can be specified without need of triaxial tests. Of course, the worth of any soil model is not only gauged by its ease of use, but also, by its ability to correctly capture the soil responses. Here too, the Hardin model performs well as demonstrated in the following section.

2. Verification of the Hardin Model for Granular Material

It would be of little significance to demonstrate the validity of the Hardin model by comparing it to the same test data on which Hardin developed his model because the parameters of his model were chosen to best fit his data. However, it is significant to compare Hardin with test data not previously "built in" to the model. To this end, an independent and comprehensive set of experimental data (Reference 9) on a uniform sand was obtained for purposes of the soil study. The tests were performed in a triaxial testing apparatus and included two hydrostatic tests, two uniaxial strain tests (K_o test) and five triaxial compression tests with measurements of lateral strain. Appendix C contains tabularized data from these tests.

Graphs of secant shear modulus versus shear strain for the five triaxial compression tests are displayed in Figure D-2. It is easily observed that the measured secant shear modulus G_s is dependent upon shear strain and stress state, in that, G_s increases with increasing confining pressure and decreases with increasing shear strain. Although the confining pressures may appear to be too high to be representative of live load stress state increments in soil, it should be kept in mind that gravity stresses must be included for proper definition of a secant modulus.

To directly compare Hardin's model with this test data the soil parameters S_1, a, and C_1 are evaluated by Equations D-6, D-7 and D-8 using the reported values: void ratio = 0.4, percent saturation = 0.0, and plasticity index = 0.0. For each data point in Figure D-2, a corresponding value for G_{max} and γ_h can be determined by means of Equations D-3, D-4, and D-5. Figure D-3 illustrates the comparison between the Hardin model and the experimental data wherein the solid line represents the Hardin model (Equation D-2) in the normalized form: $G_s/G_{max} = 1/(1+\gamma_h)$. The accompanying data points are plotted in the same form using measured values of G_s together with the corresponding computed values of G_{max} and γ_h.

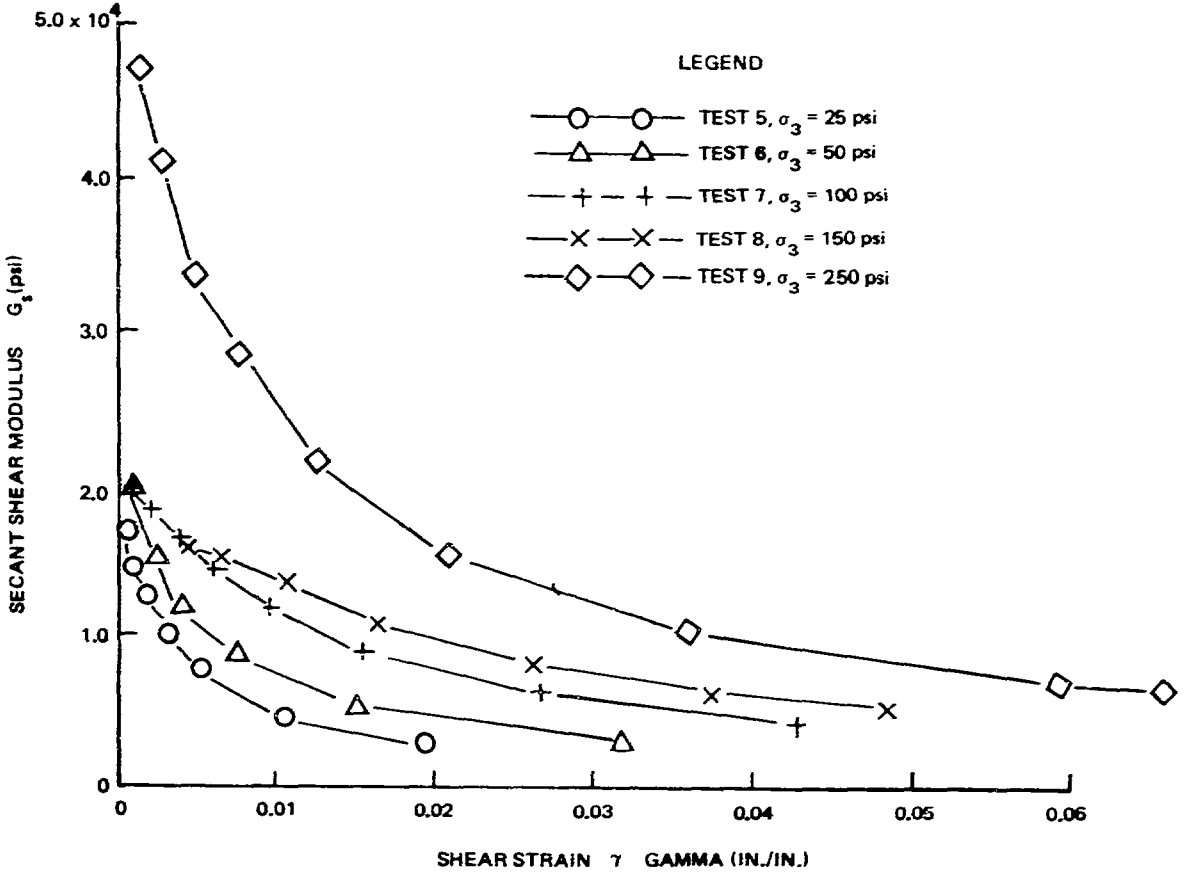

Figure D-2. G_s Versus Gamma

The agreement between the Hardin prediction and the test data is quite good over the entire range of γ_h. The significant result of Hardin's model is that it condenses the observed secant shear modulus into a single general relationship which provides a means to establish a computational algorithm for determining the shear modulus as a function of the stress and strain state.

It is re-emphasized that the above comparison was not based on curve fitting, but rather on a straightforward application of Hardin's shear model. In the next section a proposed relationship for Poisson's ratio is introduced to form the extended Hardin soil law.

3. Extended Hardin Model, Poisson Ratio Function

In order to develop a general variable modulus constitutive model for isotropic materials two "elastic" parameters (functions) must be specified. The secant shear modulus, G_s (Equation D-2), supplies one of these "elastic" parameters. For the second "elastic" parameter any one of several may be selected, such as Young's modulus, or bulk modulus, or Poisson's ratio. The specification of any two elastic parameters automatically infers the specification of the remaining parameters through well known elastic relationships.

The bulk modulus is the natural choice to compliment the shear modulus, G_s, however, any candidate bulk modulus relationship, $B_s = G_s\ (\sigma,\varepsilon)$, must be such that $B_s > (2/3)G_s$ in order to avoid an undesired inverse Poisson effect. That is, if B_s is specified less than $(2/3)G_s$ for example, the model would respond with transverse dilation under uniaxial tension, which is clearly unrepresentative of soil behavior. Because of this potential problem, it is difficult to directly specify an independent function for B_s which will at all times satisfy the above requirements. However, it can be done indirectly by first specifying an admissible function for Poisson's ratio, ν_s, and then using elastic relationships to define B_s.

Based on the above, the secant Poisson's ratio was selected as the second "elastic" functional relationship to be developed in a form similar to Equation D-2. Note, if the Poisson ratio function, $\nu_s\ (\sigma,\varepsilon)$, is such that the range is within the limits $0 < \nu_s < 0.5$ the theoretical energy considerations are satisfied regardless of the value of G_s.

For the first step in developing the functional relationship, observed values of Poisson's ratio are examined from experimental tests.

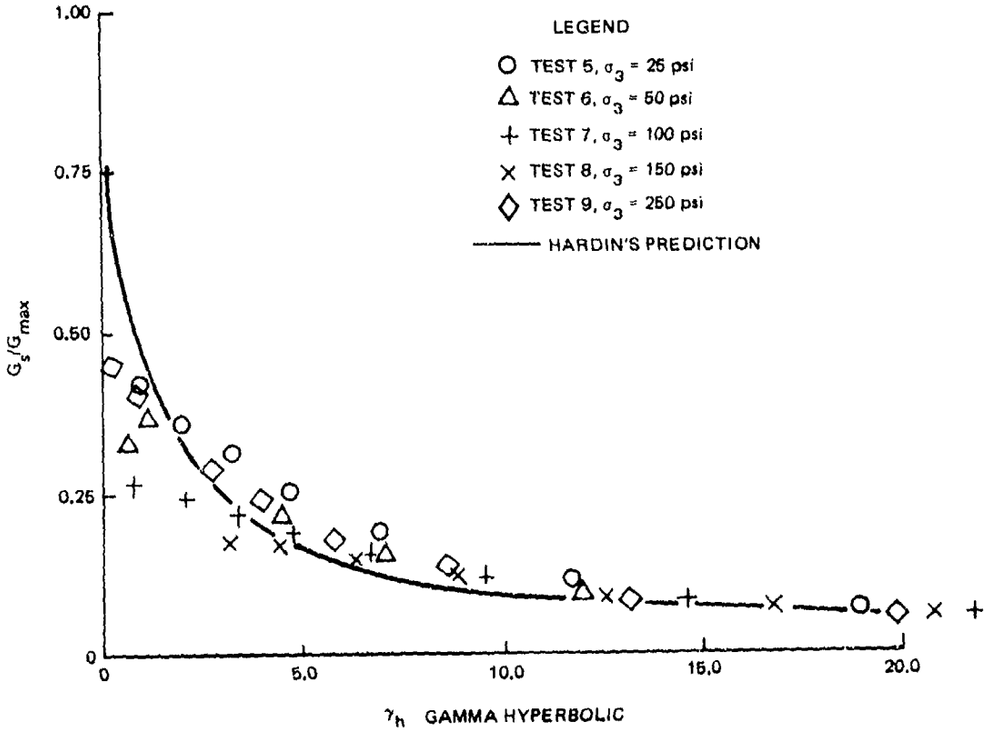

Figure D-3. G_s/G_{max} Versus Gamma Hyperbolic

From Hook's law the observed value of Poisson's ratio can be determined from a known stress-strain state by:

$$\nu_s = \frac{\sigma_m/3\phi - 2\,\tau/\gamma}{2\sigma_m/3\phi + 2\tau/\gamma} \qquad \text{(D-9)}$$

where ν_s = secant Poisson ratio

σ_m = $(1/3)(\sigma_{11} + \sigma_{22} + \sigma_{33})$, average normal stress

ϕ = $(\varepsilon_{11} + \varepsilon_{22} + \varepsilon_{33})$, volume change

τ = maximum shear stress

γ = maximum shear strain

Equation D-9 reduces to $\nu_s = -\varepsilon_1/\varepsilon_2$ for a one-dimensional stress state.

To examine the nature of the secant Poisson ratio, the test data of the five triaxial compression tests of Appendix C were used to calculate Poisson's ratio from Equation D-9. Note, in Appendix C the tabularized values of axial and radial strain do not include hydrostatic straining due to confining pressure. Therefore, in order to obtain the total strains, ε_{kk} and γ, the corresponding hydrostatic strains from the two hydrostatic tests were averaged and added to the tabularized values.

Motivated by Hardin's approach for the shear modulus, the data in Figure D-4 was replotted as a function of the ratio of shear strain to reference shear strain (γ/γ_r, see Equation D-5). These results are illustrated in Figure D-5 wherein it is observed the data collapses into a single curve. This suggests that a relationship for Poisson's ratio using γ/γ_r as the independent variable is reasonable. Again, paralleling Hardin's work, a hyperbolic relationship given by Equation D-10 is hereby proposed as a general relationship for Poisson's ratio.

$$\nu_s = \frac{\nu_{min} + \gamma_p\ \nu_{max}}{1 + \gamma_p} \qquad \text{(D-10a)}$$

and

$$\gamma_p = q\ \gamma/\gamma_r \qquad \text{(D-10b)}$$

where ν_s = Poisson ratio as function of γ_p

ν_{min} = Poisson ratio at zero shear strain

ν_{max} = Poisson ratio at large shear strain (failure)

q = dimensionless parameter for curve shape

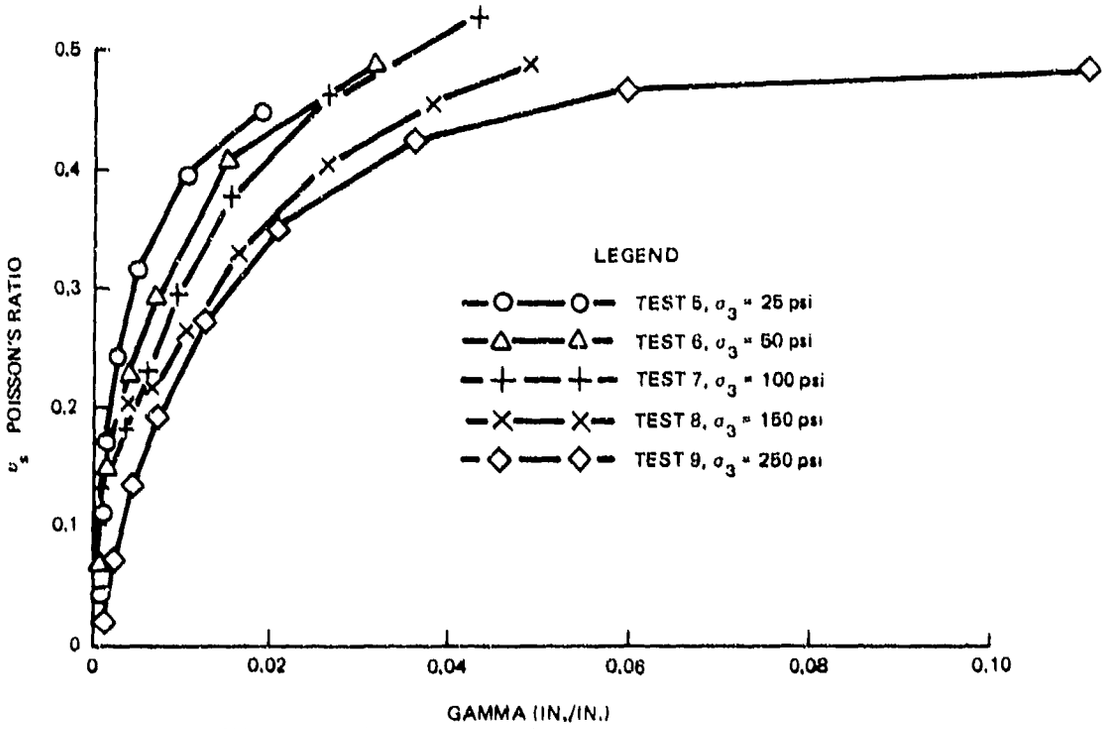

Figure D-4. Poisson's Ratio Versus Gamma

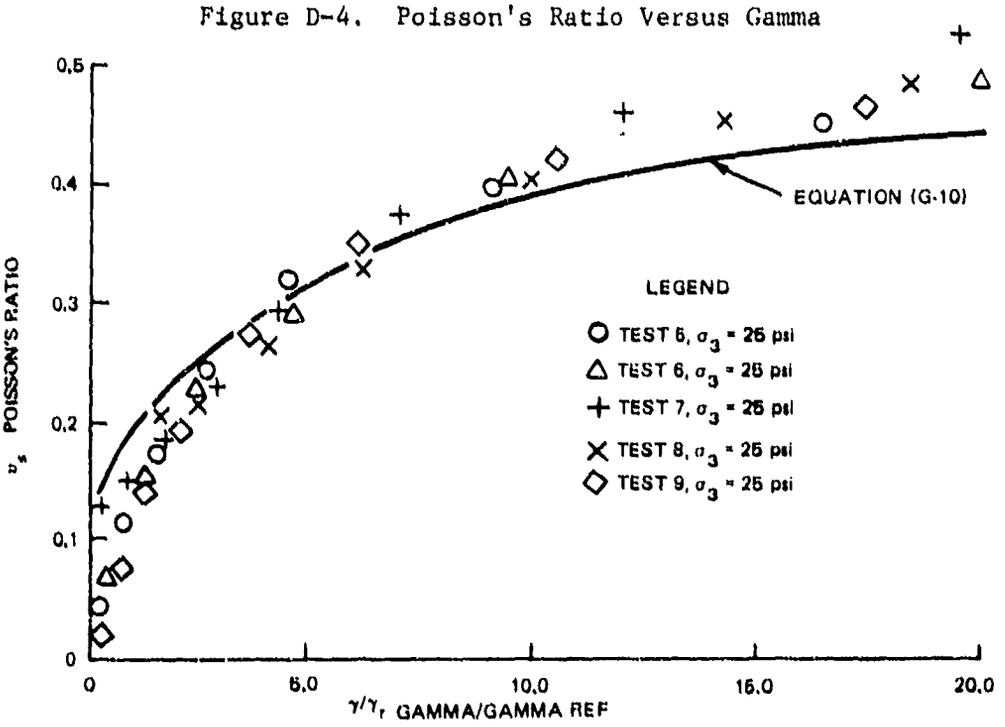

Figure D-5. Poisson's Ratio Versus Gamma/Gamma Ref

The terms ν_{min}, ν_{max}, and q are parameters dependent on the type and characteristics of the soil, and are selected by simple curve fitting techniques discussed at the end of this appendix. The solid line in Figure D-5 represents Equation D-10 for the parametric values:

$$\nu_{min} = 0.10$$

$$\nu_{max} = 0.49$$

$$q = 0.258$$

It is observed that the proposed curve for Poisson's ratio is in good agreement with the test data over the entire range of shear strain.

Of course, the general validity of Equation D-10 is by no means substantiated by a single set of tests. Confidence in the model can only be obtained through further testing of many types of soils in different loading environments. Nonetheless, it is felt Equation (D-10) is sufficiently general to model most soils. Certain features of Equation (D-10) are particularly useful. For example, the theoretical limits of Poisson's ratio, $0 < \nu_s < 0.5$, are easily maintained by the parameters ν_{min} and ν_{max}. Also, the shape of the curve can be varied from concave to convex by the parameter q. Carried to its logical end, expressions for ν_{min}, ν_{max}, and q can be developed in terms of basic soil characteristics such as void ratio, saturation and plasticity index, thereby providing an alternative to triaxial testing.

The combination of the shear modulus and Poisson ratio relationships constitute the extended Hardin soil model. In the next section the versatility of the extended Hardin model is demonstrated on a one-dimensional confined compression test, (K_o Test).

4. Extended Hardin Versus K_o Test for Granular Material

A severe test of any soil model is to compare it to test data from a load environment different from the one upon which the model was based. To this end, the K_o tests of Appendix C provide experimental data for determining the coefficient of lateral earth pressure K_c and the confined modulus M_s. K_c is determined by the ratio of lateral stress-to-axial stress, i.e., (σ_3/σ_1), and M_s is determined by the ratio axial stress-to-axial strain, i.e., (σ_1/ε_1). The corresponding "extended Hardin" prediction is determined by solving a one-dimensional plane strain boundary value problem characterized by the following set of nonlinear equations:

$$\tau = \sigma_1(1 - 2\nu_s)/2(1 - \nu_s) \qquad \text{(D-11)}$$

$$\sigma_m = \sigma_1[1 + 2\nu_s/(1 - \nu_s)]/3 \qquad \text{(D-12)}$$

By utilizing the "extended" Hardin model, Equations (D-1 through D-10) the above equations may be solved in an iterative manner to determine the predicted responses for each axial load, σ_1. Figure D-6 shows the comparison between measured and predicted values for the coefficient of lateral earth pressure as a function of axial stress. It is observed that the agreement is excellent. More significantly, the results indicate that K_c is constant for this load environment. Since K_c is directly related to Poisson's ratio by the expression $K_c = \nu_s/(1 - \nu_s)$, one might carelessly conclude from this type of test that Poisson's ratio remains constant for soils regardless of the load environment. This conclusion is invalid as previously demonstrated in Figure D-4. The reason Poisson's ratio remains practically constant for this type of test can be understood by examining the variable, γ_p, of Equation (D-10). Since Poisson's ratio is constant, it follows that γ_p is constant. But γ_p is directly proportional to shear strain (8) and inversely proportional to the square root of the spherical stress (σ_m). Consequently, in this loading environment the shear strain increases directly with the square root of spherical stress producing a relatively constant Poisson ratio.

For the last comparison, Figure (D-7) depicts the measured and predicted value of the confined modulus, M_s, as a function of axial stress. In this instance, the predicted values average about 25 percent lower than the measured values. However, the shapes of the two curves are practically identical. Keeping in mind that the analytical prediction of M_s is based on the generalized relationship for the secant shear modulus, the discrepancy between the curves is not viewed as a defect of the model. That is, it would be a simple matter to adjust the parameters S_1, a, and C_1 of Equations (D-3 and D-4) to produce analytical predictions of M_s that more precisely coincide with the measured values. However, here the objective is to demonstrate the general applicability of the extended Hardin model and not curve fitting results.

5. Comparison of Extended Hardin with Compacted Clays

The extended Hardin model has been shown in the foregoing to be capable of modeling the behavior of dense sand with a high degree of accuracy under various types of loading, i.e., hydrostatic, confined compression, and triaxial shear. General application of Hardin's approach to modeling soil stiffness, however, requires knowledge of the previous

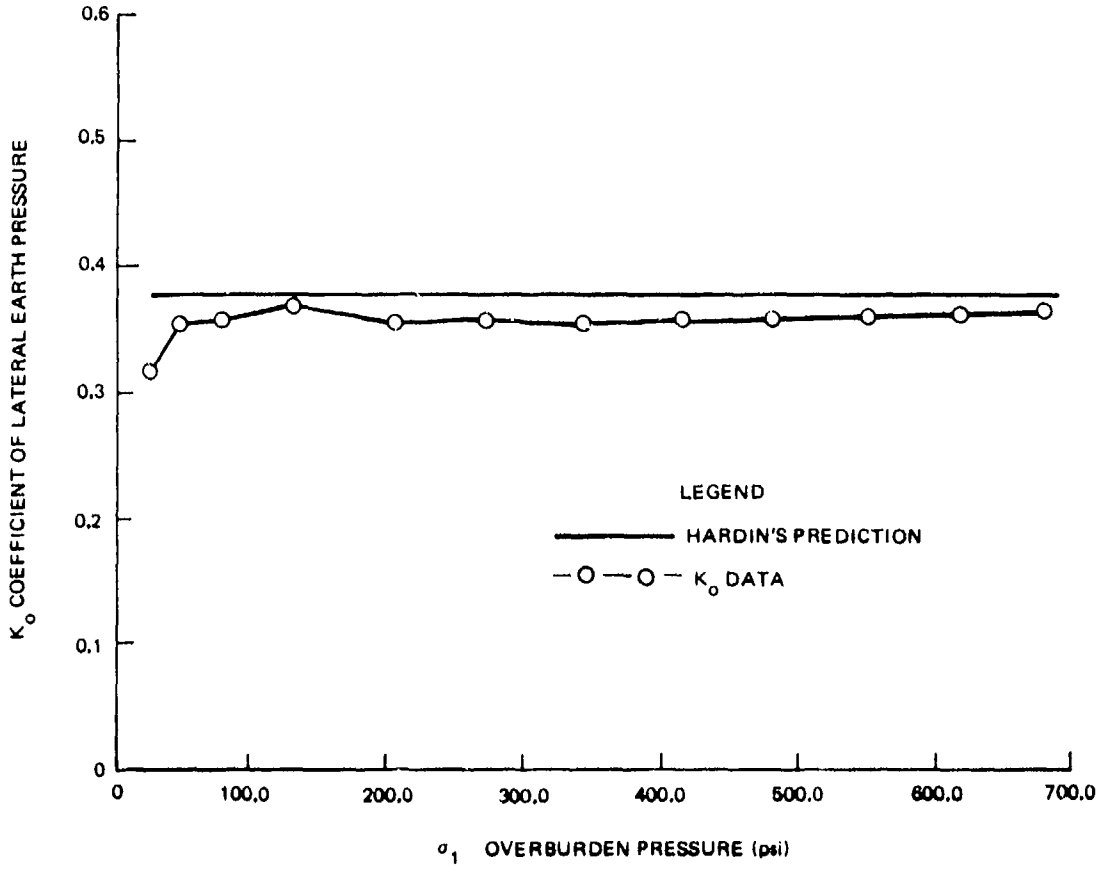

Figure D-6. k Versus Overburden Pressure

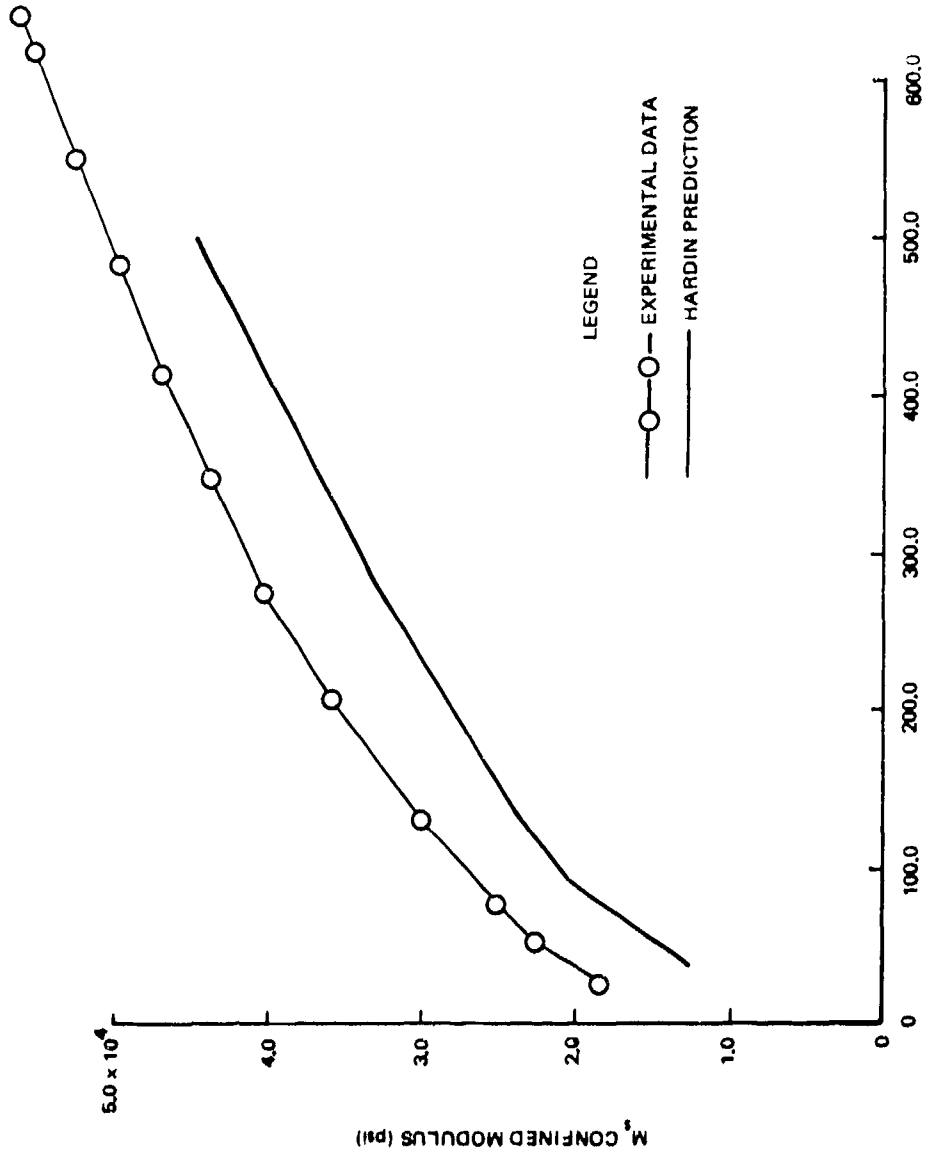

Figure D-7. M_s Versus Overburden Pressure

stress, loading history, and confining stress. These conditions are not easily assessed for compacted clays. For example, the compactive history or, in effect, the existing over consolidation ratio is difficult to estimate. Furthermore, the effects of partial saturation cause large pore water tensions within the soil matrix and exert a level of effective confining stress which is not readily measurable. Thus a plot of shear stress versus shear strain, from a triaxial shear test for a compacted clay, would not have the characteristic of a normally consolidated soil as shown in shape Figure D-1 but rather a much steeper initial section as shown in Figure D-8. This steeper initial section is largely due to the preconditioning of the compactive effort. In addition, the stress strain curves, due to the influence of pore pressure effects, show an insensitivity to confining pressure which increases with increasing degree of saturation.

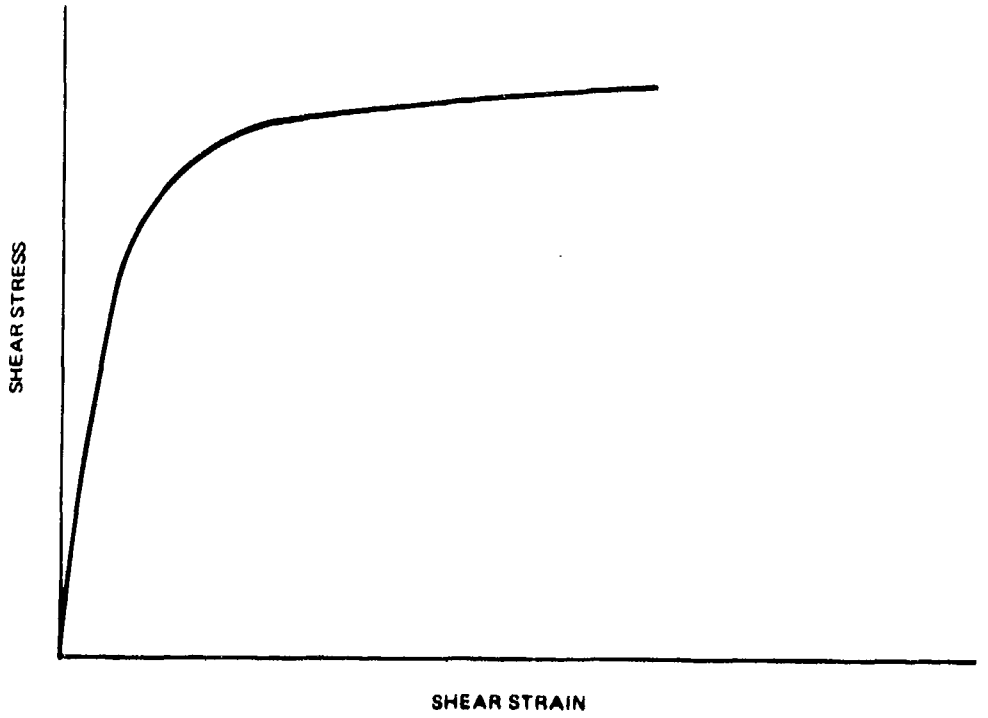

Figure D-8. Typical Stress-Strain Curve for a Compacted Clay

Figures D-9 through D-11 illustrate the shear stiffness of the individual clay specimens. The principal stress difference, plotted along the ordinate, is two times the value of the maximum shear stress acting on any plane within the soil specimen, whereas the abscissa is used to represent shear strain. (No consideration of stress irregularities due to loading caps, etc., are considered herein). Thus the slopes of the curves in Figures D-9 to D-11 represent values of 2 times the shear modulus. It may be noted on Figures D-9 to D-11 that the shear stiffness of the clay is reasonably independent of the initial confining stress (σ_3), particularly within the initial portions of the stress-strain curves. Attempts to fit these curves by means of the Hardin model will concentrate on test series B (Figure D-10) which has the intermediate range of saturation (about 59%). In Figure D-12 are shown measured values of secant shear modulus from tests B-2, B-4 as well as average values for the test series B-2 through B-7. Since it is noted that both test B-2 at a confining pressure of 19.7 psi (1.36 bars) and B-4 at a confining pressure of 59.2 psi (4.08 bars) provide a reasonable estimate of the average for the test series, regardless of the level of initial confinement, test B-4 is selected for fitting. Figure D-13 shows measured values of secant shear modulus plotted versus shear strain for triaxial test B-4. Also shown on Figure D-13 are calculated values of shear modulus based upon different fitted values for the constants in Hardin's model, S_1, C_1 and for a confining pressure (σ_3) of 40 psi (as opposed the confining pressures of about 20 psi and 60 psi for tests B-2 and B-4 respectively and a range of 20 to 91 psi for the series). It is shown in Figure D-13 that the following values for Hardin's parameters give a reasonable simulation of shear behavior for test B-4:

$$S_1 = 2000$$

$$C_1 = 3 \times 10^6$$

$$a = 1/2$$

Also shown in Figure D-13 is a plot using the above values for Hardin's parameters and a confining pressure of 5 psi. The calculated modulus values again appear to give a reasonable simulation of the shear behaviour for the compacted clay within this range of saturation. Comparisons of the foregoing curve fit parameter values were also made with typical tests from the wetter and dryer test series, see Figures D-14 and D-15. Figure D-14 shows relatively good agreement between the Hardin values of shear modulus and experimental values for test C-7, particularly in the higher shear strain ranges where initial specimen reconditioning due to compaction history is not so prevalent. Figure D-15 shows that Hard.. theoretical values of shear modulus for confining pressures of 5 and 40 psi bracket values of shear modulus for test A-1, which is typical of the A series.

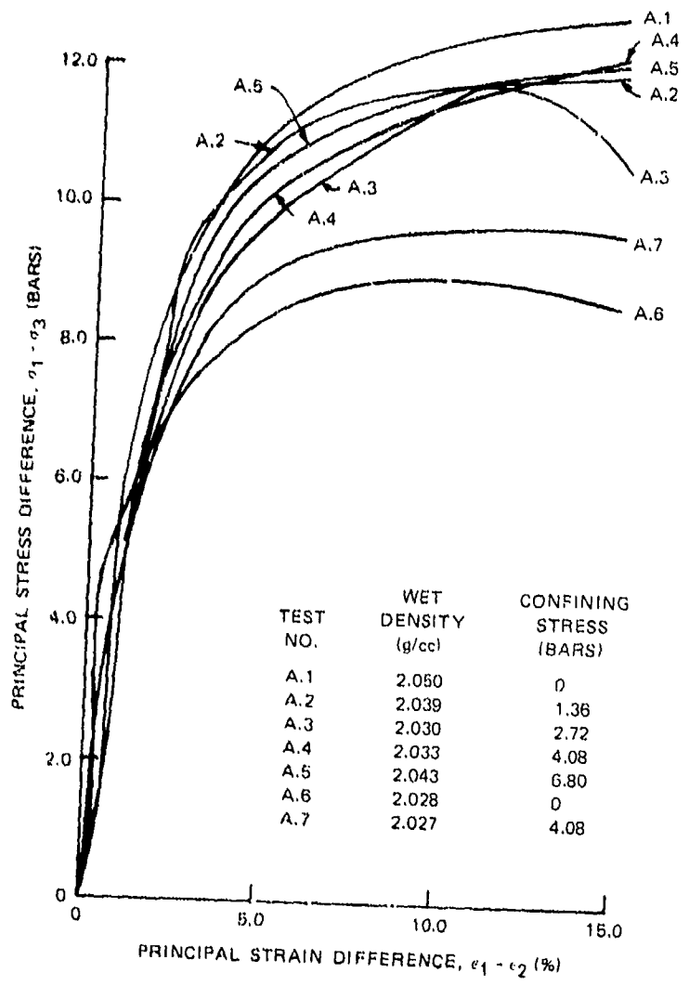

Figure D-9. Triaxial Shear Test Data for Series A Tests

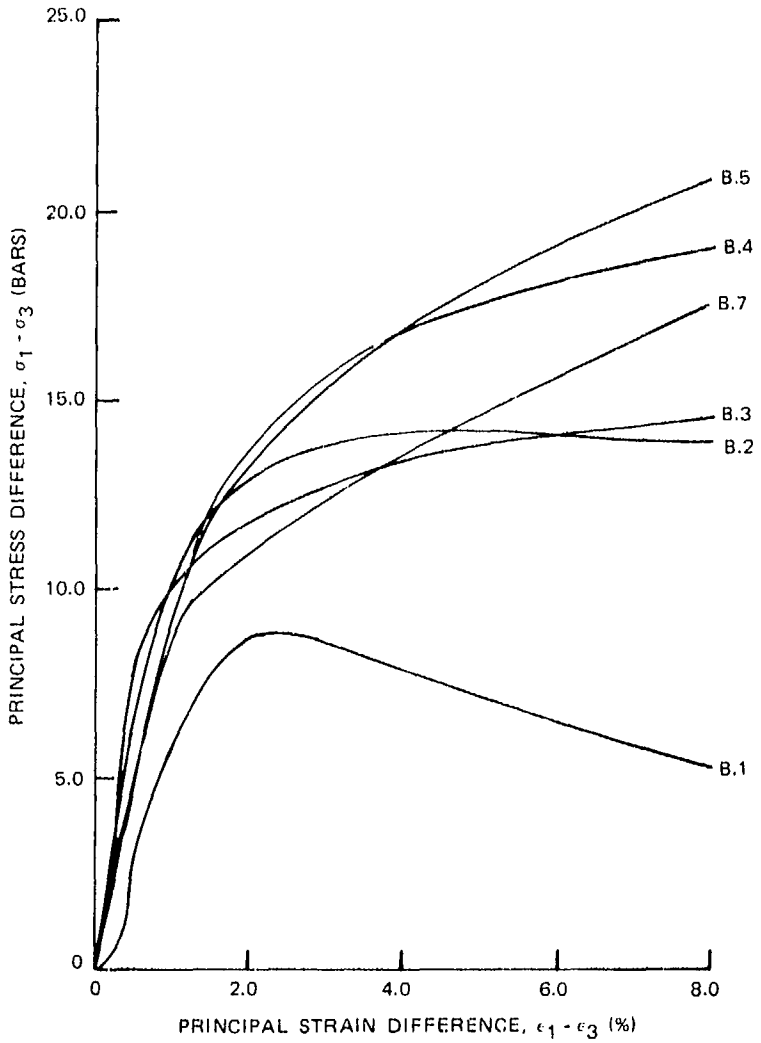

Figure D-10. Triaxial Shear Test Data for Series B Tests

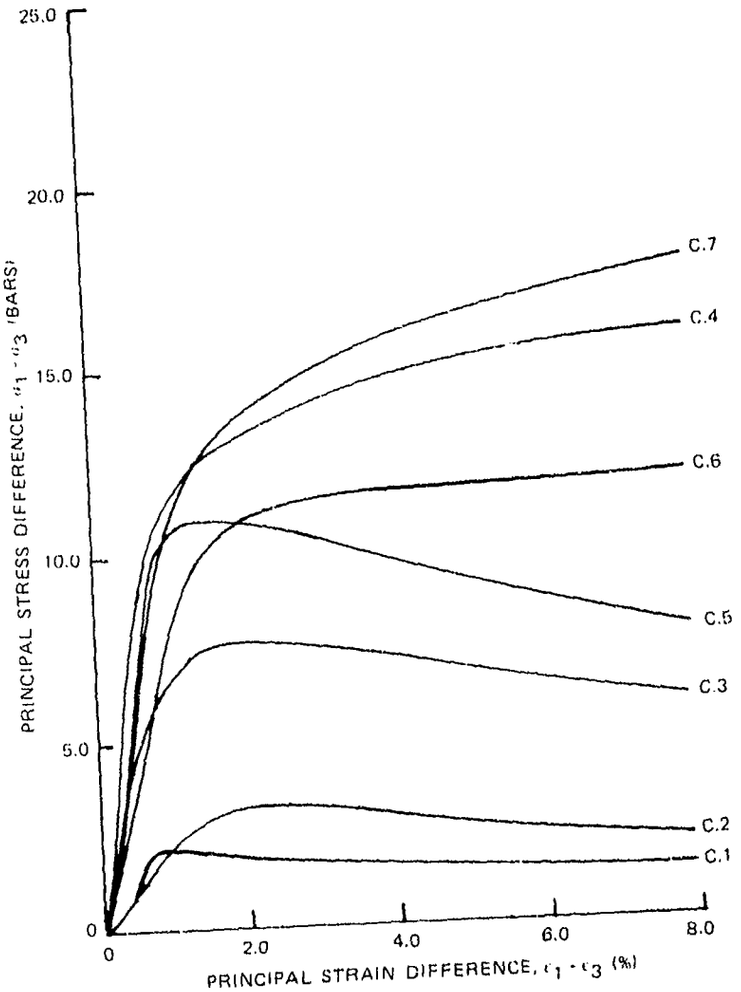

Figure D-11. Triaxial Shear Test Data for Series C Tests

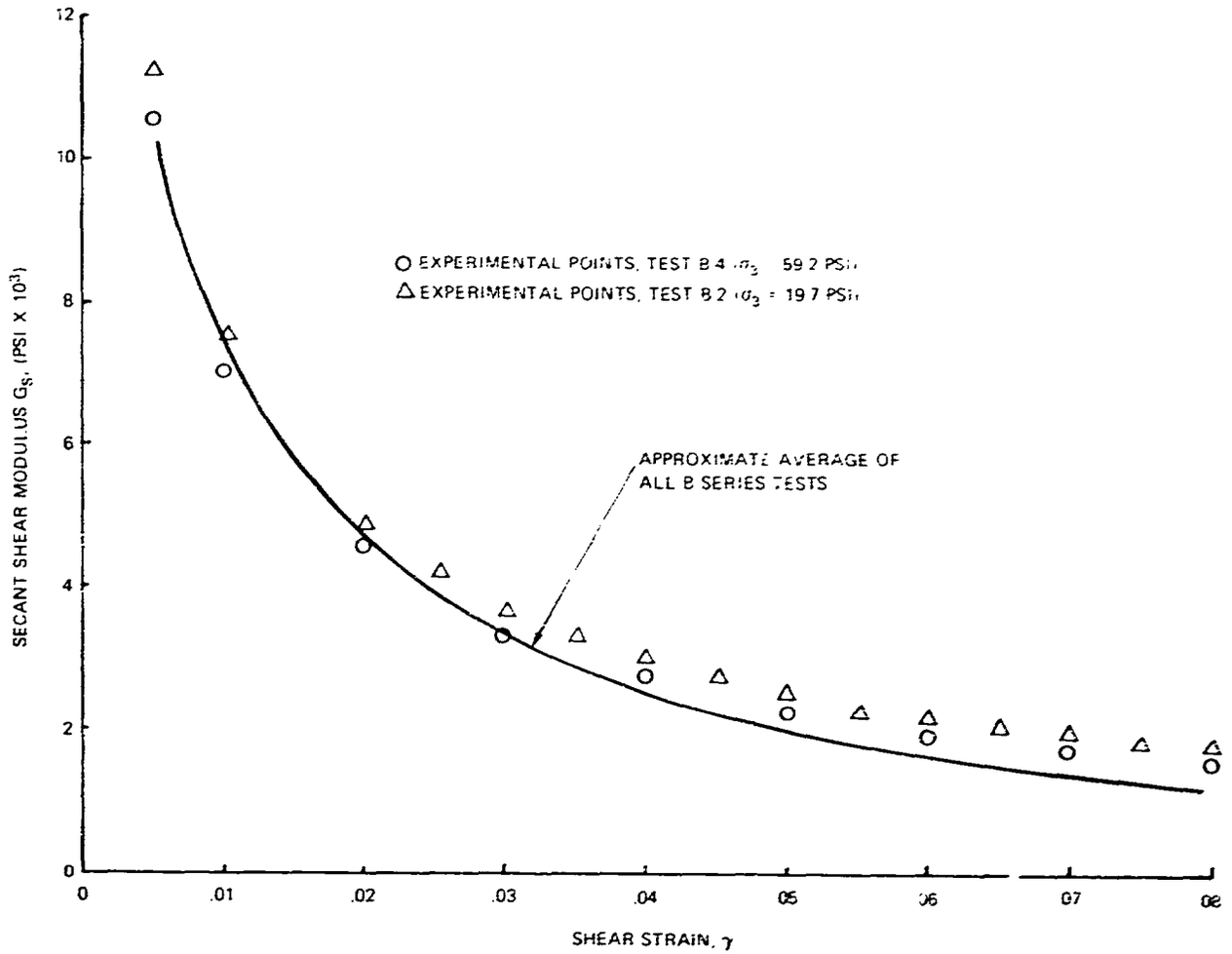

Figure D-12. Measured Values of Secant Shear Modulus for Test Series B

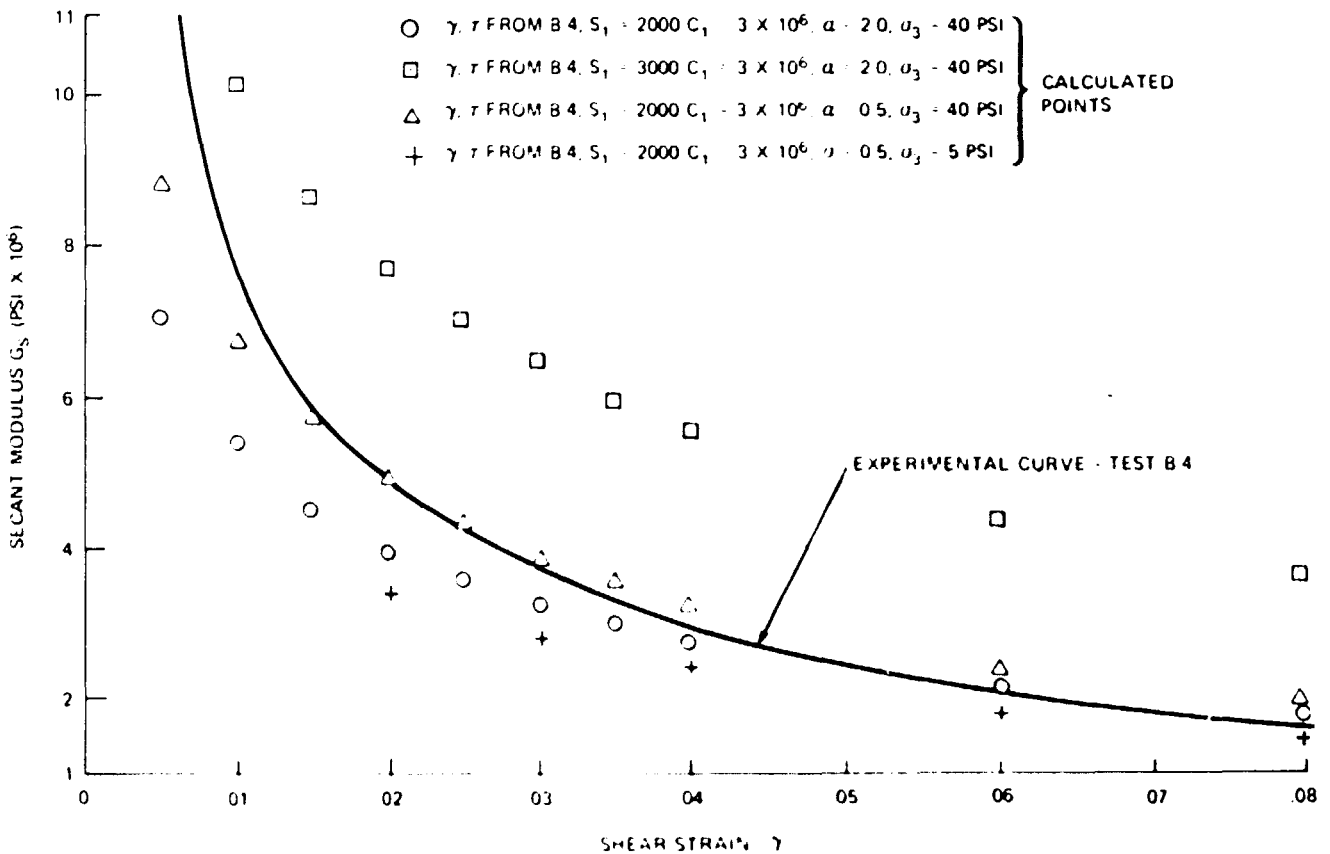

Figure D-13. Calculated Versus Measured Values of Secant Shear Modulus

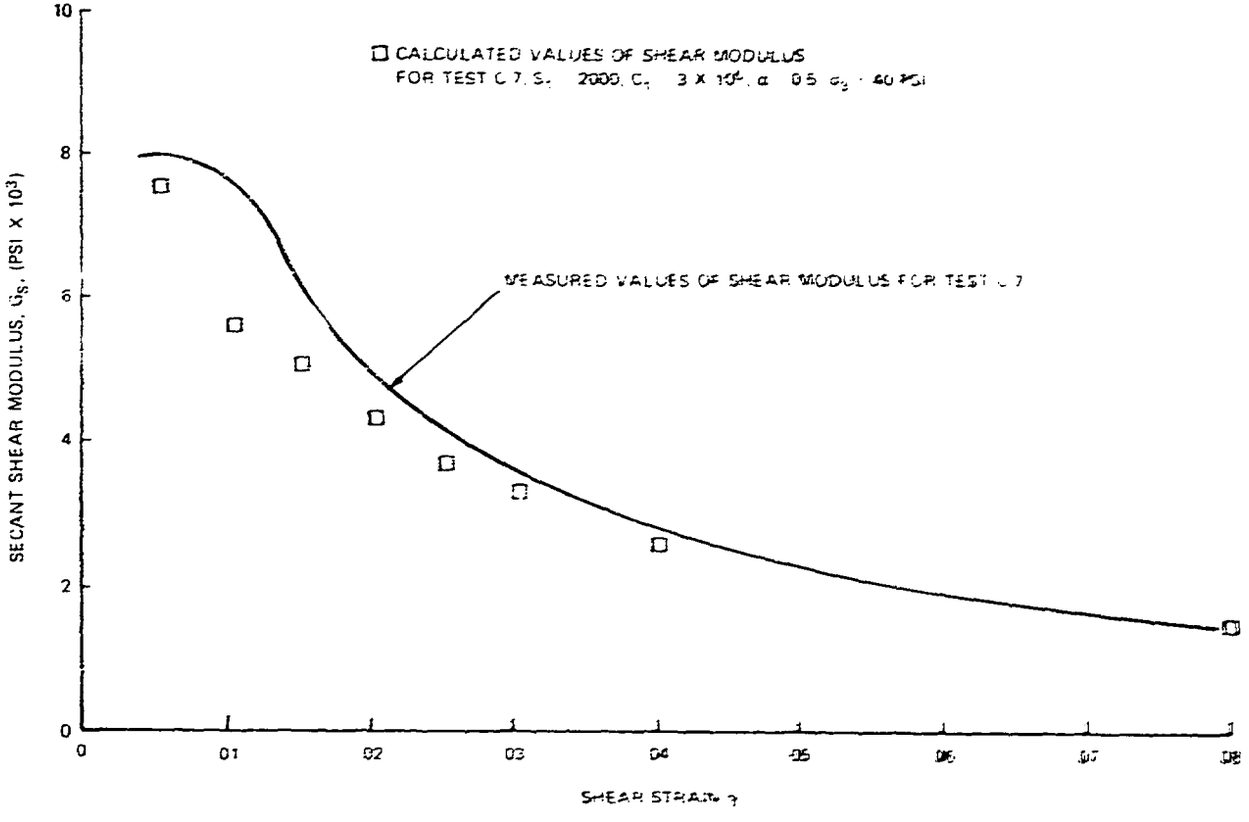

Figure D-14. Measured Versus Computed Values of Shear Modulus for Test C-7

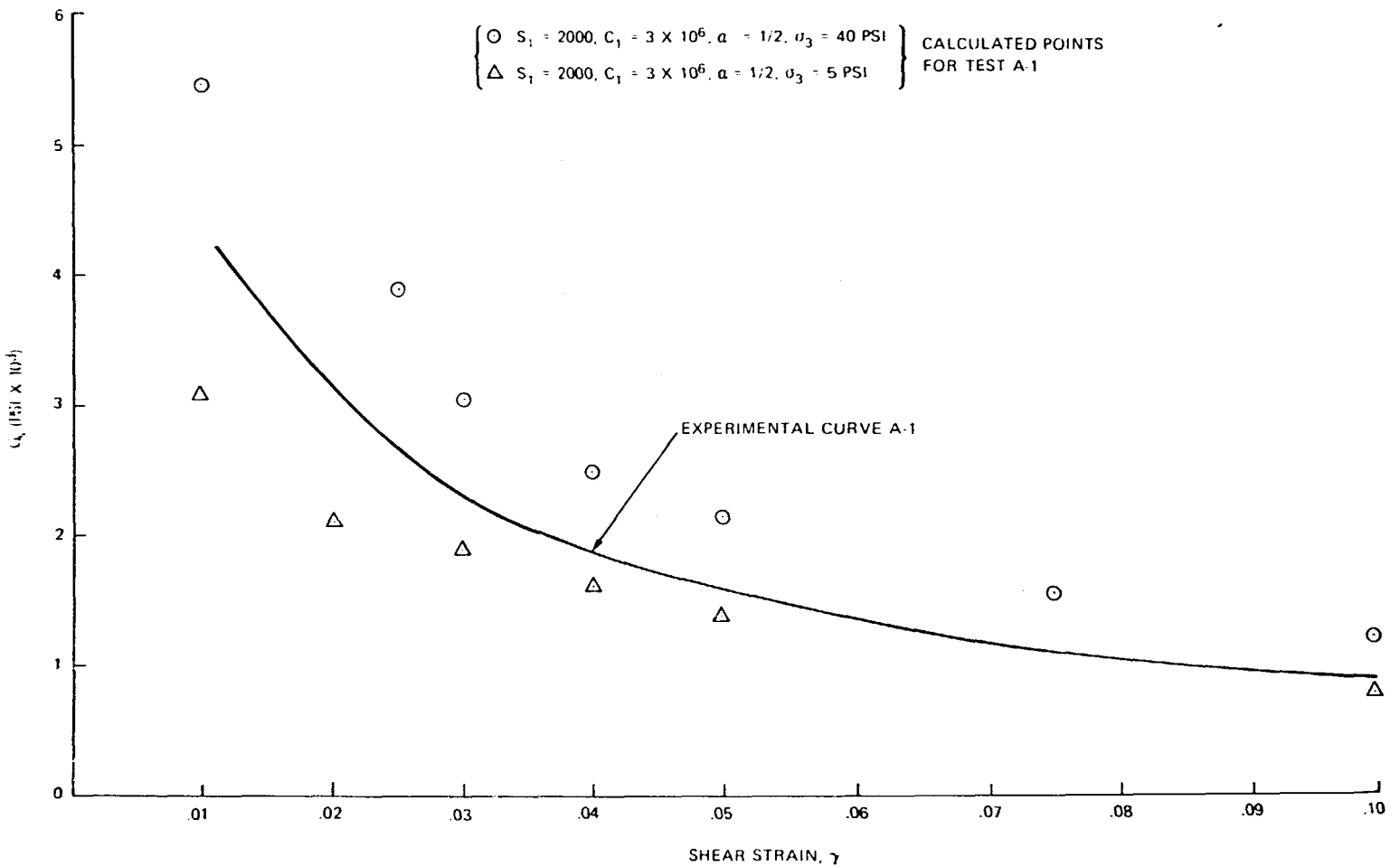

Figure D-15. Measured Versus Computed Values of Shear Modulus for Test Al

POISSON'S RATIO FITTING

Although values of Poisson's ratio for normally consolidated clays are generally thought to be close to 1/2, high air void contents in compacted clays can be expected to reduce this value, at least in the lower stress ranges prior to collapse of the air bubbles. Figure D-16 shows typical measured values of Poisson's ratio for the three different triaxial test series. As would be expected, the test points representative of the A series, which has the highest degree of saturation (around 90 percent) are very close to 0.5. Alternatively, the data from the other two series which had degrees of saturation of about 34 and 58 percent are found to be somewhat lower. Parameter values for fitting this data by means of the extended Hardin model were selected to provide intermediate values of Poisson's ratio somewhat between the wettest and driest specimens as shown in Figure D-16.

Parameter values of: $\nu_{min} = 0.10$

$\nu_{max} = 0.49$

$q = 1.0$

are noted to provide values of Poisson's ratio falling within the shaded area of Figure D-16 for values of confining pressure, σ_3, between 5 and 40 psi. It is noted that the value of Poisson's ratio in using the extended Hardin formulation is only slightly influenced by the σ_3, level. Thus it is obvious the effects of such factors as pore water tension in compacted materials make it very difficult to calculate any type of reliable constitutive laws on a theoretical basis.

OTHER TYPES OF SOIL BEHAVIOR

The crucial test for any soil model is its ability to model types of soil response different from that which was used to fit it. This is the area in which the great host of proposed soil models abounding in the literature break down. Using the previous soil parameter values determined on the basis of triaxial tests, namely:

$S_1 = 2000$ $\quad C_1 = 3 \times 10^6$ $\quad a = 0.5$

$\nu_{min} = 0.10$ $\quad \nu_{max} = 0.49$ $\quad q = 1.0$

it will be interesting to investigate other types of behavior, in this case the compacted clay response under both hydrostatic and uniaxial strain compression tests. For hydrostatic tests, since the shear strain is theoretically zero, the relationship for bulk modulus, $K = \frac{2G(1+\nu)}{3(1-2\nu)}$, becomes $K = 0.92G$. Thus bulk modulus would be slightly less

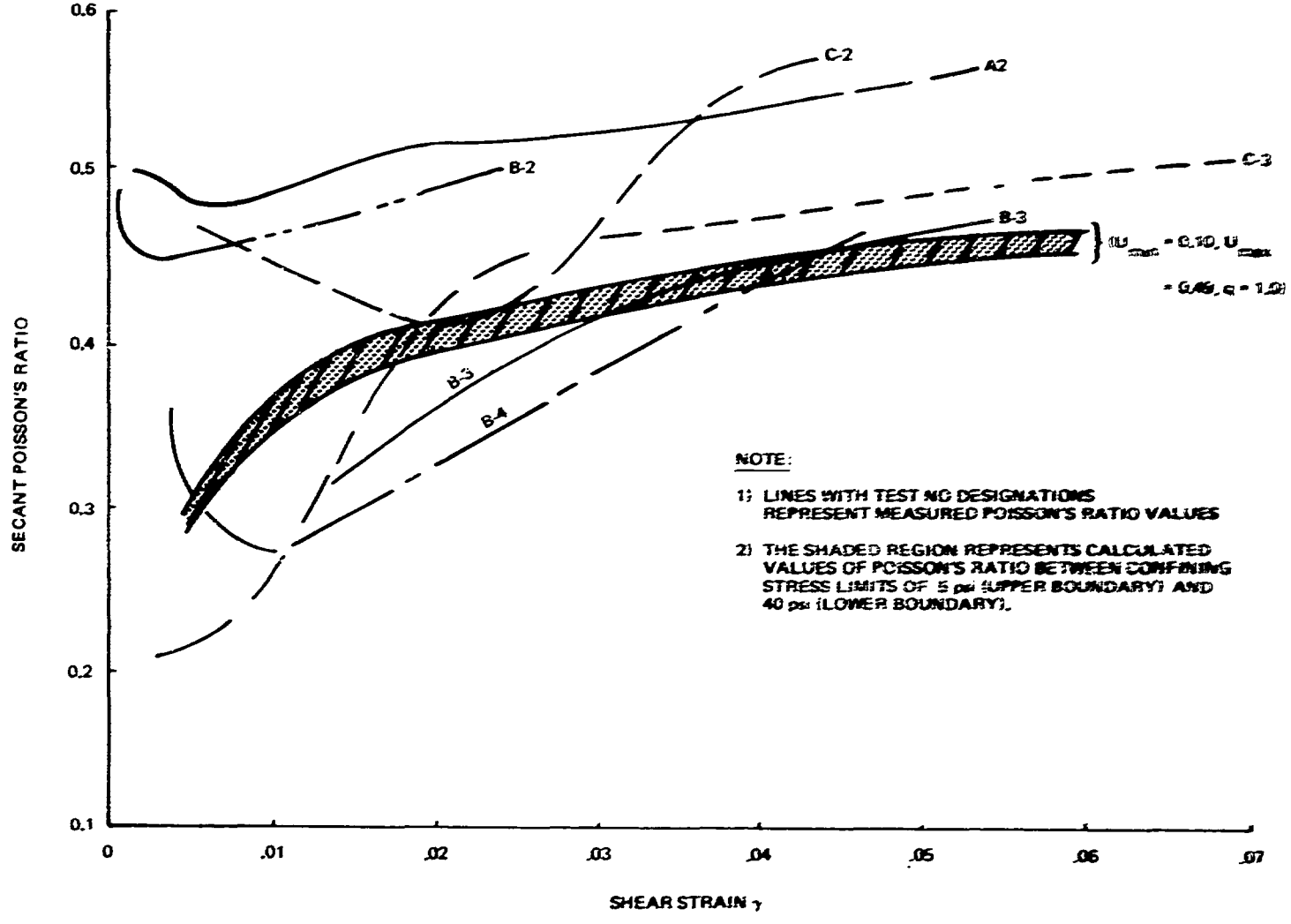

Figure D-16. Measured and Calculated Values of Secant Poisson's Ratio

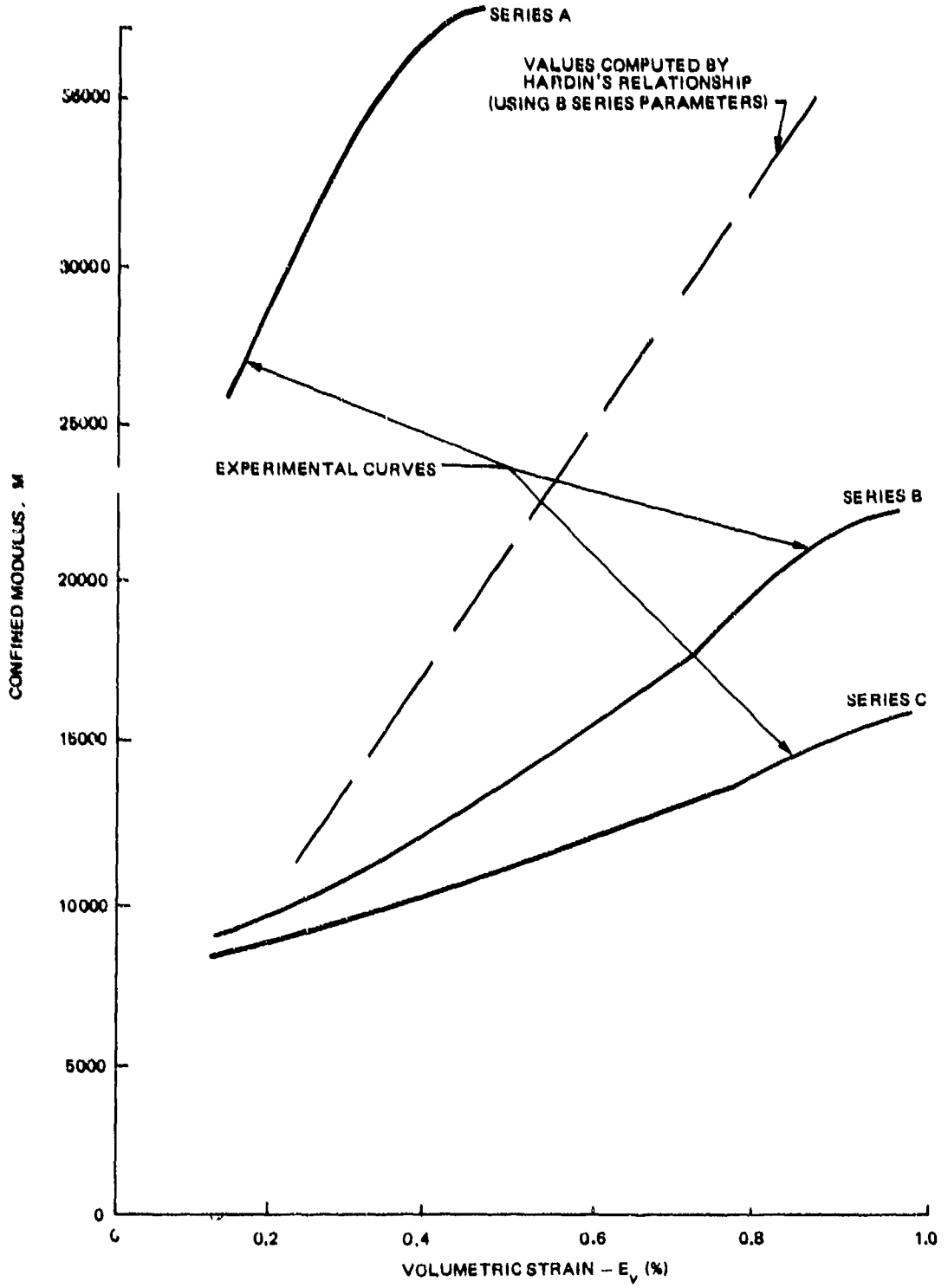

Figure D-17. Calculated Versus Measured Values of Confined Modulus

than shear modulus by this particular parameter selection. For the large air void contents involved with low saturation levels this is acceptable.

Measured values of average confined modulus measured for the three series of uniaxial (K_o) tests are shown in Figure D-17 versus volumetric strain, ε_n. As might be expected, the confined modulus is very much a function of the degree of saturation. Also shown on Figure D-17 is a plot of confined modulus based upon the foregoing parameter values inserted into the extended Hardin model. Again it is obvious that the Hardin model is not very appropriate for compacted fat clays, nevertheless the calculated values are a reasonable compromise between the various measured values, and tend to match the values for the drier two series reasonably well in the lower shear strain range. Thus for the compacted clays, the Hardin model can be used as a framework to define material response, but it must be fitted in a phenomenological manner and not extended to other situations theoretically.

6. Parameters for Extended Hardin Model

Complete identification of the extended Hardin model requires specifying the parameters S_1, a and C_1 for defining the secant shear modulus (Equations D-3 to D-5), and the parameters ν_{min}, ν_{max}, and q for Poisson's ratio (Equation D-10).

As a general rule of thumb, it is always more desirable to determine the parameters directly from soil test specimens taken from the field under investigation. Moreover, the specimens should be tested in a load environment closely resembling actual field conditions. (That this is a necessity with compacted fat clays has been shown in the foregoing.) However, all too often engineers are faced with analyzing soil-structure systems without available test data of soil specimens. In such cases Equations D-6 to D-8 can be used directly to determine S_1, a and C_1 for most soils. Unfortunately, similar expressions for ν_{min}, ν_{max}, and q are not yet developed. It is hoped that this report will stimulate further work toward that end. In the meantime, the Poisson ratio parameters will have to be determined from test data similar to Appendix C and/or engineering judgment.

Outlined below is a step-by-step procedure for determining the complete set of parameters for the extended Hardin model based on a triaxial test with axial strain, ε_1, and radial strain, ε_3, measurements.

Shear modulus parameters. To begin with, a graph of shear stress, $\tau = (\sigma_1 - \sigma_3)/2$, versus shear strain, $\gamma = \varepsilon_1 - \varepsilon_3$, is plotted similar to Figure D-1.

1. Construct the initial tangent at zero shear strain and denote its value as G_{max}. The parameter S_1 is given by:

$$S_1 = G_{max}/\sqrt{\sigma_3}$$

2. Determine the maximum stress, τ_{max}, at failure. The parameter C_1 is computed by:

$$C_1 = S_1^2(2/3 + \sigma_3/\tau_{max})$$

3. At the shear stress level $\bar{\tau} = \tau_{max}/2$ determine the corresponding measured shear strain and denote it as $\bar{\gamma}$. Also compute the reference shear, $\bar{\gamma}_r$, at this stress level given by the expression:

$$\bar{\gamma}_r = \frac{S_1}{C_1}\sqrt{\sigma_3 + \tau_{max}/3}$$

Then, the parameter a is given by:

$$a = \exp(r)^{0.4}\left(\frac{6\rho + 2}{3\rho + 2}\right) - \left(\frac{1 + r}{r}\right)$$

where $r = \bar{\gamma}/\bar{\gamma}_r$, $(r > 0)$

$\rho = \sigma_3/\tau_{max}(\rho > 0)$

Poisson ratio parameters. Poisson's ratio may be computed from the results of a triaxial test by the relation:

$$\nu_s = \frac{\sigma_3/\sigma_1 - \varepsilon_3/\varepsilon_1}{1 + (\sigma_3/\sigma_1)(1 - 2\varepsilon_3/\varepsilon_1)}$$

Note, in the above equation, ε_3 and ε_1 must include the volumetric strain due to confining pressure. Also the signs of ε_3 and ε_1 must be strictly observed. Hence, the ratio $\varepsilon_3/\varepsilon_1$ varies from positive to negative with increased axial stress.

1. The expression for ν_s is undefined at the origin, i.e., at hydrostatic loading. Therefore, to obtain the value of the parameter ν_{min} it is necessary to evaluate at the first few data points and extrapolate to the origin, (See Figure D-4). Any error arising from this extrapolation will generally be diminished since the influence of ν_{min} on the Poisson's ratio function decreases with increasing shear strain.

2. To obtain ν_{max}, ν_s is evaluated at maximum failure stress; i.e., $\sigma_1 = \sigma_{1max}$ and $\varepsilon_1 = \varepsilon_{1max}$.

3. Lastly, to compute the parameter q the data obtained at the stress level τ defined in step 3 of Part A is used as follows: ν_s is evaluated for $\bar{\nu}_s$ using $\bar{\varepsilon}_1 = \bar{\gamma} + \bar{\varepsilon}_3$, and $\bar{\sigma}_1 = \sigma_3 + 2\bar{\tau}$, then q is given by:

$$q = \frac{1}{r} \frac{\bar{\nu}_s - \nu_{min}}{\nu_{max} - \nu_s}$$

The above procedure is only one of a multitude of possible curve fitting techniques. For example, a least squares procedure could also be used. For different types of soil tests similar procedures can readily be developed to define the parameters.

It must be emphasized here that the Hardin model was developed for natural soils. Therefore, although it has demonstrated its validity in this region, and with compacted granular materials, it may be used with caution for compacted highly cohesive soils, which contain unknown levels of pore water tension and pre-consolidation conditioning.

Appendix E

COMPUTER PROGRAM XHARDN

An elastic layer analysis requires the specification of two elasticity constants (normally E and ν) for each layer of the pavement/soil system. The XHARDN computer program can be used as an aid in the determination of E and ν for a soil. Additionally, this program punches as output the cards necessary to operate the ELAST program described in Reference 1.

The XHARDN program is designed to operate either with minimal input corresponding to the situation where no specific materials information is available (based on Section 2 and 4 of Appendix D) or with input determined experimentally (preferably from a triaxial test as described in Section 6 of Appendix D). The latter method, which is preferable, requires that for each layer of soil the S, PI, e, density, layer thickness, G_{max}, ν_{min}, ν_{max}, and q parameters be specified. The expedient procedure which should be limited to "ball park" calculations selects values for e, S, PI, and ν_{min}, ν_{max}, and q according to soil type (shown in Table E-1 as default values). G_{max} is computed using equation (D-3). Table E-1 also shows acceptable parameter values; any input outside these ranges causes the program to terminate. The user manual for the XHARDN computer program is shown in Figure E-1.

1. Example Problem

The following input data for the XHARDN program was obtained from Reference 30 and was used to generate the results shown in Figure E-2 for the first section shown in Figure E-3.

```
   USNAS MOFFETT FIELD HANGER NO 3 K 380
CONC      7.3       150.      3000000.      0.2       2
GRAN      16.0      110.
                                0.467         0.534
GRAN      20.0      110.
                                0.385         0.5605
LCOHE               110.
                                                      22.
STOP
```

Table E-1. Default Values and Acceptable Range for Material Constants

Type of Soil	Void Ratio, e		Saturation, S		Plastic Index, PI		Poisson's Ratio Parameters		
	Min-Max	Default	Min-Max	Default	Min-Max	Default	ν_{min}	c	ν_{max}
Granular	0.1-1.0	0.6	0.0-1.0	0.0	0-0	0	0.1	0.26	0.49
Mixed	0.1-1.0	0.5	0.0-1.0	0.5	0-50	5	0.2	0.35	0.49
Cohesive	0.3-3.0	1.0	0.0-1.0	0.9	0-100	20	0.3	0.40	0.49

```
C
C- - - -M A N U A L - - - -M A N U A L - - - -M A N U A L - - - -M A
C
C
C
C - - - - - - - - - - - - - - - - - - - - - - - - - - - - - - - - - -
C
C * * * * * * * * * * * * * * * * * * * * * * * * * * * * * * * * *
C
C - - - - - - - - - - - - - - - - - - - - - - - - - - - - - - - - - -
C
C    CARD TYPE 1 TITLE (20A)
C                DESCRIPTION OF THE SECTION
C                (STOP BEGINNING IN COL 1 ENDS PROGRAM)
C
C - - - - - - - - - - - - - - - - - - - - - - - - - - - - - - - - - -
C
C * * * * * * * * * * * * * * * * * * * * * * * * * * * * * * * * *
C
C - - - - - - - - - - - - - - - - - - - - - - - - - - - - - - - - - -
C
C    CARD TYPE 2.  DEFINES TYPE OF MATERIAL AND GIVES LINEAR ELASTIC
C                PROPERTIES IF KNOWN.  (A1,A4,5X,4F10.0,I5)
C
C    COL 1            LAST, ANY NON BLANK CHARACTER INDICATES LAST LAYER
C
C    COL 2 TO 5       MATNUM, TYPE OF MATERIAL
C                         GRAM = GRANULAR MATERIAL
C                         MIXE = MIXED MATERIAL
C                         COHE = COHESIVE MATERIAL
C                         NOTE THESE COL ARE TO BE BLANK IF KTYPE = 2.
C
C    COL 11 TO 20     HEIGHT, HEIGHT OF SOIL LAYER
C
C    COL 21 TO 30     DENS, DENSITY OF THE SOIL MATERIAL.
C
C                     DEFAULT = 90 PCF
C
C    COL 31 TO 40     E, YOUNGS MODULUS (USED ONLY IF KTYPE = 2)
C
C    COL 41 TO 50     V, POISSONS RATIO (USED ONLYE IF KTYPE = 2)
C
C    COL 51 TO 55     KTYPE, DETERMINES TYPE OF MATERIAL PROPERTY GENERATION
C                         KTYPE = 0, EXTENDED HARDIN MATERIAL WITH TYPICAL
C                                    SOIL INPUT (CARD 3A)
C
```

Figure E-1. User Manual for XHARDN Computer Program (Sheet 1 of 3)

```
C                   KTYPE = 1, EXTENDED HARDIN SOIL WITH TRIAXIS INPUT
C                              (CARD 3B)
C                   KTYPE = 2, LINEAR INPUT PROPERTIES DEFINED ON THIS CARD
C                              COLS 31 TO 40 (E) AND COL 41 TO 50 (V).
C                              NO CARD TYPE 3.
C
C
C
C
C - - - - - - - - - - - - - - - - - - - - - - - - - - - - - - - - - - - - -
C
C * * * * * * * * * * * * * * * * * * * * * * * * * * * * * * * * * * * *
C
C - - - - - - - - - - - - - - - - - - - - - - - - - - - - - - - - - - - - -
C
C    CARD TYPE 3A. EXTENDED HARDIN FOR TYPICAL SOILS (5F10.0)
C
C      COL 1 TO 10   XNUMIN, POISSON RATIO AT LOW SHEAR STRAIN
C                           GRANULAR,XNUMIN = 0.10
C                           MIXED   ,XNUMIN = 0.2
C                           COHESIVE,XNUMIN = 0.3
C
C      COL 11 TO 20  XNUMAX, POISSON RATIO AT HIGH SHEAR STRAIN, FOR
C                           ALL CLASSIFICATIONS, DEFAULT = 0.49
C
C      COL 21 TO 30  XQ, SHAPE PARAMETER Q FOR POISSON FUNCTION.
C                           GRANULAR,XQ = 0.26
C                           MIXED   ,XQ = 0.35
C                           COHESIVE,XQ = 0.40
C
C      COL 31 TO 40  VOIDR, VOID RATIO OF SOIL, RANGE IS 0.1 to 3.0.
C                          DEFAULT VALUES FOR EACH CLASSIFICATION,
C
C                              GRANULAR, VOIDR = 0.6
C                              MIXED   , VOIDR = 0.5
C                              COHESIVE, VOIDR = 1.0
C
C      COL 41 TO 50  SAT, PERCENTAGE SATURATION, RANGE IS 0.0 TO 1.0.
C                         DEFAULT VALUES FOR EACH CLASSIFICATION.
C
C                            GRANULAR, SAT = (LEAVE BLANK)
C                            MIXED   , SAT = 0.5
C                            COHESIVE, SAT = 0.9
C
C      COL 51 TO 60  PI, PLATICITY INDEX, RANGE IS 0.0 TO 100.,
C                        DEFAULT VALUES FOR EACH CLASSIFICATION
```

Figure E-1. User Manual for XHARDN Computer Program (Sheet 2 of 3)

```
C
C                              GRANULAR, PI = (LEAVE BLANK)
C                              MIXED   , PI = 5
C                              COHESIVE, PI = 20
C
C
C
C
C - - - - - - - - - - - - - - - - - - - - - - - - - - - - - - - - - - - -
C
C * * * * * * * * * * * * * * * * * * * * * * * * * * * * * * * * * * * *
C
C - - - - - - - - - - - - - - - - - - - - - - - - - - - - - - - - - - - -
C
C    CARD TYPE 3B.  EXTENDED HARDIN TRIAXIAL DATA.  (6F10.0)
C                   HARDIN MODEL FOR USE WITH TRIAXIAL SOIL DATA.(6F10.0)
C
C      COL 1 TO 10     XNUMIN, POISSON RATIO FOR NO AXIAL LOAD ONLY
C                             CONFINING PRESSURE. DEFAULT = 0.1
C
C      COL 11 TO 20    XNUMAX, POISSON RATIO AT MAXIMUM AXIAL LOAD,
C                             DEFAULT = 0.49
C
C      COL 21 TO 30    XQ, SHAPE PARAMETER Q FOR POISSON FUNCTION.
C                          FOR ALL CLASSIFICATIONS, DEFAULT = 0.26
C
C      COL 31 TO 40    S1, HARDIN PARAMETER USED TO CALCULATE GMAX.
C
C      COL 41 TO 50    C1, HARDIN PARAMETER USED TO CALCULATE
C                          REFERENCE SHEAR STRAIN.
C
C      COL 51 TO 60     A, HARDIN PARAMETER USED TO CALCULATE
C                          HYPERBOLIC SHEAR STRAIN.
C
C
C - - - - - - - - - - - - - - - - - - - - - - - - - - - - - - - - - - - -
C
C * * * * * * * * * * * * * * * * * * * * * * * * * * * * * * * * * * * *
C
C - - - - - - - - - - - - - - - - - - - - - - - - - - - - - - - - - - - -
C
C - - - - M A N U A L - - - - M A N U A L - - - - M A N U A L - - - - M A
C
C * * * * * * * * * * * * * * * * * * * * * * * * * * * * * * * * * * * *
C
C - - - - O U T P U T - - - - O U T P U T - - - - O U T P U T - - - - -
```

Figure E-1. User Manual for XHARDN Computer Program (Sheet 3 of 3)

```
ALOHA MATERIAL PROPERTY GENERATION PROGRAM

USNAS MOFFETT FIELD HANGER NO 3 STA K = 380

TYPE OF MATERIAL . . . . . CONC
HEIGHT . . . . . 7.30
DENSITY OF MATERIAL. . . . . 150.00
YOUNGS MODULUS . . . . . .30000E+07
POISSONS RATIO . . . . . .2000
TYPE OF MATERIAL . . . . . 2
      0 = EXTENDED HARDIN WITH HARDEN CONSTANTS
      1 = EXTENDED HARDIN WITH TRIAXIS DATA
      2 = LINEAR ELASTIC

TYPE OF MATERIAL . . . . . GRAN
HEIGHT . . . . . 16.00
DENSITY OF MATERIAL. . . . . 110.00
YOUNGS MODULUS . . . . . -0.
POISSONS RATIO . . . . . -0.0000
TYPE OF MATERIAL . . . . . -0
      0 = EXTENDED HARDIN WITH HARDEN CONSTANTS
      1 = EXTENDED HARDIN WITH TRIAXIS DATA
      2 = LINEAR ELASTIC

HARDIN MATERIAL, INPUT PROPERTIES

MINIMUM POISSON RATIO. . . . . -0.000
MAXIMUM POISSON RATIO. . . . . -0.000
POISSON RATIO AT GAM-R . . . . -0.000
VOID RATIO . . . . . .467
PERCENT OF SATURATION. . . . . .534
PLASTICITY INDEX . . . . . -0.000

TYPE OF MATERIAL . . . . . GRAN
HEIGHT . . . . . 20.00
DENSITY OF MATERIAL. . . . . 110.00
YOUNGS MODULUS . . . . . -0.
POISSONS RATIO . . . . . -0.0000
TYPE OF MATERIAL . . . . . -0
      0 = EXTENDED HARDIN WITH HARDEN CONSTANTS
      1 = EXTENDED HARDIN WITH TRIAXIS DATA
      2 = LINEAR ELASTIC
```

Figure E-2. XHARDN Output (Sheet 1 of 3)

HARDIN MATERIAL, INPUT PROPERTIES

```
MINIMUM POISSON RATIO. . . . . -0.000
MAXIMUM POISSON RATIO. . . . . -0.000
POISSON RATIO AT GAM-R . . . . -0.000
VOID RATIO . . . . . .385
PERCENT OF SATURATION. . . . . .561
PLASTICITY INDEX . . . . . -0.000

TYPE OF MATERIAL . . . . . COHE
HEIGHT . . . . . -0.00
DENSITY OF MATERIAL. . . . . 110.00
YOUNGS MODULUS . . . . . -0.
POISSONS RATIO . . . . . -0.0000
TYPE OF MATERIAL . . . . . -0
      0 = EXTENDED HARDIN WITH HARDEN CONSTANTS
      1 = EXTENDED HARDIN WITH TRIAXIS DATA
      2 = LINEAR ELASTIC
```

HARDIN MATERIAL, INPUT PROPERTIES

```
MINIMUM POISSON RATIO. . . . . -0.000
MAXIMUM POISSON RATIO. . . . . -0.000
POISSON RATIO AT GAM-R . . . . -0.000
VOID RATIO . . . . . -0.000
PERCENT OF SATURATION. . . . . -0.000
PLASTICITY INDEX . . . . . 22.0
```

HARDIN MATERIAL, STANDARD SOIL PROPERTIES

```
SOIL CLASSIFICATION. . . . . GRAN
MINIMUM POISSON RATIO. . . . .100
MAXIMUM POISSON RATIO. . . . .490
POISSON RATIO AT GAM-R . . . .260
VOID RATIO . . . . . .467
PERCENT OF SATURATION. . . . .534
PLASTICITY INDEX . . . . . 0.000
```

HARDIN MATERIAL, STANDARD SOIL PROPERTIES

```
SOIL CLASSIFICATION. . . . . GRAN
MINIMUM POISSON RATIO. . . . .100
MAXIMUM POISSON RATIO. . . . .490
POISSON RATIO AT GAM-R . . . .260
VOID RATIO . . . . . .385
PERCENT OF SATURATION. . . . .561
PLASTICITY INDEX . . . . . 0.000
```

Figure E-2. XHARDN Output (Sheet 2 of 3)

HARDIN MATERIAL, STANDARD SOIL PROPERTIES

SOIL CLASSIFICATION.	COHE
MINIMUM POISSON RATIO.	.300
MAXIMUM POISSON RATIO.	.490
POISSON RATIO AT GAM-R	.400
VOID RATIO	1.000
PERCENT OF SATURATION.	-0.000
PLASTICITY INDEX	22.0

* * * LISTINGS OF DATA ON PUNCHED CARDS * * *

CARD NUMBER

1	USNAS MOFFETT FIELD HANGER NO 3 STA K = 380			
2	411111	1.00	15.00	0.00
	YOUNGS MODULUS		POISSONS RATIO	HEIGHT
3	3000000.		.2000	7.30
4	7407.		.2356	16.00
5	12102.		.2309	20.00
6	11760.		.3655	20.00

END OF DATA $ $ $ $ $ PROGRAM PAU $ $ $ $

Figure E-2. XHARDN Output (Sheet 3 of 3)

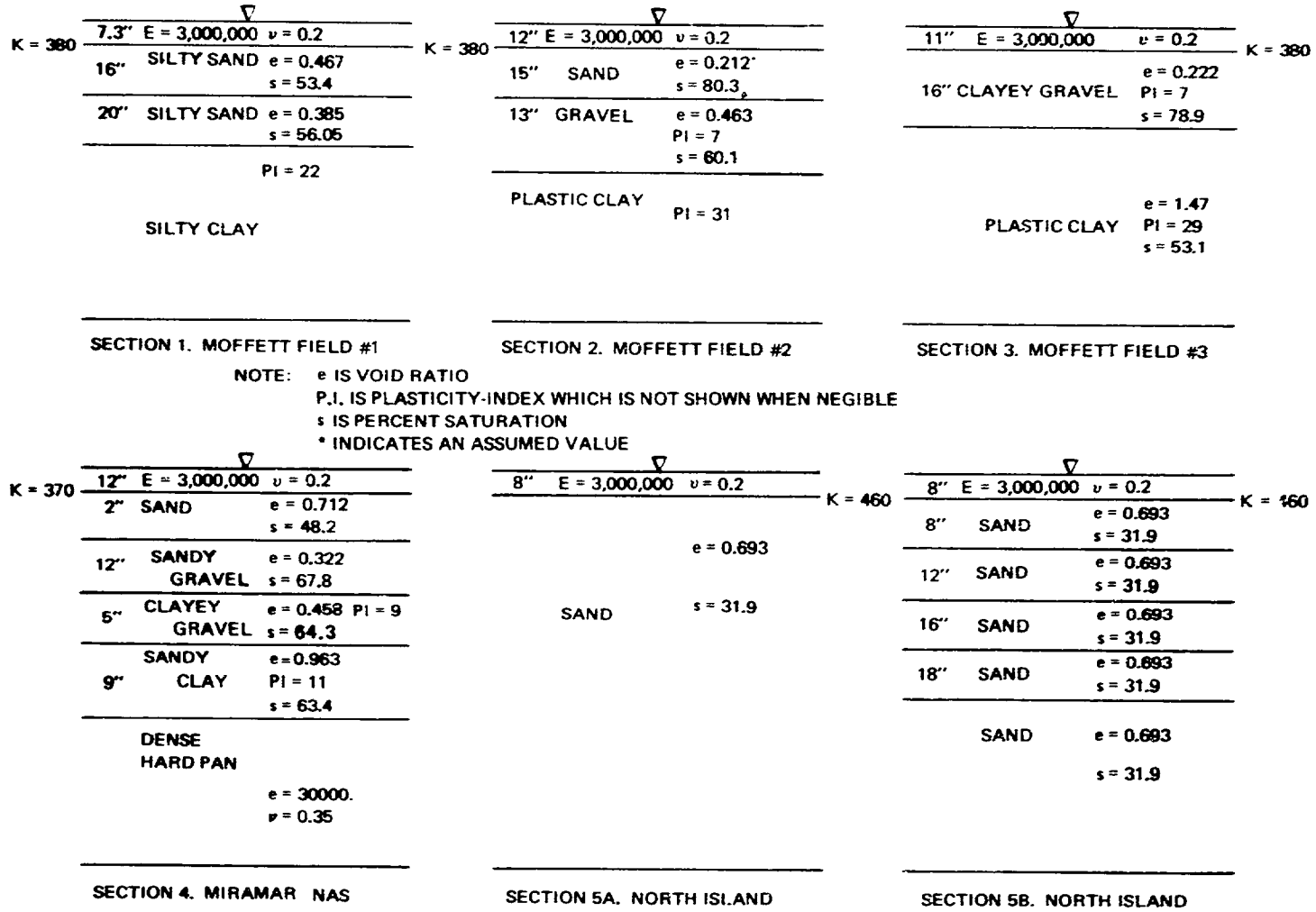

Figure E-3. Pavement Sections Taken From Condition Surveys

2. Discussion of the Output

The output consists of a reflection of the input along with any default values used. A summary of the secant material parameters E_s and ν_s is printed next as well as some additional information that allows the programs output to be used as input to the ELAST program. The first line of the summary will be a heading to signal the start of the listing of the punched output. The title of the section is on the next line and is also the first punched card. A parameter card (card type 2, ELAST code) is the next card punched and line printed. The parameters contained on this card are the numbers of layers, pressure load, radius of the load and the Westergaard k. The last three are default values for all sections (pressure load = 42.44 psi, radius of the load = 15 inches and k = 0.0). It may be desired to change these before running ELAST. The next punched cards and lines of output contain E, ν, and depth of the pavement/soil layers.

3. Program Organization

XHARDN is written in FORTRAN IV and is approximately 500 cards long. The code requires 13,000 decimal words to execute on a CDC 6600 and has been sucessfully run on the CDC 6600, UNIVAC 1110, and IBM 370 computers.

4. Computational Details

Overburden is the predominant load on the subsurface layers of an airfield except in the regions immediately adjacent to the tire load. For elastic analysis the most appropriate values for material characterization are the secant approximations of the material's stiffness under dead load. The error introduced by neglecting the live load effects is a function of the pavement's stiffness and depth. However, the attempt to incorporate the effects of live load is basically at odds with the concepts of linear analysis.

The overburden pressure is computed at the middle of each layer except for the last layer where it is computed at the top. Where the last layer is sufficiently close to the pavement surface, it is necessary to divide it into a number of fictitious layers in the preparation of input. This artificially forces a more accurate representation of the overburden within the layer.

Using the overburden pressure as a load, a plane strain boundary value problem is solved iteratively using Equations (E-1) and (E-2) and "guess" values for the material parameters G and ν.

$$\tau = \sigma_{old}(1 - 2\nu)/2(1 - \nu) \qquad \text{(E-1)}$$

$$\sigma_{new} = \sigma_{old}(1 - 2\nu/(1 - \nu))/3$$

Each time the problem is solved new values for G and ν derived from Hardin's law are used in the next cycle's computation for σ and τ. When σ and τ do not change between cycles the process is stopped and G and ν are declared the winners.

5. Application of the XHARDN Program with the Westergaard Functionals

Most major airfields, especially those of the Department of Defense, have been subjected to a "condition" survey. For almost all Naval airfields, these surveys are in report form and usually contain sufficient data to implement the extended Hardin model. Thus, they provide an invaluable aid in design and analysis of existing pavement systems. Data from three of these reports (References 33, 34, 35) has been used to construct Figure E-3.

The data for each section shown in Figure E-3 was input into the XHARDN computer program. The resulting material parameters [i.e., E and ν] were in turn input into ELAST. The functional k_w^1* computed by ELAST is shown in Table E-2 along with the measured Westergaard constant, k. Remarkably good agreement is achieved for these sections which is in contrast to the results reported in Reference 1.** Admittedly, this is only a "small piece of evidence," but it is encouraging to note that - by using standard, available soil data (such as, e and PI) coupled with the extended Hardin model of the XHARDN computer code - it is possible to predict reasonable values of Young's modulus, shear modulus, and Westergaard functional k_w^1. To reiterate, taking only the data shown on Figure E-3, it is possible to compute elastic responses (i.e., k_w^1) which agree favorably with response data (i.e., k) collected in the field.

To illustrate the impact and the necessity to include the effects of σ_m (or indirectly the overburden pressure), section 5 in Figure E-3 was considered in two alternative forms: (5A) considers the sand as one mass where σ_m is computed at a depth of 8 inches while (5B) considers the sand mass in several layers for the purposes of computing more appropriate values of σ_m for a given region of sand. Table E-2 shows the impact that a careful consideration of σ_m has on the subgrade's stiffness.

---

*This functional is described in Reference 1 and provides a mathematical equivalent Westergaard parameter based on the properties of an elastic layer idealization.

**Neglecting section 5A, the average error is 17% with a standard deviation of $\pm$10%. For similar section types where materials data was derived without use of material models, the average error reported in Reference 1 was 47% with a standard deviation of $\pm$22%.

Table E-2. Computed Versus Measured Westergaard Constant

Section Number	k PCI	k_w^1 PCI	% Error $\frac{(k_w^1-k)}{k} \times 100$
1	380	310	18
2	380	460	21
3	380	391	3
4	370	425	15
5A[a]	460	170	63
5B	460	325	29

[a]Note that the rather erroneous values of Section 5A are significantly improved by a more careful consideration of overburden, Section 5B.

While the successful results of Table E-2 are encouraging, reliance on the procedures of Section D-2 to determine G (using e, PI, and S) and the default value that XHARDN selects for Poisson's ratio is not recommended or warranted. The most appropriate utilization of the Hardin concept and XHARDN is through the application of the procedures of Section D-6. This includes triaxial tests for the soils over the range of parameters (both levels of stress/strain and e, PI, and S) that occur in the field.

REFERENCES

1. Crawford, J.E., Hopkins, J.S., and Smith, James, "Theoretical Relationships Between Moduli for Soil Layers Beneath Concrete Pavements," Report No. FAA-RD-75-140, Federal Aviation Administration, Washington, DC, May 1976.

2. Federal Aviation Administration, "Airport Pavement Design and Evaluation," Advisory Circular AC 150/5320-6B, Washington, D.C, May 1974.

3. Department of Defense, "Unified Soil Classification System for Roads, Airfields, Embankments, and Foundations, "Military Standard No. MIL-STD-619B, Washington, D.C., June 1968.

4. American Society for Testing and Materials, "Determining the Density of Soil and Soil Aggregate in Place by Nuclear Methods (Shallow Depth)," Designation: D2922-71, 1972 Annual Book of ASTM Standards, Part II, Philadelphia, Pennsylvania, April 1972.

5. American Society for Testing and Materials. "Test for Density of Soil in Place by the Sand-Cone Method," Designation: D1556-68, 1972 Annual Book of ASTM Standards, Part 11, Philadelphia, Pennsylvania, April 1972.

6. Bison Instruments Incorporated, "Bison Instruments, Soil Strain Gage, Model 4101A, Instruction Manual," Minneapolis, Minnesota.

7. Ailtech, "Embedment Gage, Model CG129, Specifications," Cutler-Hammer Company, Industry, California.

8. The American Association of State Highway Official. "Moisture-Density Relations of Soils Using a 10-Lb Rammer and an 18-In. Drop," Designation T180-70, 1971 Standard Specifications for Highway Materials and Methods of Sampling and Testing, Part II, Washington, D.C., 1971.

9. Ballard, J. T., Personal communication to the Naval Civil Engineering Laboratory, Sep 6, 1973.

10. Dorris, J. M., and Chang, Chin-Yung, "Nonlinear Analysis of Stress and Strain in Soils," Journal of the Soil Mechanics and Foundations Division, ASCE Vol. 96, No. SM5, Proc. Paper 7513, Sep 1970 pp 1629-1653.

11. Ehrgott, J., Personal communication to the Civil Engineering Laboratory, April 1975.

12. Hardin, B. O., "Constitutive Relations for Air Field Subgrade and Base Course Materials," Technical Report UKY 32-71-CE5, University of Kentucky, College of Engineering, Soil Mechanics Series No. 4, Lexington, KY, 1970.

13. Hardin, B. O., "Effects of Strain Amplitude on the Shear Modulus of Soils," Technical Report AFWL-TR-72-201, Air Force Weapons Laboratory, Kirtland Air Force Base, NM, Mar 1973.

14. Kondner, R. L., "Hyperbolic Stress-Strain Response: Cohesive Soils," Journal of the Soil Mechanics and Foundations Division, ASCE, Vol. 89, No. SM1, Proc. Paper 3429, 1963, pp 115-143.

15. Kondner, R. L., and Zelasko, J. W., "Hyperbolic Stress-Strain Formulation for Sands." Proceedings, 2nd Pan-American Conference on Soil Mechanics and Foundation Engineering, Brazil, Vol. 1, 1963, pp 289-324.

16. Isenberg, J., "Nuclear Geoplosics, Part 2 mechanical properties of earth materials," DNA AD-755 488, Agbabian Associates, Nov 1972.

17. Nayak, G. D. and Zienkiewicz, O. C., Elasto-plastic stress Analysis, Generalization for various constitutive relations including strain softening," International Journal of Num. Methods in Eng., Vol 5, pp 113-135, 1972.

18. Nielsen, John P. The Modulus of Deformation of Asphaltic Concrete, Technical Note N-822, U. S. Naval Civil Engineering Laboratory, Port Hueneme, California Jun 1966.

19. Richards B. E. The Role of the Environment in Flexible Pavement Design. Institute of Engineers, Australia, Civil Engineering Transactions, Vol CE 10, No. 2 Oct 1968.

20. Smith and Nair. Report No. FHWA-RD-74-61.

21. FAA Advisory Circular, AC No. 150/5370-10, Oct 24, 1974.

22. Appendix C, "Full-Depth Asphalt Pavements for Air Carrier Airports," Manual Serial No. 11. The Asphalt Institute, Jan 1973.

23. Suddath, L. P. and Thompson, M. R., Load Deflection Behavior of Lime-Stabilized Layers. Technical Report N-118. Construction Engineering Research, Lake Urbane, ILL. Jan 1975.

24. Nielsen, John P. and Glenn T. Baird, "Non-destructive pavement load rating," 13th Annual Paving Conference, University of New Mexico, Jan 1976.

25. Edwards, J. M., and C. P. Valkering, "Structure Design of Asphalt Pavements for Heavy Aircraft," Shell Printing Limited, Shell Center, London 1970.

26. Federal Aviation Administration, "Standards for Specifying Construction of Airports," Advisory Circular AC 150/5370-10, Washington, D.C., October 1974.

27. American Society for Testing and Materials. "Making and curing Concrete Compressive and Flexural Strength Test Specimens in the Field," Designation: C31-69, 1970 Annual Book at ASTM Standards, Part 10, Philadelphia, Pennsylvania, November 1970.

28. American Society for Testing and Materials. "Compressive Strength of Molded Concrete Cylinders," Designation C39-66, 1970 Annual Book of ASTM Standards, Part 10, Philadelphia, Pennsylvania, November 1970.

29. American Society for Testing and Materials. "Specifications for Special Finishing Hydrated Lime," Designation C206- , Annual Book of ASTM Standards, Part 9, Philadelphia, Pennsylvania.

30. Clough, R. W., and Woodward, R. J., "Analysis of Embankment Stresses and Deformations," Journal of Soil Mechanics and Foundations Division, Proc., ASCE, Jul 1967, pp 529-549.

31. Duncan, J. M., and Chang, Chin-Yung, "Nonlinear Analysis of Stress and Strain in Soils," Journal of the Soil Mechanics and Foundations Division, ASCE, Vol 96, No. SM5, Proc. Paper 7513, Sep 1970, pp 1629-1653.

32. Kulawy, F. H., and Duncan, J. M., "Finite Element Analysis of Stresses and Movements in Dams During Construction," Report No. TE 69-4, Office of Research Services, University of California, Berkeley, 1970.

33. Lowe, R. J., and Chamberlin, W. H., "Airfield Pavement Evaluation, USNAS Moffett Field, CA," NCEL Technical Note, N-809, Feb 1966.

34. _____ . "Airfield Pavement Evaluation, USNAS Miramar, CA," NCEL Technical Note, N-718, May 1965.

35. _____ . "Airfield Pavement Evaluation, USNAS North Island, CA," NCEL Technical Note, N-813, Apr 1966.